UNCOVERING MECHANISMS OF CADMIUM TOLERANCE IN A *Euglena mutabilis* FUNGAL-ALGAL-BACTERIAL (FAB) CONSORTIUM

A dissertation submitted to the Committee of Graduate Studies

in partial fulfillment of the requirements

for the degree of

Doctor of Philosophy

in the Faculty of Arts and Science.

Trent University

Peterborough, Ontario, Canada

Environmental and Life Sciences Ph.D. Graduate Program

January 2026

ABSTRACT

Uncovering mechanisms of cadmium tolerance in a *Euglena mutabilis* fungal-algal-bacterial (FAB) consortium

Emma Kaszecki

Acid mine drainage (AMD) and metal-contaminated tailings represent some of the most inhospitable aquatic environments on Earth, characterized by low pH, elevated metal concentrations, and chronic carbon limitation. Yet these systems support microbial consortia with remarkable resilience. Among the most conspicuous inhabitants is *Euglena mutabilis*, an acidophilic protist traditionally regarded as an indicator species of AMD but seldom thoroughly investigated. This thesis reframes *E. mutabilis* at the center of a fungal-algal-bacterial (FAB) consortium, demonstrating that its cadmium tolerance and persistence are emergent properties of the consortium.

Culture-based experiments revealed that *E. mutabilis* survival under cadmium stress declined when fungal and bacterial partners were disrupted, underscoring their indispensability. Glucose supplementation revealed the consortium's capacity for structural and metabolic reorganization: fungal hyphae bound algal cells into flocs, bacterial associates proliferated, and hormone production shifted. Hormone profiling suggested a distributed signaling system in which fungi contributed cytokinins (CKs) and gibberellins while algae produced methyl-thiolated CKs, jasmonic acid, and salicylic acid. Transmission electron microscopy revealed bacterial-like inclusions within algal vacuoles, suggesting facultative endosymbiosis or phagotrophic retention. Transcriptomic analyses revealed that cadmium stress suppresses light-harvesting complexes and growth-promoting

hormone biosynthesis while activating metal transporters and chloroplast sequestration mechanisms.

Beyond stress physiology, the FAB consortium unlocked chemical diversity inaccessible to axenic cultures. Molecular networking revealed that environmental consortia consistently produced unique metabolite families, often linked to silent biosynthetic pathways. Metagenomic sequencing linked these products to bacterial gene clusters further supporting the view that metabolic innovation is an emergent property of the collective.

Together, these findings suggest that the FAB consortium should be understood not as a loose association but as a microbial superorganism. This framing extends beyond the holobiont concept by dissolving the hierarchy between host and symbiont: *E. mutabilis*, fungi, and bacteria are all indispensable, and the identity of the host itself becomes blurred.

By reframing *E. mutabilis* as the nucleus of a microbial superorganism, this work highlights both theoretical and applied significance. It advances ecological understanding of how life persists under geochemical extremes, while pointing to new opportunities for sustainable bioremediation and natural product discovery through the deliberate cultivation of naturally evolved microbial consortia.

Keywords: Bioremediation · Algal symbiosis · Co-culture · Microscopy · Hormones · Transcriptomics

PREFACE

This thesis is presented in manuscript form. Chapter 1 serves as an introduction to the central concepts underpinning the work. Content from Chapter 2 encompasses published experimental work. Chapters 3 and 4 encompass experimental work that is presently under review for publication. All co-authors and their associated contributions are listed in the preface of each chapter. Copyright authorization associated with published chapters is presented in the preface of each chapter. References across all chapters have been uniformly presented in the style of the Journal of Forensic Science (JFS), and a digital object identifier (DOI) has been provided when available.

Additional publications not included in this thesis:

Kennedy V, **Kaszecki E**, Donaldson ME, Saville BJ. The impact of elevated sulfur and nitrogen levels on cadmium tolerance of *Euglena* species. Sci Rep 2024;14(11):11734. doi: 10.1038/s41598-024-61964-w

Kaszecki E, Kennedy V, Shah M, Maciszewski K, Karnkowska A, Linton E, et al. Meeting report: Euglenids in the age of symbiogenesis: Origins, innovations, and prospects, November 8–11, 2021. Protist. 2022;173(4):125894. doi: 10.1016/j.protis.2022.125894.

ACKNOWLEDGEMENTS

After a decade at Trent University, this thesis represents the final step in a long and meaningful journey – one I couldn't have completed without the help of many.

To Dr. Barry Saville – thank you for taking a chance on me and believing in me when I didn't have the confidence to believe in myself. Thank you for listening to my crazy ideas – and not only helping me achieve them but also adding to the craziness. Your knowledge and guidance shaped every part of my graduate school journey. To be your student meant to be pushed academically, which made me a better writer, a more curious thinker, and a life-long learner. This work is a culmination of the wild ideas we dreamed up together, and I'm forever grateful that we got to take this journey side-by-side.

To Dr. Neil Emery – I am profoundly grateful for your kindness, unwavering support, and inspiring dedication. Thank you for creating a nurturing and motivating environment where curiosity is celebrated and challenges are embraced as new learning opportunities. Your genuine care for your students goes far beyond the typical role of a supervisor – you consistently go above and beyond to ensure we not only succeed academically but also grow personally and professionally. I feel incredibly fortunate to have had the chance to learn from you, and any accomplishments along the way would not have been possible without your support.

To Dr. Michael Donaldson – when I began my graduate school journey you asked me what kind of student I wanted to be. I've reflected on that over the years, using it as motivation to do as much as I can with the time I've been given. Thank you for lighting the fire underneath me and helping to guide my work. To Dr. Erin Morrison – thank you for being available to talk, whether it was to sort out my research rabbit holes or sharing daily goings-on. Your insight and suggestions pushed me to get the most out of my work. To Dr. Karen Thompson – thank you for reminding me to take a holistic approach towards my research. You invited me to examine problems from a different angle which challenged me to grow not only as a researcher, but as a thinker.

As the final member of the Saville Lab, I would like to thank the countless members that came before me. You helped build a legacy that made the Saville Lab one of Trent's leading research groups. Without your example, I wouldn't have pushed myself as hard as I did. To Dr. Colleen Doyle – thank you for being available to help. I took great comfort knowing you were right across the hall, and I could count on you whenever I felt lost or overwhelmed. To Dr. Amanda Seto and Emilee Storfie – thank you for being such steady guides throughout my graduate journey. Your wisdom, support, and leadership made the path clearer and the challenges easier to face. To Victoria Kennedy – thank you for generously sharing your time and experience. Your mentorship helped me find my footing when I needed it most. To Monique Lariviere – thank you for consistently making time to

support me, both in and out of the lab. Your generosity and availability never went unnoticed.

To the past and present members of the Emery Lab – endless thanks for your support. I've never been surrounded by so many people who care so deeply for one another. It has been a privilege to be part of such a special group. To Zeynab Azimychetabi, Mark Seegobin, and Vedanti Ghatwala – thank you for your patience and kindness. You were always willing to answer my questions, and never once made me feel like I was asking a stupid one. I truly mean it when I say that without you, I might still not know what a hormone is. To Peter Andras, Galair Prevost, Stacy James, and Linh Tran – thank you for making the lab a fun and welcoming environment. You never fail to make me laugh and remind me that I have friends to lean on for extra support. To Michael Capperauld and Chetan Dhanjal – thank you for eagerly lending a hand whenever you could. It was a pleasure sharing a bench with you.

To my colleagues and friends at the University of Nottingham – thank you for the opportunity to learn and grow as a scientist. To Dr. Ellis O'Neill – thank you for inviting me to work with you. My experience was invaluable. To Oskar Fields and Harry Cagney – thank you for being so welcoming and supportive. It was a pleasure to be in the company of two incredible scientists who I'm proud to call my friends. To Harrison Leedham – thank you for taking on the impossible task of trying to teach chemistry to a biologist. You were an excellent mentor.

To my dear office mate Erin Stewart, who experienced every step of my degree with me. Sharing the highs, lows, and everyday moments of graduate life with you made the experience not just bearable, but enjoyable. To Angela Sikma and Chris Williams – there is not enough thanks in the world for everything you do. You keep the lights on, the autoclaves running, and research producing. I couldn't imagine doing this without you. To Dr. Karla Newman and Dr. Naomi Stock – thank you for being there whenever I needed you. Knowing I could turn to you made all the difference. To Erin Davidson and Sasha Trivett – thank you for being a bright light in my life and two of my biggest cheerleaders. I cherish the happy memories of the times we've shared. To Dr. Emily Slepkov – I am so grateful to know you. Thank you for your advice, for making me laugh, and reminding me that somehow everything turns out alright.

To my parents, who nurtured and encouraged my scientific curiosity, thank you for your unwavering support throughout what sometimes felt like a never-ending academic journey. The opportunities you provided me growing up shaped who I am today. I am grateful for the foundation that made this possible. To my siblings – John and Ainsley – thank you for simply being family. Your presence in my life has been a constant source of comfort and strength, and I'm grateful for the bond we share. To Kristin and Mikayla – thank you for putting up with me, cheering me on, and reminding me to take breaks and have fun. You made this journey so much better just by being you.

Finally, to my husband, Dr. Daniel Palberg – my greatest supporter and partner through every step of this journey. Sharing the bench and working alongside you made this experience even more special. You never let me forget how capable I am, and your unwavering belief in me lifted me up during the toughest moments. Thank you for being there whenever I needed anything, for your endless encouragement, and for being my rock. I truly couldn't have done this without you.

This research was made possible by generous funding from the Natural Sciences and Engineering Research Council of Canada (NSERC), the Ontario Graduate Scholarship (OGS) in Science and Technology, UK Research and Innovation (UKRI), the Trent University School of Graduate Studies, and the Environmental and Life Sciences Program at Trent University.

DEDICATION

For anyone who didn't believe they could – and proved themselves wrong.

TABLE OF CONTENTS

INDEX OF FIGURES

INDEX OF TABLES

INDEX OF ABBREVIATIONS

ABC	ATP-binding cassette
ABA	abscisic acid
AMD	acid mine drainage
ANOVA	analysis of variance
antiSMASH	antibiotics & secondary metabolite analysis shell
ASV	amplicon sequence variants
ATP	adenosine triphosphate
BGC	bioactive gene cluster
BLAST	basic local alignment search tool
BP	biological process
bp	base pair
BSC	biological soil crusts
BVC	bacteria containing vacuole
Cat. No.	catalogue number
CC	cellular component
CDF	cation diffusion facilitator
cDNA	complementary DNA
CFU	colony forming units
chl	chlorophyll
CK	cytokinin
cm	centimeter
COG	clusters of orthologous genes
CPCC	Canadian Phycological Culture Centre
*c*Z	*cis*-Zeatin
DEG	differentially expressed gene
DGE	differential gene expression
dH2O	deionized water
DMSP	dimethylsulfoniopropionate
DNA	deoxyribonucleic acid
EA	endophytic actinomycetes
EG	*Euglena gracilis* medium
EPS	extracellular polymeric substances
ESI-MS/MS	electrospray ionization tandem mass spectrometry
eV	electronvolt
FAB	fungal-algal-bacterial
FB	freebase
FDR	false discovery rate
fmol	femtomole
FV	food vacuole
G	glucose
GA	gibberellin
g	gram
gDNA	genomic DNA
GNPS	global natural product social

GO	gene ontology
GSH	glutathione
GSSG	oxidized glutathione
h	hours
HM	heavy metal
HPLC	high performance liquid chromatography
HSD	honest significant difference
Hz	hertz
IAA	indole-3-acetic acid
ICP-MS	inductively coupled plasma mass spectrometer
ICP-QQQ-MS	trile quadrupole inductively coupled plasma mass spectrometer
IPT	isopentenyltransferase
IS	internal standard
ITS	internal transcribed spacer
JA	jasmonic acid
JM	Jaworski's medium
KEGG	Kyoto Encyclopedia of Genes and Genomes
KGD	α-ketoglutaric dehydrogenase
L	litre
LCA	lowest common ancestor
LC-MS	liquid chromatography mass spectrometry
LC-MS/MS	liquid chromatography tandem mass spectrometry
LD	light-dark
LHC	light-harvesting complex
LOG	Lonely Guy
m	meter
m/z	mass-to-charge ratio
MAM	modified acid medium
MeSZ	methylthio-*trans*-Zeatin
MeSZR	methylthio-trans-Zeatin riboside
MetE	methionine E
MetH	methionine H
MF	molecular function
min	minute
mL	millilitre
mM	millimole
MQ	MilliQ
MS/MS	tandem mass spectrometry
MΩ	megaohm
µg	microgram
µL	microliter
µM	micromolar
µmol	micromole
NCBI	National Center for Biotechnology Information
ng	nanogram

nm	nanometer
NP	natural product
NRPS	non-ribosomal peptide synthase
NT	nucleotide
ORF	open reading frame
OTU	operational taxonomic units
padj	adjusted p-value
PCA	principal component analysis
PBS	phosphate buffered saline
PDA	potato dextrose agar
PDB	potato dextrose broth
PE	paired-end
PES	polyethersulfone
pg	picogram
PKS	polyketide synthase
pmol	picomole
PSII	photosystem II
PTFE	polytetrafluoroethylene
QS	quorum sensing
R2A	Reasoner's 2A
RB	riboside
RCF	relative centrifugal force
RF	radio frequency
RIM	RNA integrity number
RNA	ribonucleic acid
RNA-seq	RNA sequencing
ROS	reactive oxygen species
RPM	revolutions per minute
RT	retention time
rRNA	ribosomal RNA
SA	salicylic acid
SAM	S-adenosylmethionine
s	second
SEM	scanning electron microscopy
SM	specialized/secondary metabolites
TE	tris-EDTA
TEM	transmission electron microscopy
tRNA	transfer RNA
TSB	tryptic soy broth
tZ	*trans*-Zeatin
U-HPLC	ultra-high performance liquid chromatography
UV	ultra-violet
w/v	weight per volume
XICs	extracted ion chromatograms
ZIP	ZRT/IRT-like protein

CHAPTER 1

1.1 PREFACE

Title: General Introduction

Author: Emma Kaszecki

CHAPTER 1

GENERAL INTRODUCTION

1.2 SYMBIOSIS

Symbiotic systems are pervasive in nature. Organisms rely on each other for survival, from intertwining mycorrhizal fungi and plant root systems, to the bacteria that live in our gut, and the inseparable interkingdom collaborations that form lichens and corals [1–4]. The classically studied symbiotic systems are those that are advantageous in nature, where the benefit of each associated organism increases because of the relationship. This is known as mutualism [5].

One of the most researched mutualistic systems combines a photosynthetic algae or cyanobacteria, communities of bacteria, and two fungi – one of which is a basidiomycete yeast – to create an organism called a lichen [6–8]. Although it is unknown when lichens began to evolve, the earliest fossils date back approximately 400-600 million-years-ago [9]. Presently, it is estimated that 20,000 known fungi can lichenize to create unique structures that cover 8% of the Earth's surface [7,10]. An oversimplified interpretation of these relationships would be that they are driven by the need to survive: the photosynthetic algae provide nutrients for the fungi, while the fungal thallus provides shelter and protection for the algae, and the bacteria assist in nutrient acquisition and resistance against environmental stressors [7,10–12]. This convergence is an example of co-dependence in nature for which the separate species in a lichen come together to serve each other's need, and in doing so, creating an entirely new organism [9,10].

Mutualism can exist outside of a defined lichen structure between free-living algae and fungi, algae and bacteria, or fungi and bacteria [13–15]. While these relationships exist everywhere in nature, they are historically understudied for the following reasons: (1) It is widely agreed that the relationship between algae and fungi, and the structure they take on when cultured together, is foundational to the formation of a lichen [14]. Therefore, this interaction in the evolutionary context of lichenization is explored as opposed to studying the free-living organisms [16]; (2) Studying two unique microbes that have evolved together is challenging because the possibility of isolating one microbe to create an axenic culture is difficult [7,14]; and (3) Fungi, bacteria, and algae have traditionally been studied axenically to make them more amenable to advanced molecular tools, therefore the biological significance of microbial associations is often lost in a laboratory setting [14,17].

Phycology, like many other disciplines over the last decade, has endeavoured to understand basic principles of physiology and ecology through a reductionist approach [18]. Laboratory settings typically used sterile culture techniques with a view to study axenic algal cultures, uncontaminated by “interference” from other microbes. More recently, with the realization of how important microbiomes are to even simple living assemblages, a new imperative has arrived to understand the true functioning of algal populations, inclusive of all its bacterial and fungal partners [19,20]. The positive associations between co-cultures of algae and fungi and/or bacteria have been highlighted in the movement towards sustainable environmentally friendly technologies. These systems are being synthetically created and investigated for potential use in bioremediation, as biofuel development, and in consumer products [21–23]. Generally, the interactions in

these co-cultures are not reflective of natural microbial relationships as much as they are an attempt to optimize their potential use [21,23,24].

Exploratory studies of interkingdom mutualism with algae have focused primarily on synthetic bipartite associations, while investigations of algal tripartite co-cultures remain limited [14,25,26]. In general, tripartite systems with free-living organisms are not widely researched outside of mycorrhizal associations, largely because their inherent complexity makes them difficult to disentangle, despite the natural association of algae such as *Euglena* sp. and *Chlorella* sp. with other organisms, at times in extreme environments [27–29]. The potential for developing biotechnology with *Euglena* and *Chlorella* has led to increased interest in the association of organisms, however their evolved associations are often substituted by the formation of synthetic co-cultures from axenic strains in these technologies [30,31].

1.3 ALGAL RELATIONSHIPS

Since the idea of "algal-bacterial" consortia was proposed in 1981, their evolutionary history, interactions, and how they can be used together for biotechnology have been extensively examined [19,22,32,33].

1.3.1 PHOTOSYNTHETIC EVOLUTION FROM CYANOBACTERIA

The theory of the evolution of organelles in algae can be traced back to the endosymbiotic theory proposed by Konstantin Mereschkowski and substantiated by Lynn Margulis [34–37]. In its modern form, the endosymbiotic theory proposes that mitochondria and plastids – including chloroplasts – originated from free-living

alphaproteobacteria and cyanobacteria, respectively, that were engulfed by an ancestral eukaryotic host through a process akin to phagocytosis. Rather than being digested, these prokaryotic symbionts established a stable, long-term endosymbiotic relationship, eventually evolving into obligate organelles through extensive genomic integration and functional interdependence with the host [34–37]. Subsequent evolutionary diversification involved additional rounds of symbiosis. In secondary endosymbiosis, a eukaryotic host engulfed another eukaryote that already contained a primary plastid. This led to plastids surrounded by three or four membranes, as seen in lineages from green and red algae [38]. These events represent a horizontal transfer of photosynthetic capacity, rather than vertical descent, and significantly expanded the diversity of photosynthetic eukaryotes.

Several species of photosynthetic algae can obtain food and energy heterotrophically in the absence of light, either by absorbing dissolved organic molecules or ingesting particles from their environment [39–42]. Under experimental heterotrophic culture conditions, *Chlorella* sp. have shown markedly increased respiration rates and biomass accumulation compared with autotrophic cultures [41–43]. Despite these observations, many algal species are obligate phototrophs and have lost the ability to grow in complete darkness [41,44,45]. Light generally stimulates growth and increases growth rates, but the highest biomass yields are often achieved under mixotrophic conditions, where cells combine autotrophic and heterotrophic nutrition and thus avoid dependence on either light or carbon as a sole nutrient source [40,41]. When the growth of *Chlamydomonas reinhardtii* were compared under autotrophic, heterotrophic, and mixotrophic conditions the highest growth rates and biomass accumulation have been observed under mixotrophy [46].

While the evolution of plastids through primary and secondary endosymbiosis is well-established, the retention or loss of phagocytosis in algal lineages provides insight into the metabolic flexibility and ecological strategies of these organisms. In particular, the Archaeplastida lineage – which includes glaucophytes, red algae, green algae, and land plants – appears to have lost phagocytotic capacity early after plastid integration, likely due to the reduced selective pressure to maintain heterotrophic feeding once efficient autotrophy was established [47]. Most green algae lack the cellular machinery necessary for phagocytosis; however, not all algae have abandoned phagotrophy [47,48]. Several algal groups derived from secondary or tertiary endosymbiotic events – including euglenoids, dinoflagellates, cryptophytes, and some chrysophytes – have retained or reacquired the ability to phagocytose particles [49,50]. These algae can use both light and organic matter as energy sources, offering a competitive advantage in nutrient-poor or variable environments. For example, *Euglena gracilis* can grow heterotrophically in the dark and phagocytose bacteria [50–52], while the dinoflagellate *Oxyrrhis marina* exhibits life stages with active ingestion of prey [53]. The presence of phagocytosis in these lineages suggests that while plastid acquisition limited phagotrophy in some groups, others have maintained it as a complementary or fallback strategy. This evolutionary pattern underscores that phagocytosis is not universally lost among algae but has been selectively retained, lost, or modified depending on ecological pressures and metabolic needs [54].

1.3.2 ALGAL-BACTERIAL SYMBIOSIS

Despite the extensive evolutionary history between algae and bacteria, the idea of an “algal-bacterial consortia” was proposed only 40 years ago [32]. Since then, the various

interactions between algae and bacteria have been extensively researched [22]. These associations can be found in virtually every aquatic habitat on Earth, including extreme environments where acidity and heavy metal concentrations do not favour species diversity [13,28,55]. Recent studies have demonstrated that these interactions can be mutually beneficial, particularly through the bidirectional exchange of nutrients, supporting the existence of symbiotic relationships [22,56–58].

There are many examples of the mutualistic relationship between algae and bacteria, but perhaps the most familiar is bacteria enhancing algal growth through the supplementation of vitamin B_{12} [57,59]. Over half of the 326 algal species surveyed by Croft *et al*. [57] require vitamin B_{12} for growth because it acts as a cofactor for methylmalonyl-CoA mutase (MCM) which is involved in amino acid and protein synthesis [3,60]. Two enzymes are responsible for methionine synthesis: vitamin B_{12}-independent MetE can synthesize methionine without B_{12}, and vitamin B_{12}-dependent MetH which relies on B_{12} as its cofactor [3,57]. There is no molecular evidence of vitamin B_{12} synthesis in the algal lineage, and it is noted that most algae have lost MetE, although *C. reinhardtii* and the diatom *Phaeodactylum tricornutum* have been reported to contain both MetE and MetH [57,61,62]. Despite this anomaly, both organisms significantly repress MetE transcript expression when treated with exogenous vitamin B_{12} [61,62]. An exogenous application of only 50 ng/L of vitamin B_{12} reduced the transcript expression of MetE by 30% [61]. This correlation suggests that there is a strong cellular advantage for the gene to remain inactive when possible and instead have the organism rely on external sources of vitamin B_{12} for MetH facilitated methionine synthesis [61,62]. This ecological dependence has been empirically demonstrated: the algae *Lobomonas rostrata* cannot grow axenically

without B_{12}, but in co-culture with B_{12} producing bacterium *Mesorhizobium loti* both partners persist through reciprocal exchange of B_{12} and organic carbon [63].

In addition to providing vitamin B_{12} some bacteria are capable of fixing nitrogen to supply the algae, who do not possess nitrogen-fixing mechanisms [22]. This is seen in the Great Lakes among the growth of *Cladophora* with an abundance of nitrogen-fixing bacteria and archaea, and in a laboratory setting upon which *Ditylum brightwellii* only survives in nitrogen-limited media when co-cultured with bacteria [64,65]. It should be noted that for nitrogen fixation the interactions exist between free-living algae and free-living bacteria, as it was recently discovered that of 437 lichen metagenomes analyzed none of them contained nitrogen-fixing bacteria [66].

Although the relationship between algae and bacteria initially appear beneficial for the algae only, the bacteria capitalize on using algae as a carbon source [59,67]. In the case of the above-mentioned with *D. brightwellii*, it was observed that bacterial growth was limited by lack of a carbon source and exhibited improved growth once co-cultured with *D. brightwellii* [64]. This phenomenon is also seen in the mutualistic interaction between a culture of *Pseudo-nitzschia multiseries* from the Pacific and Atlantic Oceans that is associated with *Sulfitobacter* [68]. Separation of the organisms resulted in significantly decreased growth for both the algae and bacteria in their respective monocultures [68]. Some bacteria produce the antioxidant dimethylsulfoniopropionate (DMSP) which is released into the environment and used as a sulfur and carbon source, although not enough is produced to supply the bacteria with sufficient carbon [69]. DMSP is also produced by algae who do not recycle it for themselves, generating an excess of DMSP in axenic

cultures; however, when co-cultured with bacteria, DMSP is almost undetectable as it is being rapidly metabolized by bacteria [69].

1.3.3 ALGAL-FUNGAL SYMBIOSIS

Lichens are an example of algal mutualistic symbiosis [70,71]. First characterized by Simon Schwendener in 1868, the algal-fungal association was widely rejected until the twentieth century when an aposymbiotic culture of the fungus *Cladonia pyxidate* and its green algal partner were successfully used to reconstitute a lichen [70,71]. This led scientists to believe that a lichen is a symbiotic relationship between a fungus – typically an Ascomycota – and a photosynthesizing partner – typically an alga or cyanobacteria [10,70,71]. Bacteria were being isolated from lichen thalli as early as the 1920s, however it was believed that these organisms did not affect the algal-fungal association and were "contaminants" [8,72]. Aschenbrenner *et al*. [73] were the first group to identify a diverse bacterial community within lichens. They recognized that the bacteria were directly interacting with thalli propagules and determined that a portion of the lichen microbiome was vertically transferred using the bacteria [73]. Additionally, Spribille *et al*. [8] characterized a basidiomycete yeast embedded in the cortex of 15 *Bryoria* spp. across Montana, U.S.A., and confirmed this interaction in 52 other lichen genera from around the world. This caused the definition of what a lichen is to be corrected. Now, it is understood that a lichen is a mutualistic interaction between a photobiont, two mycobionts, and a plethora of bacteria [8,72]. Approximately 20,000 lichen-forming fungal species and 156 species of photobionts have been identified, however the consistent flow of new information about lichens underscores how much remains unknown [10,71,74].

Often, physical interaction is regarded as the earliest stage in the development of a lichen and has been frequently used as a criterion to distinguish lichen from the simple cohabitation of two organisms [14,29,75,76]. Lichens form defined structures that can be described as crust-like, leaf-like (foliose), or shrub-like (fruticose) in which the fungal hyphae surrounding the photobiont forms a colourful growth chamber called a thallus [77]. The organisms that make-up a lichen are unable to re-lichenize following intentional separation, suggesting the thallus structure formed in co-culture is critical to the survivability of the lichen relationship [16,78–80].

A transitional case was illustrated by Watanabe *et al*. [29], who documented the first mutualistic association involving *Chlorella*, fungi, and bacteria. Their study revealed that both fungal and bacterial populations adhered directly to *Chlorella* cells, indicating colonization. From this community, they successfully isolated a fungal strain, CSSF-1, closely related (98.8%) to the *Acremonium*-like hyphomycete KR21-2, and demonstrated that it could be cultured independently. When co-cultured for seven days, *Chlorella* and CSSF-1 exhibited significantly enhanced growth rates compared to their respective axenic cultures. The authors attributed this growth promotion to a mutualistic nutrient exchange between the fungus and alga. Notably, although reminiscent of lichen symbioses, the co-culture did not result in a lichenized structure, and the symbiotic relationship could be re-established after physical separation [29]. This study highlights the continuum between strict lichenization and more flexible algal-fungal partnerships.

The absence of clear criteria distinguishing between mere association, co-habitation, and true lichenization presents a challenge for accurately defining these

relationships. This ambiguity limits our understanding of their ecological significance and hinders the exploration of their potential applications in emerging biotechnologies such as bioremediation [81] and biofuel [21,33]. Currently, most of the literature which concerns relationships between algae and fungi concentrate on lichens, while other mutualistic associations are rarely discussed. In the absence of a clear standard for classifying algal-fungal interactions, the term "lichen" has become increasingly ambiguous. More concerning, the overuse of the label has led to a proliferation of reductive language – such as "lichen-like" – which risks oversimplifying or overlooking the complexity of these associations [82,83]. As a result, important insights into the biochemical and ecological dynamics that underpin these symbioses may be obscured, contributing to persistent knowledge gaps in our understanding of their natural roles and potential applications.

Such flexibility becomes apparent when considering algal symbiosis outside of the fungal context. For example, the dinoflagellate *Symbiodinium* is commonly associated with corals across vast geological ranges, including the Great Barrier Reef and the Caribbean, with diverse host specificities [84,85]. Through photosynthesis, the alga promotes coral growth and calcification, while the corals themselves provide the photobiont with refuge from the nutrient-poor open ocean [86]. Unfortunately, rising ocean temperatures from climate change has placed immense heat stress on corals resulting in the expulsion or digestion of its photosynthetic partner, and bleaching [87,88]. Disrupted nutrient cycling which occurred during the onset of heat stress was later identified as the mechanism behind functional breakdown of this system and loss of the symbiotic relationship [88]. Examples such as this demonstrate that "lichen-like" interaction with algae, though structurally distinct, are equally important to recognize as traditional lichens.

The ambiguity of the term "lichen" complicates these discussions. Some researchers argue that any association between fungi and a photobiont should be classified as a lichen, while others take a more cautious approach – emphasizing technical definitions, functional distinctions, and phylogenetic evidence to more precisely delineate these relationships [80,87–89]. Beyond its original context, the term is now being applied to interactions that do not exclusively involve algae and fungi. Algae found in association with animals such as *Hydra* spp. and *Spongilla* spp. have been described as "animal lichens," while symbiotic relationships between bacteria and viruses have even been termed "microlichens" [82,83,89].

A clearer picture of this complexity emerges from microbial co-culture studies. Hom and Murray [90] documented obligate mutualism between *Saccharomyces cerevisiae* and *Chlamydomonas reinhardtii*, driven by bidirectional nutrient exchange. The organisms formed a close wall-to-wall interface without hyphal penetration or complex morphological structures associated with lichenization. In this relationship, *S. cerevisiae* supplied CO_2 via glucose metabolism to fuel algal photosynthesis, while *C. reinhardtii* reduced nitrite to ammonia for fungal use. Interestingly, co-culturing *C. reinhardtii* with *Aspergillus nidulans* – a fungus that also requires nitrite – failed to yield obligate mutualism, suggesting that functional complementarity, not just metabolic overlap, is critical to establishing interdependence [90].

In a related study, Du *et al*. [91] explored carbon and nitrogen exchange between *Nannochloropsis oceanica* and *Mortierella elongata*. They found that physical contact was

essential for efficient carbon transfer from alga to fungus, although the alga could still acquire carbon from the fungus regardless of its viability. When the organisms were separated by a membrane, carbon transfer to the fungus was significantly reduced, while algal uptake remained largely unaffected. Notably, nitrogen transfer from fungus to alga was more than double the amount transferred in reverse and did not require direct contact [91].

Beyond nutrient exchange, fungal partners provide algae with both physical and biochemical protection in symbiotic systems [10,91,92]. Krespach *et al*. [92] investigated the interaction between *Chlamydomonas reinhardtii* and *Aspergillus nidulans* under exposure to the algicidal bacterium *Streptomyces iranensis*. In co-culture, *A. nidulans* was observed to attract *C. reinhardtii* and envelop it in developing mycelium, effectively embedding the alga within its fungal structure. This physical shielding protected the algal cells from azalomycin F, a secreted algicide produced by *S. iranensis* in response to *C. reinhardtii*. The authors found that *A. nidulans* produces polar lipids that bind and neutralize azalomycin F, thereby preventing algal bleaching. Algal cells encased within the fungal matrix exhibited significantly higher tolerance and survival rates compared to unprotected cells grown outside the mycelium [92].

Similarly, Kranner *et al*. [93] investigated the model lichen *Cladonia vulcani*, composed of the mycobiont *Cladonia* sp. and the photobiont *Trebouxia excentrica*. The study explored how the intact lichen responds to desiccation stress by maintaining a dynamic antioxidant system centered on glutathione (GSH). When cultured separately, both partners suffered oxidative damage from reactive oxygen species (ROS) during desiccation.

The alga showed some desiccation tolerance, though its photoprotection was reduced, while the fungus displayed a diminished capacity to maintain glutathione homeostasis. Upon rehydration, neither isolated partner fully restored antioxidant function. In contrast, the intact lichen showed robust oxidative stress management, rapidly converting oxidized glutathione (GSSG) back to its reduced form and resuming metabolic activity. This demonstrates that biochemical cooperation in the symbiotic state enhances desiccation tolerance through shared antioxidant strategies [93].

Some have proposed the fungal–algal relationship as helotism, a form of symbiosis in which the fungus parasitizes the alga, exploiting its photosynthetically derived nutrients for metabolic gain [73,94,95]. In this framework, the fungus benefits disproportionately: carbon flow from the photobiont often exceeds the mineral supplementation returned by the mycobiont, positioning the fungus as the dominant partner. However, the interaction remains stable because the photobiont receives shelter and protection, which are critical to sustaining the symbiosis [72,96]. Indeed, increased thallus growth – where the photobiont resides – is positively correlated with photosynthetic activity, further highlighting the importance of carbon fixation to the overall system [12,97,98]. This association reflects a self-serving survival strategy for both partners, rather than a purely cooperative interaction [11,96]. While the degree of mutual dependency remains under debate, aforementioned studies have demonstrated enhanced growth, metabolic exchange, and stress tolerance in algal–fungal co-cultures compared to their axenic counterparts [93,99–101].

1.4 INTERKINGDOM COMMUNICATION

Diverse microbial communities engage in complex interactions that are often dynamic and non-harmonious. Each organism tends to act in its own self-interest, and even slight environmental changes can alter the nature of these interactions [22,102,103], microbial coordination frequently results in mutual or community-level benefits [20,22,57]. Two major forms of chemical communication that mediate such interactions are phytohormone signaling and quorum sensing (QS), which allow microbes to perceive and respond to their environment [104–107]. QS, a well-studied bacterial communication system, enables cells to detect population density by sensing autoinducers, triggering collective behavioral changes [105,108,109]. Phytohormones, on the other hand, are low-molecular-weight metabolites which modulate growth, metabolism, and stress responses in neighboring organisms [110]. Originally discovered in plants, they have since been detected in algae, bacteria, and fungi [106,111,112].

Microbial communication in algal systems often relies on the production of secondary metabolites – organic compounds not essential for primary growth or reproduction but instead providing competitive or ecological advantages [113,114]. Among these are QS molecules produced by bacteria and analogous compounds secreted by algae, such as pheromones, homoserine derivatives, fucoserratene, and ectocarpene. These molecules have been implicated in regulating reproductive behavior and enhancing biomass accumulation [115,116]. Such compounds often exert allelopathic effects or inhibit key biological processes in competing species, thereby conferring a selective advantage [114,117].

Algae also communicate stress states through the release of signaling molecules that can stimulate antioxidant responses [113,118,119]. For example, Brisson *et al*. [118] identified several extracellular metabolites – including lunichrome, monolaurin, and aleuritic acid – that impact algal growth and physiology. In a different study, Ramachandran *et al*. [119] isolated five endophytic actinomycetes (EA) from *Caulerpa racemosa* that produced novel secondary metabolites with antagonistic effects against drug-resistant bacteria. These EA-derived metabolites – likely flavonoid and alkaloid in nature – were active against *Escherichia coli*, *Pseudomonas aeruginosa*, and *Enterobacter* sp., demonstrating the dual ecological and biotechnological relevance of secondary metabolite production by algal-associated microbes [119].

In addition to their antimicrobial or allelopathic roles, secondary metabolites may also enable interkingdom communication. Kessler *et al*. [120] demonstrated that *Ulva mutabilis* releases dimethylsulfoniopropionate (DMSP), a secondary metabolite that attracts beneficial bacteria such as *Roseovarius* sp. and *Maribacter* sp. These bacteria, in turn, secrete morphogenic compounds that enhance algal growth. This reciprocal exchange of nutrients and signals illustrates a sophisticated form of metabolic coordination, dependent on diffusion at ecologically relevant concentrations [120].

Unlike secondary metabolites, primary metabolites are involved in fundamental processes such as energy production and cellular development. These include amino acids, nucleotides, vitamins, and organic acids [121,122]. Phytohormones classified as auxins and cytokinin (CK), though derived from primary metabolites, occupy a grey area between primary and secondary metabolites due to their broad roles in growth and development

[123,124]. Auxins, particularly indole-3-acetic acid (IAA), promote cell elongation and division, stimulate root formation in plants, and play vital roles in plant-microbe symbioses [125–127]. IAA-producing rhizobacteria enhance plant stress tolerance and root development, facilitating nutrient acquisition and nodulation [128,129]. CKs support chloroplast development, vascular differentiation, and cell proliferation, while also improving resistance to abiotic stressors such as heavy metals and salinity [110,130,131]. Other phytohormones, such as abscisic acid (ABA), jasmonic acid (JA), and salicylic acid (SA) are often regarded as secondary metabolites due to their specialized functions in stress mitigation [123,124].

Although less is known about phytohormone biosynthesis in algae, species such as *Euglena gracilis*, *Chlorella* spp., and *Scenedesmus* spp. are known to produce CKs, while others including *Dunaliella* spp., *Stigeoclonium* spp., and *Chlamydomonas* spp. have been shown to synthesize ABA under stress conditions [132–134]. In parallel, fungi produce a suite of phytohormones – CKs, IAA, ABA, and JA – some of which support their own development, while others are linked to parasitic behavior or encourage mutualistic growth [107,135–137].

Interactions between algae and bacteria, particularly *Chlorella* and rhizobacteria, have demonstrated that co-cultures often yield greater algal biomass than axenic cultures [19,22,26]. Bacteria can stimulate algal growth through phytohormone production, while algae in turn produce compounds that promote bacterial growth [138]. Peng *et al*. [139] demonstrated that *Azospirillum brasilense*, a plant growth-promoting bacterium (PGPB), increased algal growth via IAA production ranging from 3.1 mg/L to 25 mg/L. However,

excessive IAA concentrations were inhibitory, underlining the importance of dosage [139]. Comparable results were obtained when *Scenedesmus* sp. was co-cultured with gibberellin-producing *Pseudomonas* sp. [138]. The bacterial secretion of gibberellins led to increased algal cell density, chlorophyll content, and photosynthetic efficiency. This effect was confirmed by axenic cultures of *Scenedesmus* sp., where exogenous gibberellin addition at a concentration of 0.1 mg/L produced the same outcomes [138].

Similar symbioses have been observed between algae and fungi. Although fungi are known to produce phytohormones, relatively little is understood about the specific role these molecules play in algal–fungal interactions [80,103,140]. Nevertheless, studies examining the endogenous phytohormone profiles of algae and fungi, correlated with comparable exogenous applications, provide a useful foundation for generating hypotheses about their ecological and physiological significance [140–143].

When cultured together, algae and fungi produce phytohormones that influence each other's physiology. Work by Pichler *et al*. [144] investigated phytohormone production by three isolated lichen mycobionts and assessed the effects of IAA on their compatible photobionts. The mycobionts released several hormones, with IAA being most abundant, alongside SA and JA. Exogenous IAA, at physiologically relevant concentrations, increased photobiont water content but did not significantly affect photosynthetic efficiency, biomass, pigment levels, or α-tocopherol content [144]. Although evidence for phytohormone signalling between algae and fungi outside of lichen systems is scarce and not well understood, recent findings by Liu *et al*. [145] indicate such signalling does occur. In non-contact co-cultures, *Clonostachys rosea* enhanced the biomass 6.5-fold and more

than doubled photosynthetic performance of *Chlorella* sp. Metabolomic and transcriptomic analyses showed increased tryptophan and IAA production by both partners, identifying IAA as a likely diffusible signal. This interaction activated algal pathways related to energy production, photosynthesis, and overall metabolism, providing new insights into algal-fungal communication [145].

Taken together, this body of evidence suggests that phytohormones are key regulators of microbial interactions in algal systems. Whether through nutrient exchange, chemical signaling, or stress mitigation, these compounds mediate complex symbioses that can be harnessed for ecological and bioremediation applications.

1.5 HEAVY METAL BIOREMEDIATION WITH ALGAE

Rapid urbanization, drastic increases in population, industrialization, and human activity have all been factors that have contributed to the deteriorating water quality around the world [146,147]. Conventional remediation approaches are costly and inefficient [148–150], driving interest in microbial biotechnology as a more sustainable alternative [151–155].

Algae are often used as bioindicators of environmental pollution due to their adaptability and inherent tolerance to harsh conditions [156]. They detoxify through biosorption and bioaccumulation of heavy metals, facilitated by abundant hydroxyl and carboxyl functional groups which bind metal ions, chelation by metallothioneins and phytochelatins, and vacuolar sequestration [157–160]. Tolerance mechanisms vary by species: *Euglena* and *Scenedesmus* produce sulfur-rich thiols, while *Chlorella* relies more

on carboxyl groups and amino acids [161–163]. Genetic engineering can enhance capacity, as shown by cadmium-tolerance *Chlamydomonas reinhardtii* expressing a plant transporter [164]. Increasingly, however, progress comes from co-culturing algae with bacteria or fungi.

1.5.1 ALGAL-BACTERIAL BIOREMEDIATION

Bacteria contribute to bioremediation by restricting metal entry, exporting ions, or transforming them enzymatically [165]. A synthetic co-culture of *Chlorella vulgaris* with *Enterobacter* sp. MN17 removed substantially more pollutants from textile wastewater than the alga alone [166]. Importantly, native consortia also show promise: cultures isolated from wastewater or metal polluted lakes removed both nutrients and metals simultaneously [81,167]. These results indicate that leveraging native algal–bacterial consortia could be a promising, underexplored strategy for simultaneous nutrient and heavy metal remediation in real-world settings.

1.5.2 ALGAL-FUNGAL BIOREMEDIATION

Fungi detoxify metals through biosorption, precipitation, and intracellular sequestration [168,169]. Co-cultures with algae can reduce toxicity and improve stability. In synthetic consortia, *Chlorella vulgaris* and *Aspergillus niger* formed pellets that enhanced cadmium biosorption while protecting algal cells [23]. Yet, the heavy metal tolerance of natural algal-fungal consortia remains almost completely unexplored, despite evidence that such organisms inhabit polluted acidic environments [25]. Addressing this gap – by isolating and characterizing natural algal–fungal partnerships from metal polluted environments or constructing consortia from pre-adapted strains – could reveal synergistic

mechanisms of tolerance and detoxification, paving the way for more robust and sustainable bioremediation strategies.

1.5.3 ALGAL-FUNGAL-BACTERIAL BIOREMEDIATION

Although most engineered bioremediation systems have focused on single algal–bacterial or algal–fungal partnerships, naturally occurring fungal-algal-bacterial consortia – often in the form of mixed biofilms – have shown considerable promise for heavy metal remediation. One of the best-characterized examples comes from acid mine drainage (AMD) sites, where Orandi *et al*. [170] isolated a metal-tolerant biofilm from the Sar Cheshmeh copper mine in Iran. The filamentous green algae *Ulothrix gigas*, fungi *Geotrichum* sp. and *Aspergillus* sp., and bacteria *Pseudomonas* sp. and *Thiobacillus* sp., was immobilized in a photo-rotating biological contactor (PRBC). Operated under continuous flow for 10 weeks, the biofilm consistently removed 20–50% of multiple metals, with removal efficiencies in the order Cu > Ni > Mn > Zn > Sb > Se > Co > Al and retained activity under the extreme acidity typical of AMD [170].

Similar mixed-kingdom systems occur in freshwater periphytic biofilms, which are defined as complex matrices of algae, bacteria, fungi, and protozoa adhered to submerged surfaces. In one study, a periphyton community achieved cadmium removal of up to 89.86% under high-light conditions, while simultaneously removing large fractions of dissolved phosphorus [171]. Zhong *et al*. [172] demonstrated that lab-grown periphyton – dominated by filamentous algae within a microbial matrix – could remove over 98% of copper at initial concentrations of 0.5–2 mg/L in under five days. Comparable performance

was reported in a periphyton tubular bioreactor, which removed 98.2% of Cu from contaminated water [173].

More recently, Zhang *et al*. [174] developed a novel tri-kingdom system by using algal-mycelial pellets as "starter nuclei" for forming self-sustaining algal–bacterial granular sludge. The pellets, comprising microalgae embedded in filamentous fungal matrices, served as structural scaffolds that facilitated rapid bacterial colonization, accelerating granulation from over 60 days in conventional systems to less than 20 days. The resulting granules maintained stable phototrophic–mycelial–bacterial interactions, promoted efficient nutrient removal, and provided high surface area for potential metal sorption and sequestration. Although this work targeted nutrient-rich wastewater rather than metal-contaminated streams, the approach demonstrates how fungal scaffolds can be engineered into algal–bacterial systems to yield highly stable, harvestable aggregates that could be adapted for multi-mechanistic heavy metal remediation [174].

Beyond aquatic systems, biological soil crusts (BSCs) in AMD settings have been shown to integrate algae, fungi, and bacteria in phototrophic surface mats capable of withstanding pH values around 3.3 and accumulating multiple metals and metalloids [175]. Across these examples, the combination of algal photosynthetic activity, fungal hyphal sorption capacity, and bacterial metabolic versatility enables multi-mechanistic detoxification – through biosorption, bioaccumulation, biomineralization, and precipitation – while maintaining tolerance under extreme environmental stress [175]. These findings highlight that tri-kingdom consortia can provide both broad-spectrum and robust removal

of heavy metals, and that their integration into engineered systems represents a promising, yet still underexplored, avenue for scalable bioremediation.

1.6 THE GENUS *Euglena*

Euglena is a genus of unicellular, flagellated eukaryotes in the phylum Euglenozoa, class Euglenophyceae [176]. Although phylogenetically distinct from true plants, *Euglena* is often regarded as microalgae because many species are photosynthetic and contribute to primary production in aquatic environments [177,178]. In the traditional five-kingdom classification, photosynthetic *Euglena* are placed among the protists, making them photosynthetic protists rather than members of the plant kingdom [179]. Taxonomically, "algae" is a functional rather than a strictly evolutionary term, referring to photosynthetic organisms that are not true plants, fungi, or bacteria [180]. Under this ecological definition, *Euglena* qualifies as an alga – Multiple studies have demonstrated the genus to have tolerance of wide ranges of salinity, pH, and inorganic and organic pollutants, and therefore makes it relevant for wastewater treatment and bioremediation [28,176,180,181]. Phylogenetically, however, *Euglena* belongs to the eukaryotic supergroup Excavata, not to the green plant lineage (Plantae), even though its chloroplasts originated from secondary endosymbiosis of a green alga [182]. Thus, *Euglena* is an alga by ecological function, but a protist by evolutionary classification.

Species of *Euglena* are mixotrophic, switching between autotrophy and heterotrophy depending on environmental conditions [52,177]. Photosynthesis occurs via chloroplasts containing chlorophylls *a* and *b* [176], but in darkness they can absorb dissolved organics or phagocytose food particles [50–52,183]. Cells are elongated and

encased in a pellicle – a flexible layer of protein strips beneath the plasma membrane – that permits shape changes [184].

One of the most extensively studied species is *Euglena gracilis*, a freshwater model organism in photosynthesis, cell biology, and environmental biotechnology [185]. It possess paramylon, a β-1,3-glucan granule storage polysaccharide that functions as an energy reserve and contributes to stress tolerance [186,187]. Its metabolic flexibility under fluctuating light and nutrients makes it highly adaptable [185].

E. gracilis shows notable resistance to salinity and heavy metals, supporting its potential in polluted water remediation. It removes metals via surface biosorption and intracellular bioaccumulation. Transcriptomic analyses have revealed upregulation of antioxidant defenses and metal transporter genes in response to mercury [188]. Pretreatment with sulfur or nitrogen further increases cadmium tolerance by boosting glutathione synthesis, stress defences, and expression of metal-binding proteins [162]. Coupled with high biomass productivity and ease of cultivation [189], these traits position *E. gracilis* as an attractive organism for biotechnology applications, especially bioremediation.

In addition to nutrient pretreatments, *E. gracilis* relies on phytohormones to survive and adapt under stress. It synthesizes a diverse suite of phytohormones, including CKs, abscisic acid (ABA), auxins, jasmonates, and salicylic acid (SA) [132] which provide an intrinsic network for growth, metabolism, and defense.

Experimental studies have shown that manipulating these pathways enhance tolerance to heavy metals. Supplementations with ABA or the CK *trans*-Zeatin (*t*Z) improved cell survival and metal removal under cadmium and lead stress, driven by hormone-induced increased in thiol-rich compounds, antioxidant metabolites, and upregulation of ROS-scavenging enzymes [190]. Phytohormone treatment also stabilized pigments, maintained photosynthesis efficiency, improved osmotic balance, and influenced broader pathways such as carbohydrate metabolism and nitrogen assimilation, collectively supporting homeostasis under adverse conditions [52].

Compared to the extensively researched model species *E. gracilis*, the related organism *Euglena mutabilis* is far less studied, yet it occupies a remarkable ecological niche as a photosynthetic, mixotrophic euglenoid capable of thriving in extreme environments. It is frequently found in extreme acidic environments such as AMD streams, where it thrives at pH values as low as 1.8–3.0 and in the presence of elevated concentrations of dissolved heavy metals, including iron, copper, zinc, and cadmium [28,181,191]. Its survival in such harsh conditions is attributed to a suite of physiological and structural adaptations, including a flexible pellicle, highly efficient antioxidant systems, and the ability to form dense benthic mats or biofilms. These mats not only protect cells from direct metal toxicity through extracellular binding and precipitation but also trap and immobilize suspended particulates, enhancing contaminant removal from the water column [191].

Unlike *E. gracilis*, which typically requires acclimation or nutrient pretreatment to achieve high heavy metal tolerance, *E. mutabilis* is naturally pre-adapted to low pH and high-metal environments, enabling immediate survival and function in conditions lethal to

many microalgae [192–194]. *In situ* observations and laboratory experiments have demonstrated that *E. mutabilis* can accumulate and sequester metals through both biosorption to cell surfaces and bioaccumulation into intracellular compartments, often in association with extracellular polymeric substances (EPS) produced by the organism or its microbial partners [195–197]. Comparative tolerance experiments show that *E. mutabilis* is markedly more resistant to most heavy metals than *E. gracilis*, making it the stronger candidate for remediation of AMD and other metal polluted waters. While both species grow well at low pH, *E. mutabilis* withstands up to 17.5-fold higher iron, 10.8-fold higher nickel, and substantially greater cadmium, aluminum, and zinc concentrations than *E. gracilis* [194]. This exceptional metal tolerance, particularly to iron, the dominant metal in AMD, rather than acidity alone, explains *E. mutabilis*' dominance in such environments and underscores its potential in bioremediation systems targeting extreme metal loads.

Although no studies have directly measured phytohormone production in *E. mutabilis*, a metatranscriptomic investigation of natural *E. mutabilis* biofilms from the acidic Río Tinto system revealed large-scale gene expression changes tied to UV stress, photosystem repair, and oxidative stress mitigation highlighting the functional breadth of its transcriptome [198]. While that study did not target hormone pathways specifically, the presence of such regulated metabolic machinery suggests that *E. mutabilis* is transcriptionally responsive to environmental stressors in ways that are analogous to hormonal regulation. Given that its close relative, *E. gracilis*, has been confirmed to produce a suite of phytohormones, it is plausible that *E. mutabilis* possesses similar biosynthetic capabilities. This inference aligns with the diverse stress tolerance observed in

E. mutabilis, though verifying it will require direct phytohormone profiling and gene-level validation.

It is also possible that the stress tolerance of *E. mutabilis* is influenced by interkingdom signaling from associated microorganisms. *E. mutabilis* is commonly associated with other microorganisms, which are thought to play a role in enhancing its extremophilic traits. Nakatsu and Hutchinson (1988) investigated *E. mutabilis* isolates from extremely acidic tundra ponds in the Smoking Hills, Northwest Territories, along with a co-occurring yeast. They assessed tolerance by measuring growth under both low pH and elevated metal concentrations. Remarkably, both *E. mutabilis* and the yeast could tolerate conditions 10 to 100 times more extreme than previously reported for algae. Importantly, the mutualistic association between the two organisms greatly enhanced their combined tolerance suggesting a generalized mutual benefit [28]. Similarly, Brake *et al*. [199] documented *E. mutabilis* interwoven with diatoms and bacteria within stromatolite structures, where these organisms collectively trap and bind ferric iron precipitates. In this assemblage, diatoms and *E. mutabilis* contribute photosynthetically derived organic matter that supports the community, while microbial interactions help stabilize the biofilm matrix under extreme acidity and high metal concentrations. Such natural associations suggest that *E. mutabilis*' stress tolerance and ecological success in AMD systems may be enhanced through cooperative interactions with other phototrophs and heterotrophs [199].

Understanding how *E. mutabilis* survives in highly acidic, metal-rich environments has direct relevance for developing biological remediation systems. AMD presents extreme challenges for most microalgae, yet *E. mutabilis* naturally tolerates, and often thrives in,

conditions with metal concentrations an order of magnitude higher than those tolerated by *E. gracilis* and other microalgae. Its frequent occurrence in multi-kingdom consortia with bacteria, fungi, and diatoms suggests that both intrinsic physiology and community-mediated interactions contribute to its tolerance. Clarifying the physiological, biochemical, and potential phytohormone-driven mechanisms behind this tolerance could inform the design of robust, biologically based systems for remediating heavy metal–polluted waters.

1.7 CORE RESEARCH OBJECTIVES

The primary objective of this research was to investigate the mechanisms underlying heavy metal tolerance in a natural *E. mutabilis* culture isolated from a gold mine in Timmins, Ontario. This culture contained unidentified bacteria and fungi that could not be separated from *E. mutabilis* despite repeated attempts. Preliminary experiments aimed at enhancing cadmium tolerance revealed that the unmodified culture was more tolerant to cadmium than *E. gracilis* [162]. These findings prompted further investigation into the interactions among the organisms in the culture in order to understand community dynamics.

The literature reviewed in this introduction demonstrates that *E. mutabilis* is an extremophilic microalga with exceptional tolerance to acidic, metal-rich environments, often surpassing that of the model species *E. gracilis*. This tolerance is likely driven by a combination of intrinsic physiological traits – such as efficient antioxidant systems, metal sequestration mechanisms, and structural adaptations – and its frequent occurrence in multi-kingdom microbial consortia, where associated bacteria and fungi may contribute to stress mitigation. Although *E. gracilis* is known to produce phytohormones that influence

stress responses, the role of such signaling in *E. mutabilis*, particularly within mixed microbial communities, remains unexplored. Together, these observations led to the central hypothesis that the heavy metal tolerance of natural *E. mutabilis* cultures arises not only from intrinsic cellular adaptations, but also from synergistic interactions with associated microbial partners.

To address this hypothesis, the research was structured around three main objectives. The first was to characterize the composition of the natural *E. mutabilis* culture and identify associated microorganisms that may contribute to its stress tolerance (Chapter 2). PacBio full-length amplicon sequencing and targeted Sanger sequencing revealed the presence of the fungus *Talaromyces* sp. and the bacterium *Acidiphilium acidophilum*. As these partners could not be separated from *E. mutabilis*, antimycotic and antibiotic agents were applied to suppress their growth and evaluate their role in cadmium tolerance. The resulting reduction in tolerance confirmed that these associated microbes contribute to the heavy metal resistance of *E. mutabilis*.

To investigate these interactions, the second objective examined how altering resource availability influenced the consortium's performance and composition (Chapter 3). Glucose supplementation experiments were conducted under both control and cadmium stress conditions to determine whether providing an additional carbon source would modify growth, photosynthetic performance, and community dynamics. The results showed that glucose enhanced *E. mutabilis* growth, chlorophyll content, and flocculation, particularly in the presence of cadmium. Both *Talaromyces* sp. and *Acidiphilium acidophilum* also exhibited improved growth under glucose enrichment. Phytohormone profiling revealed

dynamic changes in CKs, gibberellins, JA, and SA in response to glucose and cadmium, pointing toward possible signaling processes that coordinate stress responses within the consortium. Together, these findings indicate that cooperative interactions, resource sharing, and hormonal signaling may all contribute to the enhanced metal tolerance of the *E. mutabilis* culture.

The third objective focused on identifying transcriptional changes in *E. mutabilis* under cadmium stress, with an emphasis on phytohormone metabolism and metal detoxification strategies (Chapter 4). A combined transcriptomic and hormonomic approach revealed unique genes linked to phytohormone biosynthesis, with significant shifts in auxin and CK pathways. In parallel, cadmium exposure induced upregulation of genes associated with metal detoxification consistent with enhanced chelation and intracellular compartmentalization of metal ions. Transcriptomic data also suggested that the *Talaromyces* sp. and *A. acidophilum* may contribute to heavy metal tolerance through extracellular metal binding, potentially supporting *E. mutabilis* metabolism and defense responses under stress. Together, these results provide molecular evidence that cadmium disrupts hormone metabolism while simultaneously activating detoxification pathways, with the microbial partners likely playing complementary roles in enhancing the consortium's overall tolerance to heavy metals.

1.8 REFERENCES

1. Allen JL, Lendemer JC. A call to reconceptualize lichen symbioses. Trends Ecol Evol. 2022;37(7):582–9. https://doi.org/10.1016/J.TRE*E*.2022.03.004.
2. Antunes PM, Goss MJ. Communication in the tripartite symbiosis formed by arbuscular mycorrhizal fungi, rhizobia and legume plants: A review. Roots and Soil Management: Interactions between Roots and the Soil. 2015. p. 199–222.
3. Lin Z, Wang L, Chen M, Zheng X, Chen J. Proteome and microbiota analyses characterizing dynamic coral-algae-microbe tripartite interactions under simulated rapid ocean acidification. Sci Total Environ. 2022;810:152266. https://doi.org/10.1016/J.SCITOTENV.2021.152266.
4. Pudlo NA, Urs K, Kumar SS, German JB, Mills DA, Martens EC. Symbiotic human gut bacteria with variable metabolic priorities for host mucosal glycans. mBio. 2015;6(6). https://doi.org/10.1128/mBio.01282-15.
5. Holland JN, Bronstein JL. Mutualism. Encycl Ecol Five-Vol Set. 2008:2485–91. https://doi.org/10.1016/B978-008045405-4.00673-X.
6. Grube M, Cardinale M, de Castro JV, Müller H, Berg G. Species-specific structural and functional diversity of bacterial communities in lichen symbioses. ISME J. 2009;3(9):1105–15. https://doi.org/10.1038/ismej.2009.63.
7. Nash TH, editor. Lichen Biology. 2nd ed. Cambridge University Press; 2008.
8. Spribille T, Tuovinen V, Resl P, Vanderpool D, Wolinski H, Aime MC, *et al*. Basidiomycete yeasts in the cortex of ascomycete macrolichens. Science. 2016;353(6298):488–92. https://doi.org/10.1126/science.aaf8287.
9. Yuan X, Xiao S, Taylor TN. Lichen-like symbiosis 600 million years ago. Science. 2005;308(5724):1017–20. https://doi.org/10.1126/science.1111347.
10. Grube M, Wedin M. Lichenized fungi and the evolution of symbiotic organization. Microbiol Spectr. 2016;4(6). https://doi.org/10.1128/microbiolspec.FUNK-0011-2016.
11. Grube M, Cernava T, Soh J, Fuchs S, Aschenbrenner I, Lassek C, *et al*. Exploring functional contexts of symbiotic sustain within lichen-associated bacteria by comparative omics. ISME J. 2015;9(2):412–24. https://doi.org/10.1038/ismej.2014.138.
12. ten Veldhuis MC, Ananyev G, Dismukes GC. Symbiosis extended: Exchange of photosynthetic O_2 and fungal-respired CO_2 mutually power metabolism of lichen symbionts. Photosynth Res. 2020;143(3):287–99. https://doi.org/10.1007/s11120-019-00702-0.
13. Cooper MB, Smith AG. Exploring mutualistic interactions between microalgae and bacteria in the omics age. Curr Opin Plant Biol. 2015;26:147–53. https://doi.org/10.1016/j.pbi.2015.07.003.
14. Gimmler H. Mutualistic relationships between algae and fungi (excluding lichens). In: Esser K, Llittge U, Kadereit JW, editors. Progress in Botany: Genetics Physiology Systematics Ecology 62. Springer-Verlag Berlin Heidelberg; 2001. p. 194–214.
15. Yu L, Zhang H, Zhang W, Liu K, Liu M, Shao X. Cooperation between arbuscular mycorrhizal fungi and plant growth-promoting bacteria and their effects on plant growth and soil quality. PeerJ. 2022;10:e13080. https://doi.org/10.7717/peerj.13080.

16. Honegger R. Lichen-Forming Fungi and Their Photobionts. In: Deising HB, editor. The Mycota. Berlin, Heidelberg: Springer Berlin Heidelberg; 2009. p. 307–33.
17. Nai C, Meyer V. From axenic to mixed cultures: Technological advances accelerating a paradigm shift in microbiology. Trends Microbiol. 2018;26(6):538–54. https://doi.org/10.1016/j.tim.2017.11.004.
18. Levins R, Lewontin R. Dialectics and reductionism in ecology. Synthese. 1980;43(1):47–78.
19. Li SN, Zhang C, Li F, Ren NQ, Ho SH. Recent advances of algae-bacteria consortia in aquatic remediation. Crit Rev Environ Sci Technol. 2022. https://doi.org/10.1080/10643389.2022.2052704.
20. Wang J, Tian Q, Cui L, Cheng J, Zhou H, Zhang Y, *et al*. Synergism and mutualistic interactions between microalgae and fungi in fungi-microalgae symbiotic system. Bioresour Technol. 2022;361:127728. https://doi.org/10.1016/j.biortech.2022.127728.
21. Muradov N, Taha M, Miranda AF, Wrede D, Kadali K, Gujar A, *et al*. Fungal-assisted algal flocculation: Application in wastewater treatment and biofuel production. Biotechnol Biofuels. 2015;8(24). https://doi.org/10.1186/s13068-015-0210-6.
22. Ramanan R, Kim BH, Cho DH, Oh HM, Kim HS. Algae-bacteria interactions: Evolution, ecology and emerging applications. Biotechnol Adv. 2016;34(1):14–29. https://doi.org/10.1016/j.biotechadv.2015.12.003.
23. Wang J, Chen R, Fan L, Cui L, Zhang Y, Cheng J, *et al*. Construction of fungi-microalgae symbiotic system and adsorption study of heavy metal ions. Sep Purif Technol. 2021;268(April):118689. https://doi.org/10.1016/j.seppur.2021.118689.
24. Song H, Ding M-Z, Jia X-Q, Ma Q, Yuan Y-J. Synthetic microbial consortia: From systematic analysis to construction and applications. Chem Soc Rev. 2014;43(20):6954–81. https://doi.org/10.1039/c4cs00114a.
25. Das BK, Roy A, Koschorreck M, Mandal SM, Wendt-Potthoff K, Bhattacharya J. Occurrence and role of algae and fungi in acid mine drainage environment with special reference to metals and sulfate immobilization. Water Res. 2009;43(4):883–94. https://doi.org/10.1016/j.watres.2008.11.046.
26. Kim BH, Ramanan R, Cho DH, Oh HM, Kim HS. Role of *Rhizobium*, a plant growth promoting bacterium, in enhancing algal biomass through mutualistic interaction. Biomass Bioenergy. 2014;69:95–105. https://doi.org/10.1016/j.biombioe.2014.07.015.
27. Ferdous AS, Islam MR, Khan H. Transkingdom signaling systems between plant and its associated beneficial microbes in relation to plant growth and development. In: Varma A, Prasad R, Tuteja N, editors. Mycorrhiza - Nutrient Uptake, Biocontrol, Ecorestoration. Springer, Cham; 2017. p. 451–72.
28. Nakatsu C, Hutchinson TC. Extreme metal and acid tolerance of *Euglena mutabilis* and an associated yeast from Smoking Hills, Northwest Territories, and their apparent mutualism. Microb Ecol. 1988;16(2):213–31. https://doi.org/10.1007/BF02018915.
29. Watanabe K, Takihana N, Aoyagi H, Hanada S, Watanabe Y, Ohmura N, *et al*. Symbiotic association in *Chlorella* culture. FEMS Microbiol Ecol. 2005;51(2):187–96. https://doi.org/10.1016/j.femsec.2004.08.004.

30. Mujtaba G, Rizwan M, Lee K. Simultaneous removal of inorganic nutrients and organic carbon by symbiotic co-culture of *Chlorella vulgaris* and *Pseudomonas putida*. Biotechnol Bioprocess Eng. 2015;20(6):1114–22. https://doi.org/10.1007/s12257-015-0421-5.
31. Toyama T, Hanaoka T, Yamada K, Suzuki K, Tanaka Y, Morikawa M, *et al*. Enhanced production of biomass and lipids by *Euglena gracilis* via co-culturing with a microalga growth-promoting bacterium, *Emticicia* sp. EG3. Biotechnol Biofuels. 2019;12(1). https://doi.org/10.1186/s13068-019-1544-2.
32. Nambiar KR, Bokil SD. Luxury uptake of nitrogen in flocculating algal-bacterial system. Water Res. 1981;15(6):667–9. https://doi.org/10.1016/0043-1354(81)90158-5.
33. Yao S, Lyu S, An Y, Lu J, Gjermansen C, Schramm A. Microalgae–bacteria symbiosis in microalgal growth and biofuel production: A review. J Appl Microbiol. 2019;126(2):359–68. https://doi.org/10.1111/jam.14095.
34. Butterfield NJ. Early evolution of the Eukaryota. Palaeontology. 2015;58(1):5–17. https://doi.org/10.1111/pala.12139.
35. Kowallik KV, Martin WF. The origin of symbiogenesis: An annotated English translation of Mereschkowsky's 1910 paper on the theory of two plasma lineages. Biosystems. 2021;199:104281. https://doi.org/10.1016/j.biosystems.2020.104281.
36. Sagan L. On the origin of mitosing cells. J Theor Biol. 1967;14(3):225-IN6. https://doi.org/10.1016/0022-5193(67)90079-3.
37. Schimper AFW. Über die Entwicklung der Chlorophyllkörner und Farbkörper. Bot Ztg. 1883;41.
38. Archibald JM. Chapter three - the evolution of algae by secondary and tertiary endosymbiosis. In: Piganeau G, editor. Advances in Botanical Research. Academic Press; 2012. p. 87–118.
39. Khoja TM. Heterotrophic growth of blue-green algae. Durham Institution; 1973.
40. Perez-Garcia O, Escalante FME, de-Bashan LE, Bashan Y. Heterotrophic cultures of microalgae: Metabolism and potential products. Water Res. 2011;45(1):11–36. https://doi.org/10.1016/J.WATRES.2010.08.037.
41. Ruiz J, Wijffels RH, Dominguez M, Barbosa MJ. Heterotrophic vs autotrophic production of microalgae: Bringing some light into the everlasting cost controversy. Algal Res. 2022;64:102698. https://doi.org/10.1016/J.ALGAL.2022.102698.
42. Zajic JE, Chiu YS. Heterotrophic culture of algae. In: Zajic JE, editor. Properties and Products of Algae. Boston, MA: Springer; 1970. p. 1–47.
43. Zheng Y, Chi Z, Lucker B, Chen S. Two-stage heterotrophic and phototrophic culture strategy for algal biomass and lipid production. Bioresour Technol. 2012;103(1):484–8. https://doi.org/10.1016/j.biortech.2011.09.122.
44. Smith AJ, London,' And J, Stanier RY. biochemical basis of obligate autotrophy in blue-green algae and *Thiobacilli*. J Bacteriol. 1967;94(4):972–83.
45. Wood AP, Aurikko JP, Kelly DP. A challenge for 21st century molecular biology and biochemistry: What are the causes of obligate autotrophy and methanotrophy? FEMS Microbiol Rev. 2004;28(3):335–52. https://doi.org/10.1016/j.femsre.2003.12.001.
46. Young EB, Reed L, Berges JA. Growth parameters and responses of green algae across a gradient of phototrophic, mixotrophic and heterotrophic conditions. PeerJ. 2022;10:e13776. https://doi.org/10.7717/peerj.13776.

47. Mills DB. The origin of phagocytosis in Earth history. Interface Focus. 2020;10(4):20200019. https://doi.org/10.1098/rsfs.2020.0019.
48. Maruyama S, Kim *E.* A modern descendant of early green algal phagotrophs. Curr Biol. 2013;23(12):1081–4. https://doi.org/10.1016/j.cub.2013.04.063.
49. Morden CW, Sherwood AR. Continued evolutionary surprises among dinoflagellates. Proc Natl Acad Sci U S A. 2002;99(18):11558–60. https://doi.org/10.1073/pnas.192456999.
50. Willey RL, Walne PL, Kivic P, Patterson DJ. Phagotrophy and the origins of the euglenoid flagellates. Crit Rev Plant Sci. 1988;7(4):303–40. https://doi.org/10.1080/07352688809382268.
51. Ebenezer TE, Low RS, O'Neill EC, Huang I, DeSimone A, Farrow SC, *et al*. *Euglena* International Network (EIN): Driving euglenoid biotechnology for the benefit of a challenged world. Biol Open. 2022;11(11):bio059561. https://doi.org/10.1242/bio.059561.
52. Kuhne AM, Morrison EN, Sultana T, Kisiala AB, Horlock-Roberts K, Noble A, *et al*. Cultivation of heterotrophic *Euglena gracilis*: The effects of recycled media on culture growth and associations with growth regulating phytohormone profiles. J Appl Phycol. 2023;35(5):2161–75. https://doi.org/10.1007/s10811-023-03062-4.
53. Roberts EC, Wootton EC, Davidson K, Jeong HJ, Lowe CD, Montagnes DJS. Feeding in the dinoflagellate *Oxyrrhis marina*: Linking behaviour with mechanisms. J Plankton Res. 2011;33(4):603–14. https://doi.org/10.1093/plankt/fbq118.
54. Mansour JS, Anestis K. Eco-evolutionary perspectives on mixoplankton. Front Mar Sci. 2021;8:666160. https://doi.org/10.3389/fmars.2021.666160.
55. Kublanovskaya A, Chekanov K, Solovchenko A, Lobakova *E.* Cyanobacterial diversity in the algal–bacterial consortia from Subarctic regions: New insights from the rock baths at White Sea Coast. Hydrobiologia. 2019;830(1):17–31. https://doi.org/10.1007/s10750-018-3844-0.
56. Cook PLM, Veuger B, Böer S, Middelburg JJ. Effect of nutrient availability on carbon and nitrogen incorporation and flows through benthic algae and bacteria in near-shore sandy sediment. Aquat Microb Ecol. 2007;49(2):165–80. https://doi.org/10.3354/ame01142.
57. Croft MT, Lawrence AD, Raux-Deery E, Warren MJ, Smith AG. Algae acquire vitamin B_{12} through a symbiotic relationship with bacteria. Nature. 2005;438(7064):90–3. https://doi.org/10.1038/nature04056.
58. Zhao D, Cheah WY, Lai SH, Ng E-P, Khoo KS, Show PL, *et al*. Symbiosis of microalgae and bacteria consortium for heavy metal remediation in wastewater. J Environ Chem Eng. 2023;11(3):109943. https://doi.org/10.1016/j.jece.2023.109943.
59. Kazamia E, Czesnick H, Nguyen TTV, Croft MT, Sherwood E, Sasso S, *et al*. Mutualistic interactions between vitamin B_{12}-dependent algae and heterotrophic bacteria exhibit regulation. Environ Microbiol. 2012;14(6):1466–76. https://doi.org/10.1111/j.1462-2920.2012.02733.x.
60. Ravanel S, Gakière B, Job D, Douce R. The specific features of methionine biosynthesis and metabolism in plants. Proc Natl Acad Sci. 1998;95(13):7805–12. https://doi.org/10.1073/pnas.95.13.7805.

61. Helliwell KE, Scaife MA, Sasso S, Paula A, Araujo U, Purton S, *et al*. Unraveling vitamin B_{12}-responsive gene regulation in algae. Plant Physiol. 2014;165(1):388–97. https://doi.org/10.1104/pp.113.234369.
62. Helliwell KE, Wheeler GL, Leptos KC, Goldstein RE, Smith AG. insights into the evolution of vitamin B_{12} auxotrophy from sequenced algal genomes. Mol Biol Evol. 2011;28(10):2921–33. https://doi.org/10.1093/molbev/msr124.
63. Grant MAA, Kazamia E, Cicuta P, Smith AG. Direct exchange of vitamin B_{12} is demonstrated by modelling the growth dynamics of algal–bacterial cocultures. ISME J. 2014;8(7):1418–27. https://doi.org/10.1038/ismej.2014.9.
64. Brussaard C, Riegman R. Influence of bacteria on phytoplankton cell mortality with phosphorus or nitrogen as the algal-growth-limiting nutrient. Aquat Microb Ecol. 1998;14:271–80. https://doi.org/10.3354/ame014271.
65. Byappanahalli MN, Nevers MB, Przybyla-Kelly K, Ishii S, King TL, Aunins AW. Great Lakes *Cladophora* harbors phylogenetically diverse nitrogen-fixing microorganisms. Environ DNA. 2019;1(2):186–95. https://doi.org/10.1002/edn3.20.
66. Tagirdzhanova G, Saary P, Cameron ES, Garber AI, Díaz Escandón D, Goyette S, *et al*. Mircobial occurrence and symbiont detection in a global sample of lichen metagenomes. PLOS Biol; 2024:22(11). https://doi.org/10.1371/journal.pbio.3002862.
67. Seymour JR, Amin SA, Raina JB, Stocker R. Zooming in on the phycosphere: The ecological interface for phytoplankton-bacteria relationships. Nat Microbiol. 2017;2. https://doi.org/10.1038/nmicrobiol.2017.65.
68. Amin SA, Hmelo LR, Van Tol HM, Durham BP, Carlson LT, Heal KR, *et al*. Interaction and signalling between a cosmopolitan phytoplankton and associated bacteria. Nature. 2015;522(7554):98–101. https://doi.org/10.1038/nature14488.
69. Segev E, Wyche TP, Kim KH, Petersen J, Ellebrandt C, Vlamakis H, *et al*. Dynamic metabolic exchange governs a marine algal-bacterial interaction. eLife. 2016;5. https://doi.org/10.7554/eLife.17473.
70. Schwendener S, Honegger R. Simon Schwendener (1829-1919) and the dual hypothesis of lichens. The Bryologist. 2000;103(2):307–13.
71. Werth S. Biogeography and phylogeography of lichen fungi and their photobionts. In: Fontaneto D, editor. Biogeography of Microscopic Organisms: Is Everything Small Everywhere? Cambridge University Press; 2011. p. 191–208.
72. Spribille T, Resl P, Stanton DE, Tagirdzhanova G. Evolutionary biology of lichen symbioses. New Phytol. 2022;234(5):1566–82. https://doi.org/10.1111/nph.18048.
73. Aschenbrenner IA, Cardinale M, Berg G, Grube M. Microbial cargo: Do bacteria on symbiotic propagules reinforce the microbiome of lichens? Environ Microbiol. 2014;16(12):3743–52. https://doi.org/10.1111/1462-2920.12658.
74. Saini KC, Nayaka S, Bast F. Diversity of lichen photobionts: Their coevolution and bioprospecting potential. In: Satyanarayana T, Das S, Johri B, editors. Microbial Diversity in Ecosystem Sustainability and Biotechnological Applications. Singapore: Springer Singapore; 2019. p. 307–23.
75. Ahmadjian V, Jacobs JB. Relationship between fungus and alga in the lichen *Cladonia cristatella* Tuck. Nature. 1981;289(5794):169–72. https://doi.org/10.1038/289169a0.

76. Joneson S, Armaleo D, Lutzoni F. Fungal and algal gene expression in early developmental stages of lichen-symbiosis. Mycologia. 2011;103(2):291–306. https://doi.org/10.3852/10-064.
77. Grube M, Berg G, S. Andrésson Ó, Vilhelmsson O, Dyer PS, Miao VPW. Lichen genomics. The Ecological Genomics of Fungi. Hoboken, NJ: John Wiley & Sons, Inc; 2013. p. 191–212.
78. Beck A, Freidl T, Rambold G. Selectivity of photobiont choice in a defined lichen community: inferences from cultural and molecular studies. New Phytol. 1998;139(4):709–20. https://doi.org/10.1046/j.1469-8137.1998.00231.x.
79. Meeßen J, Ott S. Recognition mechanisms during the pre-contact state of lichens: I. Mycobiont-photobiont interactions of the mycobiont of *Fulgensia bracteata*. Symbiosis. 2013;59(3):121–30. https://doi.org/10.1007/s13199-013-0232-4.
80. Pichler G, Candotto Carniel F, Muggia L, Holzinger A, Tretiach M, Kranner I. Enhanced culturing techniques for the mycobiont isolated from the lichen *Xanthoria parietina*. Mycol Prog. 2021;20(6):797–808. https://doi.org/10.1007/s11557-021-01707-7.
81. Sousa JF, Amaro HM, Ribeirinho-Soares S, Esteves AF, Salgado EM, Nunes OC, *et al*. Native microalgae-bacteria consortia: A sustainable approach for effective urban wastewater bioremediation and disinfection. Microorganisms. 2024;12(7):1421. https://doi.org/10.3390/microorganisms12071421.
82. Sapp J. The symbiotic self. Evol Biol. 2016;43(4):596–603. https://doi.org/10.1007/s11692-016-9378-3.
83. Sapp J. Symbiosis: Evolution in Action. Evolution by Association: A History of Symbiosis. New York: Oxford University Press; 1994. p. 3–14.
84. Dougan KE, González-Pech RA, Stephens TG, Shah S, Chen Y, Ragan MA, *et al*. Genome-powered classification of microbial eukaryotes: Focus on coral algal symbionts. Trends Microbiol. 2022. https://doi.org/10.1016/J.TIM.2022.02.001.
85. Ulstrup KE, Van Oppen MJH. Geographic and habitat partitioning of genetically distinct zooxanthellae (*Symbiodinium*) in Acropora corals on the Great Barrier Reef. Mol Ecol. 2003;12(12):3477–84. https://doi.org/10.1046/j.1365-294X.2003.01988.x.
86. Roth MS. The engine of the reef: Photobiology of the coral-algal symbiosis. Front Microbiol. 2014;5. https://doi.org/10.3389/fmicb.2014.00422.
87. Maruyama S, Mandelare-Ruiz PE, McCauley M, Peng W, Cho BG, Wang J, *et al*. Heat stress of algal partner hinders colonization success and alters the algal cell surface glycome in a cnidarian-algal symbiosis. Microbiol Spectr. 2022;10(3). https://doi.org/10.1128/spectrum.01567-22.
88. Rädecker N, Pogoreutz C, Gegner HM, Cárdenas A, Roth F, Bougoure J, *et al*. Heat stress destabilizes symbiotic nutrient cycling in corals. Proc Natl Acad Sci. 2021;118(5). https://doi.org/10.1073/pnas.2022653118.
89. d'Herelle F. The bacteriophage and its behavior. Baltimore: Williams and Wilkins; 1926.
90. Hom EFY, Murray AW. Niche engineering demonstrates a latent capacity for fungal-algal mutualism. Science. 2014;345(6192):94–8. https://doi.org/10.1126/science.1253320.

91. Du Z-Y, Zienkiewicz K, Pol NV, Ostrom NE, Benning C, Bonito GM. Algal-fungal symbiosis leads to photosynthetic mycelium. Front Plant Sci. 2019;12. https://doi.org/10.7554/eLife.47815.001.
92. Krespach MKC, García-Altares M, Flak M, Hanno Schoeler, Scherlach K, Netzker T, *et al*. Lichen-like association of *Chlamydomonas reinhardtii* and *Aspergillus nidulans* protects algal cells from bacteria. ISME J. 2020;14(11):2794–805. https://doi.org/10.1038/s41396-020-0731-2.
93. Kranner I, Cram WJ, Zorn M, Wornik S, Yoshimura I, Stabentheiner E, *et al*. Antioxidants and photoprotection in a lichen as compared with its isolated symbiotic partners. Proc Natl Acad Sci. 2005;102(8):3141–6. https://doi.org/10.1073/pnas.0407716102.
94. Honegger R. Functional aspects of the lichen symbiosis. Annu Rev Plant Physiol Plant Mol Biol. 1991;42(1):553–78. https://doi.org/10.1146/annurev.pp.42.060191.003005.
95. Quispel A. The mutual relations between algae and fungi in lichens. Recl Trav Bot Néerl. 1946;40(1):413–541.
96. Nazem-Bokaee H, Hom EFY, Warden AC, Mathews S, Gueidan C. Towards a systems biology approach to understanding the lichen symbiosis: Opportunities and challenges of implementing network modelling. Front Microbiol. 2021;12. https://doi.org/10.3389/fmicb.2021.667864.
97. Roth R, Goodenough U. Lichen 1. Solo fungal and algal partners. Algal Res. 2021;58:102334. https://doi.org/10.1016/J.ALGAL.2021.102334.
98. Shantz AA, Lemoine NP, Burkepile DE. Nutrient loading alters the performance of key nutrient exchange mutualisms. Ecol Lett. 2016;19(1):20–8. https://doi.org/10.1111/ele.12538.
99. Boucher DH, James S, Keeler KH. The ecology of mutualism. Annu Rev Ecol Syst. 1982;13:315–47.
100. Hawksworth DL. The variety of fungal-algal symbioses, their evolutionary significance, and the nature of lichens. Bot J Linn Soc. 1988;96(1):3–20. https://doi.org/10.1111/j.1095-8339.1988.tb00623.x.
101. Văcar CL, Covaci E, Chakraborty S, Li B, Weindorf DC, Frențiu T, *et al*. Heavy metal-resistant filamentous fungi as potential mercury bioremediators. J Fungi. 2021;7(5). https://doi.org/10.3390/jof7050386.
102. Bengtson P, Sterngren AE, Rousk J. Archaeal abundance across a pH gradient in an arable soil and its relationship to bacterial and fungal growth rates. Appl Environ Microbiol. 2012;78(16):5906–11. https://doi.org/10.1128/AEM.01476-12.
103. Wang XY, Wei XL, Luo H, Kim JA, Jeon HS, Koh YJ, *et al*. Plant hormones promote growth in lichen-forming fungi. Mycobiology. 2010;38(3):176. https://doi.org/10.4489/MYCO.2010.38.3.176.
104. Kudoyarova G, Arkhipova T, Korshunova T, Bakaeva M, Loginov O, Dodd IC. Phytohormone mediation of interactions between plants and non-symbiotic growth promoting bacteria under edaphic stresses. Front Plant Sci. 2019;10. https://doi.org/10.3389/fpls.2019.01368.
105. Miller MB, Bassler BL. Quorum sensing in bacteria. Annu Rev Microbiol. 2001;55:165–99.
106. Tarakhovskaya ER, Maslov YI, Shishova MF. Phytohormones in algae. Russ J Plant Physiol. 2007;54(2):163–70. https://doi.org/10.1134/S1021443707020021.

107. Morrison EN, Knowles S, Hayward A, Greg Thorn R, Saville BJ, Emery RJN. Detection of phytohormones in temperate forest fungi predicts consistent abscisic acid production and a common pathway for cytokinin biosynthesis. Mycologia. 2015;107(2). https://doi.org/10.3852/14-157.
108. Deryabin D, Galadzhieva A, Kosyan D, Duskaev G. Plant-derived inhibitors of AHL-mediated quorum sensing in bacteria: Modes of action. Int J Mol Sci. 2019;20(22). https://doi.org/10.3390/ijms20225588.
109. Hu T, Wang S, Shan Y, Zhang Y, Zhu Y, Zheng L. complete genome of marine microalgae associated algicidal bacterium *Sulfitobacter pseudonitzschiae* H46 with quorum sensing system. Curr Microbiol. 2021;78(10):3741–50. https://doi.org/10.1007/s00284-021-02632-4.
110. Emery RJN, Kisiala A. The roles of cytokinins in plants and their response to environmental stimuli. Plants Basel. 2020;9(9):4–7.
111. Chanclud E, Morel J-B. Plant hormones: a fungal point of view. Mol Plant Pathol. 2016;17(8):1289–97. https://doi.org/10.1111/mpp.12393.
112. Wang C, Qi M, Guo J, Zhou C, Yan X, Ruan R, *et al*. The active phytohormone in microalgae: The characteristics, efficient detection, and their adversity resistance applications. Molecules. 2022;27(1). https://doi.org/10.3390/molecules27010046.
113. Gerwick L, Boudreau P, Choi H, Mascuch S, Villa FA, Balunas MJ, *et al*. Interkingdom signaling by structurally related cyanobacterial and algal secondary metabolites. Phytochem Rev. 2013;12(3):459–65. https://doi.org/10.1007/s11101-012-9237-5.
114. Zak A, Kosakowska A. Cyanobacterial and microalgal bioactive compounds-the role of secondary metabolites in allelopathic interactions. Oceanol Hydrobiol Stud. 2016;45(1):131–43. https://doi.org/10.1515/ohs-2016-0013.
115. Das S, Das S, Ghangrekar MM. Quorum-sensing mediated signals: A promising multi-functional modulators for separately enhancing algal yield and power generation in microbial fuel cell. Bioresour Technol. 2019;294:122138. https://doi.org/10.1016/J.BIORTECH.2019.122138.
116. Hombeck M, Boland W. Biosynthesis of the algal pheromone fucoserratene by the freshwater diatom *Asterionella formosa* (Bacillariophyceae). Tetrahedron. 1998;54(37):11033–42. https://doi.org/10.1016/S0040-4020(98)00660-7.
117. Dow L. How do quorum-sensing signals mediate algae–bacteria interactions? Microorganisms. 2021;9(7). https://doi.org/10.3390/microorganisms9071391.
118. Brisson V, Mayali X, Bowen B, Golini A, Thelen M, Stuart RK, *et al*. Identification of effector metabolites using exometabolite profiling of diverse microalgae. mSystems. 2021;6(6).
119. Ramachandran G, Rajivgandhi G, Maruthupandy M, Manoharan N. Extraction and partial purification of secondary metabolites from endophytic actinomycetes of marine green algae *Caulerpa racemosa* against multi drug resistant uropathogens. Biocatal Agric Biotechnol. 2019;17:750–7. https://doi.org/10.1016/J.BCAB.2019.01.016.
120. Kessler RW, Weiss A, Kuegler S, Hermes C, Wichard T. Macroalgal-bacterial interactions: Role of dimethylsulfoniopropionate in microbial gardening by *Ulva* (Chlorophyta). Mol Ecol. 2018;27(8):1808–19. https://doi.org/10.1111/mec.14472.

121. Sanchez S, Demain AL. Metabolic regulation and overproduction of primary metabolites. Microb Biotechnol. 2008;1(4):283–319. https://doi.org/10.1111/j.1751-7915.2007.00015.x.
122. Zaynab M, Fatima M, Sharif Y, Zafar MH, Ali H, Khan KA. Role of primary metabolites in plant defense against pathogens. Microb Pathog. 2019;137:103728. https://doi.org/10.1016/J.MICPATH.2019.103728.
123. Fàbregas N, Fernie AR. The reliance of phytohormone biosynthesis on primary metabolite precursors. J Plant Physiol. 2022;268:153589. https://doi.org/10.1016/j.jplph.2021.153589.
124. Gasperini D, Howe GA. Phytohormones in a universe of regulatory metabolites: lessons from jasmonate. Plant Physiol. 2024;195(1):135–54. https://doi.org/10.1093/plphys/kiae045.
125. Skalický V, Kubeš M, Napier R, Novák O. Auxins and Cytokinins—The Role of Subcellular Organization on Homeostasis. Int J Mol Sci. 2018;19(10):3115. https://doi.org/10.3390/ijms19103115.
126. Tate JJ, Gutierrez-Wing MT, Rusch KA, Benton MG. The effects of plant growth substances and mixed cultures on growth and metabolite production of green algae *Chlorella* sp.: A review. J Plant Growth Regul. 2013;32(2):417–28. https://doi.org/10.1007/s00344-012-9302-8.
127. Keswani C, Singh SP, Cueto L, García-Estrada C, Mezaache-Aichour S, Glare TR, *et al*. Auxins of microbial origin and their use in agriculture. Appl Microbiol Biotechnol. 2020;104(20):8549–65. https://doi.org/10.1007/s00253-020-10890-8.
128. Alemneh AA, Zhou Y, Ryder MH, Denton MD. Mechanisms in plant growth-promoting rhizobacteria that enhance legume–rhizobial symbioses. J Appl Microbiol. 2020;129(5):1133–56. https://doi.org/10.1111/jam.14754.
129. Yousef NMH. Capability of plant growth-promoting rhizobacteria (PGPR) for producing indole acetic acid (IAA) under extreme conditions. Eur J Biol Res. 2018;8(4):174–82.
130. Li S-M, Zheng H-X, Zhang X-S, Sui N. Cytokinins as central regulators during plant growth and stress response. Plant Cell Rep. 2021;40(2):271–82. https://doi.org/10.1007/s00299-020-02612-1.
131. Reckova S, Tuma J, Dobrev P, Vankova R. Influence of copper on hormone content and selected morphological, physiological and biochemical parameters of hydroponically grown *Zea mays* plants. Plant Growth Regul. 2019;89(2):191–201. https://doi.org/10.1007/s10725-019-00527-w.
132. Noble A, Kisiala A, Galer A, Clysdale D, Emery RJN. *Euglena gracilis* (Euglenophyceae) produces abscisic acid and cytokinins and responds to their exogenous application singly and in combination with other growth regulators. Eur J Phycol. 2014;49(2):244–54. https://doi.org/10.1080/09670262.2014.911353.
133. Hirsch R, Hartung W, Gimmler H. Abscisic acid content of algae under stress. Bot Acta. 1989;102(4):326–34. https://doi.org/10.1111/j.1438-8677.1989.tb00113.x.
134. Tietz A, Ruttkowski U, Kohler R, Kasprik W. Further investigations on the occurrence and the effects of abscisic acid in algae. Biochem Physiol Pflanz. 1989;184(3):259–66. https://doi.org/10.1016/S0015-3796(89)80011-3.
135. Fu S-F, Wei J-Y, Chen H-W, Liu Y-Y, Lu H-Y, Chou J-Y. Indole-3-acetic acid: A widespread physiological code in interactions of fungi with other organisms. Plant

Signal Behav. 2015;10(8):e1048052. https://doi.org/10.1080/15592324.2015.1048052.
136. Pichler G, Stoggl W, Carniel FC, Muggia L, Ametrano CG, Holzinger A, *et al*. Abundance and extracellular release of phytohormones in aero-terrestrial microalgae (Trebouxiophyceae, Chlorophyta) as a potential chemical signaling source. J Phycol. 2020;56(5):1295–307. https://doi.org/10.1111/jpy.13032.
137. Grich N, Huynh T, Kisiala A, Palberg D, Emery RJN. The biosynthesis and impacts of cytokinins on growth of the oyster mushroom, *Pleurotus ostreatus*. Mycologia. 2025;117(1):76–94. https://doi.org/10.1080/00275514.2024.2401320.
138. Dao G, Wang S, Wang X, Chen Z, Wu Y, Wu G, *et al*. Enhanced *Scenedesmus* sp. growth in response to gibberellin secretion by symbiotic bacteria. Sci Total Environ. 2020;740:140099. https://doi.org/10.1016/J.SCITOTENV.2020.140099.
139. Peng H, de-Bashan LE, Higgins BT. Comparison of algae growth and symbiotic mechanisms in the presence of plant growth promoting bacteria and non-plant growth promoting bacteria. Algal Res. 2021;53:102156. https://doi.org/10.1016/J.ALGAL.2020.102156.
140. Tiwari P, Bajpai M, Singh LK, Mishra S, Yadav AN. Phytohormones producing fungal communities : Metabolic engineering for abiotic stress tolerance in crops. In: Yadav A, Mishra S, Kour D, Yadav N, Kumar A, editors. Agriculturally Important Fungi for Sustainable Agriculture. Springer, Cham; 2020. p. 171–97.
141. Piotrowska-Niczyporuk A, Bajguz A, Kotowska U, Bralska M, Talarek-Karwel M. Growth, Metabolite Profile, Oxidative Status, and Phytohormone Levels in the Green alga *Acutodesmus obliquus* exposed to exogenous auxins and cytokinins. J Plant Growth Regul. 2018;37(4):1159–74. https://doi.org/10.1007/s00344-018-9816-9.
142. Piotrowska-Niczyporuk A, Bajguz A, Zambrzycka-Szelewa E, Bralska M. Exogenously applied auxins and cytokinins ameliorate lead toxicity by inducing antioxidant defence system in green alga *Acutodesmus obliquus*. Plant Physiol Biochem. 2018;132(July):535–46. https://doi.org/10.1016/j.plaphy.2018.09.038.
143. Piotrowska-Niczyporuk A, Bajguz A, Kotowska U, Zambrzycka-Szelewa E, Sienkiewicz A. Auxins and cytokinins regulate phytohormone homeostasis and thiol-mediated detoxification in the green alga *Acutodesmus obliquus* exposed to lead stress. Sci Rep. 2020;10(1):1–14. https://doi.org/10.1038/s41598-020-67085-4.
144. Pichler G, Stöggl W, Trippel D, Candotto Carniel F, Muggia L, Ametrano CG, *et al*. Phytohormone release by three isolated lichen mycobionts and the effects of indole-3-acetic acid on their compatible photobionts. Symbiosis. 2020;82(1–2):95–108. https://doi.org/10.1007/s13199-020-00721-9.
145. Liu J, Sun S, Chen K, Gao S, Chen D, Zhang Y, *et al*. Discerning promotion mechanisms of fungi *Clonostachys rosea* on growth of freshwater microalga *Chlorella* sp. by non-contact culture. Algal Res. 2025;86:103967. https://doi.org/10.1016/j.algal.2025.103967.
146. Chen Y di, Duan X, Zhou X, Wang R, Wang S, Ren N qi, *et al*. Advanced oxidation processes for water disinfection: Features, mechanisms and prospects. Chem Eng J. 2021;409:128207. https://doi.org/10.1016/J.CEJ.2020.128207.
147. Naidu G, Ryu S, Thiruvenkatachari R, Choi Y, Jeong S, Vigneswaran S. A critical review on remediation, reuse, and resource recovery from acid mine drainage.

Environ Pollut. 2019;247:1110–24. https://doi.org/10.1016/J.ENVPOL.2019.01.085.
148. Skousen JG, Sexstone A, Ziemkiewicz PF. Acid mine drainage control and treatment. Reclam Drastically Disturb Lands. 2000;(January):131–68. https://doi.org/10.2134/agronmonogr41.c6.
149. Akcil A, Koldas S. Acid mine drainage (AMD): Causes, treatment and case studies. J Clean Prod. 2006;14(12-13 SPEC. ISS.):1139–45. https://doi.org/10.1016/j.jclepro.2004.09.006.
150. Hedin RS, Watzlaf GR, Nairn RW. Passive treatment of acid mine drainage with limestone. J Environ Qual. 1994;23:1338–45. https://doi.org/10.2134/jeq1994.00472425002300060030x.
151. Hassan Z ul, Ali S, Rizwan M, Ibrahim M, Nafees M, Waseem M. Role of bioremediation agents (bacteria, fungi, and algae) in alleviating heavy metal toxicity. In: Kumar V, Kumar M, Sharma S, Prasad R, editors. Probiotics in Agroecosystem. 2017. p. 517–37.
152. Waluyo L, Prihanta W, Bachtiar Z, Permana TI. Potential bioremediation of lead (Pb) using marine microalgae *Nannochloropsis oculata*. AIP Conf Proc. 2018;2231:040088. https://doi.org/10.1063/5.0002441.
153. Salgueiro JL, Pérez L, Maceiras R, Sánchez A, Cancela A. Bioremediation of wastewater using *Chlorella Vulgaris* microalgae: Phosphorus and organic matter. Int J Environ Res. 2016;10(3):465–70.
154. Dell'Anno F, Rastelli E, Buschi E, Barone G, Beolchini F, Dell'Anno A. Fungi can be more effective than bacteria for the bioremediation of marine sediments highly contaminated with heavy metals. microorganisms. 2022;10(5):993. https://doi.org/10.3390/microorganisms10050993.
155. Anusha P, Natarajan D. Bioremediation potency of multi metal tolerant native bacteria *Bacillus cereus* isolated from bauxite mines, kolli hills, Tamilnadu- A lab to land approach. Biocatal Agric Biotechnol. 2020;25:101581. https://doi.org/10.1016/j.bcab.2020.101581.
156. Sen B, Tahir M, Sonmez F, Turan Kocer MA, Canpolat O. Relationship of algae to water pollution and waste water treatment. In: Elshorbagy W, editor. Water Treatment. InTech; 2013.
157. Zhang J, Zhou F, Liu Y, Huang F, Zhang C. Effect of extracellular polymeric substances on arsenic accumulation in *Chlorella pyrenoidosa*. Sci Total Environ. 2020;704:135368. https://doi.org/10.1016/J.SCITOTENV.2019.135368.
158. Salama E-S, Roh H-S, Dev S, Khan MA, Abou-Shanab RAI, Chang SW, *et al*. Algae as a green technology for heavy metals removal from various wastewater. World J Microbiol Biotechnol. 2019;35(5):75. https://doi.org/10.1007/s11274-019-2648-3.
159. Cheng SY, Show P-L, Lau BF, Chang J-S, Ling TC. New prospects for modified algae in heavy metal adsorption. Trends Biotechnol. 2019;37(11):1255–68. https://doi.org/10.1016/j.tibtech.2019.04.007.
160. Nowicka B. Heavy metal–induced stress in eukaryotic algae—mechanisms of heavy metal toxicity and tolerance with particular emphasis on oxidative stress in exposed cells and the role of antioxidant response. Environ Sci Pollut Res. 2022;29:1–52. https://doi.org/10.1007/s11356-021-18419-w.
161. Mangal V, Stock NL, Guéguen C. Molecular characterization of phytoplankton dissolved organic matter (DOM) and sulfur components using high resolution

Orbitrap mass spectrometry. Anal Bioanal Chem. 2016;408(7):1891–900. https://doi.org/10.1007/s00216-015-9295-9.
162. Kennedy V, Kaszecki E, Donaldson ME, Saville BJ. The impact of elevated sulfur and nitrogen levels on cadmium tolerance in *Euglena* species. Sci Rep. 2024;14(1):11734. https://doi.org/10.1038/s41598-024-61964-w.
163. Saitoh T, Nakagaki N, Uchida Y, Hiraide M, Matsubara C. Spectrophotometric determination of some functional groups on *Chlorella* for the evaluation of their contribution to metal uptake. Anal Sci. 2001;17(6):793–5. https://doi.org/10.2116/analsci.17.793.
164. Ibuot A, Webster RE, Williams LE, Pittman JK. Increased metal tolerance and bioaccumulation of zinc and cadmium in *Chlamydomonas reinhardtii* expressing a AtHMA4 C-terminal domain protein. https://doi.org/10.1002/bit.27476.
165. Greeshma K. The emerging potential of natural and synthetic algae-based microbiomes for heavy metal removal and recovery from wastewaters. Environ Res. 2022;215(1):114238. http://doi.org/10.1016/j.envres.2022.114238.
166. Mubashar M, Naveed M, Mustafa A, Ashraf S, Shehzad Baig K, Alamri S, *et al*. Experimental investigation of *Chlorella vulgaris* and *Enterobacter* sp. mn17 for decolorization and removal of heavy metals from textile wastewater. Water. 2020;12(11):3034. https://doi.org/10.3390/w12113034.
167. Altammar F, El Semary N, Aldayel M. The use of some species of bacteria and algae in the bioremediation of pollution caused by hydrocarbons and some heavy metals in Al Asfar lake water. Sustainability. 2024;16(18):7896. https://doi.org/10.3390/su16187896.
168. Goutam J, Sharma J, Singh R, Sharma D. Fungal-mediated bioremediation of heavy metal–polluted environment. In: Panpatte DG, Jhala YK, editors. Microbial Rejuvenation of Polluted Environment. Singapore: Springer Singapore; 2021. p. 51–76.
169. Sağ Y. Biosorption of heavy metals by fungal biomass and modeling of fungal biosorption: A review. Sep Purif Methods. 2001;30(1):1–48. https://doi.org/10.1081/SPM-100102984.
170. Orandi S, Lewis DM. Biosorption of heavy metals in a photo-rotating biological contactor—a batch process study. Appl Microbiol Biotechnol. 2013;97(11):5113–23. https://doi.org/10.1007/s00253-012-4316-5.
171. Zhang J, Liu Y, Liu J, Shen Y, Huang H, Zhu Y, *et al*. Removal of phosphorus and cadmium from wastewaters by periphytic biofilm. Water. 2023;15(18):3314. https://doi.org/10.3390/w15183314.
172. Zhong W, Zhao W, Song J. Responses of periphyton microbial growth, activity, and pollutant removal efficiency to cu exposure. Int J Environ Res Public Health. 2020;17(3):941. https://doi.org/10.3390/ijerph17030941.
173. Ma L, Wang F, Yu Y, Liu J, Wu Y. Cu removal and response mechanisms of periphytic biofilms in a tubular bioreactor. Bioresour Technol. 2018;248:61–7. https://doi.org/10.1016/j.biortech.2017.07.014.
174. Zhang B, Wu L, Shi W, Zhang Z, Lens PNL. A novel strategy for rapid development of a self-sustaining symbiotic algal-bacterial granular sludge: Applying algal-mycelial pellets as nuclei. Water Res. 2022;214:118210. https://doi.org/10.1016/J.WATRES.2022.118210.

175. Kuang X, Peng L, Chen S, Peng C, Song H. Immobilization of metal(loid)s from acid mine drainage by biological soil crusts through biomineralization. J Hazard Mater. 2023;443:130314. https://doi.org/10.1016/j.jhazmat.2022.130314.
176. Zakryś B, Milanowski R, Karnkowska A. Evolutionary origin of *Euglena*. In: Schwartzbach SD, Shigeoka S, editors. *Euglena*: Biochemistry, Cell and Molecular Biology. Cham: Springer International Publishing; 2017. p. 3–17.
177. Nakano Y, Miyatake K, Okuno H, Hamazaki K, Takenaka S, Honami N, *et al*. Growth of photosynthetic algae *Euglena* in high co2 conditions and its photosynthetic characteristics. Acta Hortic. 1996;(440):49–54. https://doi.org/10.17660/ActaHortic.1996.440.9.
178. Ludwig HF, Oswald WJ, Gotaas HB, Lynch V. Algae symbiosis in oxidation ponds: I. Growth characteristics of *Euglena* Gracilis cultured in sewage. Sew Ind Wastes. 1951;23(11):1337–55.
179. Kostygov AY, Karnkowska A, Votýpka J, Tashyreva D, Maciszewski K, Yurchenko V, *et al*. Euglenozoa: taxonomy, diversity and ecology, symbioses and viruses. Open Biol. 2021;11(3):200407. https://doi.org/10.1098/rsob.200407.
180. Guiry MD. How many species of algae are there? J Phycol. 2012;48(5):1057–63. https://doi.org/10.1111/j.1529-8817.2012.01222.x.
181. Casiot C, Bruneel O, Personné JC, Leblanc M, Elbaz-Poulichet F. Arsenic oxidation and bioaccumulation by the acidophilic protozoan, *Euglena mutabilis*, in acid mine drainage (Carnoulès, France). Sci Total Environ. 2004;320(2–3):259–67. https://doi.org/10.1016/j.scitotenv.2003.08.004.
182. Inwongwan S, Kruger NJ, Ratcliffe RG, O'Neill EC. *Euglena* central metabolic pathways and their subcellular locations. Metabolites. 2019;9(6):115. https://doi.org/10.3390/metabo9060115.
183. Dahoumane SA, Yéprémian C, Djédiat C, Couté A, Fiévet F, Coradin T, *et al*. Improvement of kinetics, yield, and colloidal stability of biogenic gold nanoparticles using living cells of *Euglena gracilis* microalga. J Nanoparticle Res. 2016;18(3):79. https://doi.org/10.1007/s11051-016-3378-1.
184. Leedale GF. Pellicle structure in *Euglena*. Br Phycol Bull. 1964;2(5):291–306. https://doi.org/10.1080/00071616400650021.
185. Inwongwan S, Pekkoh J, Pumas C, Sattayawat P. Metabolic network reconstruction of *Euglena gracilis*: Current state, challenges, and applications. Front Microbiol. 2023;14. https://doi.org/10.3389/fmicb.2023.1143770.
186. Yuan S, Fu W, Du M, Yao R, Zhang D, Li C, *et al*. Enhanced cold tolerance mechanisms in *Euglena gracilis*: Comparative analysis of pre-adaptation and direct low-temperature exposure. Front Microbiol. 2024;15. https://doi.org/10.3389/fmicb.2024.1465351.
187. Zhang K, Wan M, Bai W, Bao Z, Duan X, Wang W, *et al*. A novel heterotrophic cultivation process of *Euglena gracilis* based on NaCl stress significantly increases the paramylon production. Algal Res. 2024;78:103391. https://doi.org/10.1016/j.algal.2024.103391.
188. Mangal V, Donaldson ME, Lewis A, Saville BJ, Guéguen C. Identifying *Euglena gracilis* metabolic and transcriptomic adaptations in response to mercury stress. Front Environ Sci. 2022;10. https://doi.org/10.3389/fenvs.2022.836732.
189. Rodríguez-Zavala JS, Ortiz-Cruz MA, Mendoza-Hernández G, Moreno-Sánchez R. Increased synthesis of α-tocopherol, paramylon and tyrosine by *Euglena gracilis*

under conditions of high biomass production: Metabolites biosynthesis by *E. gracilis*. J Appl Microbiol. 2010;109(6):2160–72. https://doi.org/10.1111/j.1365-2672.2010.04848.x.
190. Nguyen NH, Nguyen QT, Dang DH, Emery RJN. Phytohormones enhance heavy metal responses in *Euglena gracilis*: Evidence from uptake of Ni, Pb and Cd and linkages to hormonomic and metabolomic dynamics. Environ Pollut. 2023;320:121094. https://doi.org/10.1016/j.envpol.2023.121094.
191. Yanagawa K, Haraguchi A, Yoshitake K, Asamatsu K, Harano M, Yamashita K, *et al*. Ubiquity of *Euglena mutabilis* population in three ecologically distinct acidic habitats in southwestern Japan. water. 2021;13(11):1570. https://doi.org/10.3390/w13111570.
192. Valente T, Gomes C. The role of two acidophilic algae as ecological indicators of acid mine drainage sites. J Iber Geol 2007. 2007;33.
193. Sittenfeld A, Mora M, Ortega JM, Albertazzi F, Cordero A, Roncel M, *et al*. Characterization of a photosynthetic *Euglena* strain isolated from an acidic hot mud pool of a volcanic area of Costa Rica. FEMS Microbiol Ecol. 2002;42(1):151–61. https://doi.org/10.1111/j.1574-6941.2002.tb01004.x.
194. Olaveson MM, Nalewajko C. Effects of acidity on the growth of two *Euglena* species. Hydrobiologia. 2000;433(1):39–56. https://doi.org/10.1023/A:1004006401516.
195. Halter D, Andres J, Plewniak F, Poulain J, Da Silva C, Arsène-Ploetze F, *et al*. Arsenic hypertolerance in the protist *Euglena mutabilis* is mediated by specific transporters and functional integrity maintenance mechanisms. Environ Microbiol. 2015;17(6):1941–9. https://doi.org/10.1111/1462-2920.12474.
196. Halter D, Goulhen-Chollet F, Gallien S, Casiot C, Hamelin J, Gilard F, *et al*. In situ proteo-metabolomics reveals metabolite secretion by the acid mine drainage bio-indicator, *Euglena mutabilis*. ISME J. 2012;6(7):1391–402. https://doi.org/10.1038/ismej.2011.198.
197. Zak MTE, Papangelakis VG, Allen DG. Biosorption selectivity of rare earth elements onto *Euglena mutabilis* suspensions and biofilms and the effect of divalent metal ions. J Rare Earths. 2025. https://doi.org/10.1016/j.jre.2025.03.018.
198. Puente-Sánchez F, Olsson S, Gómez-Rodriguez M, Souza-Egipsy V, Altamirano-Jeschke M, Amils R, *et al*. Solar radiation stress in natural acidophilic biofilms of *Euglena mutabilis* revealed by metatranscriptomics and pam fluorometry. Protist. 2016;167(1):67–81. https://doi.org/10.1016/j.protis.2015.12.003.
199. Brake SS, Hasiotis ST, Dannelly HK. Diatoms in acid mine drainage and their role in the formation of iron-rich stromatolites. Geomicrobiol J. 2004;21(5):331–40. https://doi.org/10.1080/01490450490454074.

CHAPTER 2

2.1 PREFACE

Title: *Euglena mutabilis* exists in a FAB consortium with microbes that enhance cadmium tolerance

Authors: Emma Kaszecki, Daniel Palberg, Mikaella Grant, Sarah Griffin, Chetan Dhanjal, Michael Capperauld, R. J. Neil Emery, Barry J. Saville

Reference: Published in *International Microbiology* (2024) 27;1249-1268
doi: 10.1007/s10123-023-00474-7

Contributions: BJS and RJNE contributed to the study's conception, design, and funding. Material preparation, data collection, and analysis were performed by EK. DP assisted with experimental design and data collection. MG conducted a bioinformatic analysis. SG, CD, and MC assisted with data collection. The first draft of this manuscript was written by EK, DP, and MG, and edits were made by BJS and RJN*E*. All other authors commented on subsequent versions of the manuscript. All authors have read and approved the final version.

CHAPTER 2

Euglena mutabilis exists in a FAB consortium with microbes that enhance cadmium tolerance

Published in: *International Microbiology* (2024) 27;1249-1268

2.2 ABSTRACT

Background: Synthetic algal–fungal and algal–bacterial cultures have been investigated as a means to enhance the technological applications of the algae. This inclusion of other microbes has enhanced growth and improved stress tolerance of the algal culture. The goal of the current study was to investigate natural microbial consortia to gain an understanding of the occurrence and benefits of these associations in nature. The photosynthetic protist *Euglena mutabilis* is often found in association with other microbes in acidic environments with high heavy metal (HM) concentrations. This may suggest that microbial interactions are essential for the protist's ability to tolerate these extreme environments. Our study assessed the Cd tolerance of a natural fungal–algal–bacterial (FAB) association whereby the algae is *E. mutabilis*.

Results: This study provides the first assessment of antibiotic and antimycotic agents on an *E. mutabilis* culture. The results indicate that antibiotic and antimycotic applications significantly decreased the viability of *E. mutabilis* cells when they were also exposed to Cd. Similar antibiotic treatments of *E. gracilis* cultures had variable or non-significant impacts on Cd tolerance. *E. gracilis* also recovered better after pre-treatment with antibiotics and Cd than did *E. mutabilis*. The recoveries were assessed by heterotrophic growth without antibiotics or Cd. In contrast, both *Euglena* species displayed increased chlorophyll production upon Cd exposure. PacBio full-length amplicon

sequencing and targeted Sanger sequencing identified the microbial species present in the *E. mutabilis* culture to be the fungus *Talaromyces* sp. and the bacterium *Acidiphilium acidophilum*.

Conclusion: This study uncovers a possible fungal, algal, and bacterial relationship, what we refer to as a FAB consortium. The members of this consortium interact to enhance the response to Cd exposure. This results in an *E. mutabilis* culture that has a higher tolerance to Cd than the axenic *E. gracilis*. The description of this interaction provides a basis to explore the benefits of natural interactions. This will provide knowledge and direction for use when creating or maintaining FAB interactions for biotechnological purposes, including bioremediation.

Keywords: Bioremediation · Biotechnology · Heavy metals · Algal symbiosis · Co-culture · Fungal–algal–bacterial (FAB)

2.3 INTRODUCTION

The association of algae with fungi is perhaps best known from lichen symbioses, but these alliances occur in a wider range of systems in which bacteria and fungi exchange key metabolites with algae [1–3] or strengthen their stress responses [4,5]. Algae have been co-cultured with bacteria or fungi to enhance levels of algal biomass [6,7] or the production of high-value products [8–10]. One natural association studied was that between the euglenoid *Euglena mutabilis* and a fungus, found in acid environments with high levels of heavy metals [11]. In the present investigation, potential associations between *E. mutabilis* and a fungus, as well as bacteria, are investigated to assess the contributions of the co-cultured species to cadmium (Cd) tolerance of the *Euglena*. Euglenoids are a group of

unicellular flagellates with a diverse ecological distribution [12,13]. They fill similar ecological niches as algae and have been investigated for applications in pharmaceuticals, cosmetics, biofuels, bioremediation, and foodstuffs [10,14–17]. *Euglena gracilis* is the model organism for this group, as it is readily cultured and has been widely studied and characterized. However, its genome sequence remains unannotated [18,19], and knowledge of gene content has relied heavily on transcriptome analyses [12,20]. Insight regarding microbial interactions with *Euglena* in various environments has been gained by establishing synthetic associations in culture. Notably, *E. gracilis* is incapable of synthesizing vitamins B1 and B12 and must obtain these from exogenous sources [21]. When it is cultured with bacteria that can produce these vitamins, *Lysinibacillus boronitolerans* or *Pseudobacillus badius*, *E. gracilis* is able to grow for several generations without exogenous vitamin application [21]. *Euglena* biomass and compound production were also enhanced when grown with the growth promoting bacteria *Emiticicia* sp. EG3 [10] or with *Vibrio natriegens*, a bacterium capable of synthesizing the phytohormone indole-3-acetic acid (IAA) [22]. While studying synthetic associations is informative and has led to many interesting findings related to fungal–algal–bacterial (FAB) associations, the full potential of *Euglena* co-cultures and FABs would be better revealed by investigating naturally occurring interactions such as those between *E. mutabilis* and its inextricably associated partner organisms [23–25].

E. mutabilis is an extremophilic Euglenoid that is often found in toxic environments such as peat bogs, volcanic lakes, and acid mine drainage (AMD) [23,26,27]. In fact, its ability to grow in these environments, where few other organisms can grow, has led to it becoming a bioindicator for AMD [28–31]. Acid drainage is naturally produced as water

seeps through iron sulfide-aggregated rocks; however, its production is dramatically enhanced by the disposal of industrial mining waste, which creates acidic pools of toxic substances, including high concentrations of heavy metals (HMs). AMD thus poses severe human and environmental health concerns. When *E. mutabilis* grows in these environments, it often associates with other microorganisms to form biofilms [11,27,32–34]. An isolate of *E. mutabilis* from an acidic pond in the Northwest Territories (Canada) was found to contain a yeast, later identified as *Cryptococcus* sp. [11]. The fungus was originally considered a contaminate, but the culture could not be cured, and the authors concluded this was a form of *E. mutabilis*–fungal mutualism [11]. The difficulty in obtaining axenic *E. mutabilis* cultures was also noted during subsequent isolation attempts from toxic environments [11,35]. This led the authors to hypothesize that partner organisms augment the stress tolerance of *E. mutabilis* and aid its ability to survive in acidic, metal polluted environments.

The objective of the presented research was to test this hypothesis by investigating the impact of antibiotic treatments on the growth and Cd tolerance of a natural *E. mutabilis*, fungal, and bacterial co-culture. A culture of *E. mutabilis* with associated fungal and bacterial organisms originally from an AMD site in Timmins, Ontario, Canada, was investigated. Extensive attempts to axenically separate fungi and bacteria from the *E. mutabilis* were not successful. Therefore, in the present study, an array of five antibiotics and two antimycotics were used in systematic attempts to suppress the growth of the partner organisms in the presence and absence of 100 µM $CdCl_2$. Our findings indicate that there is a significant decrease in the number of viable *E. mutabilis* cells across all antibiotics and $CdCl_2$ treatments compared to *E. mutabilis* co-cultures that are only exposed to $CdCl_2$. This

indicates that the associated microbes play a role in modulating the HM stress responses of *Euglena*. Suppressing bacterial and fungal growth also revealed the complexity of the interactions in this naturally occurring FAB association and supports the further investigation of natural interactions as model FABs for use in microbe technologies, including bioremediation.

2.4: METHODS

Culture selection and growth of *E. mutabilis* and *E. gracilis*

Field samples of *E. mutabilis* were obtained from the Canadian Phycological Culture Centre (CPCC, University of Waterloo, Canada). The strain of *E. mutabilis* (CPCC 657) contained unidentified bacteria and fungi. The CPCC did not have an axenic culture of *E. mutabilis*, therefore an axenic culture of *E. gracilis* (CPCC 95) was obtained to act as an experimental control. Both organisms were grown autotrophically in 250-mL Pyrex Erlenmeyer flasks capped with foam stoppers and aluminum foil under standard aeration (100 RPM on a Thermo Fisher Scientific MaxQ 3000) while cycling light and temperature (16:8 LD cycle at 260 μmol s^{-1} m^{-1}; 24°C ± 0.5°C in light and 18°C ± 0.5°C in dark) in a Conviron PCG20 environmental chamber [36]. Stock cultures were grown in a modified acid medium (MAM), a defined inorganic medium [37], with modifications recommended by the CPCC and adjusted to a pH between 4.3 and 4.5 [38]. Filter-sterilized F/2 vitamin mix was added after the medium was autoclaved.

Antibiotic Preparation

The five antibiotics and two antimycotic stock solutions were prepared with appropriate solvents. Kanamycin monosulfate (Bioshop Cat. No. KAN201) and tetracycline hydrochloride (Fisher Scientific Cat. No. A39246) were reconstituted in sterile MilliQ (13.4 MΩ·cm) water at a concentration of 1280 µg/mL. Rifampicin (Fisher Scientific Cat. No. 5573031GM), chloramphenicol (Fisher Scientific Cat. No. AAB2084122), and cycloheximide (Fisher Scientific Cat. No. AAJ6690103) were reconstituted in MeOH, 100% EtOH, and 95% EtOH, respectively, at a concentration of 1280 µg/mL [39–41]. A penicillin–streptomycin blend was purchased in solution (Fisher Scientific Cat. No. 15140122) and diluted using sterile MilliQ (13.4 MΩ·cm) water to a concentration of 1280 units/L. Amphotericin B was also purchased as a solution (Fisher Scientific Cat. No. 15290026), and its concentration was not modified (250 mg/L). Antibiotics were stored at−20°C in sterile polypropylene test tubes (VWR Cat. No. CA60819-761) with parafilm around the lid. Most of the antimicrobial agents selected have a broad spectrum of impact. Their mechanisms of action include inhibition of protein synthesis (kanamycin, bactericidal; tetracycline, bacteriostatic; chloramphenicol, bacteriostatic; penicillin–streptomycin, bactericidal) [42,43], inhibition of nucleic acid synthesis (rifampicin, bactericidal; cycloheximide, fungicidal) [42,44], and disrupting the cell membrane permeability (amphotericin B, fungicidal) [42,44].

***E. mutabilis* and *E. gracilis* antibiotic treatments**

Cell counts of *Euglena* from stock cultures of *E. mutabilis* were performed using a hemocytometer (Hausser Scientific) at 10x magnification. A 1-mL volume of 500,000 cells was aliquoted into 1.5 mL microfuge tubes, which were centrifuged (6000RCF for 5 min),

and the supernatant was removed using a micropipette. The pelleted cells were inoculated into a well of a 12-well culture plate (VWR Cat. No. 10861–556) containing 1 mL of media per well.

Separate 12-well culture plates (VWR Cat. No. 10861–556) were prepared for each antibiotic and antimycotic in the format of a minimum inhibitory concentration assessment used by Weigand *et al* [45] (Figure S2.1a) . Culture plates contained a sterile control (900 µL of MAM and 100 µL of antibiotic solvent), growth control (900 µL of MAM, 100 µL of sterile MilliQ (13.4 MΩ·cm) water, and 500,000 cells), and growth "check" (900 µL of MAM, 100 µL of alcohol, and an aliquot of cells) if an antibiotic was reconstituted in an alcohol. Wells that contained antibiotics were prepared using serial dilutions beginning with 1800 µL of MAM and 200 µL of an antibiotic or antimycotic in well A4. Upon completion of serial dilutions, each well contained a final volume of 1000 µL of media with antibiotic concentrations of 64, 32, 16, 8, 4, 2, 1, 0.5, and 0.25 µg/mL. Due to its stock concentration, modifications were made to the volume of media and antimycotic in culture plates containing amphotericin B; however, the final antibiotic concentrations were the same (Figure S2.1b). Cells were added to each well in the culture plate, except for the sterile control. Culture plates were sealed with parafilm and stored in the Conviron PGC20 environmental chamber under the same temperature and light conditions (16:8 LD cycle at 260 µmol s^{-1} m^{-1}; 24°C ±0.5°C in light and 18°C ±0.5°C in dark; shaking at 120 RPM) as the stock cultures with aeration (120 RPM) for 72 h. This time was previously determined to be the maximum length for which amphotericin B and penicillin–streptomycin remained fully effective [46].

An identical method and analysis were used for *E. gracilis*. Each experiment was replicated 3 times.

Euglena cell viability after antibiotic and antimycotic exposure

Seventy-two hours post-inoculation, 100 µL aliquots were taken from each well containing cells. 400µL of a 0.4% solution of Trypan Blue (Bioshop Cat. No. TRY477.100) in PBS (Bioshop, Cat. No. PBS404.100) was added to each aliquot. *Euglena* cell viability was assessed by visualizing differential uptake of the Trypan Blue stain, and cell counts were performed using a hemocytometer (Hausser Scientific) at 10x magnification. Each sample was counted twice per replicate, for a total of 6 counts per treatment. This was carried out on both *E. mutabilis* and *E. gracilis*.

Assessment of chlorophyll content

A modification of the methanol (MeOH) extraction procedure developed by Warren [47] was used to extract chlorophyll. In the modified procedure, 500 µL aliquots from each well in the culture plates were added to 2 mL Eppendorf tubes containing 200 µL of glass beads (Sigma Aldrich Cat. No. G8772). The media was decanted after centrifugation at 4°C (maximum speed for 2 min); 1 mL of chilled MeOH was added to the Eppendorf tubes, and samples were bead-beaten at 30 Hz for 2 min (Retsch Mixer Mill MM 400). Tubes were then centrifuged at 4°C (maximum speed for 2 min), and MeOH was aliquoted into a fresh 2-mL Eppendorf tube. This method was repeated so the final volume of extracted chlorophyll was 2 mL in MeOH; 200 µL of extract was added to each of three 96-well optic plates (ThermoFisher Scientific Cat. No. 165305) for triplicate readings on a BioTek Synergy HTX Multimode Reader at 652 and 665 nm wavelengths. Chlorophyll content was

determined using the equations from Warren [47], and chlorophyll content was normalized against the amount of chlorophyll per each *Euglena* cell.

Growth recovery and cultures after antibiotic treatment

Recovery of *E. gracilis* and *E. mutabilis* cultures after growth in antibiotic and $CdCl_2$ was assessed to distinguish between growth-inhibiting and cell-killing effects by plating on media without selection and allowing heterotrophic growth. Reasoner's 2A (R2A) and potato dextrose agar (PDA) plates were prepared using a 1.4% (w/v) agar mixture. Solutions were autoclaved to sterilize, and then 15 mL of media was added to each plate (Greiner Bio-One Cat. No. 633181). In sterile MilliQ (13.4 MΩ·cm) water, 100 µL aliquots were taken from wells in the culture plates containing cells and diluted with 900 µL of sterile 0.9% NaCl; 50 µL of diluted sample was added to an agar plate, sealed with parafilm, and incubated in darkness at 24℃ for 7 days. Cultures treated with antibiotics were plated on R2A, while cultures treated with antimycotics were plated on PDA. The number of *Euglena*, fungal, and bacterial colony-forming units (CFUs) were noted every 24 h throughout the 7-day incubation period.

Cadmium tolerance of *E. mutabilis* and *E. gracilis* with antibiotics

Kanamycin, rifampicin, chloramphenicol, tetracycline hydrochloride, penicillin–streptomycin, and amphotericin B at concentrations of 64, 32, 16, 8, 4, and 2 µg/mL were used to assess the impact of antibiotics and antimycotics on the $CdCl_2$ tolerance of *E. mutabilis* and *E. gracilis*. Cultures treated with cycloheximide at concentrations higher than 16 µg/mL did not contain viable cells, and therefore this antimycotic was not used in $CdCl_2$ trials. The inoculation of 12-well plates was carried out in the same manner as indicated for

the cell viability assessment (2.4 METHODS: *Euglena* cell viability after antibiotic and antimycotic exposure), with 500,000 cells being added to each well and the antibiotics added through serial dilution as described (Figure S2.1cd) [45]. Each well in the plate containing antibiotics or antimycotics received 10 µL of $CdCl_2$ at a stock concentration of 10,000 µM, resulting in a final concentration of 100 µM $CdCl_2$. A $CdCl_2$ concentration of 100 µM was selected because it is comparable to the concentration of $CdCl_2$ found in Canadian AMD [36], and *E. mutabilis* has previously demonstrated tolerance to this concentration of $CdCl_2$ under the conditions used in this experiment [48]. One well in each plate was a $CdCl_2$ control containing only $CdCl_2$ at a concentration of 100 µM and cells. Culture plates were sealed with parafilm and incubated in the environmental chamber under the same conditions (16:8 LD cycle at 260 µmol s^{-1} m^{-1}; 24°C ±0.5°C in light and 18°C ±0.5°C in dark; shaking at 120 RPM) as the initial antibiotic trials for 72 h. After 72 h assessments of cell count, cell viability, chlorophyll content, and agar plate growth checks were carried out using the methods described.

This method of assessing Cd tolerance, including subsequent analyses, was carried out on *E. mutabilis* and *E. gracilis*. All experiments were performed in triplicate.

DNA isolation

Total genomic DNA (gDNA) was isolated from cultures of CPCC 657 grown in different media to selectively enhance or limit the growth of *E. mutabilis* and its unidentified bacterial and fungal partners. CPCC 657 was grown in MAM (pH 4.3), MAM with $CdCl_2$ at a concentration of 100 µM (pH 4.3), MAM (pH 2.7), MAM with $CdCl_2$ at a concentration of 100 µM (pH 2.7), potato dextrose broth (PDB) grown in light, PDB grown

in dark, tryptic soy broth (TSB) grown in light, and TSB grown in dark. Cultures were grown for 7 days in the Conviron PGC20 environmental growth chamber under standard aeration (100RPM on a Thermo Fisher Scientific MaxQ 3000) with cycling light and temperature (16:8 LD cycle at 260 μmol s^{-1} m^{-1}; 24℃ ± 0.5℃ in light and 18℃ ± 0.5℃ in dark).

After 7 days, 1 mL of culture was aliquoted into a microfuge tube, centrifuged (6000 RCF for 5 min), and media decanted. Total cellular DNA isolations were carried out according to Hoffman and Winston (1987), with modifications [49]. Cells were resuspended in 300 μL of Triton solution and transferred to a 1.5-mL screw-cap tube containing 100 μL of glass beads and 300 μL 25 phenol:24 chloroform:1 isoamyl alcohol. Samples were vortexed for 6 min, then 200 μL of Tris-EDTA (TE) buffer was added, and the tubes were centrifuged at 4℃ (maximum speed for 5 min). The aqueous layer was transferred to a fresh 1.5-mL microfuge tube. Samples were precipitated in 1 mL of ice-cold 100% EtOH and centrifuged at 4℃ (maximum speed for 2 min) before decanting the EtOH; 400 μL of TE and 1.5 μL of RNAase A solution (20 mg/mL) were added to each tube, and samples were incubated at 37℃ for 30 min. After incubation, 10 μL of 4 M ammonium acetate and 1 mL of ice-cold 100% EtOH were added to each tube; they were then mixed, centrifuged at 4℃ (maximum speed for 2 min), and decanted. The pellet was washed with ice-cold 70% EtOH. Following centrifugation, the EtOH was decanted, and the pellets were air-dried and dissolved in 50 μL T*E.* Samples were visualized on a 0.8% (w/v) agarose (BioShop Canada Inc.) gel in 0.5×TE with ethidium bromide gel to assess the integrity of the gDNA and quantified using spectrophotometry (Thermo Fisher Scientific Nanodrop 8000 Spectrophotometer).

16S and ITS full-length amplicon PacBio sequencing

High-quality gDNA samples (at least 100 ng/μL and a 260/280 ratio of approximately 1.80 as determined using a Thermo Fisher Scientific Nanodrop 8000 Spectrophotometer) were sent to the Integrated Microbiome Resource (IMR, Dalhousie University, Canada) for library preparation and sequencing on a PacBio Sequel II sequencer. Full 16S (forward primer: 27F(Paliy)=5′-AGRGTTYGATYMTGG CTCAG-3′; reverse primer: 1492R = 5′-RGYTACCTT GTTACGACTT-3′) and full ITS (forward primer: 5′-ITS1FKYO2-3′ = 5′-TAGAGGAAGTAAAAGTCGTAA-3′; reverse primer: ITS4KYO1=5′-TCCTCCGCTTWTTGW TWTGC-3′) sequences were obtained for identification of the unidentified bacteria and fungus, respectively, and reported in the form of hif.fastq.gz file types.

Bioinformatic analysis

16S and ITS sequencing data were processed using the PacBio CCS pipeline (Comeau *et al* [50]) of the Quantitative Insights Into Microbial Ecology 2 (QIIME2) v 2022.11 software [51]. The dada2 algorithm was used to denoise raw sequences [52]. Taxonomic classification was performed against the SILVA 138.1 SSU Ref NR99 full-length database for 16S data [53] and the ITS custom classifier for all eukaryotes generated from the UNITE database [50], using the SK-Learn command from the q2-feature-classifier plugin [54]. Reads were then rarefied to filter out low-depth samples and amplicon sequence variants (ASVs) with frequencies of less than 100, as well as mitochondrial, chloroplast, and unclassified sequences. Resultant tables from QIIME2 were imported into

R-Studio for visualization and graphical analysis. The relative abundance of each ASV was plotted using the phyloseq package in R [55].

PCR amplification

PCR amplification was performed in a total reaction volume of 50 µL containing 4 µL of template DNA, 27.5 µL of sterile deionized water, 4 µL of dNTPs, 10 µL of Phusion Buffer HF (Thermo Scientific™), 0.5 µL of Phusion DNA Polymerase (Thermo Scientific™), and 2 µL of each primer (5 µM). The ITS region was amplified [56] (forward primer: ITSF=5′-CTTGGTCATTTAGAGGAA GTAA-3′; reverse primer: ITS4=5′-TCCTCCGCTTATTGA TATGC-3′), and the 16S region was amplified [57] (forward primer: 68F=5′-TNANACATGCAAGTCG RRCG-3′; reverse primer: 518R=5′-WITACCGCGGCTGC TGG-3′). Amplifications were performed with a Veriti™ Thermocycler (Applied Biosystem™), using the following program: denaturation for 30 s at 98 °C; then 35 cycles consisting of 98 °C for 10 s, 61 °C for 30 s, and 72 °C for 30 s; and a final extension step at 72 °C for 10 min. Each sample was amplified by 6 separate reactions with a volume of 50 µL and subsequently pooled for a total sample volume of 300 µL.

Gel extraction and DNA purification

60 µL of loading dye was added to each pooled sample, and amplification products were analyzed by electrophoresis in a 0.8% (w/v) agarose (BioShop Canada Inc.) gel in 0.5×TE with ethidium bromide in order to visualize DNA bands. ITS amplification resulted in a DNA fragment of approximately 460 bp, while 16S amplification resulted in a DNA fragment of approximately 400 bp. The DNA band visualized on the gel at the appropriate

location was subsequently cut out and purified using the PureLink™ Quick Gel Extraction Kit (Invitrogen™).

Sanger sequencing

Gel-purified DNA was prepared for Sanger sequencing using the BigDye™ Terminator v3.1 Cycle Sequencing Kit with modifications. Template DNA was normalized to approximately 70 ng/μL, and 3.00 μL was added to a 96-well plate (Progene Cat. No. 87-C96-ABI-2) along with 3.20 μL of primer (0.5 μM), 1.33 μL of Ready Reaction (Applied Biosystems™), 1.33 μL of BigDye Buffer (Applied Biosystems™), and 1.14 μL of deionized water for a total volume of 10.00 μL in each well. Six primers were selected for ITS identification [56], and 2 primers were used for 16S identification [57] (Table S2). Amplifications were performed with a Veriti™ Thermocycler (Applied Biosystem™), using the following program: denaturation for 1 min at 96 °C; then 40 cycles consisting of 96 °C for 10 s, 50 °C for 5 s, and 60 °C for 4 min. Following amplification, 2.5 μL of 125 mM EDTA and 30 μL of 100% cold EtOH were added to each well. The plate was sealed, inverted 4 times to mix, covered with aluminum foil, incubated at room temperature for 15 min, and then centrifuged for 4°C (2500 × g for 30 min). The plate was then decanted by being placed upside down in a centrifuge and spun (190 × g for 60 s); 30 μL of ice-cold 70% EtOH was added to each well. The plate was sealed, inverted 4 times to mix, and then centrifuged for 4°C (1650×g for 15 min). The plate was then decanted by being placed upside down in a centrifuge and spun (190×g for 60 s); 15 μL of Hi-Di™ Formamide (Applied Biosystems™) was added to each well; the plate was sealed and quickly centrifuged and covered in aluminum foil for a 15-min incubation at room temperature. The plate was run on an ABI 3730 (Applied Biosystems™), and bases were called using

SequencingAnalysis v5.4 to produce .phd1 flees. The quality of the files was assessed using Seq Scanner 2 (v. 2.0; Applied Biosystems), and the data were assembled into contiguous (contig) sequences using SeqMan Pro (v. 11.2.1; DNASTAR). The average read length±the standard deviation was assessed for each contig assembly. Generated contigs were then analyzed using Nucleotide BLAST.

2.5: RESULTS

Antibiotic treatments and $CdCl_2$

After 72 h of growth, control *E. mutabilis* cells reached at a concentration of approximately $9.4 \times 10^5 \pm 6.4 \times 10^4$ cells/ mL, while cells exposed to 100 µM $CdCl_2$ were approximately $5.5 \times 10^5 \pm 1.7 \times 10^4$ cells/mL (a 41% reduction in cells). Similarly, control *E. gracilis* cells grew to a concentration of approximately $8.0 \times 10^5 \pm 8.1 \times 10^4$ cells/mL, while cells exposed to 100 µM $CdCl_2$ grew to approximately $5.4 \times 10^5 \pm 3.3 \times 10^4$ cells/mL (a 31% reduction in cells). A *t*-test revealed that the application of 100 µM $CdCl_2$ statistically ($p < 0.05$) decreases the number of viable *E. mutabilis* and *E. gracilis* cells in culture, confirming that the application of $CdCl_2$ inhibits the growth of *Euglena*.

Cell counts of *E. mutabilis* and *E. gracilis* following antibiotic exposure revealed influences of antibiotics on algal growth (Table S2.1). Applications of kanamycin, rifampicin, chloramphenicol, and amphotericin B produced similar growth responses in both *Euglena* species. Neither *Euglena* sp. was affected by kanamycin, as evidenced by the lack of statistical (*t*-test; $p < 0.05$) difference in cell counts, while rifampicin, chloramphenicol, and amphotericin B resulted in significant decreases in cell counts at concentrations of 8–64 µg/mL (Table S2.1). Notably, the influence of the penicillin–

streptomycin blend and tetracycline differed between *E. mutabilis* and *E. gracilis*. Treatment with the penicillin–streptomycin blend here showed a significant reduction in *E. gracilis* cell counts across all concentrations; however, these antibiotics did not significantly impact on *E. mutabilis* cell counts. This was also seen with the application of tetracycline to *E. gracilis*, which displayed statistical decreases in cell counts across all concentrations of tetracycline, while *E. mutabilis* was only significantly impacted at 8 and 64 µg/ mL concentrations (Table S2.1).

Although some antibiotics impacted the growth of *E. mutabilis* and *E. gracilis*, the combination of antibiotics and $CdCl_2$ reveals more substantial differences in response between the organisms (Figure 2.1). The number of viable cells in *E. mutabilis* treated with both 100 µM $CdCl_2$ and any concentration of antibiotics was significantly less than cells treated with only antibiotics (*t*-test, $p < 0.05$; denoted by * in Figure 2.1). This was seen across all treatments of antibiotics and antimycotics in *E. mutabilis*. In contrast, statistical decreases in *E. gracilis* cells under the same treatments were only observed with a select concentration of antibiotic treatment (Figure 2.1). The addition of 100 µM $CdCl_2$ resulted in decreases in viable *E. mutabilis* cells ranging from 31 to 92%, while decreases in *E. gracilis* cells ranged from 1 to 44%. The biggest differences in cell counts were observed in samples treated with chloramphenicol and 100 µM $CdCl_2$, which resulted in decreases in cell counts ranging from 64 to 92% in *E. mutabilis* and 9 to 44% in *E. gracilis*, compared to cells treated with only chloramphenicol. Additionally, *E. mutabilis* cells treated with antibiotics and 100 µM $CdCl_2$ resulted in statistical decreases in cell counts compared to *E. mutabilis* cells treated with only 100 µM $CdCl_2$ (*t*-test, $p < 0.05$; denoted by a dagger (†) in Figure 2.1). This result was observed for every concentration of antibiotic and antimycotic

application in *E. mutabilis*. In contrast, about one-third of the antibiotic treatments reduced cell counts in *E. gracilis*. Although both *E. gracilis* and *E. mutabilis* showed similar numbers of viable cells under 100 μM $CdCl_2$, *E. mutabilis* consistently maintained a higher total cell count at every antibiotic concentration tested in combination with100 μM $CdCl_2$. This suggested that the addition of antibiotics had a greater impact on the $CdCl_2$ tolerance of the *E. mutabilis* co-cultures compared to those of axenic *E. gracilis*.

The antibiotics that resulted in the greatest decrease in *Euglena* cell viability were rifampicin and chloramphenicol, for which 64 μg/mL treatments resulted in no viable *E. mutabilis* or *E. gracilis* cells (Figure 2.1). However, the pattern of response to different concentrations of chloramphenicol was distinct for the two species. Treatment with 32 μg/mL of chloramphenicol revealed the greatest number of viable *E. mutabilis* cells, which remained as high as control conditions, while the least number of viable cells was seen at a concentration of 2 μg/mL. By contrast, the lowest number of viable *E. gracilis* cells was observed at 32 μg/mL, while the greatest number appeared at 2 μg/mL. When *E. mutabilis* was treated with 100 μM $CdCl_2$, it displayed the same trend as *E. gracilis* (Figure 2.1).

Evaluation of chlorophyll content after antibiotic treatments and $CdCl_2$

The total chlorophyll content (chl *a* +chl *b*) of *E. mutabilis* and *E. gracilis* cultures treated with antibiotics and 100 μM $CdCl_2$ was on average 1.95- and 1.82-fold higher, respectively, than cells only treated with antibiotic (Figure 2.2). When exposed to kanamycin, rifampicin, tetracycline, or penicillin–streptomycin, the chlorophyll content of both *E. mutabilis* and *E. gracilis* is below 0.2 μg/100,000 cells; however, upon the addition

of 100 μM $CdCl_2$, the concentration of chlorophyll significantly increases across every antibiotic concentration. An exception to the impact of antibiotic treatments was the exposure of *E. mutabilis* to amphotericin B, which resulted in an increased chlorophyll content; however, when treated with $CdCl_2$ and amphotericin B, the level of chlorophyll was significantly higher than the treatment with antimycotic alone. In contrast to these similar responses, *E. mutabilis* showed increased chlorophyll concentration at all concentrations of rifampin, while the *E. gracilis* response was variable. Furthermore, both species showed variability in the level of chlorophyll present across the various concentrations of chloramphenicol with $CdCl_2$, but chlorophyll production was much higher in *E. mutabilis*.

Growth recovery following antibiotic treatments and $CdCl_2$ exposure

Recovery of *Euglena* and the fungus co-cultured with *E. mutabilis*, following growth in antibiotics or antimycotics in the presence or absence of $CdCl_2$, was assessed by plating on non-selective media. The plates were incubated in the dark for 7 days, leading to only heterotrophic growth. The growth of bacterial colonies was too numerous to count, often exhibiting confluent growth, and therefore colony numbers were not recorded. Intimate growth was observed between colonies of *E. mutabilis* and the fungus (Figure S2.2). The control for the experiment was phototrophic growth in MAM ± 100 μM $CdCl_2$ without antibiotics, followed by heterotrophic growth on either R2A or PDA plates. In the control, there were large numbers of *E. mutabilis* colonies, but no fungal CFUs (Table 2.1). Generally, *E. mutabilis* cells treated with antibiotics exhibited decreased recovery compared to control growth, except for tetracycline. Phototrophic growth in MAM + $CdCl_2$, followed by heterotrophic growth, exhibited both *E. mutabilis* and fungal colonies. Pre-

growth in the presence of antibiotics, with and without $CdCl_2$, led to reduced numbers of colonies for both *Euglena* species for most of the antibiotics. An exception to this was *E. mutabilis* pre-grown with tetracycline alone, which did not affect heterotrophic growth, while pre-growth with tetracycline and $CdCl_2$ did. A notable pattern in fungal recovery growth response was the reduced recovery following growth in kanamycin and amphotericin B indicating both treatments had a negative impact on fungal viability, but this impact did not occur when $CdCl_2$ was present (Table 2.1).

PacBio sequencing and culture identification

A total of 372,830 reads were obtained from sequencing the full-length 16S ribosomal RNA (rRNA) gene. Reads per sample ranged from 7297 to 62,135. Sequencing the full-length internal transcribed spacer (ITS) gene obtained a total of 154,027 reads, ranging from 165 to 29,136 per sample. Denoising left 229,321 reads (62%), with an average of 22,932 sequences per sample for 16S, and 141,901 reads (92%), with an average of 14,190 sequences per sample for ITS. Filtering of low-level amplicon sequence variants (ASVs), low-depth samples, as well as unclassified, chloroplast, and mitochondrial sequences resulted in the exclusion of six samples and reserved a total of 34,857 reads (9%), with an average of 8714 reads per sample for 16S. The filtering process resulted in the exclusion of three samples from ITS and reserved 140,242 sequences (91%), averaging 20,034 sequences per sample. The sequences that passed the denoising and filtering processes were clustered into four ASVs for 16S and three ASVs for ITS. In total, 91% of the 16S sequences were excluded due to low sample depth or low frequency or were classified as mitochondrial, chloroplast, or unclassified at the genus level. Of these, 187,716 sequences were classified as *Euglena*, alluding to the overrepresentation of this contributor.

16S sequencing identified one bacterial genus, *Acidiphilium* (Figure 2.3a). Of the sequences classified at the genus level as *Acidiphilium*, 46% were further classified at the species level as *Acidiphilium acidophilum*. The remaining sequences could not be classified at the species level. Thus, the major bacterial contributor is determined to be *Acidiphilium acidophilum*. ITS sequencing identified three fungal genera: *Acidomyces*, *Exophiala*, and *Talaromyces* (Figure 2.3b); only one ASV could be classified to the species level (*Exophiala oligosperma*). Of the total ITS sequences that passed filtering, 98% were classified as *Talaromyces*, whereas *Exophiala* and *Acidomyces* contributed only 2.13% and 0.09% of sequences, respectively. Thus, the major fungal contributor is determined to be a species of the genus *Talaromyces*.

Sanger sequencing results

Sanger sequencing for ITS samples generates high-quality reads of 235±119 bp, with initially ambiguous bases being manually called. *Talaromyces amestolkiae* showed a 93.63% match with the raw data (562 bp length), which was increased to 94.64% upon manually calling ambiguous bases (565 bp length). The 16S reads generated were of medium quality, with a mean ± standard deviation of 151±27 base pairs. The contig assembly produced one single contig with a length of 281 bp, approximately 62% of the target region. The top match for the sequence was a 94.58% match to an uncultured bacteria isolated from acidic soils, while the next result was a 94.22% match to *Acidiphilium* sp.

2.6: DISCUSSION

The Cd tolerance of an *E. mutabilis* natural co-culture with unknown fungi and bacteria was investigated. Although extensive attempts were made, the culture bank was

unable to create an axenic *E. mutabilis* culture from any natural isolate. Therefore, we used an axenic *E. gracilis* culture as a control for assessing the impact of antibiotic treatments on the *E. mutabilis* co-culture. *E. gracilis* is the model euglenoid and has been the focus of antibiotic and heavy metal (HM) experiments using a euglenoid [58–61]. A recent investigation revealed *E. mutabilis* had greater tolerance to $CdCl_2$ than *E. gracilis*, and that it responded differently to pre-growth under nutrient conditions [48]. For the current study, cultures were grown in the presence of antibiotics with and without $CdCl_2$. Comparing the results between the two species allowed us to gain insight into the other microbes growing with *E. mutabilis*.

Cultures were treated with five antibiotics and two antimycotics. There was no impact on the viability of *E. gracilis* or *E. mutabilis* when grown in the presence of kanamycin; however, the viability of *E. mutabilis* decreased in the presence of $CdCl_2$ and kanamycin, while *E. gracilis* viability was not influenced by this treatment. These results were consistent with previous research investigating *Euglena* sp. responses to kanamycin [60,61] and indicated that any impact of kanamycin on the chloroplast or mitochondria of these *Euglena* species did not influence their viability. Therefore, the impact of kanamycin on $CdCl_2$ tolerance can be attributed to kanamycin inhibiting the translation of a culture member that is providing $CdCl_2$ tolerance to the consortium. Furthermore, since kanamycin is active against gram-negative bacteria with little impact on gram-positive bacteria [62] and no impact on fungi [63], this suggests that the consortium enhancing tolerance is a gram-negative bacterium.

The viability of both *Euglena* species was zero at 64 μg/ mL rifampin, while other rifampin concentrations had a greater impact on *E. gracilis* viability than that of *E. mutabilis*. We propose that this impact on viability was likely due to a negative impact on organelle transcription [64]. In the presence of $CdCl_2$, both *Euglena* species have reduced viability at a rifampin concentration of up to 8 μg/mL, which may suggest that organelle transcription provides a component of the protection against the $CdCl_2$ challenge. This is consistent with earlier research indicating chloroplasts in *E. gracilis* play a role in $CdCl_2$ tolerance [14].

Chloramphenicol at 64 μg/mL kills all *Euglena* cells, likely through its inhibition of organelle translation [65]. Chloramphenicol has also been shown to inhibit the synthesis of ribulose diphosphate carboxylase (RuBisCO) and NADP-linked glyceraldehyde-3-phosphate dehydrogenase (NADP-GAPDH) in *Euglena* [66]. These carbon fixation enzymes are located in the chloroplast, and their inhibition is a potential aspect of reduced chloroplast function caused by chloramphenicol [66,67], which could negatively influence Cd tolerance. Interestingly, the viability of *E. mutabilis* decreases with decreasing chloramphenicol concentrations, while the viability of *E. gracilis* increases with decreased chloramphenicol concentrations. This unexpected difference in response may be due to the presence of other consortium organisms in the *E. mutabilis* culture. The presence of chloramphenicol-metabolizing enzymes in some bacteria enables them to inactivate and breakdown the antibiotic, using it as a carbon source [68,69]. An *E. mutabilis* FAB consortia organism with this function could influence the response of the culture to chloramphenicol contributing to the observed dose curve response.

Previous studies have shown that *E. gracilis* can tolerate tetracycline concentrations ranging from 100 to 300 μg/mL [61,70]. The results here indicate that tetracycline has an impact on *E. gracilis* viability at a concentration as low as 2 μg/mL, which does not align with previous research, whereas the impact on *E. mutabilis* viability at all concentrations was not significant except at 8 μg/mL. However, tetracycline significantly reduces *E. mutabilis* viability in the presence of $CdCl_2$ while its influence on *E. gracilis* viability in the presence of $CdCl_2$ is not significant. This suggests that tetracycline is inhibiting the translation of a consortium member in the *E. mutabilis* culture [71]. The broad-spectrum activity of tetracycline does not allow the nature of this consortium member to be determined.

Penicillin and streptomycin are antibiotics that have repeatedly been shown to bleach *E. gracilis* [60,70,72,73]. The results here indicate that the addition of a combination of penicillin and streptomycin does not affect the viability of *E. mutabilis* but does have an influence on *E. gracilis* viability; however, the combined antibiotics had a significant impact on the viability of *E. mutabilis* exposed to $CdCl_2$. There was no impact of the combined antibiotics on *E. gracilis* CdCl2 tolerance. This suggested that these antibiotics are inhibiting a consortium member that influences the $CdCl_2$ tolerance of the *E. mutabilis* culture. While penicillin has a greater effect on gram-positive bacteria, streptomycin is a broad-spectrum bacteriostatic that may also impact fungal growth [40], so the nature of the consortium member influenced by this treatment cannot be determined.

The viability of both *Euglena* species was affected by amphotericin B; however, the impact of amphotericin B treatment on Cd sensitivity was consistently significant only for

the *E. mutabilis* culture. The greater impact on Cd tolerance in *E. mutabilis* is supported by the results, in that a consortium member – specifically, a fungus – likely aids in the Cd tolerance of the *E. mutabilis* culture. While all these results could reflect differences in *E. mutabilis* responses relative to *E. gracilis*, we note that one major difference between the cultures is the presence of other microbes. As such, we propose the microorganisms growing with *E. mutabilis* in the tolerance of the culture to $CdCl_2$ and suggest that the organisms supporting $CdCl_2$ tolerance are a gram-negative bacterium and a fungus susceptible to amphotericin B.

The presence of microbes assisting a photobiont (algae, cyanobacteria, or Euglenoid) is numerous. Many algae rely on exogenous vitamin B12 (cobalamin) and nitrogen, which can be supplied by co-cultured bacteria [2,74,75] in exchange for the bacteria receiving a carbon source from the algae [76,77]. Furthermore, the growth of the marine diatom *Ditylum brightwellii* in nitrogen-limiting media and its symbiotic bacterium in carbon-limited media are both lower relative to co-cultures [78]. Similarly, an investigation of a symbiotic culture of *Chlorella vulgaris* and *Bacillus subtilis* revealed that co-culturing resulted in increased growth, photosynthetic activity, carbon fixation, and vitamin B12 content of the alga [79].

Fungi can influence algae by supplying nutrients and providing protective mechanisms when grown together in co-culture [79–81]. When *Chlamydomonas reindhardtii* was cultured with *Aspergillus nidulans* and exposed to the algicide azalomycin F, algal cells grew within fungal hyphae, avoiding contact with the algicide [81]. Additionally, the presence of azalomycin F prompted *A. nidulans* to produce polar lipids,

which attract the algicide and effectively neutralize it [81]. Fungi also provide protection from reactive oxygen species (ROS) generated during HM exposure and produce extracellular polymeric substances (EPS) and organic acids that can bind HMs, reducing their toxicity when co-cultured with algae [82–84]. Further examples that are more directly related to the potential biotechnological application of the results here come from research that shows several algae have been investigated for bioremediation of textiles, organic pollutants, and HMs [85–88], and recent studies have suggested that co-culturing algae with bacteria or fungi provides benefits to these applications. These include increased flocculation efficiency, increased biomass, independent nutrient exchange, and enhanced tolerance to extreme environments [7,89–93]. The creation of artificial associations with algae, fungi, and bacteria has also been used to enhance heavy metal uptake [94], and the model euglenoid *E. gracilis* has been co-cultured with other microbes to enhance nutrient availability [21,95]. Given these previously described examples of microbes assisting photobionts, it is not unreasonable to propose that the data presented here supports a role for bacterial and fungal species as members of a FAB consortium with *E. mutabilis*, and that they contribute to the Cd tolerance of this consortium.

Although we observed a decrease in the number of viable *Euglena* cells following treatment with antibiotics and CdCl2, there was an increase in chlorophyll production by *Euglena* in the presence of Cd (Figure 2.2). This was unexpected because Cd is known to disrupt the physiological and metabolic processes of phototrophic organisms, including algae, cyanobacteria, and plants, primarily by reducing the photosynthetic rate and chlorophyll concentration [96–100]. Both *E. mutabilis* and *E. gracilis* display significantly greater chlorophyll content per 100,000 cells under Cd exposure. Furthermore, the amount

of chlorophyll being produced in the presence of Cd appears unaffected by the addition of antibiotics, suggesting that the impact does not affect the associated bacteria. This phenomenon has been reported in higher plants that have taken up Cd from their surroundings [101,102]. The structural foundation of a chlorophyll molecule is Mg; however, Mg is also essential for several other metabolic processes, including enzyme activation, sucrose transport, and energy metabolism [103]. It has been shown that Cd can replace Mg in the central position of a chlorophyll molecule as they are both divalent metals [101]. Furthermore, the Cd hyperaccumulator *Sedum alfredii* demonstrated no noticeable reduction in photosynthetic activity and a simultaneous increase in chlorophyll content following Cd treatments, despite negative impacts on leaf and root growth [102]. A similar result was observed in *Chlamydomonas reinhardtii* under excess Cu exposure, which is also a divalent metal [104]. A correlation was observed between increased chlorophyll and cell survivability, which was suggested to be the result of chlorophyll accumulation in cells that do not divide [104]. Here we showed that Cd treatment of *Euglena* led to a reduction in cell viability and an increase in the amount of chlorophyll produced per cell. This could indicate that although exposure to divalent HMs debilitates overall culture health, Cd may be able to replace the Mg in chlorophyll, leaving a less efficient but more plentiful photosynthetic apparatus that allows the *Euglena* to survive some HM toxicity.

Despite the increasing chlorophyll content per cell, *E. mutabilis* is unable to recover from antibiotic and Cd exposure during subsequent heterotrophic growth (Table 2.1). The effects of antibiotics on *E. gracilis* have been extensively studied [60,70,73,105–107], and the results here are consistent with previous findings; however, there has been no work on the impact of antibiotics on *E. mutabilis*. Based on CFU comparisons, *E. mutabilis* recovers

after antibiotic exposure better than *E. gracilis*, but *E. gracilis* shows better recovery following treatment with antibiotics and Cd. This is notable because a synergistic effect can occur where toxicity is increased through the formation of antibiotic and divalent HM complexes [108,109]. The increased chlorophyll content in the presence of Cd suggests that both *Euglena* species can generate energy and survive the treatment. Upon transfer to nutrient-rich media plates, both species could shift to heterotrophic growth and employ a number of ways to recover from Cd stress, including the use of major facilitator superfamily (MFS) transporters, transmembrane (TrkA) transporters, and HM pumps (P1 B ATPase) [110,111]. We postulate that while both *Euglena* species can recover, the recovery by the fungi and bacteria co-cultured with *E. mutabilis* occurs more quickly than that of *E. mutabilis*; consequently, substantial fungal and bacterial growth in heterotrophic conditions results in fewer *E. mutabilis* colonies being formed.

The fungi and bacteria in the *E. mutabilis* co-culture recovered well following antibiotic and $CdCl_2$ exposure and often grew to take over the entire plate. In heterotrophic cultures containing fungi and microalgae, a similar overgrowth by the fungus was previously observed [112–115]. The observations that extensive fungal colonies were visible following heterotrophic growth after antibiotic exposure and not while the culture was previously grown under phototrophic conditions in MAM suggest that antibiotic and $CdCl_2$ treatment suppressed bacterial growth and allowed the fungus to access nutrients typically taken up by the bacteria, thus giving it an improved ability to recover during heterotrophic growth. However, the results show that the number of fungal CFUs decreases with the concentration of antibiotics (Table S3), suggesting that the fungal-bacterial interaction is not simply a matter of presence or absence. Together, these results suggest

that co-cultures, in which the carbon source comes from *E. mutabilis* photosynthesis, requires a specific light regimen and organism ratio to ensure the fungus and/or bacteria do not overwhelm the photobiont. Interactions between the fungus and the bacteria were further informed by determining the species present.

Sequence analysis of DNA extracted from the *E. mutabilis* FAB co-culture was used to identify the prominent constituent organisms present in the co-culture. The fungus was determined to belong to the genus *Talaromyces*, with a possible species identification being *T. amestolkiae*, while the bacteria were determined to belong to the genus *Acidiphilium*, with a probable species identification being *A. acidophilum* (Figure 2.3). Consistent with the fungus belonging to *Talaromyces* was the observation of yellow and red fungal colonies on PDA plates following amphotericin B and cycloheximide exposure (Figure S2.3) [116]. Sequence analysis also detected a low-level sequence with similarity to *Exophiala oligosperma*; however, this may have been an artifact since *E. oligosperma* colonies are black in color, and there is no evidence that *E. oligosperma* can tolerate HMs [117,118]. *Talaromyces* sp., on the other hand, have been characterized by their ability to produce different colored pigments based on the carbon source present and in response to stress or predators [116,119,120]. Furthermore, they have been isolated from HM-polluted areas and can withstand high concentrations of Cr, As, Pb, Ni, Cu, and Cd [121–123]. Red pigment is produced by fungi that are susceptible to cycloheximide and carry the recessive *ade2* gene, which, when repressed, results in red pigmentation from the accumulation of phosphoribosylaminoimidazole, an intermediate in the biosynthesis of adenine [124–128]. The yellow pigmentation following amphotericin B and cycloheximide exposure is most likely composed of products of the azaphilone family, namely mitorubrinol and

mitorubrinic acid [116,129,130]. These compounds are found in numerous *Talaromyces* sp. and are proposed virulence factors regulated by polyketide synthesis genes *pks11* and *pks12*, which become activated under stress [116,129–131]. *Talaromyces* sp. are known to be susceptible to amphotericin B, which may activate the *pks11* and *pks12* genes and cause the pigmentation seen during heterotrophic growth [132]. This cumulative information, in combination with confirmatory Sanger sequencing results, indicates that the predominant fungus present in the *E. mutabilis* co-culture is a *Talaromyces* sp.

The production of pigments by *Talaromyces* sp. only when stressed or acting as a pathogen suggests that fungus in co-culture, where it does not produce pigments, is not stressed or acting as a pathogen. Instead, we propose that the fungus has a positive role in the FAB co-culture. Based on what is known about *Talaromyces* sp., we can attribute several possible impacts provided by the fungal consortium member. The fermented broth of red pigmentation produced by *T. amestolkiae* has shown antimicrobial activity against *Staphylococcus aureus*, although the pigmentation was significantly less cytotoxic to gram-negative bacteria and displayed low cytotoxicity against fibroblasts NIH.3 T3 [133,134]. If the consortium came under stress from an invading gram-positive bacterium, *Talaromyces* pigment production may offer protection. However, since no pigment formation was noted in the co-culture, the *Talaromyces* antibiotic production did not likely affect the experiments carried out here. *Talaromyces* sp. are also known to produce the plant growth-promoting hormone indole-3-acetic acid (IAA), and they display tolerance to Cd when growing in soil [135]. As such, when this fungus was cultured with *Arabidopsis thaliana*, it reduced the amount of Cd in the soil and underground plant tissues while simultaneously increasing plant growth. It was postulated that the fungus promoted nutrient uptake and

IAA production to promote plant development [136] and provided protection by increasing the essential nutrient bioavailability under low Cd concentrations, thereby effectively diluting the presence of Cd and enhancing plant HM tolerance [135]. These mechanisms are prevalent during other plant-fungal interactions [137–139] and may be fundamental to stress response in algal-fungal symbiosis [84,137,140,141], as well as being present in the *Euglena–Talaromyces* interaction. Therefore, the *Talaromyces* sp. in the consortium may be providing protection from gram-positive bacteria, enhanced Cd tolerance and it may enhance the *E. mutabilis* growth.

Finding that the predominant bacterial species in the FAB co-culture is an *Acidiphilium* species is consistent with this species being found in acidic environments with high HM concentrations [142–144]. *A. acidophilum* is an obligate heterotroph that could act as a nutrient source for other organisms in the FAB co-culture as it is a facultative, sulfur-reducing mixotroph [145–147]; however, there is only evidence of heterotrophic growth in AMD [148,149]. When growing heterotrophically, the main energy source for *A. acidophilum* is ferrous iron, which it can reduce to generate a usable form [147,149] and is abundant in AMD [28]. *A. acidophilum* is a gram-negative bacterium and therefore less susceptible to the potential cytotoxic effects of the *Talaromyces* member of the consortium. In the presence of fungal-produced gram-positive affecting antibiotics, *A. acidophilum* would have a competitive advantage. Cytotoxicity effects of *A. acidophilum* have not been reported. The production of an antibiotic by the fungal component of the consortium and a carbon source by the photobiont *E. mutabilis* suggests benefits for *A. acidophilum* in the association. The results of the antibiotic experiments suggest that, in return, *A. acidophilum* contributes to the Cd tolerance and possibly other stresses the consortium is exposed to.

The characteristics of *Talaromyces* sp. and *A. acidophilum* are consistent with their persistence in the FAB co-culture and suggest they have a role in the stress protection of and nutrient exchange with *E. mutabilis*. If the production of compounds by the fungal member of the consortium is confirmed and they are shown to elicit an effect on other members of the consortia, then this association would be interpreted as a commensal or holobiont type of interaction [81,150–152]. Future research on FAB co-cultures could aim to identify the mechanisms mediating the interactions between organisms.

Current methods for treating waterbodies that have been polluted with HMs include neutralization processes, chemical precipitation, coagulation/flocculation, and adsorption; however, these processes suffer from high costs, inefficient HM removal, and may produce secondary pollution [28,153–155]. As a result, biotechnological methods are being employed to enhance the bioremediation potential of microbes [92,94,156–159]. Several algae have been investigated for bioremediation of textiles, organic pollutants, and HMs [85–88], and recent studies have suggested that co-culturing algae with bacteria or fungi provides benefits that include increased flocculation efficiency, increased biomass, independent nutrient exchange, and enhanced tolerance to extreme environments [7,89–93]. However, the discoveries here show that *E. mutabilis* and its naturally associated microbial partners offer substantial insight into how organisms interact in a co-culture and provide a model to use for developing enhanced technological applications and potential use in bioremediation.

2.7: CONCLUSIONS

This study provides the first report of treating an *E. mutabilis* culture with both antibiotics and a heavy metal (HM), with DNA-sequencing enabling interpretation of the results by identifying the species present. The results indicated that the culture is a FAB consortium consisting of an HM-tolerant, potentially antibiotic-producing, and plant growth-promoting, fungus *Talaromyces* sp., the extremophilic photobiont *Euglena mutabilis*, and an acidophilic bacterium *Acidiphilium acidophilum*. The FAB isolate originated from acid mining runoff in Timmins, Ontario, Canada. Antibiotic and antimycotic suppression of the bacterial and fungal members of the consortium decreased the viability of *E. mutabilis* upon exposure to the $CdCl_2$. This indicates the consortium members have a role in responding to Cd stress and possibly other stresses. However, *E. mutabilis* cells that survived had increased chlorophyll production, potentially resulting from Cd supplementing Mg as a component of the chlorophyll pigment. Indicating it can also adapt to the Cd challenge. These interactions, combined with the inability to separate the organisms, suggest interdependence and possibly a tripartite commensal relationship, which we have coined the FAB consortium. This FAB consortium thus can be considered a holobiont consisting of constituent organisms from three separate kingdoms. Together, they can withstand exposure to high concentrations of HM and possibly other stresses. The discovery of this holobiont FAB consortium offers insight into the types of FAB interactions that could be used to create a self-sustaining bioremediation technology.

2.8: FIGURES AND TABLES

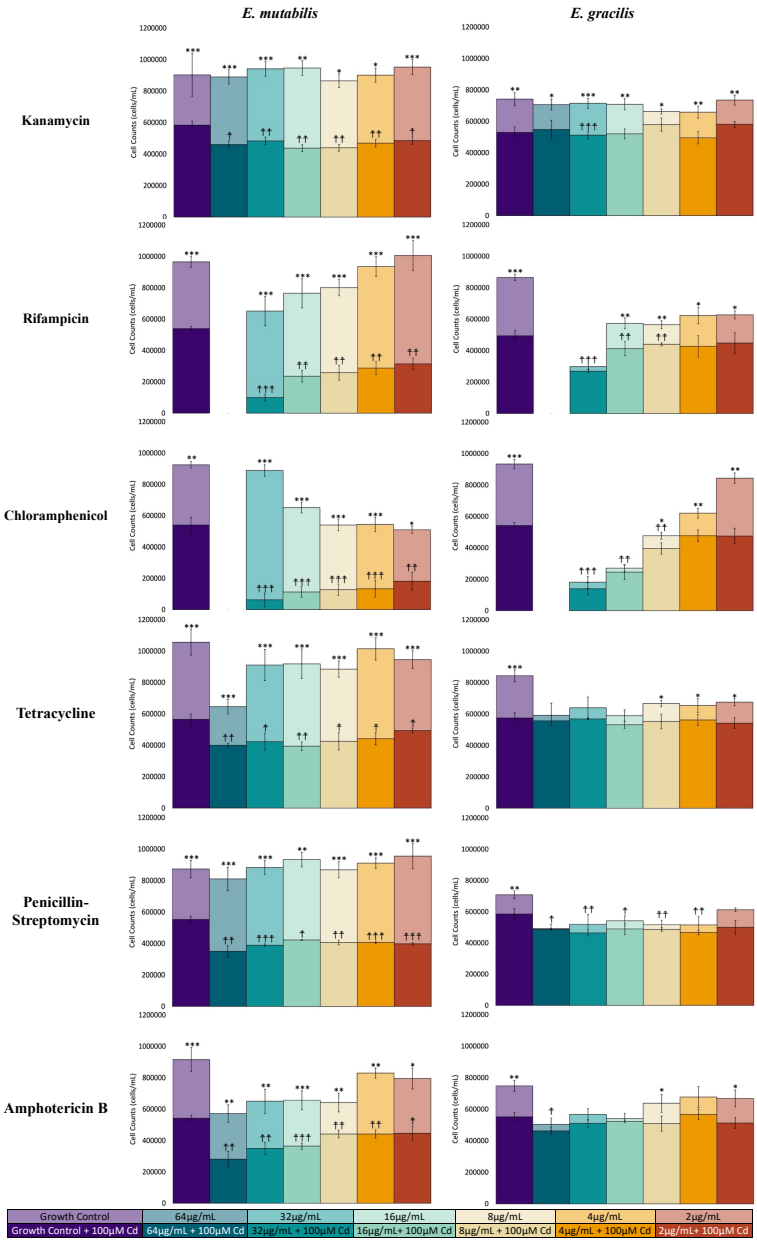

Figure 2.1: Antibiotic and $CdCl_2$ treatment reveal differences in cell viability between *E. mutabilis* and *E. gracilis*. Cultures were grown in MAM for 72 h. Light-colored bars indicate the inclusion of a dilution series of antibiotics alone, while darker-colored bars indicate exposure to antibiotics at a fixed concentration, 100 µM, of $CdCl_2$. Colors indicating different antibiotic concentrations are indicated in the legend at the bottom of the figure. Error bars represent standard deviation (n = 3). A star (*) indicates statistical difference (t-test) between cells exposed to antibiotics and cells exposed to the same concentration of antibiotics with the addition of 100 µM $CdCl_2$ (* $p < 0.05$, ** $p < 0.01$, *** $p < 0.001$). A dagger (†) indicates statistical difference (t-test) between control cells exposed to 100 µM $CdCl_2$ and those exposed to antibiotics and $CdCl_2$ († $p < 0.05$, †† $p < 0.01$, ††† $p < 0.001$).

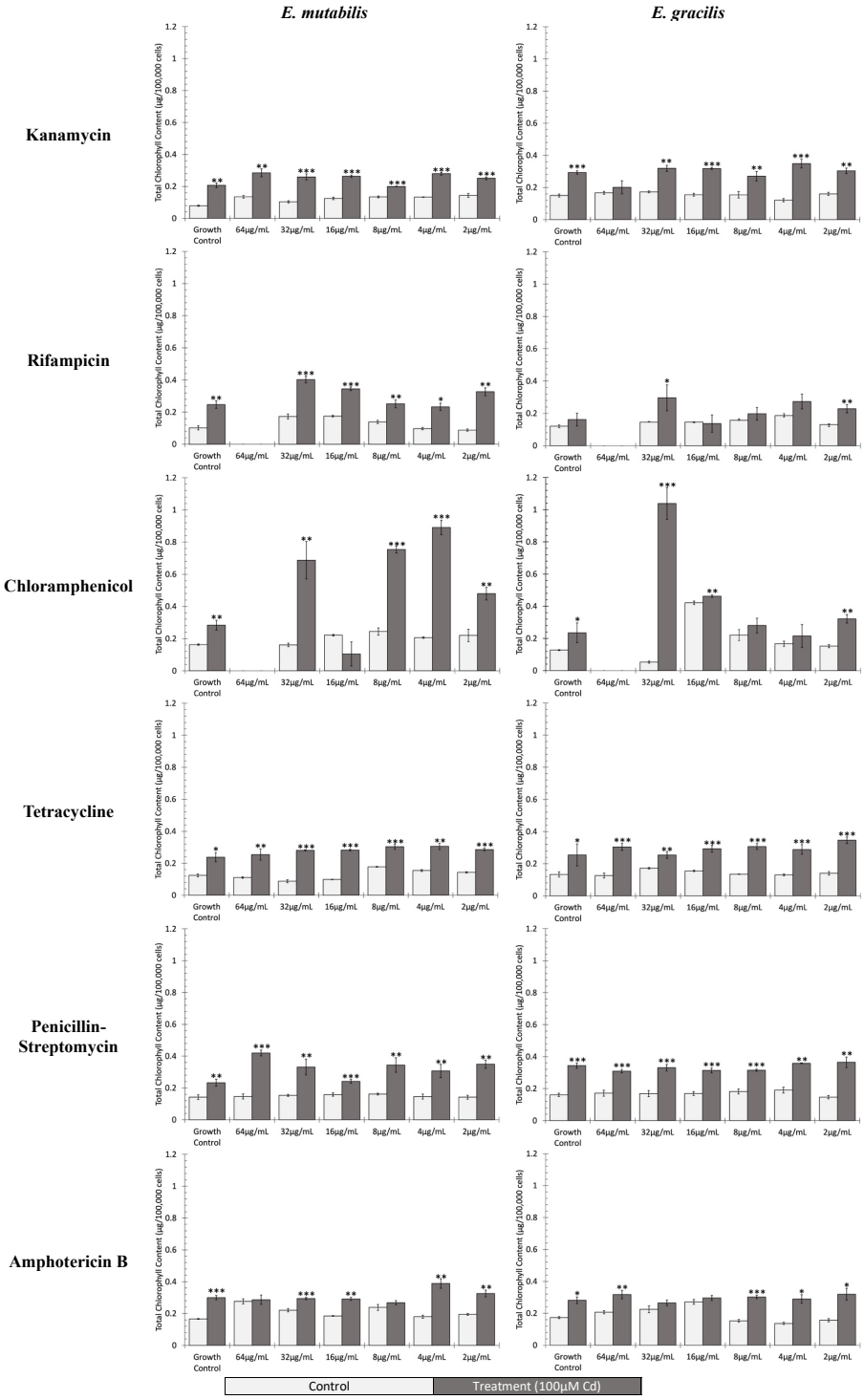

Figure 2.2: Cadmium exposure increases the chlorophyll content of *Euglena* cultures. Total chlorophyll content (chl *a* + chl *b*) per 100,000 *Euglena* cells was determined after 72 h of exposure to varying concentrations of antibiotics (light-coloured bars) and varying concentrations of antibiotics + 100 µM $CdCl_2$ (dark-coloured bars). Error bars represent standard deviation (n = 3). The statistical difference between total chlorophyll content in control and treatment conditions was assessed using a *t*-test, and significant differences are denoted by a star (* $p < 0.05$, ** $p < 0.01$, *** $p < 0.001$).

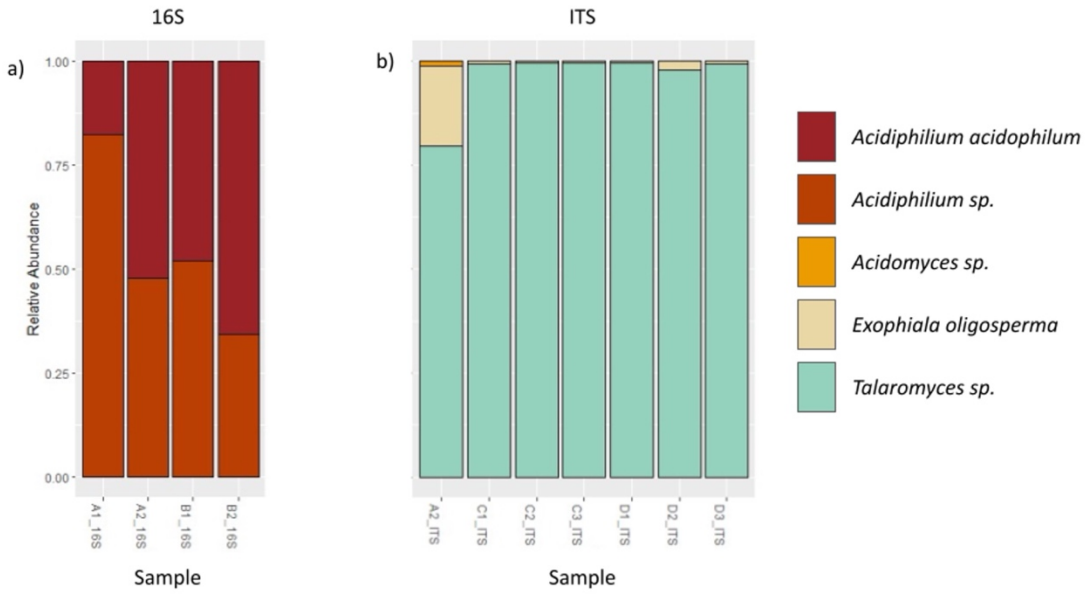

Figure 2.3: PacBio sequencing identifies a major bacterial and a major fungal partner for *E. mutabilis*. Relative abundance taxa bar plot of *E. mutabilis* co-culture (CPCC 657) grown in MAM at pH 4.3 (A samples), MAM at pH 2.7 (B samples), TSB grown in light (C samples), and TSB grown in dark (D samples). Taxa (targeting the full 16S region of bacterial rDNA and full ITS region of fungal rDNA) are represented at the species level where possible where a) displays bacteria taxa and b) displays fungal taxa.

Table 2.1: Cell viability test (n = 3) comparing colony-forming units of *E. mutabilis* (CPCC 657) and uncharacterized fungal growth, in addition to *E. gracilis* (CPCC 95) after 7 days of incubation at 24 °C in darkness.

	E. mutabilis		*Fungi*		*E. gracilis*	
	Media Only	100 µM $CdCl_2$	Media Only	100 µM $CdCl_2$	Media Only	100 µM $CdCl_2$
Control	+++	++	-	+++	++	+++
	32 µg/mL	32 µg/mL + 100 µM $CdCl_2$	32 µg/mL	32 µg/mL + 100 µM $CdCl_2$	32 µg/mL	32 µg/mL + 100 µM $CdCl_2$
Kanamycin	++	+	+	+++	++	+++
Rifampicin	+	+	+++	+++	+	+
Chloramphenicol	+	+	+++	+++	+	++
Tetracycline	+++	+	+++	+++	+	++
Penicillin-Streptomycin	++	+	+++	+++	+	++
Amphotericin B	++	+	+	+++	+	+++

(–) no CFU, (+) if < 50 CFU, (+ +) if 50 >< 150 CFU, and (+ + +) if >150 or complete lawn present and CFU count impossible.

2.9: SUPPLEMENTARY MATERIALS

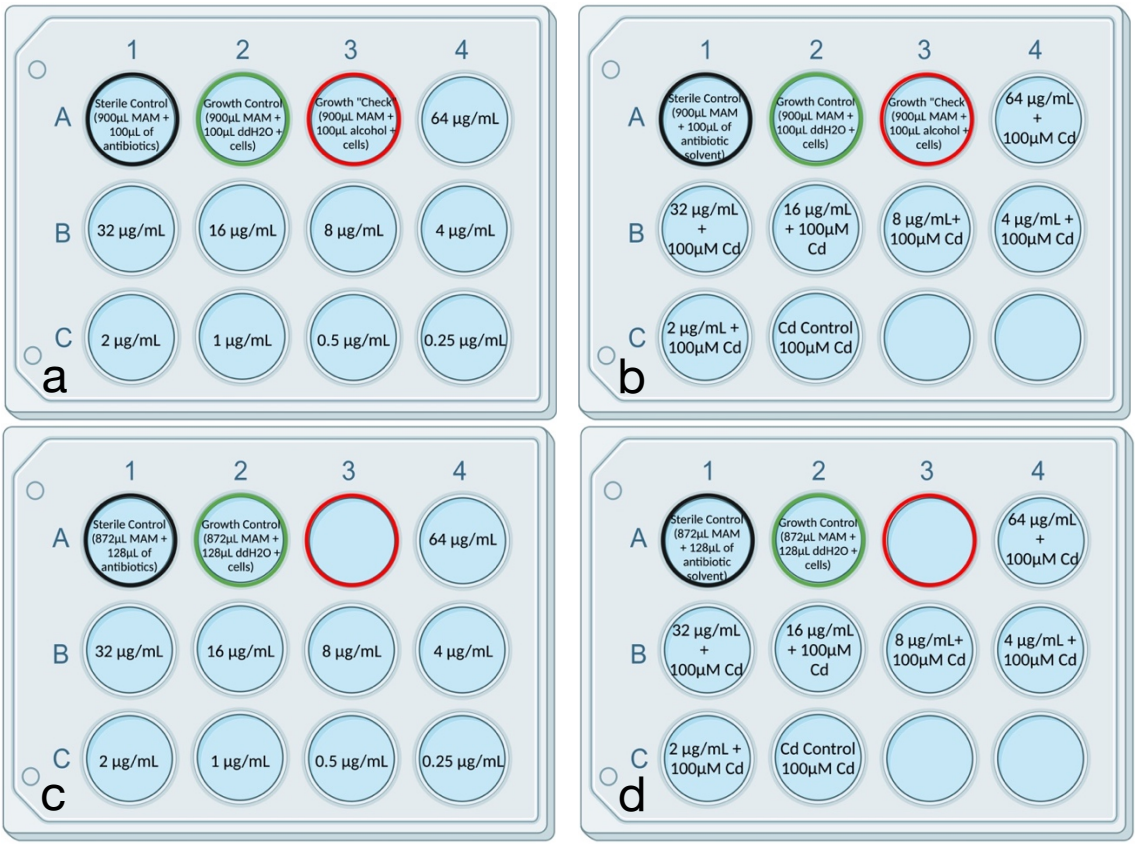

Figure S2.1: Schematic of a modified minimum inhibitory concentration (MIC) assay in 12-well plates. Each plate contains a sterile control in A1 (MAM + antibiotic) and a growth control in A2 (MAM + water + cells). Antibiotics that have been reconstituted in alcohol (rifampicin, chloramphenicol, cycloheximide) also contain a growth check condition in A3 (MAM + alcohol + cells). The initial treatment of cell cultures with antibiotics begins in A4 with a concentration of 64µg/mL which is serially diluted in subsequent wells to a final concentration of 0.25µg/mL in C4 (a, b). This is repeated with the addition of 100µM $CdCl_2$ to assess Cd tolerance against antibiotic treatments ranging from 2-64µg/mL (c, d). Plates containing $CdCl_2$ also have a Cd control in C2 (MAM + 100µM $CdCl_2$). It can be noted that the lower stock concentration of amphotericin B precludes the addition of the antimycotic at the same volume as other antibiotics in this study, therefore adjustments were made to account for an increase in the volume required to obtain the accurate concentrations required (b, d). Images were created with BioRender.com.

Table S2.1: Relative growth of viable *E. mutabilis* (CPCC 657) and *E. gracilis* (CPCC 95) following 72 hours of antibiotic exposure at various concentrations compared to control conditions (MAM only) where *nil* indicates there was no difference in growth, *ng* indicates no *Euglena* cells were detected, an up arrow (↑) indicates the growth of *Euglena* after antibiotic exposure increase, and a down arrow (↓) indicates the growth of *Euglena* after antibiotic exposure decreased. A star (*) is used to denote the difference in growth (* = $p < 0.05$, ** = $p < 0.01$, *** = $p < 0.001$) determined by a *t*-test.

Antibiotic Concentrations (µg/mL)		*E. mutabilis*	*E. gracilis*
Kanamycin	64	*nil*	*nil*
	32	*nil*	*nil*
	16	*nil*	*nil*
	8	*nil*	*↓
	4	*nil*	*nil*
	2	*nil*	*nil*
Rifampicin	64	*ng*	*ng*
	32	***↓	***↓
	16	**↓	**↓
	8	***↓	***↓
	4	*nil*	**↓
	2	*nil*	***↓
Chloramphenicol	64	*ng*	*ng*
	32	*nil*	***↓
	16	***↓	***↓
	8	***↓	***↓
	4	***↓	***↓
	2	***↓	*↓
Tetracycline	64	**↓	*↓
	32	*nil*	*↓
	16	*nil*	**↓
	8	*↓	**↓
	4	*nil*	**↓
	2	*nil*	**↓
Penicillin Streptomycin	64	*nil*	***↓
	32	*nil*	*↓
	16	*nil*	**↓
	8	*nil*	***↓
	4	*nil*	*↓
	2	*nil*	**↓
Amphotericin B	64	***↓	**↓
	32	**↓	**↓
	16	**↓	**↓
	8	**↓	*nil*
	4	*nil*	*nil*
	2	*nil*	*nil*

Table S2.2: ITS and 16S primers selected for the identification of constituent fungal and bacterial organisms in an *E. mutabilis* co-culture (CPCC 657) through Sanger sequencing. ITS primers were selected from Raja *et al* [56] while 16S primers were selected from Thijs *et al* [57].

	Primer	Sequence (5'→3')
ITS	ITS1F	CTTGGTCATTTAGAGGAAGTAA
	ITS1	TCCGTAGGTGAACCTGCGG
	ITS2	GCTGCGTTCTTCATCGATGC
	ITS3	GCATCGATGAAGAACGCAGC
	ITS4	TCCTCCGCTTATTGATATGC
	ITS5	GGAAGTAAAAGTCGTAACAAGG
16S	68F	TNANACATGCAAGTCGRRCG
	518R	WITACCGCGGCTGCTGG

Table S2.3: Cell viability test ($n = 3$) comparing colony forming units of *E. mutabilis* (CPCC 657) and uncharacterized fungal growth, in addition to *E. gracilis* (CPCC 95) after 7 days incubation at 24°C in darkness.

	E. mutabilis		*Fungi*		*E. gracilis*	
	Media Only	100 µM $CdCl_2$	Media Only	100 µM $CdCl_2$	Media Only	100 µM $CdCl_2$
Control	+++	++	-	+++	++	+++
	16 µg/mL	16 µg/mL + 100 µM $CdCl_2$	16 µg/mL	16 µg/mL + 100 µM $CdCl_2$	16 µg/mL	16 µg/mL + 100 µM $CdCl_2$
Kanamycin	+	+	-	+++	++	+++
Rifampicin	+++	+	+	+++	+	+
Chloramphenicol	++	+	-	+	+	++
Tetracycline	++	+	+	+++	+	++
Penicillin-Streptomycin	++	+	-	+++	+	++
Amphotericin B	+	+	+	+++	+	+++
	8 µg/mL	8 µg/mL + 100 µM $CdCl_2$	8 µg/mL	8 µg/mL + 100 µM $CdCl_2$	8 µg/mL	8 µg/mL + 100 µM $CdCl_2$
Kanamycin	+	+	-	+++	++	+++
Rifampicin	++	+	+	+++	+	+
Chloramphenicol	++	+	+	+	+	++
Tetracycline	+++	+	+	+++	+	++
Penicillin-Streptomycin	+	+	-	+++	+	+++
Amphotericin B	+	+	-	+++	+	+
	4 µg/mL	4 µg/mL + 100 µM $CdCl_2$	4 µg/mL	4 µg/mL + 100 µM $CdCl_2$	4 µg/mL	4 µg/mL + 100 µM $CdCl_2$
Kanamycin	+	+	-	+++	++	+++
Rifampicin	++	++	+	+++	+	+
Chloramphenicol	+++	+++	+	+	+	++
Tetracycline	++	++	+	+++	+	++
Penicillin-Streptomycin	+	+	-	+++	+	++
Amphotericin B	+	+	+	+++	+	++

	2 µg/mL	2 µg/mL + 100 µM $CdCl_2$	2 µg/mL	2 µg/mL + 100 µM $CdCl_2$	2 µg/mL	2 µg/mL + 100 µM $CdCl_2$
Kanamycin	+	+	-	+++	++	+++
Rifampicin	++	+	+	+++	+	+
Chloramphenicol	++	+	+	+++	+	+++
Tetracycline	+++	+	-	+++	+	++
Penicillin-Streptomycin	+	+	+	+++	+	++
Amphotericin B	+	+	+	+++	+	++

(–) no CFU, (+) if < 50 CFU, (+ +) if 50 ><150 CFU, and (+ + +) if >150 or complete lawn present and CFU count impossible.

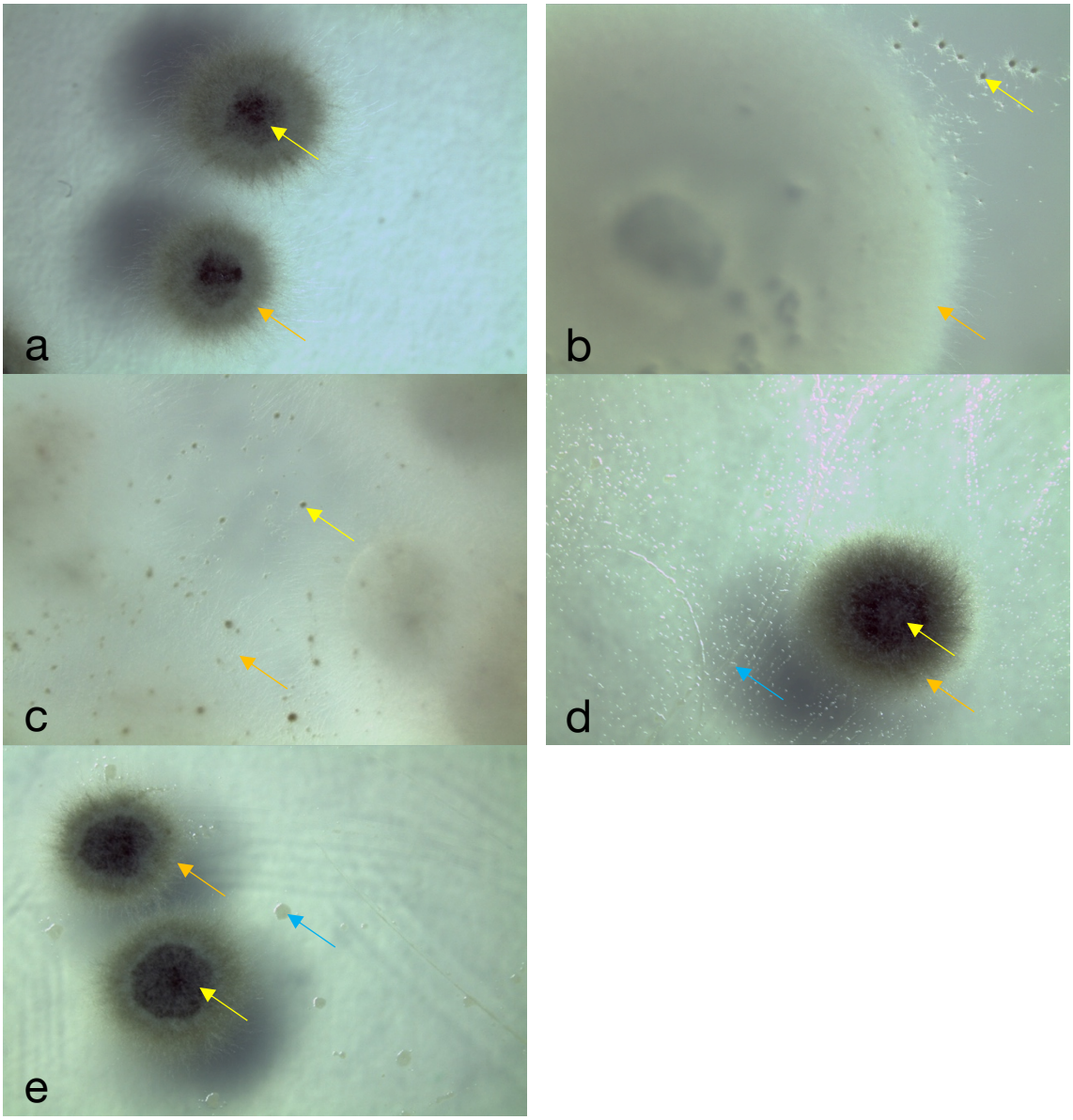

Figure S2.2: Plate photographs of an *E. mutabilis* co-culture (CPCC657) after 7 days on R2A plates in control conditions (a), following 72 hours of exposure to 8 µg/mL of cycloheximide (b), 64 µg/mL of cycloheximide (c), 32 µg/mL of kanamycin (d), and after 7 days on PDA plates following 72 hours of exposure to 4 µ/mL of amphotericin B and 100 µM $CdCl_2$ (e). Growth of *E. mutabilis* (yellow arrows) exhibits intimate interactions with constituent bacterial (blue arrows) and fungal (orange arrows) organisms which prohibits the isolation on single colonies.

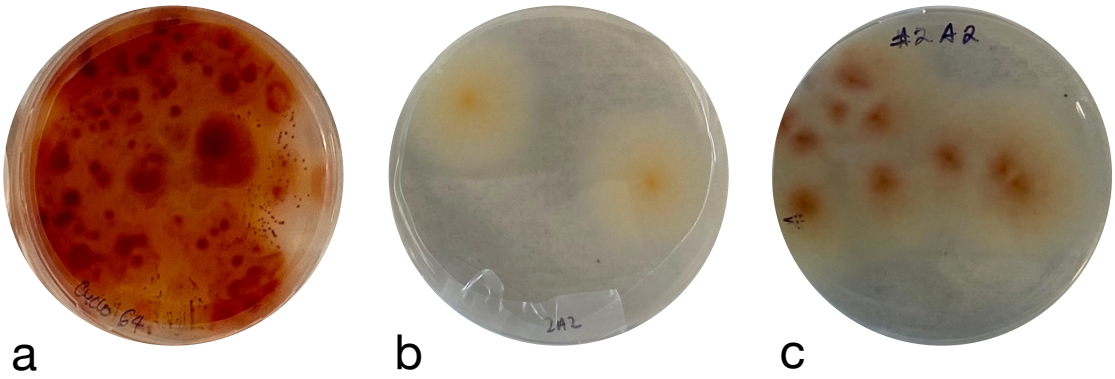

Figure S2.3: Plate photographs of an *E. mutabilis* co-culture (CPCC 657) after 7 days on PDA plates following 72 hours of exposure to 64µg/mL of cycloheximide (a) and 2µg/mL of exposure to amphotericin B (b, c).

2.10: REFERENCES

1. Cantin NE, van Oppen MJH, Willis BL, Mieog JC, Negri AP. Juvenile corals can acquire more carbon from high-performance algal symbionts. Coral Reefs. 2009;28(2):405–14. https://doi.org/10.1007/s00338-009-0478-8.
2. Croft MT, Lawrence AD, Raux-Deery E, Warren MJ, Smith AG. Algae acquire vitamin B_{12} through a symbiotic relationship with bacteria. Nature. 2005;438(7064):90–3. https://doi.org/10.1038/nature04056.
3. Matthews JL, Crowder CM, Oakley CA, Lutz A, Roessner U, Meyer E, *et al*. Optimal nutrient exchange and immune responses operate in partner specificity in the cnidarian-dinoflagellate symbiosis. Proc Natl Acad Sci. 2017;114(50):13194–9. https://doi.org/10.1073/pnas.1710733114.
4. Ramanan R, Kim BH, Cho DH, Oh HM, Kim HS. Algae-bacteria interactions: Evolution, ecology and emerging applications. Biotechnol Adv. 2016;34(1):14–29. https://doi.org/10.1016/j.biotechadv.2015.12.003.
5. Zan J, Li Z, Tianero MaD, Davis J, Hill RT, Donia MS. A microbial factory for defensive kahalalides in a tripartite marine symbiosis. Science. 2019;364(6445). https://doi.org/10.1126/science.aaw6732.
6. Berthold DE, Shetty KG, Jayachandran K, Laughinghouse HD, Gantar M. Enhancing algal biomass and lipid production through bacterial co-culture. Biomass Bioenergy. 2019;122:280–9. https://doi.org/10.1016/j.biombioe.2019.01.033.
7. Fuentes JL, Garbayo I, Cuaresma M, Montero Z, González-Del-Valle M, Vílchez C. Impact of microalgae-bacteria interactions on the production of algal biomass and associated compounds. Mar Drugs. 2016;14(5). https://doi.org/10.3390/md14050100.
8. Lutzu GA, Dunford NT. Interactions of microalgae and other microorganisms for enhanced production of high-value compounds. Front Biosci. 2018;23(8):1487–504. https://doi.org/10.2741/4656.
9. Magdouli S, Brar SK, Blais JF. Co-culture for lipid production: Advances and challenges. Biomass Bioenergy. 2016;92:20–30. https://doi.org/10.1016/j.biombioe.2016.06.003.
10. Toyama T, Hanaoka T, Yamada K, Suzuki K, Tanaka Y, Morikawa M, *et al*. Enhanced production of biomass and lipids by *Euglena gracilis* via co-culturing with a microalga growth-promoting bacterium, *Emticicia* sp. EG3. Biotechnol Biofuels. 2019;12(1). https://doi.org/10.1186/s13068-019-1544-2.
11. Nakatsu C, Hutchinson TC. Extreme metal and acid tolerance of *Euglena mutabilis* and an associated yeast from Smoking Hills, Northwest Territories, and their apparent mutualism. Microb Ecol. 1988;16(2):213–31. https://doi.org/10.1007/BF02018915.
12. Ebenezer TE, Low RS, O'Neill EC, Huang I, DeSimone A, Farrow SC, *et al*. *Euglena* International Network (EIN): Driving euglenoid biotechnology for the benefit of a challenged world. Biol Open. 2022;11(11):bio059561. https://doi.org/10.1242/bio.059561.
13. Kostygov AY, Karnkowska A, Votýpka J, Tashyreva D, Maciszewski K, Yurchenko V, *et al*. Euglenozoa: Taxonomy, diversity and ecology, symbioses and viruses. Open Biol. 2021;11(3):200407. https://doi.org/10.1098/rsob.200407.

14. Khatiwada B, Hasan MT, Sun A, Kamath KS, Mirzaei M, Sunna A, *et al*. Probing the role of the chloroplasts in heavy metal tolerance and accumulation in *Euglena gracilis*. Microorganisms. 2020;8(1). https://doi.org/10.3390/microorganisms8010115.
15. Li J, Zheng Z, Du M, Chen J, Zhu H, Hu Z, *et al*. *Euglena gracilis* and its aqueous extract constructed with chitosan-hyaluronic acid hydrogel facilitate cutaneous wound healing in mice without inducing excessive inflammatory response. Front Bioeng Biotechnol. 2021;9. https://doi.org/10.3389/fbioe.2021.713840.
16. Nakashima A, Yamada K, Iwata O, Sugimoto R, Atsuji K, Ogawa T, *et al*. β-Glucan in foods and its physiological functions. J Nutr Sci Vitaminol (Tokyo). 2018;64(1):8–17. https://doi.org/10.3177/jnsv.64.8.
17. Yamamoto FY, Sutili FJ, Hume M, Gatlin III DM. The effect of β-1,3-glucan derived from *Euglena gracilis* (Algamune^{TM}) on the innate immunological responses of Nile tilapia (*Oreochromis niloticus* L.). J Fish Dis. 2018;41(10):1579–88. https://doi.org/10.1111/jfd.12871.
18. Borst P, Sabatini R. Base J: Discovery, biosynthesis, and possible functions. Annu Rev Microbiol. 2008;62(1):235–51. https://doi.org/10.1146/annurev.micro.62.081307.162750.
19. O'Neill EC, Trick M, Hill L, Rejzek M, Dusi RG, Hamilton CJ, *et al*. The transcriptome of *Euglena gracilis* reveals unexpected metabolic capabilities for carbohydrate and natural product biochemistry. Mol Biosyst. 2015;11(10):2808–20. https://doi.org/10.1039/C5MB00319A.
20. Ebenezer TE, Zoltner M, Burrell A, Nenarokova A, Novák Vanclová AMG, Prasad B, *et al*. Transcriptome, proteome and draft genome of *Euglena gracilis*. BMC Biol. 2019;17(1):1–23. https://doi.org/10.1186/s12915-019-0626-8.
21. Lukáčová A, Beck T, Koptašiková L, Benda A, Tomečková L, Trniková M, *et al*. *Euglena gracilis* can grow in the mixed culture containing *Cladosporium westerdijkiae*, *Lysinibacillus boronitolerans* and *Pseudobacillus badius* without the addition of vitamins B_1 and B_{12}. J Biotechnol. 2022;351:50–9. https://doi.org/10.1016/j.jbiotec.2022.04.013.
22. Kim JY, Oh J-J, Jeon MS, Kim G-H, Choi Y-*E.* Improvement of *Euglena gracilis* paramylon production through a cocultivation strategy with the indole-3-acetic acid-producing bacterium *Vibrio natriegens*. Appl Environ Microbiol. 2019;85(19):e01548-19. https://doi.org/10.1128/AEM.01548-19.
23. Casiot C, Bruneel O, Personné JC, Leblanc M, Elbaz-Poulichet F. Arsenic oxidation and bioaccumulation by the acidophilic protozoan, *Euglena mutabilis*, in acid mine drainage (Carnoulès, France). Sci Total Environ. 2004;320(2–3):259–67. https://doi.org/10.1016/j.scitotenv.2003.08.004.
24. Sabater S, Buchaca T, Cambra J, Catalan J, Guasch H, Ivorra N, *et al*. Structure and function of benthic algal communities in an extremely acid river. J Phycol. 2003;39(3):481–9. https://doi.org/10.1046/j.1529-8817.2003.02104.x.
25. Searles PS, Kropp BR, Flint SD, Caldwell MM. Influence of solar UV-B radiation on peatland microbial communities of southern Argentinia. New Phytol. 2001;152(2):213–21. https://doi.org/10.1046/j.0028-646X.2001.00254.x.
26. Gross W, Oesterhelt C, Tischendorf G, Lederer F. Characterization of a non-thermophilic strain of the red algal genus *Galdieria* isolated from Soos (Czech

Republic). Eur J Phycol. 2002;37(3):477–82. https://doi.org/10.1017/S0967026202003773.
27. Sittenfeld A, Mora M, Ortega JM, Albertazzi F, Cordero A, Roncel M, *et al*. Characterization of a photosynthetic *Euglena* strain isolated from an acidic hot mud pool of a volcanic area of Costa Rica. FEMS Microbiol Ecol. 2002;42(1):151–61. https://doi.org/10.1111/j.1574-6941.2002.tb01004.x.
28. Akcil A, Koldas S. Acid mine drainage (AMD): Causes, treatment and case studies. J Clean Prod. 2006;14(12-13 SPEC. ISS.):1139–45. https://doi.org/10.1016/j.jclepro.2004.09.006.
29. Halter D, Goulhen-Chollet F, Gallien S, Casiot C, Hamelin J, Gilard F, *et al*. In situ proteo-metabolomics reveals metabolite secretion by the acid mine drainage bio-indicator, *Euglena mutabilis*. ISME J. 2012;6(7):1391–402. https://doi.org/10.1038/ismej.2011.198.
30. Valente T, Gomes C. The role of two acidophilic algae as ecological indicators of acid mine drainage sites. J Iber Geol 2007. 2007;33.
31. Halter D, Casiot C, Heipieper HJ, Plewniak F, Marchal M, Simon S, *et al*. Surface properties and intracellular speciation revealed an original adaptive mechanism to arsenic in the acid mine drainage bio-indicator *Euglena mutabilis*. Appl Microbiol Biotechnol. 2012;93(4):1735–44. https://doi.org/10.1007/s00253-011-3493-y.
32. Brake SS, Hasiotis ST, Dannelly HK. Diatoms in acid mine drainage and their role in the formation of iron-rich stromatolites. Geomicrobiol J. 2004;21(5):331–40. https://doi.org/10.1080/01490450490454074.
33. Ňancucheo I, Barrie Johnson D. Acidophilic algae isolated from mine-impacted environments and their roles in sustaining heterotrophic acidophiles. Front Microbiol. 2012;3. https://doi.org/10.3389/fmicb.2012.00325.
34. Yanagawa K, Haraguchi A, Yoshitake K, Asamatsu K, Harano M, Yamashita K, *et al*. Ubiquity of *Euglena mutabilis* population in three ecologically distinct acidic habitats in southwestern Japan. Water. 2021;13(11):1570. https://doi.org/10.3390/w13111570.
35. Prigent S, Frioux C, Dittami SM, Thiele S, Larhlimi A, Collet G, *et al*. Meneco, a topology-based gap-filling tool applicable to degraded genome-wide metabolic networks. PLOS Comput Biol. 2017;13(1):e1005276. https://doi.org/10.1371/journal.pcbi.1005276.
36. Olaveson MM, Nalewajko C. Effects of acidity on the growth of two *Euglena* species. Hydrobiologia. 2000;433(1):39–56. https://doi.org/10.1023/A:1004006401516.
37. Olaveson MM, Stokes PM. Reponses of the acidiphilic alga *Euglena* mutablilis (Euglenophyceae) to carbon enrichent at pH 3. J Phycol. 1989;25(3):529–39. https://doi.org/10.1111/j.1529-8817.1989.tb00259.x.
38. Canadian Phycological Culture Centre. Modified acid medium (MAM). University of Waterloo. 2017. https://uwaterloo.ca/canadian-phycological-culture-centre/cultures/culture-media/modified-acid-medium.
39. Holstege CP. Rifampin. Encyclopedia of Toxicology. Elsevier; 2014. p. 134–6.
40. Schneck DW, Tyrrell DLJ, Marks GS. Drug-induced porphyrin biosynthesis—III. Biochem Pharmacol. 1971;20(11):2999–3007. https://doi.org/10.1016/0006-2952(71)90104-3.

41. Szulczewski D, Eng F. Chloramphenicol. Analytical Profiles of Drug Substances. Elsevier; 1975. p. 47–90.
42. Garrett ER, Won CM. Kinetics and mechanisms of drug action on microorganisms XVII: Bactericidal effects of penicillin, kanamycin, and rifampin with and without organism pretreatment with bacteriostatic chloramphenicol, tetracycline, and novobiocin. J Pharm Sci. 1973;62(10):1666–73. https://doi.org/10.1002/jps.2600621018.
43. Kapoor G, Saigal S, Elongavan A. Action and resistance mechanisms of antibiotics: A guide for clinicians. J Anaesthesiol Clin Pharmacol. 2017;33(3):300. https://doi.org/10.4103/joacp.JOACP_349_15.
44. Mousavi SAA, Robson GD. Oxidative and amphotericin B-mediated cell death in the opportunistic pathogen *Aspergillus fumigatus* is associated with an apoptotic-like phenotype. Microbiology. 2004;150(6):1937–45. https://doi.org/10.1099/mic.0.26830-0.
45. Wiegand I, Hilpert K, Hancock REW. Agar and broth dilution methods to determine the minimal inhibitory concentration (MIC) of antimicrobial substances. Nat Protoc. 2008;3(2):163–75. https://doi.org/10.1038/nprot.2007.521.
46. Perlman D. [7] Use of antibiotics in cell culture media. Methods in Enzymology. Elsevier; 1979. p. 110–6.
47. Warren CR. Rapid measurement of chlorophylls with a microplate reader. J Plant Nutr. 2008;31(7):1321–32. https://doi.org/10.1080/01904160802135092.
48. Kennedy V, Kaszecki E, Donaldson ME, Saville BJ. The impact of elevated sulfur and nitrogen levels on cadmium tolerance in *Euglena* species. Sci Rep. 2024;14(1):11734. https://doi.org/10.1038/s41598-024-61964-w.
49. Hoffman CS, Winston F. A ten-minute DNA preparation from yeast efficiently releases autonomous plasmids for transformaion of *Escherichia coli*. Gene. 1987;57(2–3):267–72. https://doi.org/10.1016/0378-1119(87)90131-4.
50. Comeau AM, Douglas GM, Langille MGI. Microbiome helper: A custom and streamlined workflow for microbiome research. mSystems. 2017;2(1):e00127-16. https://doi.org/10.1128/mSystems.00127-16.
51. Bolyen E, Rideout JR, Dillon MR, Bokulich NA, Abnet CC, Al-Ghalith GA, *et al*. Reproducible, interactive, scalable and extensible microbiome data science using QIIME 2. Nat Biotechnol. 2019;37(8):852–7. https://doi.org/10.1038/s41587-019-0209-9.
52. Callahan BJ, McMurdie PJ, Rosen MJ, Han AW, Johnson AJA, Holmes SP. DADA2: High-resolution sample inference from Illumina amplicon data. Nat Methods. 2016;13(7):581–3. https://doi.org/10.1038/nmeth.3869.
53. Quast C, Pruesse E, Yilmaz P, Gerken J, Schweer T, Yarza P, *et al*. The SILVA ribosomal RNA gene database project: improved data processing and web-based tools. Nucleic Acids Res. 2012;41(D1):D590–6. https://doi.org/10.1093/nar/gks1219.
54. Bokulich NA, Kaehler BD, Rideout JR, Dillon M, Bolyen E, Knight R, *et al*. Optimizing taxonomic classification of marker-gene amplicon sequences with QIIME 2's q2-feature-classifier plugin. Microbiome. 2018;6(1):90. https://doi.org/10.1186/s40168-018-0470-z.

55. McMurdie PJ, Holmes S. phyloseq: An R package for reproducible interactive analysis and graphics of microbiome census data. PLoS ON*E.* 2013;8(4):e61217. https://doi.org/10.1371/journal.pone.0061217.
56. Raja HA, Miller AN, Pearce CJ, Oberlies NH. Fungal identification using molecular tools: A primer for the natural products research community. J Nat Prod. 2017;80(3):756–70. https://doi.org/10.1021/acs.jnatprod.6b01085.
57. Thijs S, De Beeck MO, Beckers B, Truyens S, Stevens V, Van Hamme JD, *et al*. Comparative evaluation of four bacteria-specific primer pairs for 16S rRNA gene surveys. Front Microbiol. 2017;8(MAR):1–15. https://doi.org/10.3389/fmicb.2017.00494.
58. Bishop DG, Smillie RM. The effect of chloramphenicol and cycloheximide on lipid synthesis during chloroplast development in *Euglena gracilis*. Arch Biochem Biophys. 1970;139(1):179–89. https://doi.org/10.1016/0003-9861(70)90059-7.
59. Gumińska N, Płecha M, Walkiewicz H, Hałakuc P, Zakryś B, Milanowski R. Culture purification and DNA extraction procedures suitable for next-generation sequencing of euglenids. J Appl Phycol. 2018;30(6):3541–9. https://doi.org/10.1007/s10811-018-1496-0.
60. He J, Liu C, Du M, Zhou X, Hu Z, Lei A, *et al*. Metabolic responses of a model green microalga *Euglena gracilis* to different environmental stresses. Front Bioeng Biotechnol. 2021;9. https://doi.org/10.3389/fbioe.2021.662655.
61. Shao Q, Jiang Y, Lei A, Hu Z, Wang J. Research progress on genetic transformation technology of *Euglena*. Acta Hydrobiol Sin. 2018;42(4):655–62. https://doi.org/10.7541/2018.081.
62. Zeng J, Duan W, Li M, Xue Y. Plasmonic metallic nanostructures as colorimetric probes for environmental pollutants. Novel Nanomaterials for Biomedical, Environmental and Energy Applications. Elsevier; 2019. p. 327–52.
63. Umezawa H, Ueda M, Maeda K, Yagishita K, Kondō S, Okami Y, *et al*. Production and isolation of a new antibiotic, kanamycin. 1957.
64. McClure WR, Cech CL. On the mechanism of rifampicin inhibition of RNA synthesis. J Biol Chem. 1978;253(24):8949–56. https://doi.org/10.1016/S0021-9258(17)34269-2.
65. Choi J, Marks J, Zhang J, Chen D-H, Wang J, Vázquez-Laslop N, *et al*. Dynamics of the context-specific translation arrest by chloramphenicol and linezolid. Nat Chem Biol. 2020;16(3):310–7. https://doi.org/10.1038/s41589-019-0423-2.
66. Hovenkamp-Obbema R, Stegwee D. Effect of chloramphenicol on the development of proplastids in *Euglena gracilis*. Z Für Pflanzenphysiol. 1974;73(5):430–8. https://doi.org/10.1016/S0044-328X(74)80112-1.
67. Davis B, Merrett MJ. The glycolate pathway and photosynthetic competence in *Euglena*. Plant Physiol. 1975;55(1):30–4. https://doi.org/10.1104/pp.55.1.30.
68. Kim S-H, Kang P-A, Han K, Lee S-W, Rhee S. Crystal structure of chloramphenicol-metabolizing enzyme EstDL136 from a metagenome. PLOS ONE. 2019;14(1):e0210298. https://doi.org/10.1371/journal.pone.0210298.
69. Nakano H, Matsuhashi Y, Takeuchi T, Umezawa H. Distribution of chloramphenicol acetyltransferase and chloramphenicol-3-acetate esterase among *Streptomyces* and *Corynebacterium*. J Antibiot (Tokyo). 1977;30(1):76–82. https://doi.org/10.7164/antibiotics.30.76.

70. Ebringer L, Krajčovič J, Polónyi J, Lahitová N, Doupovcová M, Dobias J. Tetracycline reduces fluoroquinolones-induced bleaching of *Euglena gracilis*. Mutat Res Genet Toxicol. 1996;340(2):141–9. https://doi.org/10.1016/S0165-1110(96)90045-7.
71. Nguyen F, Starosta AL, Arenz S, Sohmen D, Dönhöfer A, Wilson DN. Tetracycline antibiotics and resistance mechanisms. Biol Chem. 2014;395(5):559–75. https://doi.org/10.1515/hsz-2013-0292.
72. Ebringer L, Nemec P, Santová H, Foltínová P. Changes of the plastid system of *Euglena gracilis* induced with streptomycin and dihydrostreptomycin. Arch Für Mikrobiol. 1970;73(3):268–80. https://doi.org/10.1007/BF00410628.
73. Zahalsky AC, Hutner SH, Keane M, Burger RM. Bleaching *Euglena gracilis* with antihistamines and streptomycin-type antibiotics. Arch Für Mikrobiol. 1962;42(1):46–55. https://doi.org/10.1007/BF00425189.
74. Kazamia E, Czesnick H, Nguyen TTV, Croft MT, Sherwood E, Sasso S, *et al*. Mutualistic interactions between vitamin B_{12}-dependent algae and heterotrophic bacteria exhibit regulation. Environ Microbiol. 2012;14(6):1466–76. https://doi.org/10.1111/j.1462-2920.2012.02733.x.
75. Liba CM, Ferrara FIS, Manfio GP, Fantinatti-Garboggini F, Albuquerque RC, Pavan C, *et al*. Nitrogen-fixing chemo-organotrophic bacteria isolated from cyanobacteria-deprived lichens and their ability to solubilize phosphate and to release amino acids and phytohormones. J Appl Microbiol. 2006;101(5):1076–86. https://doi.org/10.1111/j.1365-2672.2006.03010.x.
76. Amin SA, Hmelo LR, Van Tol HM, Durham BP, Carlson LT, Heal KR, *et al*. Interaction and signalling between a cosmopolitan phytoplankton and associated bacteria. Nature. 2015;522(7554):98–101. https://doi.org/10.1038/nature14488.
77. Seymour JR, Amin SA, Raina JB, Stocker R. Zooming in on the phycosphere: The ecological interface for phytoplankton-bacteria relationships. Nat Microbiol. 2017;2. https://doi.org/10.1038/nmicrobiol.2017.65.
78. Brussaard C, Riegman R. Influence of bacteria on phytoplankton cell mortality with phosphorus or nitrogen as the algal-growth-limiting nutrient. Aquat Microb Ecol. 1998;14:271–80. https://doi.org/10.3354/ame014271.
79. Kranner I, Cram WJ, Zorn M, Wornik S, Yoshimura I, Stabentheiner E, *et al*. Antioxidants and photoprotection in a lichen as compared with its isolated symbiotic partners. Proc Natl Acad Sci. 2005;102(8):3141–6. https://doi.org/10.1073/pnas.0407716102.
80. Grube M, Wedin M. Lichenized fungi and the evolution of symbiotic organization. Microbiol Spectr. 2016;4(6). https://doi.org/10.1128/microbiolspec.FUNK-0011-2016.
81. Krespach MKC, García-Altares M, Flak M, Hanno Schoeler, Scherlach K, Netzker T, *et al*. Lichen-like association of *Chlamydomonas reinhardtii* and *Aspergillus nidulans* protects algal cells from bacteria. ISME J. 2020;14(11):2794–805. https://doi.org/10.1038/s41396-020-0731-2.
82. Park D, Yun Y-S, Hye Jo J, Park JM. Mechanism of hexavalent chromium removal by dead fungal biomass of *Aspergillus niger*. Water Res. 2005;39(4):533–40. https://doi.org/10.1016/j.watres.2004.11.002.
83. Shen L, Li Z, Wang J, Liu A, Li Z, Yu R, *et al*. Characterization of extracellular polysaccharide/protein contents during the adsorption of Cd(II) by *Synechocystis* sp.

PCC6803. Environ Sci Pollut Res. 2018;25(21):20713–22. https://doi.org/10.1007/s11356-018-2163-3.
84. Wang J, Tian Q, Cui L, Cheng J, Zhou H, Zhang Y, *et al*. Synergism and mutualistic interactions between microalgae and fungi in fungi-microalgae symbiotic system. Bioresour Technol. 2022;361:127728. https://doi.org/10.1016/j.biortech.2022.127728.
85. Rehman A. Heavy metals uptake by *Euglena proxima* isolated from tannery effluents and its potential use in wastewater treatment. Russ J Ecol. 2011;42(1):44–9. https://doi.org/10.1134/S1067413611010085.
86. Salgueiro JL, Pérez L, Maceiras R, Sánchez A, Cancela A. Bioremediation of wastewater using *Chlorella Vulgaris* microalgae: Phosphorus and organic matter. Int J Environ Res. 2016;10(3):465–70.
87. Waluyo L, Prihanta W, Bachtiar Z, Permana TI. Potential bioremediation of lead (Pb) using marine microalgae *Nannochloropsis oculata*. Tangerang Selatan, Indonesia; 2020. p. 040088.
88. Znad H, Al Ketife AMD, Judd S, AlMomani F, Vuthaluru HB. Bioremediation and nutrient removal from wastewater by *Chlorella vulgaris*. Ecol Eng. 2018;110:1–7. https://doi.org/10.1016/j.ecoleng.2017.10.008.
89. Ayangbenro AS, Babalola OO, Aremu OS. Bioflocculant production and heavy metal sorption by metal resistant bacterial isolates from gold mining soil. Chemosphere. 2019;231:113–20. https://doi.org/10.1016/j.chemosphere.2019.05.092.
90. Lal A, Banerjee S, Das D. *Aspergillus* sp. assisted bioflocculation of *Chlorella* MJ 11/11 for the production of biofuel from the algal-fungal co-pellet. Sep Purif Technol. 2021;272:118320. https://doi.org/10.1016/J.SEPPUR.2021.118320.
91. Mujtaba G, Rizwan M, Lee K. Simultaneous removal of inorganic nutrients and organic carbon by symbiotic co-culture of *Chlorella vulgaris* and *Pseudomonas putida*. Biotechnol Bioprocess Eng. 2015;20(6):1114–22. https://doi.org/10.1007/s12257-015-0421-5.
92. Nazari MT, Freitag JF, Cavanhi VAF, Colla LM. Microalgae harvesting by fungal-assisted bioflocculation. Rev Environ Sci Biotechnol. 2020;19(2):369–88. https://doi.org/10.1007/s11157-020-09528-y.
93. Zhang Z, Nair S, Tang L, Zhao H, Hu Z, Chen M, *et al*. Long-term survival of S*ynechococcus* and heterotrophic bacteria without external nutrient supply after changes in their relationship from antagonism to mutualism. mBio. 2021;12(4). https://doi.org/10.1128/mBio.01614-21.
94. Wang J, Chen R, Fan L, Cui L, Zhang Y, Cheng J, *et al*. Construction of fungi-microalgae symbiotic system and adsorption study of heavy metal ions. Sep Purif Technol. 2021;268(April):118689. https://doi.org/10.1016/j.seppur.2021.118689.
95. Rubiyatno, Mori K, Inoue D, Kim S, Yu J, Lee T, *et al*. Isolation and characterization of *Euglena gracilis*-associated bacteria, *Enterobacter* sp. CA3 and *Emticicia* sp. CN5, capable of promoting the growth and paramylon production of *E. gracilis* under mixotrophic cultivation. Microorganisms. 2021;9(7):1496. https://doi.org/10.3390/microorganisms9071496.
96. Andresen E, Küpper H. Cadmium toxicity in plants. In: Sigel A, Sigel H, Sigel RK, editors. Cadmium: From Toxicity to Essentiality. Dordrecht: Springer Netherlands; 2013. p. 395–413.

97. Choppala G, Saifullah, Bolan N, Bibi S, Iqbal M, Rengel Z, *et al*. Cellular mechanisms in higher plants governing tolerance to cadmium toxicity. Crit Rev Plant Sci. 2014;33(5):374–91. https://doi.org/10.1080/07352689.2014.903747.
98. Jamers A, Blust R, De Coen W, Griffin JL, Jones OAH. An omics based assessment of cadmium toxicity in the green alga *Chlamydomonas reinhardtii*. Aquat Toxicol. 2013;126:355–64. https://doi.org/10.1016/j.aquatox.2012.09.007.
99. Trevors JT, Stratton GW, Gadd GM. Cadmium transport, resistance, and toxicity in bacteria, algae, and fungi. Can J Microbiol. 1986;32(6):447–64. https://doi.org/10.1139/m86-085.
100. Du J, Qiu B, Pedrosa Gomes M, Juneau P, Dai G. Influence of light intensity on cadmium uptake and toxicity in the cyanobacteria *Synechocystis* sp. PCC6803. Aquat Toxicol. 2019;211:163–72. https://doi.org/10.1016/j.aquatox.2019.03.016.
101. Grajek H, Rydzyński D, Piotrowicz-Cieślak A, Herman A, Maciejczyk M, Wieczorek Z. Cadmium ion-chlorophyll interaction – Examination of spectral properties and structure of the cadmium-chlorophyll complex and their relevance to photosynthesis inhibition. Chemosphere. 2020;261:127434. https://doi.org/10.1016/j.chemosphere.2020.127434.
102. Zhou W, Qiu B. Effects of cadmium hyperaccumulation on physiological characteristics of *Sedum alfredii* Hance (Crassulaceae). Plant Sci. 2005;169(4):737–45. https://doi.org/10.1016/j.plantsci.2005.05.030.
103. Ishfaq M, Wang Y, Yan M, Wang Z, Wu L, Li C, *et al*. Physiological essence of magnesium in plants and its widespread deficiency in the farming system of China. Front Plant Sci. 2022;13:802274. https://doi.org/10.3389/fpls.2022.802274.
104. Jiang Y, Zhu Y, Hu Z, Lei A, Wang J. Towards elucidation of the toxic mechanism of copper on the model green alga *Chlamydomonas reinhardtii*. Ecotoxicology. 2016;25(7):1417–25. https://doi.org/10.1007/s10646-016-1692-0.
105. Ebringer L, Mego JL, Jurášek A. Mitomycins and the bleaching of *Euglena gracilis*. Arch Für Mikrobiol. 1969;64(3):229–34. https://doi.org/10.1007/BF00425628.
106. Ebringer L. Are plastids derived from prokaryotic micro-organisms? Action of antibiotics on chloroplasts of *Euglena gracilis*. J Gen Microbiol. 1972;71(1):35–52. https://doi.org/10.1099/00221287-71-1-35.
107. Scott NS. Precursors of chloroplast ribosomal RNA in *Euglena gracilis*. Phytochemistry. 1976;15(8):1207–13. https://doi.org/10.1016/0031-9422(76)85079-0.
108. Fu Y, Zhu Y, Dong H, Li J, Zhang W, Shao Y, *et al*. Effects of heavy metals and antibiotics on antibiotic resistance genes and microbial communities in soil. Process Saf Environ Prot. 2023;169:418–27. https://doi.org/10.1016/j.psep.2022.11.020.
109. Khurana P, Pulicharla R, Kaur Brar S. Antibiotic-metal complexes in wastewaters: Fate and treatment trajectory. Environ Int. 2021;157:106863. https://doi.org/10.1016/j.envint.2021.106863.
110. Grenson M. Physiology and cytology of chloroplast formation and "loss" in *Euglena*. International Review of Cytology. Elsevier; 1964. p. 37–59.
111. Khatiwada B, Hasan MT, Sun A, Kamath KS, Mirzaei M, Sunna A, *et al*. Proteomic response of *Euglena gracilis* to heavy metal exposure – Identification of key proteins involved in heavy metal tolerance and accumulation. Algal Res. 2020;45(June 2019):101764. https://doi.org/10.1016/j.algal.2019.101764.

112. Bansfield D, Spilling K, Mikola A, Piiparinen J. Bioflocculation of *Euglena gracilis* via direct application of fungal filaments: A rapid harvesting method. J Appl Phycol. 2022;34(1):321–34. https://doi.org/10.1007/s10811-021-02651-5.
113. Bhattacharya A, Malik A, Malik HK. A mathematical model to describe the fungal assisted algal flocculation process. Bioresour Technol. 2017;244:975–81. https://doi.org/10.1016/J.BIORTECH.2017.08.062.
114. Gultom S, Hu B. Review of microalgae harvesting via co-pelletization with filamentous fungus. Energies. 2013;6(11):5921–39. https://doi.org/10.3390/en6115921.
115. Wyatt KH, Seballos RC, Shoemaker MN, Brown SP, Chandra S, Kuehn KA, *et al*. Resource constraints highlight complex microbial interactions during lake biofilm development. J Ecol. 2019;107(6):2737–46. https://doi.org/10.1111/1365-2745.13223.
116. Morales-Oyervides L, Ruiz-Sánchez JP, Oliveira JC, Sousa-Gallagher MJ, Méndez-Zavala A, Giuffrida D, *et al*. Biotechnological approaches for the production of natural colorants by *Talaromyces*/*Penicillium*: A review. Biotechnol Adv. 2020;43:107601. https://doi.org/10.1016/j.biotechadv.2020.107601.
117. Kennes C, Veiga MC. Fungal biocatalysts in the biofiltration of VOC-polluted air. J Biotechnol. 2004;113(1–3):305–19. https://doi.org/10.1016/j.jbiotec.2004.04.037.
118. Tokuhisa Y, Hagiya Y, Hiruma M, Nishimura K. Phaeohyphomycosis of the face caused by *Exophiala oligosperma*: Facial phaeohyphomycosis caused by *E. oligosperma*. Mycoses. 2011;54(4):e240–3. https://doi.org/10.1111/j.1439-0507.2009.01845.x.
119. Koolen HHF, Menezes LS, Souza MP, Silva FMA, Almeida FGO, Souza AQLD, *et al*. *Talaroxanthone*, a novel xanthone dimer from the endophytic fungus *Talaromyces* sp. associated with *Duguetia stelechantha* (Diels) R. E. Fries. J Braz Chem Soc. 2013. https://doi.org/10.5935/0103-5053.20130104.
120. Yilmaz N, Houbraken J, Hoekstra ES, Frisvad JC, Visagie CM, Samson RA. Delimitation and characterisation of *Talaromyces purpurogenus* and related species. Persoonia - Mol Phylogeny Evol Fungi. 2012;29(1):39–54. https://doi.org/10.3767/003158512X659500.
121. Guerra Sierra BE, Arteaga-Figueroa LA, Sierra-Pelaéz S, Alvarez JC. *Talaromyces santanderensi*s: A new cadmium-tolerant fungus from cacao soils in Colombia. J Fungi. 2022;8(10):1042. https://doi.org/10.3390/jof8101042.
122. Nam I-H, Murugesan K, Ryu J, Kim JH. Arsenic (As) removal using *Talaromyces* sp. KM-31 isolated from As-contaminated mine soil. Minerals. 2019;9(10):568. https://doi.org/10.3390/min9100568.
123. Priyanka, Dwivedi SK. Hexavalent chromium (Cr^{+6}) detoxification potential and stress response of fungus *Talaromyces pinophillus* isolated from tannery wastewater. Environ Adv. 2023;13:100417. https://doi.org/10.1016/j.envadv.2023.100417.
124. Ajimura M, Leem SH, Ogawa H. Identification of new genes required for meiotic recombination in *Saccharomyces cerevisiae*. Genetics. 1993;133(1):51–66. https://doi.org/10.1093/genetics/133.1.51.
125. Granot D, Snyder M. Carbon source induces growth of stationary phase yeast cells, independent of carbon source metabolism. Yeast. 1993;9(5):465–79. https://doi.org/10.1002/yea.320090503.

126. Mano Y, Kobayashi TJ, Nakayama J, Uchida H, Oki M. Single cell visualization of yeast gene expression shows correlation of epigenetic switching between multiple heterochromatic regions through multiple generations. PLoS Biol. 2013;11(7):e1001601. https://doi.org/10.1371/journal.pbio.1001601.
127. Parry JM, Zimmerman FK. The detection of monosomic colonies produced by mitotic chromosome non-disjunction in the yeast *Saccharomyces cerevisiae*. Mutat Res Mol Mech Mutagen. 1976;36(1):49–66. https://doi.org/10.1016/0027-5107(76)90020-8.
128. Vyas VK, Barrasa MI, Fink GR. A *Candida albicans* CRISPR system permits genetic engineering of essential genes and gene families. Sci Adv. 2015;1(3):e1500248. https://doi.org/10.1126/sciadv.1500248.
129. Tam E, Tsang C-C, Lau S, Woo P. Polyketides, toxins and pigments in *Penicillium marneffei*. Toxins. 2015;7(11):4421–36. https://doi.org/10.3390/toxins7114421.
130. Woo PCY, Lam C-W, Tam EWT, Leung CKF, Wong SSY, Lau SKP, *et al*. First discovery of two polyketide synthase genes for mitorubrinic acid and mitorubrinol yellow pigment biosynthesis and implications in virulence of *Penicillium marneffei*. PLoS Negl Trop Dis. 2012;6(10):e1871. https://doi.org/10.1371/journal.pntd.0001871.
131. Wang F, Han R, Chen S. An overlooked and underrated endemic mycosis—Talaromycosis and the pathogenic fungus *Talaromyces marneffei*. Clin Microbiol Rev. 2023;36(1):e00051-22. https://doi.org/10.1128/cmr.00051-22.
132. Sheng L, Shen Q, Zhou J. Efficacy of different antifungal drugs as initial treatment for patients with talaromycosis: A systematic review and meta-analysis. J Med Mycol. 2021;31(1):101108. https://doi.org/10.1016/j.mycmed.2020.101108.
133. Mussagy CU, Oshiro AA, Lima CA, Amantino CF, Primo FL, Santos-Ebinuma VC, *et al*. Natural fluorescent red colorants produced by *Talaromyces amestolkiae* as promising coloring agents for custom-made latex gloves. J Ind Eng Chem. 2023;119:357–66. https://doi.org/10.1016/j.jiec.2022.11.056.
134. Zaccarim BR, De Oliveira F, Passarini MRZ, Duarte AWF, Sette LD, Jozala AF, *et al*. Sequencing and phylogenetic analyses of I*alaromyces amestolkiae* from amazon: A producer of natural colorants. Biotechnol Prog. 2019;35(1):e2684. https://doi.org/10.1002/btpr.2684.
135. Xiao Y, Chen R, Chen L, Yang B, Jiang L, Fang J. Endophytic fungus *Talaromyces* sp. MR1 promotes the growth and cadmium uptake of *Arabidopsis thaliana* L. under cadmium stress. Curr Microbiol. 2023;80(11):346. https://doi.org/10.1007/s00284-023-03453-3.
136. Emery RJN, Longnecker NE, Atkins CA. Branch development in *Lupinus angustifolius* L. II. relationship with endogenous ABA, IAA and cytokinins in axillary and main stem buds. J Exp Bot. 1998;49(320):555–62. https://doi.org/10.1093/jxb/49.320.555.
137. Sudová R, Vosátka M. Differences in the effects of three arbuscular mycorrhizal fungal strains on P and Pb accumulation by maize plants. Plant Soil. 2007;296(1–2):77–83. https://doi.org/10.1007/s11104-007-9291-8.
138. Velivelli SLS, Sessitsch A, Prestwich BD. The role of microbial inoculants in integrated crop management systems. Potato Res. 2014;57(3–4):291–309. https://doi.org/10.1007/s11540-014-9278-9.

139. Yang G-L, Zheng M-M, Tan A-J, Liu Y-T, Feng D, Lv S-M. Research on the mechanisms of plant enrichment and detoxification of cadmium. Biology. 2021;10(6):544. https://doi.org/10.3390/biology10060544.
140. Du Z-Y, Zienkiewicz K, Pol NV, Ostrom NE, Benning C, Bonito GM. Algal-fungal symbiosis leads to photosynthetic mycelium. Front Plant Sci. 2019;12. https://doi.org/10.7554/eLife.47815.001.
141. Li B, Zhang T, Yang Z. Immobilizing unicellular microalga on pellet-forming filamentous fungus: Can this provide new insights into the remediation of arsenic from contaminated water? Bioresour Technol. 2019;284:231–9. https://doi.org/10.1016/j.biortech.2019.03.128.
142. Li L, Liu Z, Zhang M, Meng D, Liu X, Wang P, *et al*. Insights into the metabolism and evolution of the genus acidiphilium, a typical acidophile in acid mine drainage. mSystems. 2020;5(6):e00867-20. https://doi.org/10.1128/mSystems.00867-20.
143. Xu L, Gu W, Bai J. *Thiobacillus acidophilus* removes lead and copper from wastewater containing low concentration of heavy metals. IOP Conf Ser Earth Environ Sci. 2021;769(2):022039. https://doi.org/10.1088/1755-1315/769/2/022039.
144. Yang W, Song W, Li J, Zhang X. Bioleaching of heavy metals from wastewater sludge with the aim of land application. Chemosphere. 2020;249:126134. https://doi.org/10.1016/j.chemosphere.2020.126134.
145. Johnson DB. Extremophiles: Acidic environments. Encyclopedia of Microbiology. Elsevier; 2009. p. 107–26.
146. Rawlings D*E*. Heavy metal mining using microbes. Annu Rev Microbiol. 2002;56(1):65–91. https://doi.org/10.1146/annurev.micro.56.012302.161052.
147. Priya A, Hait S. Biometallurgical recovery of metals from waste printed circuit boards using pure and mixed strains of *Acidithiobacillus ferrooxidans* and *Acidiphilium acidophilum*. Process Saf Environ Prot. 2020;143:262–72. https://doi.org/10.1016/j.psep.2020.06.042.
148. Johnson DB, Bridge TAM. Reduction of ferric iron by acidophilic heterotrophic bacteria: Evidence for constitutive and inducible enzyme systems in *Acidiphilium* spp. J Appl Microbiol. 2002;92(2):315–21. https://doi.org/10.1046/j.1365-2672.2002.01535.x.
149. Liu H, Yin H, Dai Y, Dai Z, Liu Y, Li Q, *et al*. The co-culture of *Acidithiobacillus ferrooxidans* and *Acidiphilium acidophilum* enhances the growth, iron oxidation, and CO_2 fixation. Arch Microbiol. 2011;193(12):857–66. https://doi.org/10.1007/s00203-011-0723-8.
150. Berlanga-Clavero MV, Molina-Santiago C, De Vicente A, Romero D. More than words: The chemistry behind the interactions in the plant holobiont. Environ Microbiol. 2020;22(11):4532–44. https://doi.org/10.1111/1462-2920.15197.
151. Rasmann S, Turlings TC. Root signals that mediate mutualistic interactions in the rhizosphere. Curr Opin Plant Biol. 2016;32:62–8. https://doi.org/10.1016/j.pbi.2016.06.017.
152. Wooldridge SA. Is the coral-algae symbiosis really 'mutually beneficial' for the partners? BioEssays. 2010;32(7):615–25. https://doi.org/10.1002/bies.200900182.
153. Hlabela P, Maree J, Bruinsma D. Barium carbonate process for sulphate and metal removal from mine water. Mine Water Environ. 2007;26(1):14–22. https://doi.org/10.1007/s10230-007-0145-7.

154. Skousen JG, Sexstone A, Ziemkiewicz PF. Acid mine drainage control and treatment. Reclam Drastically Disturb Lands. 2000;(January):131–68. https://doi.org/10.2134/agronmonogr41.c6.
155. Yang W, Tang Q, Wei J, Ran Y, Chai L, Wang H. Enhanced removal of Cd(II) and Pb(II) by composites of mesoporous carbon stabilized alumina. Appl Surf Sci. 2016;369:215–23. https://doi.org/10.1016/j.apsusc.2016.01.151.
156. Das PK, Rani J, Rawat S, Kumar S. Microalgal co-cultivation for biofuel production and bioremediation: Current status and benefits. BioEnergy Res. 2022;15:1–26. https://doi.org/10.1007/s12155-021-10254-8/Published.
157. Hassan Z ul, Ali S, Rizwan M, Ibrahim M, Nafees M, Waseem M. Role of bioremediation agents (bacteria, fungi, and algae) in alleviating heavy metal toxicity. In: Kumar V, Kumar M, Sharma S, Prasad R, editors. Probiotics in Agroecosystem. 2017. p. 517–37.
158. Higgins BT, Gennity I, Fitzgerald PS, Ceballos SJ, Fiehn O, VanderGheynst JS. Algal–bacterial synergy in treatment of winery wastewater. Npj Clean Water. 2018;1(1):6. https://doi.org/10.1038/s41545-018-0005-y.
159. Pei XY, Ren HY, Liu BF. Flocculation performance and mechanism of fungal pellets on harvesting of microalgal biomass. Bioresour Technol. 2021;321:124463. https://doi.org/10.1016/J.BIORTECH.2020.124463.

CHAPTER 3

3.1 PREFACE

Title: Glucose amendments alter cultural and cellular features of FAB (Fungal-Algal-Bacterial) consortium and uncover a link to dynamic hormone shifts

Authors: Emma Kaszecki, R. J. Neil Emery, Barry J. Saville

Reference: This chapter is under review in the journal *FEMS Microbiology Ecology*. The published version may appear different than presented here.

Contributions: Study conception, experimental design, material preparation, data collection, and analysis were carried out by EK. RJNE and BJS contributed to experimental design and funding. The manuscript was written by EK with edits from RJNE and BJS. All authors have approved the final version of the manuscript.

CHAPTER 3

Glucose amendments alter cultural and cellular features of FAB (Fungal-Algal-Bacterial) consortium and uncover a link to dynamic hormone shifts

3.2 ABSTRACT

The fungal-algal-bacterial (FAB) consortium composed of *Euglena mutabilis*, *Talaromyces*, and *Acidiphilium acidophilum* exhibits unique resilience to heavy metal (HM) stress, yet the mechanisms underpinning this tolerance remain undefined. Here, we increased glucose availability in the FAB, which altered community structure, hormone production, and Cd tolerance. Glucose supplementation promoted dense fungal hyphal growth, greater bacterial abundance, and pronounced flocculation, as well as higher *Euglena* cell densities under Cd stress. Hormone profiling revealed elevated extracellular levels of bioactive *trans*-Zeatin (*t*Z) and gibberellin GA_7 – compounds known to promote growth and stress adaptation – specifically in Cd- and glucose-treated cultures. Methyl-thiolated cytokinins (CKs) and jasmonic acid (JA) also accumulated under these conditions, indicating that glucose stimulates coordinated, multi-partner hormonal responses linked to Cd detoxification and sustained growth. Transmission electron microscopy (TEM) identified intracellular bacterial-like structures in *E. mutabilis*, suggesting possible facultative endosymbiosis or phagocytosis that could aid microbial persistence during nutrient limitation. Together, these findings show that glucose shapes both the physical organization and biochemical signalling of the FAB – enhancing fungal, algal, and bacterial performance under HM stress – and provides a framework for designing engineered microbial consortia for bioremediation.

Keywords: Bioremediation · Symbiosis · *Euglena* · Stress Response · Hormones · Microscopy

3.3 INTRODUCTION

Canada is recognized as a leader in the global mining sector, generating $71.9 billion in 2023 through a combination of metal, non-metal, and mineral production [1]. Despite its economic significance, the Canadian mining industry produces over one hundred million metric tonnes of solid waste each year in the form of waste rock and tailings [2]. Although regulatory frameworks and engineering interventions have been implemented to address mining-related environmental impacts [3–5], even the most robust practices cannot guarantee environmental or human safety. The catastrophic failure of the Mount Polley gold and copper mine tailings dam in British Columbia released approximately seventeen million cubic meters of water and eight million cubic meters of tailings into the surrounding environment [6]. The spill prompted a local water use ban and ultimately cost an estimated $70 million in cleanup efforts [6]. Although the Mount Polley failure occurred at an active mining site, it highlighted a broader concern; over 10,000 abandoned mine sites across Canada contain hazardous and toxic waste that remain insufficiently monitored [7]. Traditional restoration practices such as backfilling, adsorption, and permeable reactive barriers can be expensive and inefficient [8,9] contributing to the proliferation of tailings.

Bioremediation offers a cost-effective and environmentally friendly solution to reduce the bioavailability and toxicity of heavy metals (HM) in soil and water systems by harnessing the natural metabolic processes of organisms to immobilize, transform, or remove pollutants from contaminated sites [10]. In recent years, microalgae, fungi, bacteria, and plants have been effectively applied in field-relevant studies to remediate HM-

contaminated environments [11–14]. These efforts have predominantly focused on the application of single organisms, such as *Trichoderma virens* [15] or *Chlorella vulgaris* [16], and aim to improve bioremediation capacity through genetic engineering [17] or by optimizing environmental conditions [18]. Emerging research has shifted from this model to co-culturing organisms to promote metal sequestering [19,20], stimulate microbial growth [21,22], increase secondary metabolite production [23,24], promote flocculation [25,26], and reduce the overall cost of the bioremediation technology [27–29]. These studies typically evaluate the productivity and efficiency of organisms chosen for their complementary individual traits that may enhance performance when co-cultured [26,30,31] disregarding those which are indigenous to contaminated and extreme environments. Microbes isolated from these environments have naturally adapted to withstand harsh conditions, allowing them to remain active in contaminated sites [32–34]. Because native microbes are already adapted to local conditions, they can integrate seamlessly into existing communities, reducing the risk of ecological imbalance and supporting sustainable remediation outcomes [35]. In the present study, the HM tolerance of an intimate relationship between a fungal-algal-bacterial (FAB) consortium isolated from a gold mine tailing in Timmins, Ontario, Canada is investigated. The consortium is comprised of a versatile ascomycete of the genus *Talaromyces*, the acidophilic bacterium *Acidiphilium acidophilum*, and the extremophilic photosynthetic protist *Euglena mutabilis* [36].

Euglenoids are a diverse group of unicellular, flagellated protists renowned for their ecological adaptability [37]. Usually found in freshwater and acidic aquatic environments, they serve as important model organisms in studies of environmental stress responses and

symbiosis [38,39]. Many species, including the widely researched *E. gracilis*, are notable for their dual metabolic capacity – capable of both heterotrophic feeding, common among protists, and photosynthesis via chloroplasts depending on environmental conditions [39]. The photosynthetic capabilities of *E. gracilis*, which resemble those of algae, have propelled its use in research spanning bioremediation, pharmaceuticals, cosmetics, biofuels, and food production [38,40]. Beyond these applications, *E. gracilis* has demonstrated resilience to HMs, synthesizing hormones like abscisic acid (ABA) and cytokinins (CKs) to support its physiological responses [41]. Studies have also shown that *E. gracilis* exhibits enhanced growth and biomass production when cultured with fungi, even when those fungal species were previously thought to inhibit proliferation [42].

These traits observed in *E. gracilis* are not unique to the species and often shared with the more extremophilic *E. mutabilis*, which thrives in harsh environments such as mine tailings, peat bogs, and volcanic lakes [43–46]. Recent investigations revealed that *E. mutabilis* is naturally more tolerant to Cd than *E. gracilis* [47]. When isolated from these extreme environments, *E. mutabilis* is frequently associated with other organisms [48]. The interactions between *E. mutabilis* and its partner organisms permits interkingdom communication [45] and is essential for withstanding harsh conditions [36,48]. The co-isolation of *E. mutabilis* with the acidophilic bacterium *A. acidophilum* from mine tailings is unsurprising, given that *A. acidophilum* is also commonly found in acid mine drainage and mine tailings [49,50]. Like *E. mutabilis*, it exhibits mixotrophic growth, utilizing chemolithotrophic pathways through sulfur compound reduction or heterotrophic metabolism of organic compound sources [50]. In contrast, the fungi of the genus *Talaromyces* are not considered extremophiles but have demonstrated considerable

tolerance to HMs [51–53] and are known to provide growth-promoting and protective benefits when in a symbiotic relationship [54]. Together, these organisms form a naturally occurring FAB consortium capable of withstanding the acidic and HM-rich conditions of mine tailings [36]. Their coordinated resistance and survival strategies in such an extreme environment offer valuable insights into developing more effective, biologically driven approaches for bioremediation.

The present study investigates the mechanisms underlying a natural FAB consortium composed of *E. mutabilis*, *A. acidophilum*, and a fungus from the genus *Talaromyces* isolated from gold mine tailings from Timmins, Ontario. The consortium's tolerance to heavy metals was assessed under exposure to 100 µM $CdCl_2$ – a concentration previously shown to inhibit *Euglena* growth [55,56] – with and without an available heterotrophic carbon source. Culture viability and performance were assessed through cell counts of *E. mutabilis*, chlorophyll content, recovery on non-selective media, and measurements of cellular Cd accumulation. This work also provides the first analysis of hormone production by *E. mutabilis*. The structural and physical associations within the FAB community were also assessed using scanning and transmission electron microscopy, revealing a potential symbiotic relationship. Collectively, these analyses uncovered close microbial associations within the FAB that contribute to its resilience in extreme environments, offering insights that advance the potential applications of natural microbial interactions in bioremediation technologies.

3.4 METHODS

Culture selection and growth conditions of *E. mutabilis*

Field samples of *E. mutabilis* were obtained from the Canadian Phycological Culture Centre (CPCC, University of Waterloo, Canada). The strain of *E. mutabilis* (CPCC 657) exists in a seemingly symbiotic relationship with fungus from the genus *Talaromyces* and the bacterium *Acidiphilium acidophilum*. Stock cultures were grown in modified acid medium (MAM) [46] with modifications recommended by the CPCC and adjusted to a pH of 4.3 [57]. Filter sterilized F/2 nutrient solution was added to autoclaved medium after it cooled. Cultures were grown autotrophically in 250 mL Pyrex Erlenmeyer flasks secured with foam stoppers covered in aluminum foil under standard aeration (100 RPM on a Thermo Fisher Scientific MaxQ 3000 shaker) while cycling light and temperature (16:8 LD cycle at 260 μm s^{-1} m^{-1}; 24°C ± 0.5°C in light and 18°C ± 0.5°C in dark) in a Conviron PCG20 environmental chamber.

Cell counts of *E. mutabilis* from stock cultures were performed using a hemocytometer (Hausser Scientific). A volume of cells from each stock containing 12 x10^6 cells was aliquoted into each 15 mL Falcon tube. Tubes were centrifuged (3,724 RCF for 10 minutes) and the supernatant was discarded. The pellet was inoculated into 250 mL Pyrex Erlenmeyer flasks containing 60 mL of media for a final concentration of 200,000 *E. mutabilis* cells/mL. Control cultures were grown in MAM with 0 g/L of glucose, MAM with 5 g/L of glucose (Fisher Scientific Cat. No. D16-1) (MAM + 5), or MAM with 2.5 g/L of glucose (MAM + 2.5). MAM with 5 g/L of glucose was serially diluted to yield MAM with 2.5 g/L of glucose. Furthermore, cultures were grown in the same three medium

conditions with the addition of 100 µM $CdCl_2$. Each experimental condition was carried out in triplicate.

Flasks were placed in the Conviron PCG20 environmental chamber under the same light and temperature conditions as the stock cultures for 5 days. During the experiment, the flasks were agitated for 1 minute every 24-hours (80 RPM on a Thermo Fisher Scientific MaxQ 3000) but were otherwise unshaken. *E. mutabilis* cell counts, culture chlorophyll content, cellular Cd uptake, and hormone profiles were assessed 1-, 3-, and 5-days post-inoculation. Aliquots from each culture were taken after 1- and 5-days post-inoculation to evaluate the growth recovery of *E. mutabilis* and *Talaromyces* which could not be quantified with a hemocytometer. Cultures were also visualized using a scanning electron microscope (SEM) after 5-days of growth.

Euglena cell viability after Cd exposure

Every 1-, 3-, and 5-days post-inoculation, 100 µL aliquots were taken from each flask and diluted with 400 µL of a 0.4% Trypan Blue solution (Bioshop Cat. No. TRY477.100) in PBS (Bioshop, Cat. No. PBS404.100). Cell viability in *E. mutabilis* was evaluated by Trypan Blue staining, with live and dead cells counted us a hemocytometer (Hausser Scientific) at 10x magnification.

Assessment of post-stress growth

Recovery of *E. mutabilis* and *Talaromyces* were assessed by plating on potato dextrose agar (PDA) plates prepared using a 1.4% (w/v) agar mixture which was sterilized by autoclaving. 15 mL of media was added to each plate (Greiner Bio-One Cat. No.

633181). 100 µL from each culture flask was diluted with 900 µL of sterile 0.9% (w/v) NaCl and 50 µL was added to an agar plate. Plates were sealed with parafilm and incubated at 22℃ in darkness. The number of *E. mutabilis* and *Talaromyces* colony forming units (CFUs) were recorded after 1 and 7 days of growth.

Assessment of chlorophyll content

Chlorophyll content was assessed according to Kaszecki *et al* [36]. Briefly, 500 µL from each flask was aliquoted into 2 mL Eppendorf tubes containing glass beads (Sigma Aldrich Cat. No. G8772) and the media was decanted after centrifugation at 4℃ (maximum speed for 2 minutes). 1 mL of chilled methanol (MeOH) was added to each tube to extract the chlorophyll, and the samples were agitated at 30 Hz for 2 minutes (Retsch Mixer Mill MM 400). After centrifugation to pellet the glass beads (maximum speed for 2 minutes), the MeOH was transferred to a fresh Eppendorf tube, and the extraction was repeated. 200 µL of extracted MeOH was added to three 96-well optic plates (ThermoFisher Scientific Cat. No. 165305) for triplicate readings on a BioTek Synergy HTX Multimode Reader at 652 and 665 nm wavelengths. Chlorophyll content was quantified according to Warren [58] and normalized against *E. mutabilis* cell counts to calculate chlorophyll content per cell.

Cellular Cd accumulation

Samples were extracted according to Metcalfe *et al* [59] with modifications. 1 mL from each flask was added to a 1.5 mL microfuge tube. The supernatant was decanted with a pipette following centrifugation (3,824 RCF for 10 minutes). Cell pellets were washed three times by resuspending in 2 mL of sterile dH_2O, centrifuging, and then decanting the supernatant. After the final wash, 300 µL of 70% (v/v) nitric acid (HNO_3) (Fisher Scientific

Ca. No. A509P500) was added and each tube was placed on a heat block at 95℃ for 20 minutes to digest the pellet. The entire volume of digested sample was diluted in 10.2 mL of sterile dH_2O for a final HNO_3 concentration of 2% (v/v) and filtered through a 0.45 µm polytetrafluoroethylene (PTFE) syringe filter (VWR Cat. No. 76479-004) into a 15 mL Falcon tube. Control media blanks for each condition were extracted in parallel to verify the absence of Cd in the control environment.

Elemental analysis was conducted using an Agilent 8900 ICP-QQQ-MS in the Water Quality Centre (Trent University). Sample introduction was executed using a MicroMist nebulizer (nominal uptake rate: 400 µL min^{-1}) coupled with a Scott double-pass spray chamber to ensure efficient aerosol formation. The instrument was operated with a radio frequency (RF) power of 1550 W and a carrier gas flow rate of 1.05 L min^{-1}, following the General-Purpose Plasma Preset parameters. The sampling depth was set to 10 mm, and an X-type extraction lens was used to optimize ion transmission. Sample introduction into the plasma was facilitated by standard nickel sampler and skimmer cones. Cadmium (Cd) was analyzed in single quadrupole mode using helium (He) as the collision cell gas. Calibration standards were prepared through serial dilution of 1000 ng mL^{-1} single-element standards in 2% HNO_3. Rhodium served as the internal standard and was introduced continuously inline throughout the analysis. All solutions were prepared using high-purity water (18.2 MΩ·cm) and ultrapure HNO_3 to ensure minimal contamination.

Hormone Profiling

Solid phase extraction and purification of hormones

From each flask (3.4 METHODS: Culture selection and growth conditions of *E. mutabilis*), 10 mL of culture was collected into a 50 mL Falcon tube 1-, 3-, and 5-days post-inoculation. The tubes were centrifuged (3,724 RCF for 10 minutes) to form a cell pellet, and the supernatant was decanted into a new 50 mL Falcon tube. From there, the supernatant was sterilized through a 0.2 µm polyethersulfone (PES) syringe filter (Fisher Scientific Cat. No. 13-1001-06) into a fresh 50 mL Falcon tube. Media blanks were prepared the same way at the same time. The cell pellets were washed by resuspension in sterile 0.9% NaCl, centrifuged, and the supernatant discarded. Prepared samples were flash-frozen with liquid nitrogen (LN_2), freeze-dried (LabConco Free Zone lyophilizer; Kansas City, MO, USA), and stored at -80°C.

Hormone extractions were performed sequentially to obtain distinct hormone fractions, following modified methods previously published [60,61]. This approach enabled the extraction of 35 CKs and acidic hormones – including abscisic acid (ABA), gibberellins (GA_1, GA_4, GA_7), indole-3-acetic acid (IAA), jasmonic acid (JA), and salicylic acid (SA) – from a single sample (Table S3.2).

To facilitate hormone quantification via the isotope dilution technique, internal standards (IS) of deuterated hormones were added to each sample in 2 mL of 50% ice-cold acetonitrile (ACN). These included 60.9 ng ABA ($[^2H_4]$ ABA) (PBI, Saskatoon, Canada), 10 ng each of IAA and SA (OLChemim, Olomouc, Czech Republic), and 10 ng each of the gibberellins GA_1, GA_4, GA_7, GA_9, and GA_{20}. Additionally, 10 ng of deuterated CK

standards were included, covering aromatic, methylthiolated, and glucoside forms (Table S3.2). While JA was not included as an internal standard, [$^2H_4$] ABA was used for JA quantification [41].

Dried cell pellets were resuspended with ice-cold 50% ACN in 2 mL Eppendorf tubes and agitated with two zirconium beads (Comeau Technique Ltd.) at 25 Hz for 5 minutes (Retsch Mixer Mill MM 400) in a 4°C cold room. Supernatant and media blanks were resuspended in ice-cold 50% ACN and vortexed to mix. All samples were centrifuged and divided equally, with 1 mL of ACN transferred to a fresh 2 mL Eppendorf tube for acidic hormone analysis and the remaining 1 mL transferred to another tube for CK analysis. Additionally, three method-blank samples were extracted in parallel to the samples.

Samples designated for acidic hormone analysis were purified through HLB cartridges (Canadian Life Sciences Cat. No. VO34445). First, the columns were preconditioned under vacuum with analytical grade MeOH, B-Pure water (18.2 MΩ·cm), and 50% aqueous (v/v) ACN. After conditioning, samples were centrifuged (10 minutes at maximum speed), and the supernatant was added to each cartridge and eluted into 5 mL tubes by gravity followed with a final wash of 2 mL of 30% aqueous (v/v) ACN. Tubes for acidic hormones and CKs were evaporated to dryness in a vacuum concentrator (Savant UVS400) at ambient temperature.

Once dried, acidic hormone samples were derivatized and CK samples were stored at -20°C. To each sample for acidic hormones, 75 µL of 1-propanol, 20 µL of B-Pure water, 5 µL of 500 mM bromocholine (TCI America Cat. No. B0577) in 70% ACN, and 1 µL of

triethylamine (Fisher Scientific Cat. No. O4884-100) were added. Samples were incubated in a water bath at 80℃ for 130 minutes and then chilled on ice for 1 hour before being evaporated to dryness in a vacuum concentrator at ambient temperature. Dry samples were stored at -20℃ ahead of analysis.

Samples designated for CK analysis were redissolved in 1 mL of 1M Formic Acid (HCOOH) in preparation for purification through MCX cartridges (Canadian Life Sciences Cat. No. VO54445). Under vacuum, the columns were preconditioned with MeOH and HCOOH. After conditioning, samples were centrifuged (10 minutes at maximum speed), and the supernatant was added to each cartridge and eluted by gravity. With the vacuum reconnected, the column was then equilibrated with 5 mL of HCOOH and 5 mL of MeOH. 5 mL of 0.35M ammonium hydroxide (NH_4OH) was eluted through the cartridge under vacuum and collected in a 5 mL tube. This fraction was used to assess the CKs in their nucleotide (NT) form. Next, 5 mL of 0.35 M NH_4OH in 60% MeOH (H_2O:MeOH 40:60 v/v) was eluted through the cartridge under vacuum and collected in a 5 mL tube. This fraction was used to assess CKs in their freebase (FB) and riboside (RB) forms. All collected fractions were evaporated to dryness in a vacuum concentrator at ambient temperature.

The dried samples for the FB fraction were stored at -20℃ ahead of analysis and the NT fraction was dephosphorylated to enable detection as ribosides by the ESI-MS/MS [62]. Dried NT samples were redissolved in 1 mL of 0.1M ethanolamine (Sigma Aldrich Cat. No. E9508-100) and 3 units (12 μL) of phosphatase enzyme mix (New England

Biolabs Cat. No. M0525L). Samples were incubated overnight at 37°C and then evaporated to dryness in a vacuum concentrator at ambient temperature.

Dried NT samples were redissolved in 1.5 mL of B-Pure water in preparation for purification with C18 cartridges (Canadian Life Science Cat. No. IS72006). The columns were first preconditioned with 3 mL of MeOH and 6 mL of B-Pure water under vacuum. Then, samples were centrifuged (10 minutes at maximum speed), and the supernatant was added to each cartridge and eluted by gravity before being washed with 3 mL of B-Pure water. Final NT samples were collected by washing the column with 1.25 mL of 80% MeOH into 2 mL Eppendorf tubes. Collected samples were then evaporated to dryness in a vacuum concentrator at ambient temperature and stored at -20°C.

All final hormone fractions were redissolved in 300 µL of 0.08% acetic acid (AcOH) in 5% ACN. Samples were quickly vortexed to mix and centrifuged (3,724 RCF for 10 minutes) to remove any solid particles before transferring 250 µL into 300 µL glass inserts in clear mass spectrometry vials. Samples were prepared the one day before analysis and stored overnight at -20°C.

Hormone analysis by ultra high-performance liquid chromatography-electrospray ionization tandem mass spectrometry (UHPLC-ESI-MS/MS)

Purified samples were analyzed for hormone content using ultra high-performance liquid chromatography-electrospray ionization-tandem mass spectrometry (UHPLC-(ESI)-MS/MS; Thermo Q-Exactive quadrupole orbitrap coupled with Thermo Dionex Ultimate 3000 UHPLC) as previously described [62]. Chromatographic separation of hormones was

performed using an HGP-3400RS dual pump and a WPS-3000 autosampler, equipped with a Kinetex C18 column (2.1 mm internal diameter × 50 mm length, 2.6 µm particle size; Phenomenex, Torrance, CA, USA). The column was operated at an approximate room temperature of 22°C. Samples were injected at a volume of 25 µL and all hormone fractions were eluted using solution A (ddH_2O with 0.08% CH_3COOH) and solution B (CH_3CN with 0.08% CH_3COOH) at a flow rate of 0.5 mL/min using a multi-step gradient. The initial condition of 5% solution B was maintained for 0.5 minutes, followed by a linear increase to 45% B over 4.5 minutes, then further increased to 95% B over the next 6.5 minutes. This condition was held for 1 minute before returning to the starting condition for 2 minutes to allow for column re-equilibration for a total run time of 8.2 minutes.

Instrument control and data acquisition were managed using Chromeleon 6.8 Chromatography Data System software (ThermoScientific, Ottawa, ON, Canada).

Quantification of hormone profiles

Quantification of hormone peaks were assessed using Xcalibur 3.0.63 software (ThermoFisher Scientific). Peaks corresponding to metabolites were initially identified by their monoisotopic mass as protonated molecules $[M+H]^+$ and by comparing their retention time (RT) to those of the IS. Extracted ion chromatograms (XICs) were generated for each hormone using the accurate masses of the two most intense fragment ions along with the unfragmented precursor ion, applying a mass tolerance of 3 ppm. Quantification was based on the area under the peak of each XIC. Quantified peaks from supernatant samples were normalized against the number of *E. mutabilis* cells in each volume of media (10 mL) and quantified peaks from pellet samples were normalized against dried weight.

Visualization with SEM

Samples of *E. mutabilis* grown in MAM in the presence and absence of Cd were prepared for SEM according to the air-drying technique for cultured micro-organisms outlined by Murtey and Ramasamy [63] with modifications. 1 mL of culture was aliquoted into 1.5 mL microfuge tubes. The supernatant was decanted with a p200 after centrifugation (3,824 RCF for 10 minutes) and the pellet was resuspended in 500 µL of 2.5% glutaraldehyde (Sigma Aldrich Cat. No. G5882-100ML) prepared in a 0.1 mol/L phosphate buffer (pH 7.2) for 16 hours at room temperature. After fixation, the sample was centrifuged (10,621 RCF for 2 minutes) and the glutaraldehyde was removed using a p200. The pellet was resuspended in 1 mL of the 0.1 mol/L phosphate buffer for 10 minutes, centrifuged to decant, and the wash step was repeated. The pellet was then dehydrated in 200 µL of EtOH through an EtOH series (35% EtOH in dH_2O, 50% EtOH in dH_2O, 75% EtOH in dH_2O, 95% EtOH in dH_2O, 2 x 100% EtOH) followed by two washes with 200 µL of HMDS (Sigma Aldrich Cat. No. 440191-100ML). At each step, the solvent was added to the tubes for 10 minutes after which the tubes were centrifuged and the supernatant discarded. After the final HMDS wash, the sample tubes were left open in a fume hood overnight to air dry.

Dehydrated samples were visualized with a Hitachi FlexSEM 1000 II connected to an energy dispersive x-ray spectrometer (QUANTAX Compact 30 with 129eV Xflash Detector 630Mini) at 15.0 kV.

Visualization with TEM

1 mL of cultures grown in MAM and MAM + 100 µM $CdCl_2$ were aliquoted into 1.5 mL microfuge tubes. The supernatant was decanted with a p200 following centrifugation, and the pellet was resuspended in 500 µL of 2.5% glutaraldehyde (Sigma Aldrich Cat. No. G5882-100ML) prepared in a 0.1 mol/L phosphate buffer (pH 7.2) for 24 hours at room temperature. Sample preparation and embedding were performed by the Cellular and Molecular Electron Microscopy core (The Hospital for Sick Children, Toronto, Canada). The fixed tissue was sectioned into 2 mm cubes and rinsed with 0.1 M sodium cacodylate buffer with 0.2 M sucrose (pH 7.3) for 10 minutes. Samples were post-fixed in 1% osmium tetroxide in the same buffer for 1.5 hours, then rinsed again with the sucrose-buffer rinse. Dehydration was performed through a graded EtOH series (70% EtOH in dH_2O, 90% EtOH in dH_2O, 3 x 100% EtOH) followed by two washes with propylene oxide. Samples were then infiltrated with a 50:50 mixture of propylene oxide and Spurr resin for 1 hour, followed by two washes of pure Spurr resin (1 hour and overnight) and then embedded in molds and polymerized at 65 °C overnight. Ultrathin sections (90 nm) were cut on an ultramicrotome using a diamond knife, mounted on copper grids, and contrasted with uranyl acetate and lead citrate before imaging on a Hitachi HT7800.

Statistical analysis

Differences in *E. mutabilis* cell counts, chlorophyll content, and hormone content were compared each day using a one-way ANOVA ($p < 0.05$) followed by Tukey's Honest Significant Difference (HSD) test. Blank media samples containing each glucose

concentration with and without Cd were processed and analyzed using the same methods to remove background hormone levels (Table S3.2).

3.5 RESULTS AND DISCUSSION

To evaluate the Cd tolerance and synergistic interactions within the FAB consortium, a series of physiological, cellular, and molecular analyses were conducted. Glucose supplementation was used to perturb the FAB consortium displaying enhancements of the growth and viability of *E. mutabilis*, particularly under Cd stress. This was observed through increased cell counts, flocculation, and chlorophyll content. Recovery assays further confirmed the importance of glucose in supporting the growth of *E. mutabilis* and its associated microbial partners, *A. acidophilum* and *Talaromyces*. Hormone profiling revealed dynamic changes in cytokinins (CKs), gibberellins (GAs), jasmonic acid (JA), and salicylic acid (SA) – modulated by both glucose availability and Cd exposure. Electron microscopy provided structural insights into the FAB, illustrating close associations among consortium members and intracellular features consistent with endosymbiotic retention. Together, these data suggest that FAB consortia deploy cooperative and metabolically adaptive strategies to persist in HM-polluted environments.

FAB growth and chlorophyll content are dependent on the presence of glucose and Cd

After 5-days of growth in liquid media without standard aeration, the FAB cultures supplemented with glucose contained flocs (Figure 3.1). Both 5 g/L and 2.5 g/L of glucose also promoted increased fungal biomass, compared to cultures without glucose. The addition of Cd to cultures with glucose supplementation did not alter the level of flocculation and the *E. mutabilis* cells remained imbedded in what appears to be a fungal-

derived mycelial mat with extracellular material (Figure 3.1de). In contrast, when cultured without glucose supplementation either in the presence or absence of Cd, the *E. mutabilis* cells were either free floating or more loosely associated with the other FAB members and the overall culture had a diffuse green cast that was not present with glucose supplementation (Figure 3.1cf). Additionally, cultures lacking both glucose and Cd displayed more limited biomass, and those exposed to Cd without glucose showed the most suppressed growth (Figure 3.2). These observations suggest a glucose- and Cd-dependent bioflocculation mechanism within the FAB, prompting comparison to existing microbial flocculation strategies.

Bioflocculation technologies are increasingly explored for wastewater treatments, biomass harvesting, and bioremediation [64,65]. Most current bioflocculation systems utilize bacterial biofilms or algal extracellular polymeric substances (EPS) that aggregate particles to facilitate separation of solid and organic matter from liquid phases [66,67]; however, these often require precise environmental conditions and are limited by low mechanical stability or slow processing rates [68–71]. To overcome such limitations, co-culturing approaches have been investigated, wherein one organism enhances the flocculating efficiency of another. For instance, the surface of *Chlorella vulgaris* cells are negatively charged, which hinders natural aggregation during harvesting [72]. To address this, the bacterium *Streptomyces* sp. HSN06 was co-cultured with *C. vulgaris*, producing a bioflocculant that neutralizes the surface charge and facilitates efficient cell aggregation [72]. Nevertheless, co-culturing microalgae with bacteria can be challenging if flocculation is required in acidic and HM-rich environments [72,73].

In contrast, fungi – particularly filamentous fungi like *Talaromyces* – offer significant advantages for bioflocculation due to their robust mycelial network, high surface area, and EPS secretion [74–76]. Fungal flocculation can proceed through either spore-assisted or pellet-assisted mechanisms [77]. Spore-assisted flocculation systems rely on dormant spores as nucleation sites around which microalgae can aggregate, whereas pellet-assisted systems – such as the one demonstrated in this study – use actively growing fungal hyphae that entangle or bind to microalgae, forming dense and stable flocs [77]. This is especially advantageous in acidic, HM-rich environments, where both *Talaromyces* and *E. mutabilis* naturally thrive. Acidic pH not only supports the growth of these organisms but also enhances pellet formation in fungi, as the lower pH increases the hydrophobicity of fungal hyphae through the protonation of surface functional groups [25,78]. In addition, fungi like *Talaromyces* actively secrete organic acids, which can further acidify the surrounding environment [79]. This acidification destabilizes algal cells by reducing their surface charge, thereby promoting close cell-to-cell contact and facilitating effective flocculation [79]. As an added benefit, *Talaromyces* possesses the ability to bind HMs [53,80]. Previous work demonstrated that prolonged interactions or environmental stress can lead microalgae to form endosymbiotic-like associations within fungal hyphae, offering protection while supporting mutual nutrient exchange [81,82]. Taken together, these traits position *Talaromyces* as both a structural and biochemical driver of bioflocculation within the FAB, supporting stable, metal-tolerant aggregates that can persist and function in extreme acidic environments.

Visual observations of culture growth in light were supported when *E. mutabilis* cell counts were performed (Figure 3.2). After 5-days, control cultures containing no Cd

but supplemented with glucose showed *E. mutabilis* cell counts approximately double those grown without glucose. Likewise, cultures exposed to Cd and supplemented with 5 g/L of glucose showed a 37% increase in cell counts compared to those exposed to Cd without glucose, and a 31% increase compared to cultures grown with 2.5 g/L glucose and Cd.

The highest total chlorophyll content (chl *a* + chl *b*) after 5 days was found in cultures grown without glucose, either with or without Cd exposure (Figure 3.3). These treatments formed the statistical group ("a") and were the only cultures that did not experience a significant decline in chlorophyll between days 3 and 5, unlike all other conditions. In contrast, cultures supplemented with 2.5 g/L and 5 g/L glucose had significantly lower chlorophyll by day 5, with 2.5 g/L + Cd falling into the lowest statistical grouping ("d") and showing the sharpest decline from day 3 (56%). Those grown with 5 g/L glucose generally maintained chlorophyll levels ("bc" to "ab" groups) exhibiting a slight (8%) decrease from day 3. Quantitatively, glucose-free cultures had 39% more chlorophyll than those grown with 5 g/L glucose and 52% more than those with 2.5 g/L glucose after 5 days. A similar pattern occurred in Cd-treated cultures, where the absence of glucose resulted in chlorophyll levels 14.6% higher than with 5 g/L glucose and 5% higher than with 2.5 g/L glucose. Overall, the results show that both glucose concentration and Cd exposure significantly influenced chlorophyll retention, with glucose supplementation generally reducing chlorophyll maintenance over prolonged growth.

The observed increase in *E. mutabilis* cell counts in glucose-supplemented cultures, particularly under Cd stress, suggests that glucose plays a critical role in growth and resilience of the FAB consortium. As a metabolically flexible protist, *Euglena* can alternate

from photoautotropic and heterotrophic metabolism in response to changes in light availability, supporting sustained growth under cyclical environmental conditions and Cd stress [83]. Glucose supplementation not only increases *Euglena* cell counts under Cd exposure, but also significantly reduced the number of dead cells compared to cultures grown without glucose (Figure S3.1). These findings suggest that glucose supplementation enhances both survival and proliferation of *E. mutabilis* under heavy metal stress, reinforcing its role as a key driver of FAB consortium stability in fluctuating and contaminated environments.

Under Cd stress, where photosynthetic efficiency may be impaired, glucose likely enables energy production through heterotrophic pathways to sustain cell proliferation. Interestingly, the highest chlorophyll content was observed in glucose-supplemented cultures also exposed to Cd. Previous research suggests that Cd could substitute for Mg in the chlorophyll molecule in *E. mutabilis*, potentially leading to increased chlorophyll accumulation while impairing photosynthetic function [36]. This substitution may result in the formation of non-functional or less efficient chlorophyll derivatives, inflating total chlorophyll content without a corresponding boost in carbon fixation by photosynthesis. Taken together, the coupled increase in cell counts and chlorophyll content suggests that the enhanced chlorophyll levels under Cd stress may represent a compensatory physiological response to metal toxicity rather than an indication of improved photosynthetic capacity.

The post-stress growth of *E. mutabilis* and *Talaromyces* reflected the observed trends in *E. mutabilis* viability and flocculation (Table 3.1). Assessing growth of the

organisms after HM exposure provides insight into microbial resilience, indicating whether they can regrow and re-establish populations once stress is removed. In the absence of Cd, post-stress growth of *E. mutabilis* was the highest in cultures supplemented with 2.5 g/L glucose, aligning with cell count data – suggesting that 2.5 g/L glucose may optimally support growth and survival of the FAB [84]. Under Cd exposure, *E. mutabilis* survivorship did not differ significantly across glucose treatments, despite clear differences in cell counts and flocculation. This discrepancy may reflect a physiological threshold in Cd tolerance that is maintained across treatments once glucose is available. Although no studies directly compare glucose supplementation to HM tolerance, previous work identified that when *E. gracilis* is grown mixotrophically it expresses more metal-transport proteins and detoxification systems [85,86]. This raises the possibility that waste-deprived carbon sources could be repurposed to enhance algal resilience in contaminated environments, creating paired systems that both recycle organic waste and improve HM bioremediation – a potential contribution to circular economy strategies. Indeed, similar approaches have already been demonstrated by *Chlorella vulgaris* in which, when grown with industrial dairy waste, exhibited enhanced growth and metabolic activity [87].

In contrast, *Talaromyces* survivorship strongly correlated with glucose availability and Cd exposure. Cultures grown with 5 g/L glucose showed the highest fungal growth after Cd exposure (Table 3.1), mirroring increased flocculation and cell viability in those conditions, while cultures grown without glucose displayed minimal fungal colonization as evidenced by the lower number of CFUs. These results support the possibility that fungal resilience – and by extension, its protective role in the FAB – is enhanced by glucose and may contribute to the improved survival and aggregation of *E. mutabilis* under metal stress.

This concept was demonstrated in a co-culture between *Chlorella vulgaris* and *Aspergillus oryzae* exposed to arsenic, where tolerance to the metal was enhanced in the presence of glucose, but only when the level of other essential nutrients were precisely balanced [88]. Similarly, although the survivorship of *Talaromyces* in this study complements trends observed in cell count and chlorophyll data, the role of glucose in maintaining the viability and functionality of the FAB consortium under HM stress may depend on a similarly fine-tuned nutrient environment and this warrants further investigation.

Cellular Cd accumulation varies with glucose supplementation

Cellular cadmium accumulation of the FAB varied over time depending on glucose availability (Figure 3.4). On day 1, all treatments showed similarly low (22-28 ng/100,000 cells) Cd levels. By day 3, Cd accumulation peaked in cultures supplemented with 5 g/L glucose (241 ng/10^6 cells), while lower levels were observed in cultures with 2.5 g/L and 0 g/L glucose. Interestingly, by day 5, Cd accumulation in the 5 g/L glucose condition decreased, whereas cultures without glucose showed a continued increase, ultimately reaching the highest Cd concentration. Cd levels in the 2.5 g/L glucose condition remained relatively stable between days 3 and 5 with a slight (1.4%) decrease (Figure 3.4). This suggests that higher glucose concentrations may initially promote Cd uptake but may later reduce retention, whereas the absence of glucose supports more sustained accumulation.

Although the glucose concentration did not significantly alter final cellular Cd levels, observed trends suggest a relationship between Cd accumulation, *E. mutabilis* cell counts, and chlorophyll content. A key factor influencing Cd accumulation in *Euglena* is the metabolic state determined by environmental conditions. In *E. gracilis*, Cd

preferentially accumulated in chloroplasts under photoautotrophic conditions, while dark-grown cells accumulate Cd primarily in the mitochondria [55,89]. As a result, heterotrophic or dark-grown cells exhibit greater Cd tolerance due to reduced chloroplast-associated accumulation [90].

By cultivating *E. mutabilis* under mixotrophic conditions, its resilience to Cd stress may be enhanced. This is consistent with findings in *Ochromonas*, where mixotrophic growth preserved photosynthetic capacity and supported continued growth under high Cd concentrations, in contrast to obligate heterotrophy [91]. In *E. gracilis*, over 60% of intracellular Cd is sequestered in chloroplasts within three days of exposure, with subsequent redistribution and a reduction in chlorophyll content, suggesting an adaptive detoxification strategy to protect vital cellular functions [89,90,92]. Thus, providing glucose may allow *Euglena* to balance energy production between photosynthesis and carbon metabolism, minimizing chloroplast stress while maintaining overall cell viability during Cd exposure. This trade-off is evident when assessing chlorophyll content, where the presence of glucose leads to a decline in chlorophyll after 5-days of Cd exposure (Figure 3.3).

Beyond *E. mutabilis*, other members of the FAB consortium also contribute to HM sequestration. *Talaromyces* contributes not only through surface adsorption of HMs [93–96], but also by engaging in interspecies signalling that can trigger protective responses in co-cultured organisms under stress [80]. For example, *Talaromyces* strain MR1 significantly enhanced Cd accumulation in plants under high Cd conditions by alleviating toxicity through the production of antioxidants and activation of host defence mechanisms

[80]. By alleviating physiological stress, the fungus enabled the plant to tolerate and accumulate more Cd than it could alone. A similar interaction may occur in this study, whereby *Talaromyces* supports *E. mutabilis* by promoting Cd bioaccumulation and mitigating stress within the consortium. However, because primarily intracellular Cd was assessed in this study, and *Talaromyces* is known to primarily sequester HMs through extracellular adsorption, it is likely that some of the metal bound by the fungus was lost during washing steps. As a result, it is possible that most, if not all, of the cellular Cd measured in the FAB cultures originated from *E. mutabilis* alone.

Electron microscopy reveals intimate, and endosymbiotic, relationships between FAB organisms

Scanning electron microscopy (SEM) provided visual evidence of microbial interactions within the *E. mutabilis* FAB and the dependence of these associations on glucose availability. In cultures supplemented with 5 g/L (Figure 3.5a) and 2.5 g/L (Figure 3.5b) glucose, dense extracellular growth of rod-shaped bacterial cells and extensive fungal hyphae were observed, indicating the active proliferation of *A. acidophilum* and *Talaromyces*, respectively. The surface of *E. mutabilis* cells in these conditions appeared intertwined within the complex microbial matrix. In contrast, cultures grown in the absence of glucose (Figure 3.5c) lacked visible bacterial or fungal structures, displaying only intact *E. mutabilis* cells with clean surfaces, suggesting minimal to no extracellular microbial activity from the partner organisms.

A similar trend was observed under Cd exposure. Cultures amended with both Cd and 5 g/L glucose (Figure 3.5d) or 2.5 g/L glucose (Figure 3.5e) retained microbial

structures similar to their non-Cd counterparts, though slight morphological differences in hyphae and decreased bacterial distribution were observed (not quantified). In the absence of glucose under Cd exposure (Figure 3.5f), no associated microbial structures were detected, paralleling the pattern seen in glucose-free controls (Figure 3.1). These results suggest that glucose is a critical driver of microbial proliferation within the FAB and support the hypothesis that associated microbial populations may exist in a dormant or minor presence in intracellular state within *E. mutabilis* under nutrient-limited conditions.

Transmission electron microscopy (TEM) analysis of *E. mutabilis* cells revealed detailed ultrastructural features and the presence of intracellular, electron-dense bodies consistent with potential endosymbiotic associations (Figure 3.6). In *E. mutabilis* cells cultured in MAM without Cd exposure (Figure 3.6a), characteristic organelles including the nucleus, chloroplasts, mitochondria, vacuoles, paramylon storage granules, and the pellicle were clearly visible. Similar structures were observed in cells grown in the presence of 100 μM Cd (Figure 3.6b), suggesting that basic cellular architecture is maintained under metal stress. Notably, in both treatments, multiple electron-dense bodies were consistently observed within vacuoles. The morphology and isolation of these structures within vacuoles resembled bacteria-containing vacuoles (BCVs) or food vacuoles (FV) at various stages of degradation, suggesting intracellular digestion or storage of microbial cells [97,98]; however, definitive identification of the electron-dense bodies requires further investigation (white arrows in Figure 3.6).

The absence of visible fungal and bacterial structures in FAB cultures grown in minimal media raises important questions about the source of these organisms once glucose

is introduced. One plausible explanation is that these microbial partners persist within *E. mutabilis* in a dormant or internalized state, only proliferating extracellularly when conditions become favorable. This retention model is supported by the presence of electron-dense inclusions (white arrows in Figure 3.6) within *E. mutabilis* vacuoles, whose morphology is consistent with BCVs observed in other protists [97–101]. In this scenario, *E. mutabilis* may act as a temporary refuge for *A. acidophilum* or other consortium members, preserving them through nutrient-limited periods until conditions permit extracellular growth.

An alternative explanation is that these inclusions represent FVs associated with active phagotrophy and digestion. The range of morphologies observed is consistent with digestive stages documented in other protists, where bacterial cells are progressively degraded. If correct, this would suggest that *E. mutabilis* retains phagotrophic capabilities that were previously thought to have been lost during its evolutionary divergence toward photoautotrophy [102]. Notably, *Euglena* species have undergone multiple endosymbiotic events during their evolutionary history [103,104], and it remains possible that *E. mutabilis* can both internalize microbial cells for digestion and, under certain conditions, maintain them in a viable state.

The interaction between *E. mutabilis* and *A. acidophilum* may represent a form of protistan grazing, a well-established ecological strategy in which protists selectively ingest bacteria to obtain energy and essential nutrients [105–107]. Although photosynthetic euglenoids are believed to have lost phagotrophy following the acquisition of plastids through secondary endosymbiosis [108], not all lineages may have lost this capacity

equally. For example, while *E. gracilis* and *E. mutabilis* are closely related [109], their differing tolerances to environmental extremes [36,47] suggest underlying physiological and genetic differences that remain poorly understood. Among euglenoid flagellates, *Entosiphon* are well-studied examples of obligate phagotrophs [102]. *Entosiphon* employs a complex ingestion apparatus, or siphon, formed by three microtubular rods arranged into a U-shaped tube that facilitates particle uptake into FVs [102]– similar to what was observed in *E. mutabilis*. Therefore, the potential for *E. mutabilis* to retain phagocytic or facultative endosymbiotic behavior cannot be excluded. The persistent detection of BCV-like structures in both control and Cd-treated cells suggests that internalized microbial partners may represent a survival mechanism or a flexible interaction strategy that shifts with environmental conditions.

Evaluation of FAB hormone production

The cytokinins

Hormone profiles in *E. mutabilis* varied markedly with glucose availability and Cd exposure over time (Tables S3.3-S3.10). The concentration of the active freebase *trans*-Zeatin (*t*Z) increased significantly over time in glucose-amended cultures, particularly in the presence of 5 g/L glucose plus Cd, which reached the highest levels (234.8 ± 87.4 fmol/mL) by day 5 (Figure 3.7a). Notably, *t*Z levels remained low in cultures not exposed to Cd, and only trace levels were detected in cultures that did not contain glucose. A similar trend was observed for the precursor *trans*-Zeatin riboside (*t*ZR), which peaked at day 5 in the 5 g/L glucose condition without Cd (149.0 ± 20.8 fmol/mL), indicating that *t*Z conjugation from *t*ZR may be sensitive to both glucose and Cd availability (Figure 3.7b).

In contrast, the precursor form *trans*-Zeatin nucleotide (*t*ZNT) accumulated dramatically in cultures grown without glucose but exposed to Cd, showing a 10- to 100-fold increase over all other conditions at each timepoint (Figure 3.7c). By day 5, the patterns in *t*ZNT were strikingly similar to those of *t*Z at the same time point.

The predominance of *t*Z over *cis*-Zeatin (*c*Z) (Table S3.3, S3.4) in FAB cultures suggests *Talaromyces* as the primary source of this hormone. Both *Euglena* [110–112] and fungi [113–115] can produce *c*Z via the *t*RNA-degradation pathway and *t*Z via the cytosolic mevalonate (MVA) pathway [114,116]; however, *Euglena* only produces *t*Z in minute quantities [111]. In our study, *t*Z concentrations greatly exceeded *c*Z in both supernatant and pellet – particularly under Cd stress with glucose – indicating that these conditions synergistically stimulate *t*Z production (Table S3.3, S3.4). Previous research shows that, under HM stress, *E. gracilis* exhibits greater HM tolerance and uptake efficiency when supplied with exogenous *t*Z [41]. Although it has not been directly reported that *Talaromyces* can produce *t*Z, it is still the more likely source compared to *E. mutabilis*. Notably, there were no detectable levels of *t*Z in the pellet of the FAB (Table S3.4), raising the possibility that *Talaromyces* releases *t*Z extracellularly to signal *E. mutabilis* to adjust endogenous hormone levels in response to Cd stress [41]. Moreover, *Talaromyces* abundance increased substantially in glucose-supplemented cultures, which may have contributed to the elevated *t*Z and *t*ZNT levels observed under glucose and Cd conditions.

The concentration of the early precursor form, *t*ZNT, was high in Cd- and glucose-treated cultures, suggesting a shift toward CK inactivation under Cd simultaneously with elevated *t*Z concentrations (Table S3.3, S3.4). While *t*ZNT can occasionally occur as a late

conjugate, it more commonly acts as a biosynthetic precursor. Given that day 5 *t*ZNT profiles trends closely mirrored those of *t*Z (Figure 3.7ac), two non-exclusive explanations are possible: 1) the *t*Z biosynthesis pathway is upregulated, reflecting elevated IPT and LOG activity, or 2) *t*Z accumulation is sufficiently high to drive back-conversion to *t*ZNT via adenine phosphoribosyl transferase 1 (APRT) in a single-step – a process for which very little is currently known in CK metabolism [117]. This interpretation is consistent with the low levels of active *t*Z observed under control growth conditions with glucose, alongside the elevated concentrations of the intermediate precursor *t*ZR, which suggest limited activation to *t*Z under those conditions.

The concentration of methylthio-*trans*-Zeatin (MeSZ) in the supernatant rose substantially by day 3 in all glucose-supplemented cultures, regardless of Cd exposure (Figure 3.8a). The most significant accumulation was observed at day 5 in the 5 g/L + Cd condition (612.9 ± 257.3 pmol/mL), suggesting an inducible response of this methyl-thiolated CK to the combination of high carbon and metal stress. By contrast, MeSZR accumulated primarily in the Cd-only condition at day 5 (18.1 ± 0.2 pmol/mL) and remained low in all other treatments (Figure 3.8b). This divergence between MeSZ and MeSZR indicates that glucose and Cd may not only regulate the production of methyl-thiolated CKs but also modulate their inter-conversions.

Methyl-thiolated CKs are evolutionarily conserved hormones identified across diverse biological domains including bacteria, protists, plants, and certain animals [118]. These compounds are synthesized exclusively via the tRNA degradation pathway, producing the *cis* configuration of CKs [118]. Although their physiological roles are poorly

characterized, growing evidence implicates methyl-thiolated CKs in stress response, cellular communication, and microbe–host interactions, where they may influence host immunity or promote growth [118–121]. For example, the methylotrophic bacterium *Methylobacterium oryzae* was shown to increase production of four methyl-thiolated CKs, including MeSZ and MeSZR, when inoculated with lentil plants under drought stress, ultimately enhancing plant growth and photosynthetic capacity through modulation of host CK pathways [120]. The increased chemical stability of methyl-thiolated CKs suggests they may function as persistent signaling intermediates or hormonal reservoirs [122]. In pathogenic systems, such as *Rhodococcus fascians* colonizing *Arabidopsis thaliana*, methyl-thiolated CKs have been shown to resist enzymatic degradation while mimicking bioactive plant hormones, thereby manipulating host development to favor microbial colonization [122].

In the context of symbiotic consortia or extreme environments, such as those experienced by the FAB community, methyl-thiolated CKs may serve adaptive functions by mediating interspecies signaling and enhancing stress tolerance. Although methyl-thiolated CKs have not been detected in axenic fungal cultures, they have been reported in fungi when grown in association with other microorganisms [116,123], suggesting that fungal synthesis of these compounds may depend on specific environmental or microbial cues. Conversely, *Euglena* has been documented to produce methyl-thiolated CKs [110,111,118], and the absence of these compounds in the cellular pellet, particularly under Cd stress, suggests rapid secretion into the extracellular environment (Table S3.6). This pattern may reflect a signaling mechanism by *E. mutabilis* to coordinate a communal

response to HM stress, although the exact functional outcome of such signaling remains to be determined.

Gibberellins

Of the 5 key GAs (Table S3.1) scanned for in the LC-MS/MS only GA_3, GA_4, and GA_7 were ever detected. GA_3 was only present in trace levels of control supernatants by day 5. No other samples of supernatant or pellet contained GA_3

GA_4, a widely regarded as an active form of GA [124], was not detected in any pellet samples and was absent in all control supernatants and the supernatants of day 1 Cd treated cultures. However, quite large quantities (from 19,398 180,399 fmol/mL) of GA_4 appeared in all glucose amended Cd treated cultures at day 3 and day 5.

The most consistent and interesting patterns were seen for gibberellin 7 (GA_7). High levels of GA_7 were detected in the supernatant of cultures exposed to Cd with glucose supplementation, particularly at 2.5 g/L where GA_7 levels sharply rose over time, peaking by Day 5 (23,409.5 ± 2,074.5 fmol/mL) (Figure 3.9a). In contrast, cultures without Cd or glucose showed minimal GA_7 production (not detected). Notably, pellet-associated GA_7 levels (Figure 3.9b) were significantly lower across all treatments (39.5 ± 3.3 – 131.2 ± 31.5 fmol/mL), suggesting that GA_7 was predominantly released extracellularly rather than retained within the cells. This trend implies that GA_7 biosynthesis and excretion are strongly stimulated by the combined presence of glucose and Cd stress, and that the hormone may play a role in extracellular signaling or environmental adaptation by the FAB consortium. The lack of intracellular GA_7 accumulation also suggests that the hormone may

be acting more as a community-level effector rather than functioning solely within the producing organism.

Only a limited number of GAs are biologically active, with GA_7 recognized for its role in promoting plant growth and stress tolerance [125]. Although *Euglena* has been shown to respond positively to exogenous applications of the bioactive gibberellin GA_3, exhibiting enhanced growth rates, evidence for endogenous production in *Euglena* remains largely uncharacterized [111,126]. In contrast, GA biosynthesis is more commonly attributed to fungi in co-culture systems [127,128]. *Talaromyces* has been reported to produce gibberellins [129], and closely related species in the genus *Penicillium* are well-known for synthesizing biologically active GAs [127,130,131]. In this study, GA_7 emerged as the predominant GA, an intriguing find given the relative instability and rapid metabolization of GA_7 in plants, where it plays a transient role during early development [132]. Moreover, although it is on occasion detected from plant samples, no enzyme has been characterized from plants for its synthesis [133].

GA_7 has previously been identified as a dominant GA in fungi [134,135] and its biosynthetic pathway has, to date, only been attributed to fungi and plants [136,137]. Additional evidence for a fungal origin of the GAs in the FAB is the co-occurrence of GA_4 with GA_7 in the supernatants of Cd-treated samples; in fungi, GA_4 is the immediate precursor to GA_7. This interpretation is further supported by the absence of GA_{20} and GA_9, neither of which is associated with fungal biosynthesis. GA_{20} is a common plant-derived intermediate, whereas GA_9 can originate from either bacteria or plants [136]. Notably, GA_9

is the only bacterial or plant precursor capable of yielding GA_4 or GA_7, and its absence strongly suggests that the detected GA_4 and GA_7 are of fungal origin.

The discovery of gibberellins in fungi originated with the identification of *Fusarmium fujikuori* (formerly *Gibberella fujikuori*), the causal agent of "foolish seedling" disease in rice [138,139]. This pathogenic fungus produces excessive amounts of GAs, promoting elongation of rice shoots, its preferred colonization site, thereby redirecting host nutrient flow to benefit its own growth [139]. Outside of a pathogenic model, bioactive GAs produced by *Penicillium* have been shown to improve copper (Cu) uptake efficiency and nutrient acquisition in *Glycine max*, enhancing plant biomass, pigment levels, and stress resistance while reducing membrane damage and lipid peroxidation under Cu stress [127].

Taken together, these findings suggest that the elevated levels of GA_7 observed in glucose-supplemented, Cd-exposed cultures may originate from *Talaromyces* and serve to signal *E. mutabilis* to sustain growth and enhance Cd tolerance. This is also consistent with the pattern of *t*Z and *t*ZNT being of fungal origin since, they too, rose sharply in the supernatant in presence of glucose and Cd. While these hormonal interactions appear beneficial to *E. mutabilis*, it raises the question of whether *Talaromyces* is the dominant member of the FAB consortium functioning not merely in mutualism, but potentially as the primary driver of a holobiont-like association aimed at preserving its own survival under extreme environmental conditions. The sharp rise in GA_7 and CKs in the supernatant points to intercellular communication as the hormonal priority, perhaps for the whole FAB consortium.

Jasmonic acid and salicylic acid

Supernatant concentrations of jasmonic acid (JA) were highest at day 3 in cultures grown with 2.5 g/L glucose and without Cd (1,751.9 ± 819.5 pmol/mL), followed by a steep decline in all treatments by day 5 (not detectable) (Figure 3.10a). Cd suppressed JA accumulation at all glucose concentrations. In the pellet, JA content was highest in 5 g/L glucose at day 1 (29,9787.0 ± 13,055.4 pmol/g [DW]) and decreased thereafter (107.6 ± 26.7 pmol/g [DW] at day 5) (Figure 3.10b), indicating an early but transient cellular retention. Salicylic acid (SA) exhibited a strikingly similar temporal pattern to JA across treatments (Figure 3.10cd). In the pellet fraction, JA and SA patterns were virtually identical, with both hormones showing highest concentrations in 0 g/L glucose treatments at day 1 and declining thereafter. This may reflect endogenous *Euglena*-derived production, as fungal and bacterial biomass was minimal in glucose-free cultures. In the supernatant, JA and SA also followed nearly parallel trajectories, with the only differences being slightly lower JA levels in all glucose treatments at day 1 and day 5. In general, glucose supplementation promoted higher extracellular JA and SA levels compared to glucose-free controls, which showed negligible or undetectable concentrations of either hormone.

In plants, JA plays a key role in regulating growth, development, and responses to abiotic stressors such as HMs [140,141]. Comparative studies between wild-type *Lycopersicon esculentum* and JA-deficient mutants have shown that Cd accumulation in roots and leaves is significantly lower in wild-type plants, indicating a potential role of JA

in restricting Cd uptake and translocation [142]. Although *Euglena* is known to biosynthesize JA [143], its functional significance in this genus remains largely unexplored. Fungi can also produce JA, though its production is often associated with virulence and pathogenicity [144], suggesting that *E. mutabilis* is the more likely source of JA in the FAB consortium. Given JA's protective role in plants, it is plausible that *E. mutabilis* secretes JA in response to Cd stress to reduce metal uptake, particularly under glucose-supplemented conditions. In support of this, JA was primarily detected in supernatant of Cd-exposed cultures grown with glucose, while intracellular retention of JA was more apparent in cultures not exposed to Cd.

Unlike JA, *Euglena* does not synthesize SA, but it is capable of perceiving SA signals from surrounding organisms and can act as an elicitor, triggering SA-mediated responses in plants [145]. For example, application of paramylon – a β-1,3-D-glucan storage polysaccharide from *E. gracilis* – to tomato roots reduced SA levels while increasing JA and abscisic acid (ABA) concentrations [145]. In our study, increased paramylon accumulation was observed in Cd-treated cultures (Figure 3.6), suggesting that Cd stress may enhance *Euglena*'s capacity to modulate hormone signaling in the FAB through paramylon-mediated interactions. Notably, SA was detected at high levels in the pellets of glucose-free cultures, where fungal and bacterial biomass was minimal, raising the possibility that *Euglena* itself may be producing SA. If confirmed, this would represent the first documented instance of endogenous SA biosynthesis in *Euglena*. While some pathogenic fungi are reported to biosynthesize SA or its derivatives [146,147], they more commonly induce SA production in plants as part of host defense against biotrophic infection [147,148]. The FAB system studied here appears to function mutualistically, with

previous findings showing that all community members are essential for Cd stress mitigation [36]. Although the origin of SA within the FAB remains uncertain, *Acidiphilium acidophilum* may contribute. SA biosynthesis is widely conserved among bacteria, including many plant growth-promoting species [149]; however, the hormone profile of *A. acidophilum* has not been characterized.

Regardless of its precise origin, SA was excreted primarily in glucose-supplemented, Cd-exposed cultures and retained intracellularly under non-glucose conditions. Exogenous SA applications have been shown to enhance Cd tolerance in algae such as *Scenedesmus obliquus* and *Chlorella pyrenoidosa* by stabilizing cell structure and chelating Cd ions [150]. Thus, the presence of SA in the FAB likely contributes to the protection of *E. mutabilis*, potentially as part of a cooperative stress mitigation strategy orchestrated at the community level.

Hormone accumulation showed clear interactions between glucose availability and Cd stress. Taken together, the hormone dynamics suggest the FAB consortium operates not as a loose association of individual organisms, but as an interdependent system capable of adapting to environmental stress through coordinated signalling. This hormonal cross talk enhances bioremediation potential by promoting sustained growth, mitigating toxicity, and optimizing resource use. Moreover, these results support a model where *Talaromyces* may serve as a central regulatory role, facilitating a functional holobiont that ensure the survival and efficacy of the FAB under extreme conditions. Our results show that the fungal partner is the likely source of key active and precursor hormones (*t*Z, *t*ZNT, GA_4, GA_7) that are likely important intercellular regulators of growth and HM resistance.

In support, glucose conditions, especially with Cd, produced dense fungal hyphae, pronounced flocculation, and greater bacterial proliferation indicating hormone-linked restructuring of community architecture (Figure 3.5). Functionally, *Euglena* cell counts increased and mortality fell with glucose under Cd, whereas chlorophyll retention by day 5 was highest without glucose and declined in glucose-amended treatments, showing that growth gains are not simply due to higher photosynthetic capacity but likely reflect mixotrophic buffering and community support under metal stress. At the molecular level, GA_7 and *t*Z accumulated predominantly in the supernatant under Cd and glucose, consistent with a fungal origin and an extracellular signalling role that coordinates partner physiology; in parallel, JA and SA showed closely matched trajectories with higher extracellular levels under glucose, linking carbon availability to shared stress-hormone dynamics across partners. Together with higher post-stress fungal survivorship at 5 g/L glucose and time-dependent cellular Cd patterns, these findings indicate that *Talaromyces*-derived hormones act as intercellular regulators of growth and HM resistance, by orchestrating a glucose-responsive, holobiont-level adjustment of metabolism, and metal handling in the consortium.

3.6 CONCLUSIONS

Microscopy revealed clear shifts in microbial organization under carbon limitation, including intracellular bacteria-like inclusions within *E. mutabilis*, suggesting possible facultative endosymbiosis or phagocytosis. These structural changes indicate that the FAB consortium can physically reorganize to maintain functionality under nutrient stress. Complementing these observations, hormonal profiling showed that glucose and Cd

exposure modulate interspecies signalling, with elevated *t*Z, GA_7, and methyl-thiolated CKs under Cd stress pointing to coordinated mechanisms that enhance metal tolerance. *Talaromyces* likely supplies bioactive GAs and CKs, while *E. mutabilis* appears to produce methylthiolated CKs, JA, and SA potentially to regulate community-level stress responses. Together, the microscopy and hormone data support a model of the FAB as a dynamic, adaptive community capable of both physical restructuring and biochemical cross-talk in response to environmental pressures. Future work should aim to resolve the genetic basis of hormone biosynthesis in each FAB member and determine whether these associations are metabolically integrated or opportunistic. Understanding these interactions can guide the design of synthetic, or enhancement of natural, algal consortia for sustainable bioremediation and environmental resilience.

3.7 FIGURES AND TABLES

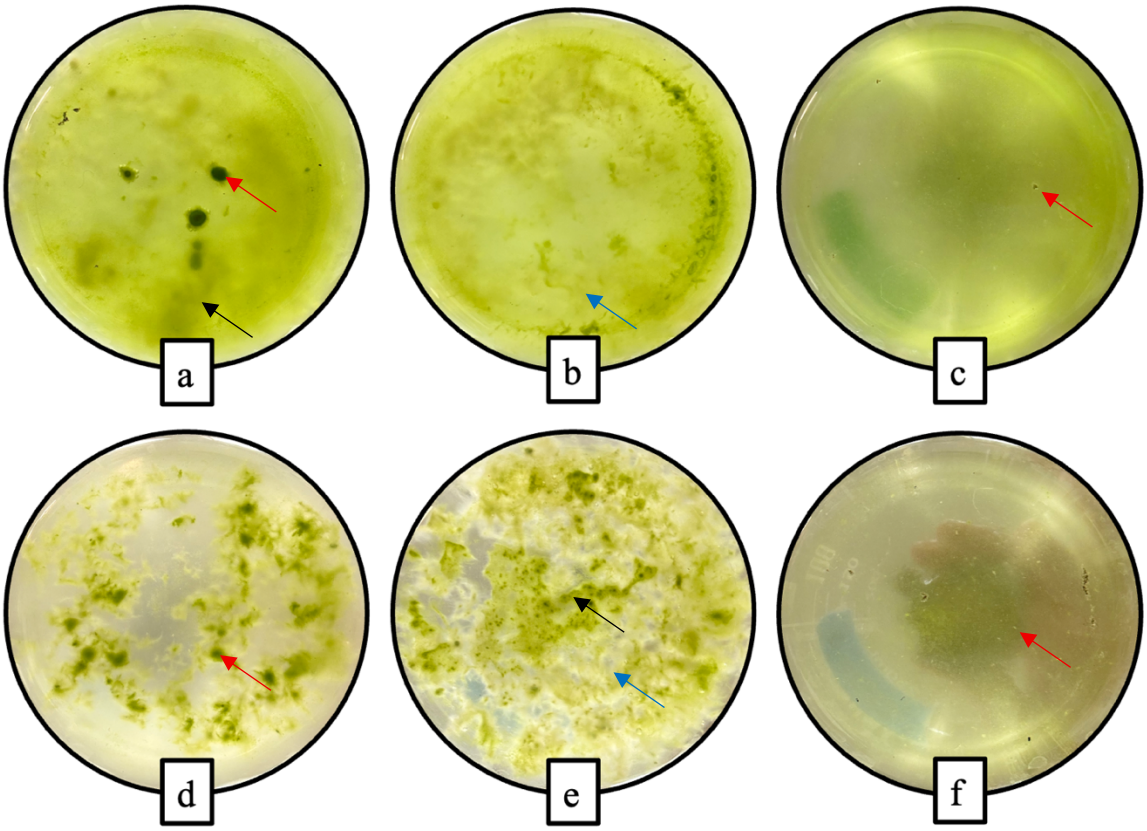

Figure 3.1: *E. mutabilis* FAB culture floc in the presence of glucose. Representative photographs from underneath culture flasks reveal enhanced fungal growth (blue arrow indicating mycelium mats) in the presence of 5 g/L (a, d) and 2.5 g/L (b, e) of glucose compared to cultures grown in the absence of glucose (c, f). Furthermore, cultures grown without $CdCl_2$ (a-c) exhibit a more even distribution of *E. mutabilis* (red arrow) throughout the medium, along with some flocculation (black arrow), whereas cultures exposed to $CdCl_2$ (d-f) tend to exhibit increased flocculation.

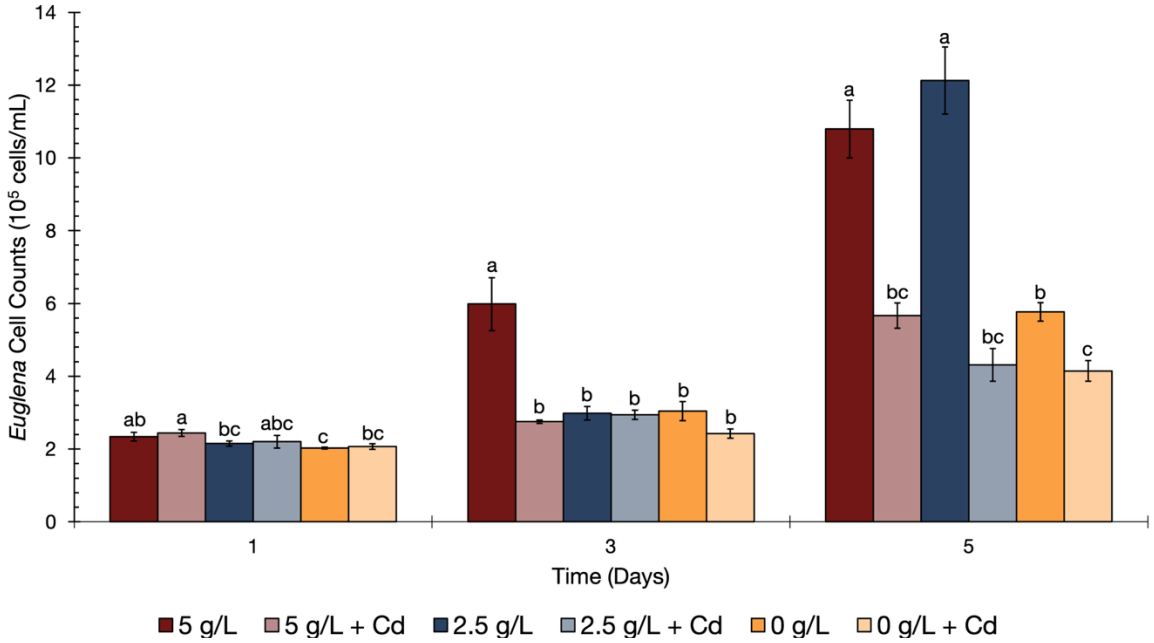

Figure 3.2: Cell counts of *E. mutabilis* increase in the presence of glucose. Cultures of *E. mutabilis* were grown in for 5 days in MAM, cycling light (16L:8D), and amended with glucose in the presence (light coloured bars) and absence (dark coloured bars) of $CdCl_2$. Error bars represent standard deviation (n = 3). Statistical significance within each timepoint was assessed using a one-way ANOVA and Tukey's HSD post-hoc test ($p < 0.05$).

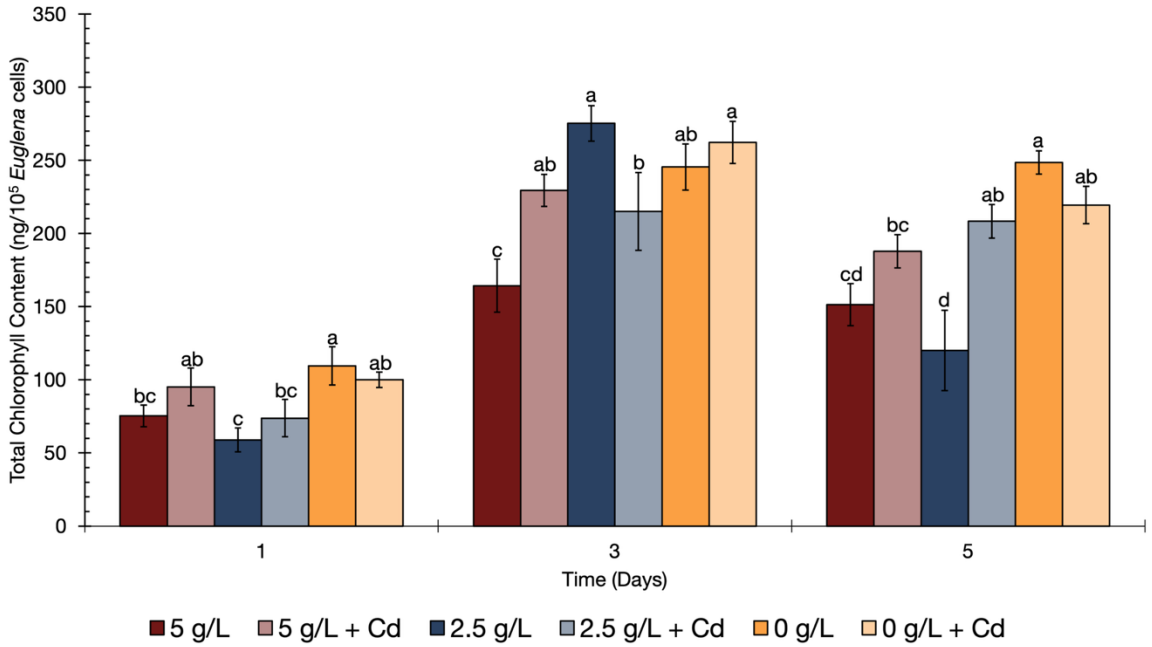

Figure 3.3: Effects of glucose and cadmium on total chlorophyll content of *E. mutabilis* over time. Cultures of *E. mutabilis* were grown for 5-days in MAM, cycling light (16L:8D), and amended with glucose in the presence (light coloured bars) and absence (dark coloured bars) of $CdCl_2$. Error bars represent standard deviation (n = 3). Statistical significance within each timepoint was assessed using a one-way ANOVA and Tukey's HSD post-hoc test ($p < 0.05$).

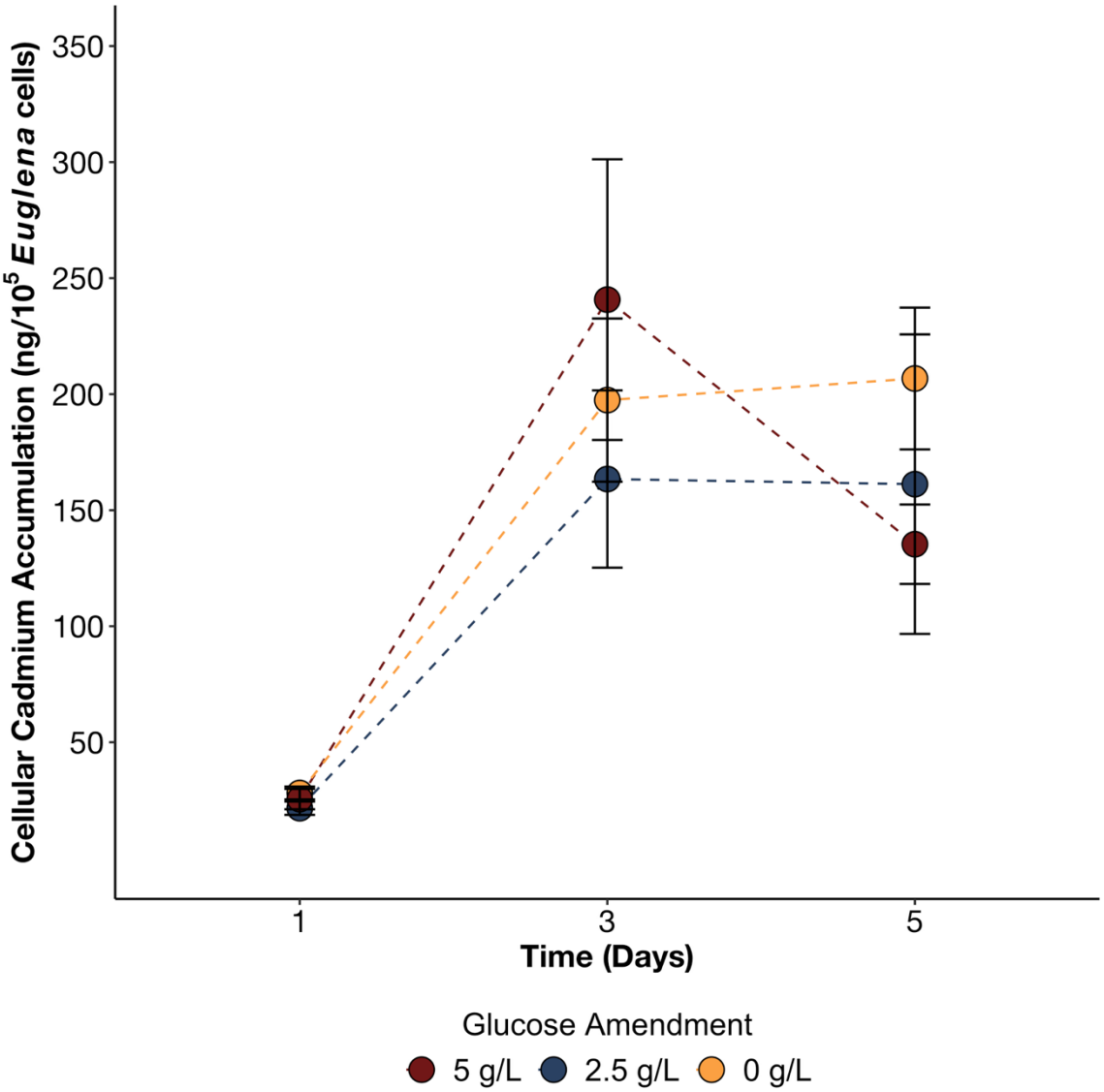

Figure 3.4: Cellular $CdCl_2$ accumulation varies depending on the amount of glucose present. Cultures were grown in MAM, cycling light (16L:8D), and exposed to 100 µM $CdCl_2$, and Cd content was measured at days 1, 3, and 5. Control media blanks for each condition (n = 3) were extracted in parallel to verify the absence of Cd in the control environment (0 ng). Each symbol represents the mean value for a given glucose treatment (n = 3): dark red circles = 5 g/L glucose, blue circles = 2.5 g/L glucose, and yellow circles = 0 g/L glucose. Dashed lines connect timepoints for the same treatment to illustrate temporal trends and are not statistical fits. Error bars represent standard deviation. Statistical significance within each timepoint was assessed using a one-way ANOVA and Tukey's HSD post-hoc test, however, no significant differences were found ($p < 0.05$).

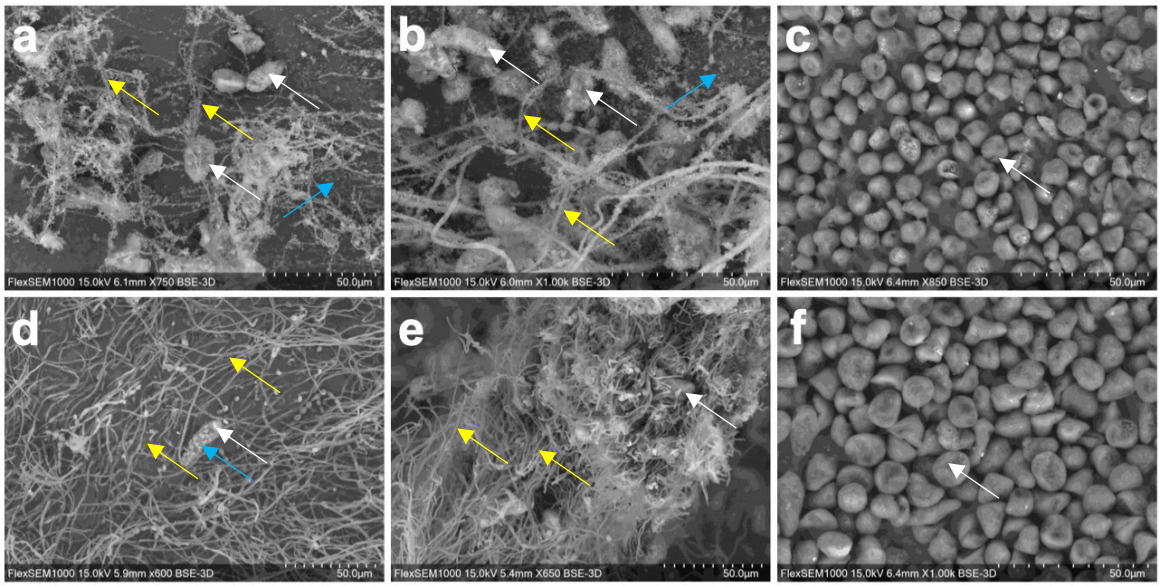

Figure 3.5: Growth of *E. mutabilis* FAB in glucose-amended media reveals the presence of bacterial and fungal associates. Cultures supplemented with 5 g/L (a) and 2.5 g/L (b) glucose showed visible proliferation of *A. acidophilum* (blue arrow) and *Talaromyces* (yellow arrow) with *E. mutabilis* (white arrow), whereas no such growth was observed in the absence of glucose (c). A similar trend was seen under Cd exposure, where cultures grown with 5 g/L (d) and 2.5 g/L (e) glucose supported microbial growth, while those without glucose (f) did not. The absence of observable extracellular microbial growth in glucose-free conditions suggests these organisms may persist intracellularly within *E. mutabilis* until environmental conditions permit their proliferation.

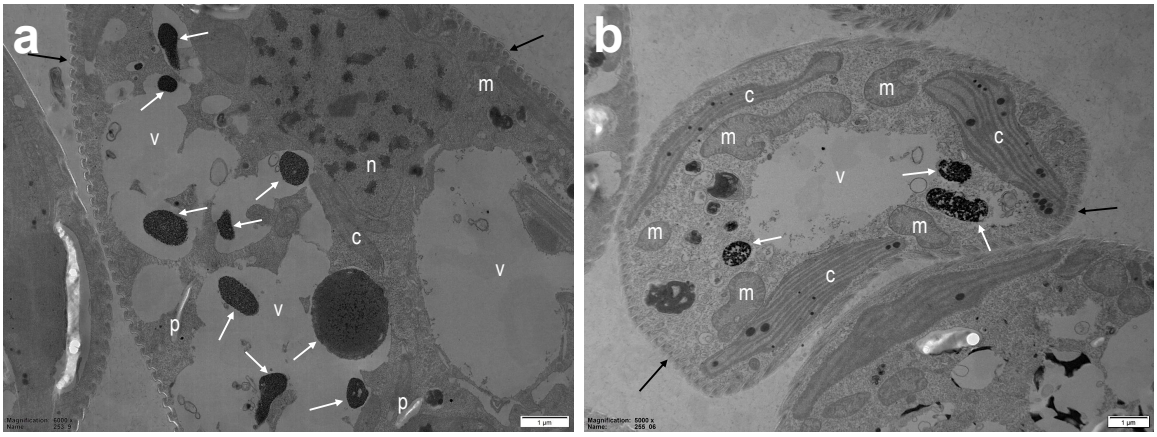

Figure 3.6: Transmission electron microscopy of *E. mutabilis* cells reveals potential endosymbiotic organisms. Images of *E. mutabilis* cross-sections grown in MAM, cycling light (16L:8D) (a), and MAM + 100 µM $CdCl_2$, cycling light (16L:8D) (b), readily display chloroplasts (c), mitochondria (m), the nucleus (n), paramylon (p), vacuoles (v), and the pellicle (black arrow). In both growth conditions, electron-dense bodies housed in vacuoles (indicated by the white arrows) resemble bacteria-containing vacuoles (BCVs) at various stages of decomposition. These BCVs suggest that *A. acidophilum* and potentially *Talaromyces* are being stored in and consumed by *E. mutabilis*.

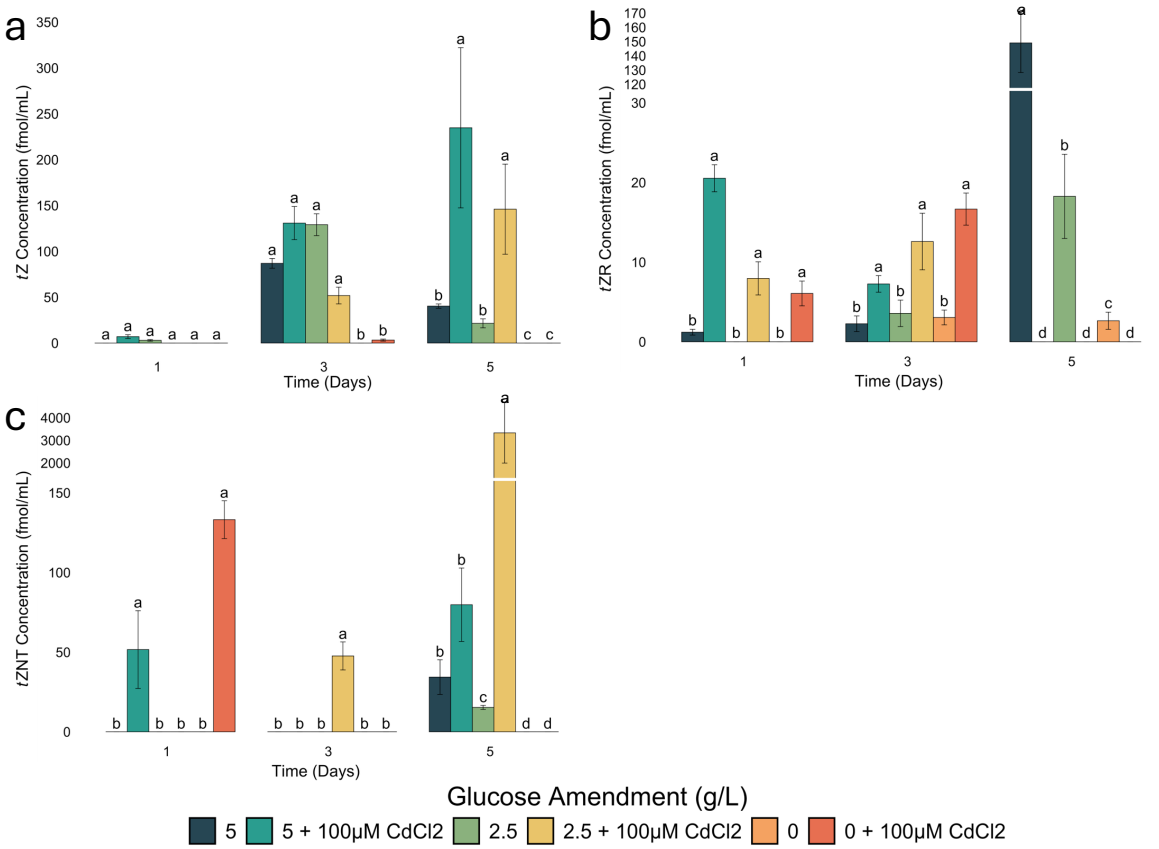

Figure 3.7: Supernatant concentrations (fmol/mL) of *t*Z (a), *t*ZR (b), and *t*ZNT (c) from an *E. mutabilis* FAB grown in varying concentration of glucose in the presence and absence of $CdCl_2$ over 5-days. Error bars represent standard error (n = 3). Statistical significance within each timepoint was assessed using a one-way ANOVA and Tukey's HSD post-hoc test ($p < 0.05$) including cultures where the hormones were not detected.

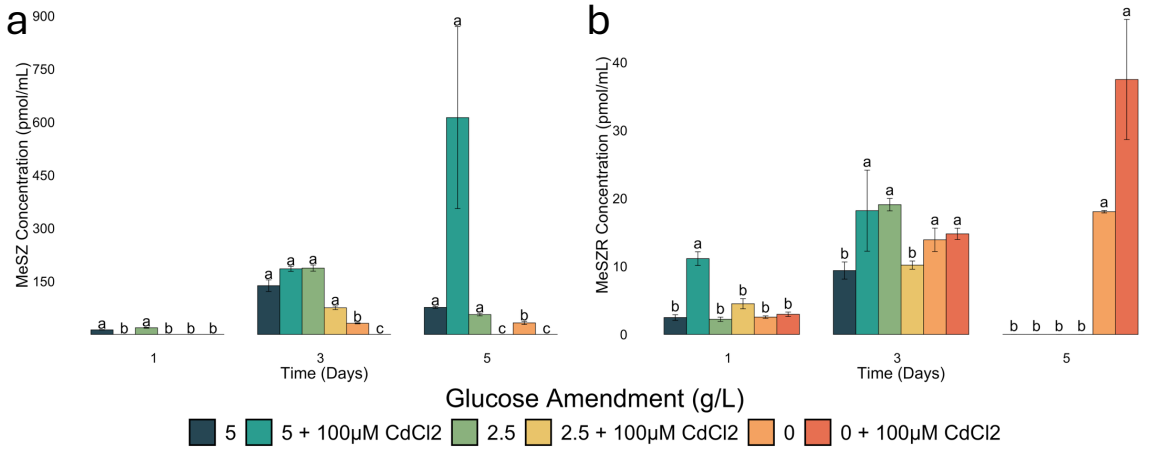

Figure 3.8: Supernatant concentrations (pmol/mL) of MeSZ (a) and MeSZR (b) from an *E. mutabilis* FAB grown in varying concentration of glucose in the presence and absence of $CdCl_2$ over 5-days. Error bars represent standard error (n = 3). Statistical significance within each timepoint was assessed using a one-way ANOVA and Tukey's HSD post-hoc test ($p < 0.05$) including cultures where the hormones were not detected.

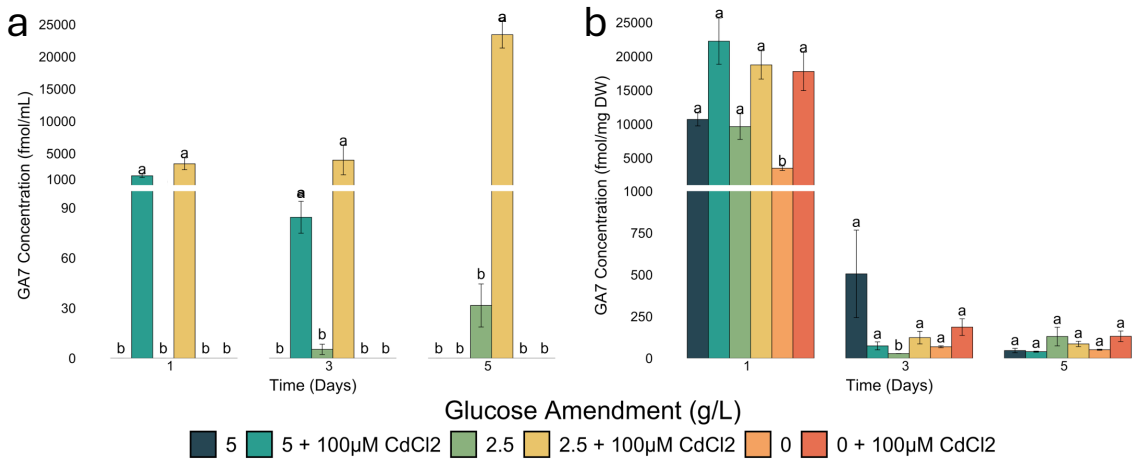

Figure 3.9: Supernatant (a) and pellet (b) concentrations (fmol/mL and fmol/mg DW) of GA7 from an *E. mutabilis* FAB grown in varying concentration of glucose in the presence and absence of $CdCl_2$ over 5-days. Error bars represent standard error (n = 3). Statistical significance within each timepoint was assessed using a one-way ANOVA and Tukey's HSD post-hoc test ($p < 0.05$) including cultures where the hormones were not detected.

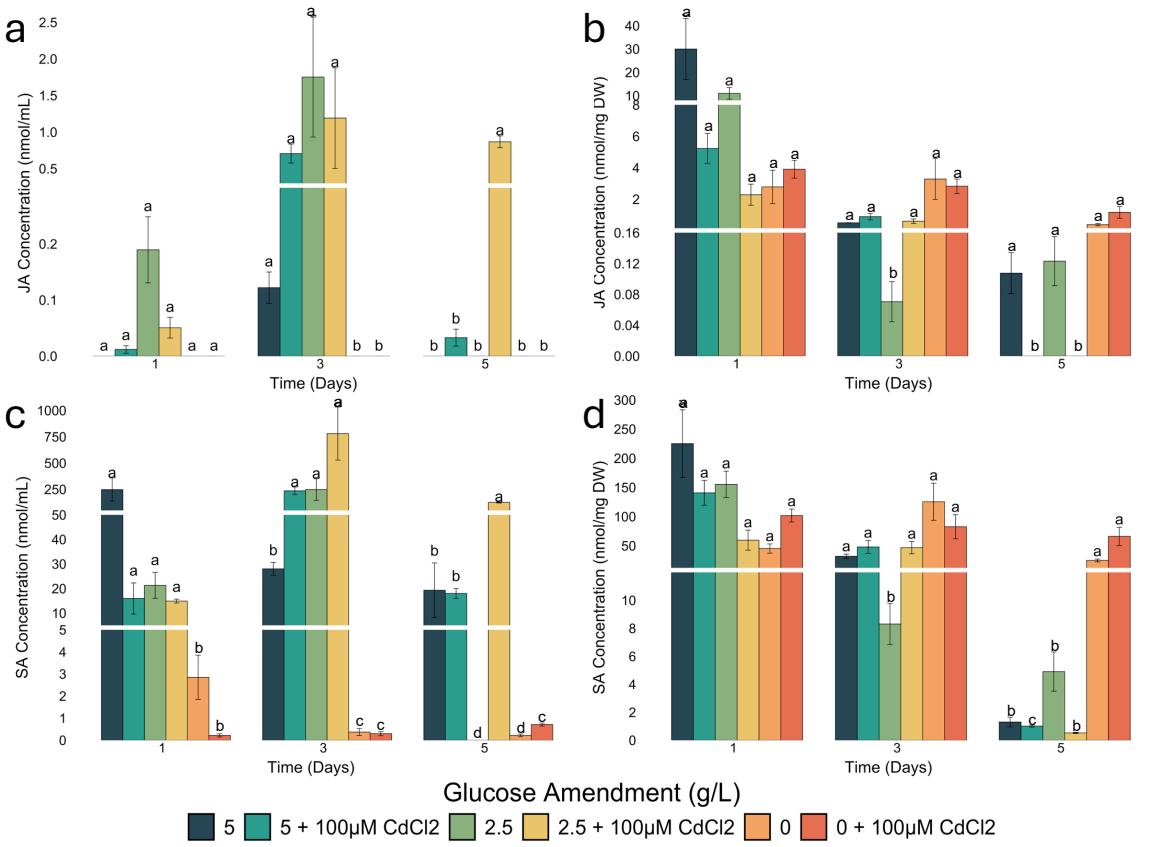

Figure 3.10: Supernatant concentration (nmol/mL) of JA (a) and SA (c) and pellet concentrations (nmol/mg DW) of JA (b) and SA (d) from an *E. mutabilis* FAB grown in varying concentration of glucose in the presence and absence of $CdCl_2$ over 5-days. Error bars represent standard error (n = 3). Statistical significance within each timepoint was assessed using a one-way ANOVA and Tukey's HSD post-hoc test ($p < 0.05$) including cultures where the hormones were not detected.

Table 3.1: Cell survivability test (n = 3) comparing colony forming units of *E. mutabilis* (CPCC 657) and *Talaromyces* after 7-days of incubation on PDA at 22°C cycling in darkness. Before plating, samples were grown in their respective media types for 5-days.

	E. mutabilis		*Talaromyces*	
	MAM only	100 µM $CdCl_2$	MAM only	100 µM $CdCl_2$
5 g/L	+ +	+ +	+ + +	+ + +
2.5 g/L	+ + +	+ +	+ + +	+ +
0 g/L	+ +	+ +	+	+

"-" if no CFU; "+" if < 50 CFU; "++" if 50><250 CFU; "+++" if >250 CFU or if a complete lawn is present and CFU count is impossible.

3.8 SUPPLEMENTARY MATERIALS

Table S3.1: Hormones, grouped accordingly, included in the UHPLC-MS/MS method using PRM mode [62]. 23 CKs (freebase, riboside, glucoside, methylthiolated, and aromatic forms) and 8 acidic hormones were analyzed directly while 4 CK nucleotides were analyzed in their dephosphorylated riboside state.

Group	Analyte	Abbreviation	Labelled Analyte
Freebases	*trans*-Zeatin	*t*Z	*t*Z-d_5
	cis-Zeatin	*c*Z	
	DihydroZeatin	DZ	DZ-d_3
	Isopentyladenine	iP	iP-d_6
Ribosides	*trans*-Zeatin riboside	*t*ZR	*t*ZR-d_5
	cis-Zeatin riboside	*c*ZR	
	DihydroZeatin riboside	DZR	DZR-d_3
	Isopentyladenosine	iPR	iPR-d_6
Nucleotides	*trans*-Zeatin riboside-5′-monophosphate	*t*ZNT	*t*ZR-d_5
	cis-Zeatin riboside-5′-monophosphate	*c*ZNT	
	DihydroZeatin riboside -5′-monophosphate	DZNT	DZR-d_3
	Isopentyladenosine-5′monophosphate	iPNT	iPR-d_6
Methylthiols	2-Methylthio-*trans*-Zeatin	MeSZ	MeSZ-d_5
	2-Methylthio-*trans*-Zeatin riboside	MeSZR	MeSZR-d_5
	2-Methylthio-isopentyladenine	MeSiP	MeSiP-d_6
	2-Methylthio-isopentyladenosine	MeSiPR	MeSiPR-d_6
Glucosides	*trans*-Zeatin-O-glucoside	*t*ZOG	*t*ZOG-d_5
	cis-Zeatin-O-glucoside	*c*ZOG	
	DihydroZeatin-O-glucoside riboside	DZOG	DZOG-d_7
	trans-Zeatin-7-glucoside	*t*Z7G	*t*Z7G-d_5
	cis-Zeatin-7-glucoside		
	trans-Zeatin-9-glucoside	*t*Z9G	*t*Z9G-d_5
	cis-Zeatin-9-glucoside	*c*Z9G	
	DihydroZeatin-9-glucoside	DZ9G	DZ9G-d_3
	Isopentenyladenine-7-glucoside	iP7G	iP7G-d_6
	Isopentenyladenine-9-glucoside	iP9G	iP7G-d_6
Aromatic CKs	Benzylaminopurine	BA	BA-d_7
	Benzylaminopurine riboside	BAR	BAR-d_7
Acids	Abscisic acid	ABA	ABA-d_6
	Gibberellin 1	GA1	GA1-d_2
	Gibberellin 3	GA3	GA3-d_2
	Gibberellic acid 4	GA4	GA4-d_2
	Gibberellin 7	GA7	GA7-d_2
	Indole-3-acetic acid	IAA	IAA-d_5
	Salicylic acid	SA	SA-d_6
	Jasmonic acid	JA	ABA-d_6

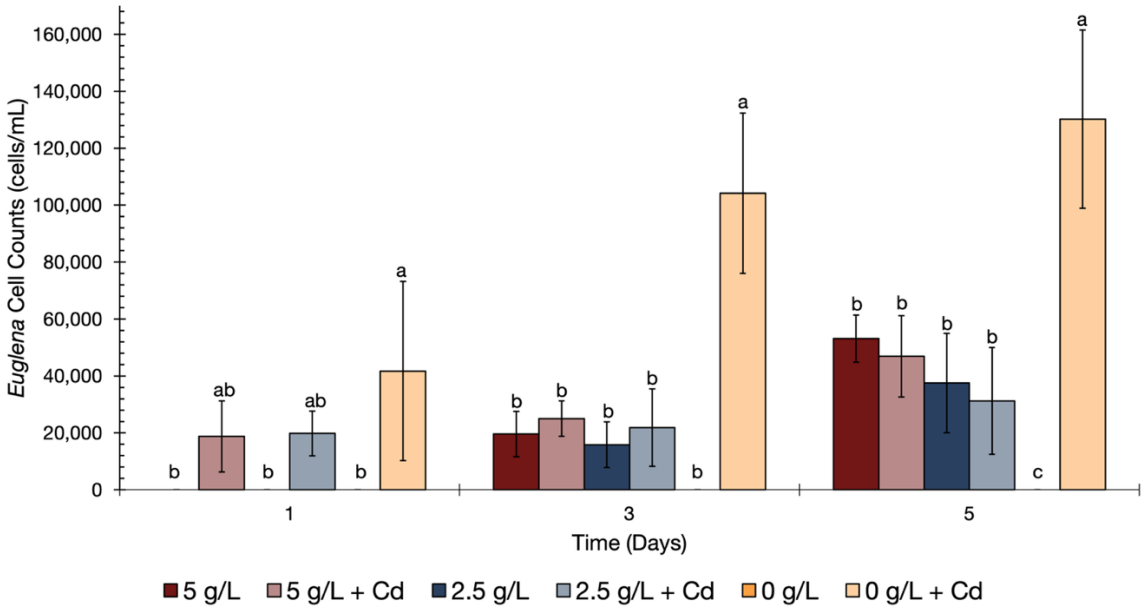

Figure S3.1: Dead cell counts of *E. mutabilis* exposed to Cd decrease when cells are grown in glucose. Culture of *E. mutabilis* were grown for 5-days in MAM amended with glucose in the presence (light coloured bards) or absence (dark coloured bars) of $CdCl_2$. The number of dead cells in each culture were determined using Trypan Blue dye and counting on a Haemocytometer. Error bars represent standard deviation (n = 3). Statistical significance within each timepoint was assessed using a one-way ANOVA and Tukey's HSD post-hoc test ($p < 0.05$).

Table S3.2: Average quantified hormone concentrations (nmol/mL) detected in the MAM media blanks grown in the presence and absence of 100 µM $CdCl_2$ and amended with glucose at concentrations of 0 g/L, 2.5 g/L, and 5 g/L. 5 hormones were detected in the media blanks and are reported; compounds absent from the media are not included.

	Glucose [g/L]	**MAM**			**MAM + 100 µM $CdCl_2$**		
		Day 1	Day 3	Day 5	Day 1	Day 3	Day 5
ABA	5	5.61	4.417	2.673	3.19	3.241	4.057
	2.5	2.894	1.840	0.760	1.721	1.823	1.411
	0	7.485	0.848	2.150	5.841	1.509	4.030
SA	5	567,680.54	633,978.565	682,269.486	1,448,339.61	400,372.699	352,517.862
	2.5	236,205.310	306,631.529	189,767.506	235,611.617	296,674.132	90,960.888
	0	23,335.500	10,268.070	12,474.069	37,192.728	20,443.743	1,090.713
JA	5	10,685.54	1,324.212	3,991.319	4,546.81	n.d.	n.d.
	2.5	n.d.	n.d.	n.d.	n.d.	680.388	n.d.
	0	n.d.	n.d.	n.d.	15.561	n.d.	32.023
GA4	5	n.d.	69.626	n.d.	59.00	n.d.	n.d.
	2.5	n.d.	n.d.	n.d.	n.d.	52.759	n.d.
	0	n.d.	n.d.	n.d.	n.d.	n.d.	n.d.
GA7	5	160.42	0.889	1.693	224.24	n.d.	155.870
	2.5	86.782	0.416	0.604	99.599	n.d.	100.323
	0	36.732	7.470	10.434	40.054	0.646	43.150

Table S.3.3: Quantified CK concentrations (fmol/mL) in the culture supernatant across experimental treatments. Values represent the mean concentration (± standard error, n = 3) of each sample measured at indicated time points. Treatments include varying glucose amendments with and without Cd exposure. Data reflect extracellular CK accumulation as part of the experimental assessment of environmental and nutrient stress on CK production.

	Glucose [g/L]	**MAM**			**Change**	**MAM + 100 µM $CdCl_2$**			**Change**
		Day 1	Day 3	Day 5		Day 1	Day 3	Day 5	
tZ	5	n.d.	86.918 ± 5.299	40.311 ± 2.324	↑	6.997 ± 2.038	130.847 ± 18.076	234.789 ± 87.413	↑
	2.5	2.957 ± 0.861	129.068 ± 11.914	21.493 ± 4.891	↑	n.d.	51.818 ± 9.097	145.986 ± 49.169	↑
	0	n.d.	n.d.	n.d.	–	n.d.	3.247 ± 1.093	n.d.	–
tZR	5	1.205 ± 0.363	2.263 ± 0.982	149.072 ± 20.789	↑	20.532 ± 1.695	7.265 ± 1.042	n.d.	↓
	2.5	n.d.	3.572 ± 1.659	18.259 ± 5.287	↑	7.959 ± 2.079	12.588 ± 3.555	n.d.	↓
	0	n.d.	3.054 ± 0.928	2.641 ± 1.077	↑	6.068 ± 1.556	16.661 ± 2.013	n.d.	↓
tZNT	5	n.d.	n.d.	34.335 ± 10.844	↑	51.621 ± 24.409	n.d.	79.771 ± 23.045	↑
	2.5	n.d.	n.d.	15.307 ± 1.283	↑	n.d.	47.610 ± 8.797	3,333.622 ± 1,335.907	↑
	0	n.d.	n.d.	n.d.	–	133.177 ± 11.857	n.d.	n.d.	↓
cZ	5	n.d.	29.635 ± 14.548	207.019 ± 19.130	↑	n.d.	n.d.	120.666 ± 59.072	↑
	2.5	n.d.	16.183 ± 8.448	131.264 ± 14.583	↑	n.d.	14.578 ± 3.856	265.705 ± 89.104	↑
	0	n.d.	n.d.	n.d.	–	n.d.	n.d.	n.d.	–
cZNT	5	n.d.	n.d.	n.d.	–	59.058 ± 23.486	95.326 ± 26.337	140.199 ± 18.734	↑
	2.5	n.d.	n.d.	15.730 ± 4.828	↑	18.455 ± 10.655	64.321 ± 19.994	3,389.643 ± 947.008	↑
	0	n.d.	n.d.	n.d.	–	77.239 ± 24.759	133.526 ± 53.396	n.d.	↓
iP	5	n.d.	3.433 ± 0.361	1.390 ± 0.430	↑	n.d.	2.444 ± 0.188	n.d.	–
	2.5	1.446 ± 0.405	2.219 ± 0.850	n.d.	↓	n.d.	4.022 ± 0.776	n.d.	–
	0	n.d.	1.018 ± 0.060	n.d.	–	n.d.	n.d.	2.614 ± 0.774	↑
iPR	5	n.d.	2.341	n.d.	–	3.332 ± 0.299	10.647 ± 3.467	n.d.	↓
	2.5	n.d.	1.244	n.d.	–	2.561 ± 0.590	3.673 ± 0.491	n.d.	↓
	0	n.d.	0.988	n.d.	–	n.d.	4.518 ± 0.446	30.642 ± 9.386	↑

Table S3.4: Quantified CK concentrations in culture pellets (fmol/g [DW]) across experimental treatments. Values represent the mean concentration (± standard error, n = 3) of each sample measured at indicated time points. Treatments include varying glucose amendments with and without Cd exposure. Data reflect intracellular CK accumulation as part of the experimental assessment of environmental and nutrient stress on CK production.

	Glucose [g/L]	**MAM**			**Change**	**MAM + 100 µM $CdCl_2$**			**Change**
		Day 1	Day 3	Day 5		Day 1	Day 3	Day 5	
tZ	5	n.d.	n.d.	n.d.	–	n.d.	n.d.	n.d.	–
	2.5	n.d.	n.d.	n.d.	–	n.d.	n.d.	n.d.	–
	0	n.d.	n.d.	n.d.	–	n.d.	n.d.	n.d.	–
tZR	5	n.d.	n.d.	349.657 ± 26.351	↑	n.d.	n.d.	520.286 ± 148.531	↑
	2.5	n.d.	n.d.	268.235 ± 36.009	↑	n.d.	n.d.	600.748 ± 332.808	↑
	0	n.d.	n.d.	n.d.	–	n.d.	n.d.	n.d.	–
tZNT	5	n.d.	n.d.	21.398 ± 6.634	↑	n.d.	n.d.	17.911 ± 5.210	↑
	2.5	1,972.490 ± 983.172	53.585 ± 28.570	113.321 ± 19.537	↓	n.d.	n.d.	n.d.	–
	0	n.d.	243.179 ± 32.772	216.652 ± 64.474	↑	n.d.	n.d.	n.d.	–
cZ	5	n.d.	n.d.	13.863 ± 4.866	↑	n.d.	n.d.	n.d.	–
	2.5	n.d.	n.d.	8.017 ± 3.454	↑	n.d.	n.d.	n.d.	–
	0	n.d.	n.d.	n.d.	–	n.d.	n.d.	n.d.	–
cZNT	5	n.d.	38.629 ± 22.302	25.280 ± 4.715	↑	n.d.	73.857 ± 38.402	200.603 ± 57.963	↑
	2.5	n.d.	122.196 ± 70.550	39.293 ± 22.686	↑	n.d.	187.686 ± 69.105	346.821 ± 141.058	↑
	0	n.d.	116.764 ± 67.414	n.d.	–	n.d.	n.d.	63.302 ± 3.187	↑
iP	5	39.135 ± 11.914	2.522 ± 0.746	n.d.	↓	n.d.	n.d.	13.557 ± 5.581	↑
	2.5	n.d.	2.339 ± 0.729	n.d.	–	n.d.	n.d.	n.d.	–
	0	n.d.	n.d.	n.d.	–	n.d.	n.d.	n.d.	–
iPR	5	n.d.	1.691 ± 0.505	100.107 ± 3.763	↑	n.d.	n.d.	n.d.	–
	2.5	n.d.	n.d.	101.023 ± 17.140	↑	n.d.	n.d.	118.496 ± 52.838	↑
	0	n.d.	n.d.	n.d.	–	n.d.	n.d.	n.d.	–

Table S3.5: Quantified methylthiolated CK concentrations (fmol/mL) in the culture supernatant across experimental treatments. Values represent the mean concentration (± standard error, n = 3) of each sample measured at indicated time points. Treatments include varying glucose amendments with and without Cd exposure. Data reflect extracellular methylated CK accumulation as part of the experimental assessment of environmental and nutrient stress on methylated CK production.

	Glucose [g/L]	**MAM**			**Change**	**MAM + 100 µM $CdCl_2$**			**Change**
		Day 1	Day 3	Day 5		Day 1	Day 3	Day 5	
MeSZ	5	12.948 ± 0.633	137.823 ± 16.279	76.492 ± 2.731	↑	n.d.	185.381 ± 7.025	612.868 ± 257.268	↑
	2.5	18.801 ± 1.288	187.489 ± 8.747	56.142 ± 3.605	↑	n.d.	75.358 ± 5.220	n.d.	–
	0	n.d.	31.493 ± 1.561	32.708 ± 4.432	↑	n.d.	n.d.	n.d.	–
MeSZR	5	2.485 ± 0.416	9.399 ± 1.256	n.d.	↓	11.150 ± 1.003	18.204 ± 5.963	37.494 ± 8.841	↑
	2.5	2.229 ± 0.319	19.083 ± 0.915	n.d.	↓	4.517 ± 0.742	10.195 ± 0.602	n.d.	↓
	0	2.551 ± 0.186	13.919 ± 1.720	18.050 ± 0.184	↑	2.965 ± 0.326	14.793 ± 0.836	n.d.	↓

Table S3.6: Quantified methylthiolated CK concentrations (fmol/g [DW]) in culture pellets across experimental treatments. Values represent the mean concentration (± standard error, n = 3) of each sample measured at indicated time points. Treatments include varying glucose amendments with and without Cd exposure. Data reflect intracellular methylated CK accumulation as part of the experimental assessment of environmental and nutrient stress on methylated CK production.

	Glucose [g/L]	**MAM**			**Change**	**MAM + 100 µM $CdCl_2$**			**Change**
		Day 1	Day 3	Day 5		Day 1	Day 3	Day 5	
MeSZ	5	n.d.	n.d.	n.d.	−	n.d.	n.d.	n.d.	−
	2.5	n.d.	n.d.	n.d.	−	n.d.	n.d.	n.d.	−
	0	n.d.	n.d.	n.d.	−	n.d.	n.d.	n.d.	−
MeSZR	5	n.d.	n.d.	n.d.	−	n.d.	n.d.	n.d.	−
	2.5	n.d.	n.d.	n.d.	−	n.d.	n.d.	n.d.	−
	0	n.d.	n.d.	n.d.	−	n.d.	n.d.	n.d.	−

Table S3.7: Quantified gibberellin concentrations in the culture supernatant (fmol/mL) across experimental treatments. Values represent the mean concentration (± standard error, n = 3) of each sample measured at indicated time points. Treatments include varying glucose amendments with and without Cd exposure. Data reflect extracellular gibberellin accumulation as part of the experimental assessment of environmental and nutrient stress on gibberellin production.

	Glucose [g/L]	Control			Change	Cadmium			Change
		Day 1	Day 3	Day 5		Day 1	Day 3	Day 5	
GA3	5	n.d.	n.d.	8.770 ± 1.234	↑	n.d.	n.d.	n.d.	–
	2.5	n.d.	n.d.	68.224 ± 38.779	↑	n.d.	n.d.	n.d.	–
	0	n.d.	n.d.	2.143 ± 0.122	↑	n.d.	n.d.	n.d.	–
GA4	5	n.d.	n.d.	n.d.	–	n.d.	180,399.436 ± 97,985.708	19,398.803 ± 7,891.018	↑
	2.5	n.d.	n.d.	n.d.	–	n.d.	157,932.445 ± 50,227.927	20,797.342 ± 10,997.882	↓
	0	n.d.	n.d.	n.d.	–	n.d.	n.d.	n.d.	–
GA7	5	n.d.	n.d.	n.d.	–	1,544.157 ± 269.850	84.335 ± 9.537	n.d.	↓
	2.5	n.d.	5.319 ± 3.071	31.574 ± 12.862	↑	3,402.130 ± 919.111	3,965.852 ± 2,264.589	23,409.480 ± 2,074.459	↑
	0	n.d.	n.d.	n.d.	–	n.d.	n.d.	n.d.	–

Table S3.8: Quantified gibberellin concentrations in culture pellets (fmol/g [DW]) across experimental treatments. Values represent the mean concentration (± standard error, n = 3) of each sample measured at indicated time points. Treatments include varying glucose amendments with and without Cd exposure. Data reflect intracellular gibberellin accumulation as part of the experimental assessment of environmental and nutrient stress on gibberellin production.

	Glucose [g/L]	MAM			Change	MAM + 100 µM $CdCl_2$			Change
		Day 1	Day 3	Day 5		Day 1	Day 3	Day 5	
GA3	5	n.d.	n.d.	n.d.	–	n.d.	n.d.	n.d.	–
	2.5	n.d.	n.d.	n.d.	–	n.d.	n.d.	n.d.	–
	0	n.d.	n.d.	n.d.	–	n.d.	n.d.	n.d.	–
GA4	5	n.d.	n.d.	n.d.	–	n.d.	n.d.	n.d.	–
	2.5	n.d.	n.d.	n.d.	–	n.d.	n.d.	n.d.	–
	0	n.d.	n.d.	n.d.	–	n.d.	n.d.	n.d.	–
GA7	5	10,690.680 ± 956.556	504.811 ± 261.805	45.982 ± 13.085	↓	22,236.410 ± 3,409.701	74.025 ± 23.717	39.449 ± 3.297	↓
	2.5	9,631.789 ± 1,885.649	27.921 ± 0.462	129.966 ± 55.723	↓	18,737.977 ± 2,091.436	123.383 ± 37.687	85.619 ± 15.959	↓
	0	3,493.200 ± 338.149	68.753 ± 5.739	51.051 ± 3.183	↓	17,769.584 ± 2,824.381	186.210 ± 49.764	131.189 ± 31.573	↓

Table S3.9: Quantified acidic hormone concentrations in the culture supernatant (pmol/mL) across experimental treatments. Values represent the mean concentration (± standard error, n = 3) of each sample measured at indicated time points. Treatments include varying glucose amendments with and without Cd exposure. Data reflect extracellular acidic hormone accumulation as part of the experimental assessment of environmental and nutrient stress on acidic hormone production.

	Glucose [g/L]	**MAM**			**Change**	**MAM + 100 µM $CdCl_2$**			**Change**
		Day 1	Day 3	Day 5		Day 1	Day 3	Day 5	
ABA	5	1.076 ± 0.158	2.780 ± 0.406	0.952 ± 0.150	↓	0.171 ± 0.028	8.085 ± 4.350	2.857 ± 1.064	↑
	2.5	0.833 ± 0.106	3.382 ± 0.232	0.402 ± 0.134	↓	0.286 ± 0.037	7.715 ± 2.066	17.487 ± 3.280	↑
	0	0.163 ± 0.024	0.448 ± 0.053	0.320 ± 0.065	↑	n.d.	0.603 ± 0.066	0.745 ± 0.041	↑
IAA	5	3.470 ± 0.179	7.569 ± 0.399	0.753 ± 0.237	↓	5.261 ± 0.356	32.347 ± 1.298	17.531 ± 6.894	↑
	2.5	3.828 ± 0.080	12.526 ± 1.416	n.d.	↓	5.184 ± 0.030	26.252 ± 3.182	n.d.	↓
	0	2.194 ± 0.035	3.533 ± 0.316	1.081 ± 0.146	↓	6.563 ± 0.017	17.798 ± 2.324	8.347 ± 1.175	↑
JA	5	n.d.	122.025 ± 27.938	n.d.	–	11.922 ± 6.883	706.392 ± 129.929	32.973 ± 15.203	↑
	2.5	189.563 ± 58.931	1,751.943 ± 819.498	n.d.	↓	50.636 ± 18.281	1,191.295 ± 687.794	866.985 ± 81.061	↑
	0	n.d.	n.d.	n.d.	–	n.d.	n.d.	n.d.	–
SA	5	247,881.983 ± 110,415.971	28,015.481 ± 2,596.282	19,287.359 ± 11,135.562	↓	15,943.776 ± 6,352.508	236,085.369 ± 36,316.032	17,990.354 ± 2,048.180	↑
	2.5	21,301.229 ± 5,571.372	248,546.777 ± 103,358.373	n.d.	↓	14,875.196 ± 787.820	780,674.129 ± 252,116.032	125,914.032 ± 5,696.654	↑
	0	2,850.578 ± 1,001.906	372.308 ± 156.192	224.440 ± 57.320	↓	220.517 ± 72.220	297.049 ± 93.276	711.275 ± 66.177	↑

Table S3.10: Quantified acidic hormone concentrations in culture pellets (pmol/g [DW]) across experimental treatments. Values represent the mean concentration (± standard error, n = 3) of each sample measured at indicated time points. Treatments include varying glucose amendments with and without Cd exposure. Data reflect intracellular acidic hormone accumulation as part of the experimental assessment of environmental and nutrient stress on acidic hormone production.

	Glucose [g/L]	**MAM**			**Change**	**MAM + 100 µM $CdCl_2$**			**Change**
		Day 1	Day 3	Day 5		Day 1	Day 3	Day 5	
ABA	5	12.814 ± 1.756	2.028 ± 0.299	2.636 ± 0.351	↓	5.756 ± 1.324	0.367 ± 0.075	0.161 ± 0.016	↓
	2.5	15.761 ± 4.713	0.955 ± 0.238	2.599 ± 0.014	↓	5.932 ± 1.578	0.344 ± 0.107	0.159 ± 0.035	↓
	0	4.723 ± 0.355	7.231 ± 1.343	5.621 ± 1.238	↑	4.026 ± 0.288	1.400 ± 0.499	2.364 ± 0.716	↓
IAA	5	1.286 ± 0.049	0.791 ± 0.068	3.888 ± 0.193	↑	n.d.	1.444 ± 0.175	8.355 ± 0.942	↑
	2.5	2.020 ± 0.646	0.880 ± 0.046	5.121 ± 0.490	↑	n.d.	1.078 ± 0.137	4.332 ± 0.817	↑
	0	0.557 ± 0.098	1.114 ± 0.181	3.036 ± 0.497	↑	n.d.	n.d.	1.411 ± 0.191	↑
JA	5	29,986.958 ± 13,055.410	501.430 ± 9.730	107.563 ± 26.654	↓	5,230.309 ± 954.169	894.898 ± 202.984	n.d.	↓
	2.5	10,976.027 ± 2,456.056	70.459 ± 25.996	123.150 ± 31.847	↓	2,285.386 ± 670.090	607.142 ± 141.289	n.d.	↓
	0	2,787.800 ± 1,061.575	3,285.327 ± 1,303.349	390.771 ± 70.113	↓	3,910.259 ± 570.027	2,828.120 ± 456.248	1,168.303 ± 374.982	↓
SA	5	225,044.465 ± 58,072.318	31,830.248 ± 3,732.080	1,302.979 ± 341.306	↓	140,719.359 ± 21,216.086	47,857.399 ± 11,076.129	1,013.295 ± 73.395	↓
	2.5	155,301.476 ± 22,528.209	8,305.608 ± 1,467.990	4,908.685 ± 1,403.061	↓	59,578.801 ± 17,199.387	46,723.513 ± 10,638.970	524.686 ± 411.758	↓
	0	45,145.799 ± 7,872.895	125,446.832 ± 31,841.829	24,698.259 ± 2,425.237	↓	101,762.493 ± 11,108.919	82,524.811 ± 20,749.825	65,966.701 ± 15,719.629	↓

3.9 REFERENCES

1. Canada NR. Minerals and the economy. 2018. https://natural-resources.canada.ca/minerals-mining/mining-data-statistics-analysis/minerals-economy/minerals-economy (accessed June 24, 2025).
2. Canada S. Human activity and the environment. Can Public Policy Anal Polit. 2012;4(4):587. https://doi.org/10.2307/3549992.
3. Canada G of CC-IR and NA. Mine closure, reclamation and monitoring. 2022. https://www.rcaanc-cirnac.gc.ca/eng/1646321588912/1646321643743?utm_source=chatgpt.com (accessed June 24, 2025).
4. Canada NR. Tailings management at NRCan. 2013. https://natural-resources.canada.ca/maps-tools-publications/publications/tailings-management-nrcan (accessed June 24, 2025).
5. Beckett C, and Keeling A. Rethinking remediation: mine reclamation, environmental justice, and relations of care. Local Environ. 2019;24(3):216–30. https://doi.org/10.1080/13549839.2018.1557127.
6. Anglin C. Mount Polley mine tailings spill: Five years later. In: Furey R, Lupo JF, editors. Mine Tailings: Perspectives for a Changing World. Englewood, Colorado: Society for Mining, Metallurgy & Exploration; 2020. p. 21–8.
7. Mining and Mineral Sciences Laboratories, CANMET-Mineral Technology Branch. Programs to enhance and sustain safety and the quality of the environment in and around orphaned and abandoned mine sites. Ottawa, Ontario: Natural Resources Canada; 2013.
8. Sun W, Ji B, Khoso SA, Tang H, Liu R, Wang L, *et al*. An extensive review on restoration technologies for mining tailings. Environ Sci Pollut Res. 2018;25(34):33911–25. https://doi.org/10.1007/s11356-018-3423-y.
9. Moodley I, Sheridan CM, Kappelmeyer U, Akcil A. Environmentally sustainable acid mine drainage remediation: Research developments with a focus on waste/by-products. Miner Eng. 2018;126:207–20. https://doi.org/10.1016/j.mineng.2017.08.008.
10. Jayapal A, Chaterjee T, Sahariah BP. Bioremediation techniques for the treatment of mine tailings: A review. Soil Ecol Lett. 2023;5(2):220149. https://doi.org/10.1007/s42832-022-0149-z.
11. Anusha P, Natarajan D. Bioremediation potency of multi metal tolerant native bacteria *Bacillus cereus* isolated from bauxite mines, kolli hills, Tamilnadu- A lab to land approach. Biocatal Agric Biotechnol. 2020;25:101581. https://doi.org/10.1016/j.bcab.2020.101581.
12. Malletzidou L, Kyratzopoulou E, Nerantzis E, Kyzaki N, Tsirliganis NC, Kazakis NA. Optimizing *Chlorella vulgaris* bioremediation of wastewater via advanced aeration systems: A pilot-scale implementation. Processes. 2025;13(6):1709. https://doi.org/10.3390/pr13061709.
13. Doni S, Macci C, Peruzzi E, Iannelli R, Masciandaro G. Heavy metal distribution in a sediment phytoremediation system at pilot scale. Ecol Eng. 2015;81:146–57. https://doi.org/10.1016/j.ecoleng.2015.04.049.
14. Dell'Anno F, Rastelli E, Buschi E, Barone G, Beolchini F, Dell'Anno A. Fungi can be more effective than bacteria for the bioremediation of marine sediments highly

contaminated with heavy metals. Microorganisms. 2022;10(5):993. https://doi.org/10.3390/microorganisms10050993.
15. Babu AG, Shim J, Bang K-S, Shea PJ, Oh B-T. *Trichoderma virens* PDR-28: A heavy metal-tolerant and plant growth-promoting fungus for remediation and bioenergy crop production on mine tailing soil. J Environ Manage. 2014;132:129–34. https://doi.org/10.1016/j.jenvman.2013.10.009.
16. Brar KK, Etteieb S, Magdouli S, Calugaru L, Brar SK. Novel approach for the management of acid mine drainage (AMD) for the recovery of heavy metals along with lipid production by *Chlorella vulgaris*. J Environ Manage. 2022;308:114507. https://doi.org/10.1016/j.jenvman.2022.114507.
17. Deng X, Jia P. Construction and characterization of a photosynthetic bacterium genetically engineered for Hg^{2+} uptake. Bioresour Technol. 2011;102(3):3083–8. https://doi.org/10.1016/j.biortech.2010.10.051.
18. Ameen FA, Hamdan AM, El-Naggar MY. Assessment of the heavy metal bioremediation efficiency of the novel marine lactic acid bacterium, Lactobacillus plantarum MF042018. Sci Rep. 2020;10(1):314. https://doi.org/10.1038/s41598-019-57210-3.
19. Liu H, Hong Z, Lin J, Huang D, Ma LQ, Xu J, *et al*. Bacterial coculture enhanced Cd sorption and As bioreduction in co-contaminated systems. J Hazard Mater. 2023;444:130376. https://doi.org/10.1016/j.jhazmat.2022.130376.
20. Wang J, Chen R, Fan L, Cui L, Zhang Y, Cheng J, *et al*. Construction of fungi-microalgae symbiotic system and adsorption study of heavy metal ions. Sep Purif Technol. 2021;268(April):118689. https://doi.org/10.1016/j.seppur.2021.118689.
21. Wang J, Tian Q, Cui L, Cheng J, Zhou H, Zhang Y, *et al*. Synergism and mutualistic interactions between microalgae and fungi in fungi-microalgae symbiotic system. Bioresour Technol. 2022;361:127728. https://doi.org/10.1016/j.biortech.2022.127728.
22. Liu J, Sun S, Chen K, Gao S, Chen D, Zhang Y, *et al*. Discerning promotion mechanisms of fungi *Clonostachys rosea* on growth of freshwater microalga *Chlorella* sp. by non-contact culture. Algal Res. 2025;86:103967. https://doi.org/10.1016/j.algal.2025.103967.
23. Xu S, Li M, Hu Z, Shao Y, Ying J, Zhang H. The Potential Use of Fungal Co-Culture Strategy for Discovery of New Secondary Metabolites. Microorganisms. 2023;11(2):464. https://doi.org/10.3390/microorganisms11020464.
24. Wang J, Tian Q, Zhou H, Kang J, Yu X, Shen L. Key metabolites and regulatory network mechanisms in co-culture of fungi and microalgae based on metabolomics analysis. Bioresour Technol. 2023;388:129718. https://doi.org/10.1016/j.biortech.2023.129718.
25. Bansfield D, Spilling K, Mikola A, Piiparinen J. Bioflocculation of *Euglena gracilis* via direct application of fungal filaments: a rapid harvesting method. J Appl Phycol. 2022;34(1):321–34. https://doi.org/10.1007/s10811-021-02651-5.
26. Chen J, Leng L, Ye C, Lu Q, Addy M, Wang J, *et al*. A comparative study between fungal pellet- and spore-assisted microalgae harvesting methods for algae bioflocculation. Bioresour Technol. 2018;259:181–90. https://doi.org/10.1016/j.biortech.2018.03.040.

27. Das PK, Rani J, Rawat S, Kumar S. Microalgal Co-cultivation for Biofuel Production and Bioremediation: Current Status and Benefits. BioEnergy Res. 2022;15:1–26. https://doi.org/10.1007/s12155-021-10254-8/Published.
28. Naseema Rasheed R, Pourbakhtiar A, Mehdizadeh Allaf M, Baharlooeian M, Rafiei N, Alishah Aratboni H, *et al*. Microalgal co-cultivation -recent methods, trends in omic-studies, applications, and future challenges. Front Bioeng Biotechnol. 2023;11:1193424. https://doi.org/10.3389/fbioe.2023.1193424.
29. Sonker S, Fulke AB, Monga A. Recent trends on bioremediation of heavy metals; an insight with reference to the potential of marine microbes. Int J Environ Sci Technol. 2024;21(15):9763–74. https://doi.org/10.1007/s13762-024-05673-x.
30. Karim A, Islam MA, Khalid ZB, Yousuf A, Khan MdMR, Mohammad Faizal CK. Microbial lipid accumulation through bioremediation of palm oil mill effluent using a yeast-bacteria co-culture. Renew Energy. 2021;176:106–14. https://doi.org/10.1016/j.renene.2021.05.055.
31. Zhang B, Wu L, Shi W, Zhang Z, Lens PNL. A novel strategy for rapid development of a self-sustaining symbiotic algal-bacterial granular sludge: Applying algal-mycelial pellets as nuclei. Water Res. 2022;214:118210. https://doi.org/10.1016/J.WATRES.2022.118210.
32. Abbasi, M, Khan I, Rehman A, Hayat A, Ur Rehman M, Shah TA, *et al*. Bioremediation of Heavy Metals Contaminated Soil by Using Indigenous Metallotolerant Bacterial Isolates. Appl Ecol Environ Res. 2024;22(2):1623–48. https://doi.org/10.15666/aeer/2202_16231648.
33. Sarkar S, Rekha PN, Ambasankar K, Vijayan KK. Bioremediation efficiency of indigenous seaweeds of Chennai coast in brackishwater system. Aquac Int. 2021;29(1):233–51. https://doi.org/10.1007/s10499-020-00621-1.
34. Talukdar D, Jasrotia T, Sharma R, Jaglan S, Kumar R, Vats R, *et al*. Evaluation of novel indigenous fungal consortium for enhanced bioremediation of heavy metals from contaminated sites. Environ Technol Innov. 2020;20:101050. https://doi.org/10.1016/j.eti.2020.101050.
35. Firincă C, Zamfir L-G, Constantin M, Răut I, Capră L, Popa D, *et al*. Microbial Removal of Heavy Metals from Contaminated Environments Using Metal-Resistant Indigenous Strains. J Xenobiotics. 2023;14(1):51–78. https://doi.org/10.3390/jox14010004.
36. Kaszecki E, Palberg D, Grant M, Griffin S, Dhanjal C, Capperauld M, *et al*. *Euglena mutabilis* exists in a FAB consortium with microbes that enhance cadmium tolerance. Int Microbiol. 2024. https://doi.org/10.1007/s10123-023-00474-7.
37. Krajčovič J, Matej Vesteg, Schwartzbach SD. Euglenoid flagellates: A multifaceted biotechnology platform. J Biotechnol. 2015;202:135–45. https://doi.org/10.1016/j.jbiotec.2014.11.035.
38. Ebenezer TE, Low RS, O'Neill EC, Huang I, DeSimone A, Farrow SC, *et al*. *Euglena* International Network (EIN): Driving euglenoid biotechnology for the benefit of a challenged world. Biol Open. 2022;11(11):bio059561. https://doi.org/10.1242/bio.059561.
39. Kostygov AY, Karnkowska A, Votýpka J, Tashyreva D, Maciszewski K, Yurchenko V, *et al*. Euglenozoa: taxonomy, diversity and ecology, symbioses and viruses. Open Biol. 2021;11(3):200407. https://doi.org/10.1098/rsob.200407.

40. Kaszecki E, Kennedy V, Shah M, Maciszewski K, Karnkowska A, Linton E, *et al*. Meeting Report: Euglenids in the Age of Symbiogenesis: Origins, Innovations, and Prospects, November 8–11, 2021. Protist. 2022;173(4):125894. https://doi.org/10.1016/j.protis.2022.125894.
41. Nguyen NH, Nguyen QT, Dang DH, Emery RJN. Phytohormones enhance heavy metal responses in *Euglena gracilis*: Evidence from uptake of Ni, Pb and Cd and linkages to hormonomic and metabolomic dynamics. Environ Pollut. 2023;320:121094. https://doi.org/10.1016/j.envpol.2023.121094.
42. Jia Y, Du J, Fang H, Zhao G, Tian X. Inhibition of freshwater algal species by co-culture with two fungi. Mater Sci Eng C. 2013;33(4):2451–4. https://doi.org/10.1016/j.msec.2013.01.034.
43. Sittenfeld A, Mora M, Ortega JM, Albertazzi F, Cordero A, Roncel M, *et al*. Characterization of a photosynthetic *Euglena* strain isolated from an acidic hot mud pool of a volcanic area of Costa Rica. FEMS Microbiol Ecol. 2002;42(1):151–61. https://doi.org/10.1111/j.1574-6941.2002.tb01004.x.
44. Gross W, Oesterhelt C, Tischendorf G, Lederer F. Characterization of a non-thermophilic strain of the red algal genus *Galdieria* isolated from Soos (Czech Republic). Eur J Phycol. 2002;37(3):477–82. https://doi.org/10.1017/S0967026202003773.
45. Halter D, Goulhen-Chollet F, Gallien S, Casiot C, Hamelin J, Gilard F, *et al*. In situ proteo-metabolomics reveals metabolite secretion by the acid mine drainage bio-indicator, *Euglena mutabilis*. ISME J. 2012;6(7):1391–402. https://doi.org/10.1038/ismej.2011.198.
46. Olaveson MM, Stokes PM. Reponses of the Acidiphilic Alga *Euglena* mutablilis (Euglenophyceae) to Carbon Enrichent at pH 3. J Phycol. 1989;25(3):529–39. https://doi.org/10.1111/j.1529-8817.1989.tb00259.x.
47. Kennedy V, Kaszecki E, Donaldson ME, Saville BJ. The impact of elevated sulfur and nitrogen levels on cadmium tolerance in *Euglena* species. Sci Rep. 2024;14(1):11734. https://doi.org/10.1038/s41598-024-61964-w.
48. Nakatsu C, Hutchinson TC. Extreme metal and acid tolerance of *Euglena mutabilis* and an associated yeast from Smoking Hills, Northwest Territories, and their apparent mutualism. Microb Ecol. 1988;16(2):213–31. https://doi.org/10.1007/BF02018915.
49. Li L, Liu Z, Zhang M, Meng D, Liu X, Wang P, *et al*. Insights into the Metabolism and Evolution of the Genus Acidiphilium, a Typical Acidophile in Acid Mine Drainage. mSystems. 2020;5(6):e00867-20. https://doi.org/10.1128/mSystems.00867-20.
50. Priya A, Hait S. Biometallurgical recovery of metals from waste printed circuit boards using pure and mixed strains of Acidithiobacillus ferrooxidans and Acidiphilium acidophilum. Process Saf Environ Prot. 2020;143:262–72. https://doi.org/10.1016/j.psep.2020.06.042.
51. El-Shahir AA, El-Tayeh NA, Ali OM, Abdel Latef AAH, Loutfy N. The Effect of Endophytic Talaromyces pinophilus on Growth, Absorption and Accumulation of Heavy Metals of Triticum aestivum Grown on Sandy Soil Amended by Sewage Sludge. Plants. 2021;10(12):2659. https://doi.org/10.3390/plants10122659.
52. Xiao Y, Chen R, Chen L, Yang B, Jiang L, Fang J. Endophytic Fungus Talaromyces sp. MR1 Promotes the Growth and Cadmium Uptake of Arabidopsis thaliana L.

Under Cadmium Stress. Curr Microbiol. 2023;80(11):346. https://doi.org/10.1007/s00284-023-03453-3.
53. Priyanka, Dwivedi SK. Hexavalent chromium (Cr^{+6}) detoxification potential and stress response of fungus Talaromyces pinophillus isolated from tannery wastewater. Environ Adv. 2023;13:100417. https://doi.org/10.1016/j.envadv.2023.100417.
54. Kharkwal AC, Joshi H, Shandilya C, Dabral S, Kumar N, Varma A. Isolation and characterization of a newly discovered plant growth-promoting endophytic fungal strain from the genus *Talaromyces*. Sci Rep. 2024;14(1):6022. https://doi.org/10.1038/s41598-024-54687-5.
55. Avilés C, Loza-Tavera H, Terry N, Moreno-Sánchez R. Mercury pretreatment selects an enhanced cadmium-accumulating phenotype in *Euglena gracilis*. Arch Microbiol. 2003;180(1):1–10. https://doi.org/10.1007/s00203-003-0547-2.
56. Mendoza-Cózatl DG, Moreno-Sánchez R. Cd^{2+} transport and storage in the chloroplast of *Euglena gracilis*. Biochim Biophys Acta BBA - Bioenerg. 2005;1706(1–2):88–97. https://doi.org/10.1016/j.bbabio.2004.09.010.
57. Canadian Phycological Culture Centre. Modified acid medium (MAM). University of Waterloo. 2017. https://uwaterloo.ca/canadian-phycological-culture-centre/cultures/culture-media/modified-acid-medium.
58. Warren CR. Rapid measurement of chlorophylls with a microplate reader. J Plant Nutr. 2008;31(7):1321–32. https://doi.org/10.1080/01904160802135092.
59. Metcalfe CD, Sultana T, Martin J, Newman K, Helm P, Kleywegt S, *et al*. Silver near municipal wastewater discharges into western Lake Ontario, Canada. Environ Monit Assess. 2018;190(9):555. https://doi.org/10.1007/s10661-018-6922-x.
60. Gibb M, Kisiala AB, Morrison EN, Emery RJN. The origins and roles of methylthiolated cytokinins: Evidence from among life kingdoms. Front Cell Dev Biol. 2020;8:605672. https://doi.org/10.3389/fcell.2020.605672.
61. Šimura J, Antoniadi I, Široká J, Tarkowská D, Strnad M, Ljung K, *et al*. Plant hormonomics: Multiple phytohormone profiling by targeted metabolomics. Plant Physiol. 2018;177(2):476–89. https://doi.org/10.1104/pp.18.00293.
62. Kisiala A, Kambhampati S, Stock NL, Aoki M, Emery RJN. Quantification of cytokinins using high-resolution accurate-mass orbitrap mass spectrometry and parallel reaction monitoring (PRM). Anal Chem. 2019;91(23):15049–56. https://doi.org/10.1021/acs.analchem.9b03728.
63. Murtey MD, Ramasamy P. Life science sample preparations for scanning electron microscopy. Acta Microsc. 2021;30(2):80–91.
64. Ramanan R, Kim BH, Cho DH, Oh HM, Kim HS. Algae-bacteria interactions: Evolution, ecology and emerging applications. Biotechnol Adv. 2016;34(1):14–29. https://doi.org/10.1016/j.biotechadv.2015.12.003.
65. Ayangbenro AS, Babalola OO, Aremu OS. Bioflocculant production and heavy metal sorption by metal resistant bacterial isolates from gold mining soil. Chemosphere. 2019;231:113–20. https://doi.org/10.1016/j.chemosphere.2019.05.092.
66. Yang Y, Guo W, Ngo HH, Zhang X, Liang S, Deng L, *et al*. Bioflocculants in anaerobic membrane bioreactors: A review on membrane fouling mitigation strategies. Chem Eng J. 2024;486:150260. https://doi.org/10.1016/j.cej.2024.150260.

67. Kurniawan SB, Imron MF, Chik CENCE, Owodunni AA, Ahmad A, Alnawajha MM, *et al*. What compound inside biocoagulants/bioflocculants is contributing the most to the coagulation and flocculation processes? Sci Total Environ. 2022;806:150902. https://doi.org/10.1016/j.scitotenv.2021.150902.
68. Matter IA, Bui VKH, Jung M, Seo JY, Kim Y-E, Lee Y-C, *et al*. Flocculation harvesting techniques for microalgae: A review. Appl Sci. 2019;9(15):3069. https://doi.org/10.3390/app9153069.
69. Viraj Krishna Mishra. Microbial flocculants and its application in wastewater treatments: A review. J Water Pollut Purif Res. 2016;3(1):1–9.
70. Manheim D, Nelson Y. Settling and bioflocculation of two species of algae used in wastewater treatment and algae biomass production. Environ Prog Sustain Energy. 2013;32(4):946–54. https://doi.org/10.1002/ep.11861.
71. Yang Y, Jiang C, Wang X, Fan L, Xie Y, Wang D, *et al*. Unraveling the potential of microbial flocculants: Preparation, performance, and applications in wastewater treatment. Water. 2024;16(14):1995. https://doi.org/10.3390/w16141995.
72. Li Y, Xu Y, Song R, Tian C, Liu L, Zheng T, *et al*. Flocculation characteristics of a bioflocculant produced by the actinomycete *Streptomyces* sp. hsn06 on microalgae biomass. BMC Biotechnol. 2018;18(1):58. https://doi.org/10.1186/s12896-018-0471-9.
73. Zhao D, Cheah WY, Lai SH, Ng E-P, Khoo KS, Show PL, *et al*. Symbiosis of microalgae and bacteria consortium for heavy metal remediation in wastewater. J Environ Chem Eng. 2023;11(3):109943. https://doi.org/10.1016/j.jece.2023.109943.
74. Nazari MT, Freitag JF, Cavanhi VAF, Colla LM. Microalgae harvesting by fungal-assisted bioflocculation. Rev Environ Sci Biotechnol. 2020;19(2):369–88. https://doi.org/10.1007/s11157-020-09528-y.
75. Muradov N, Taha M, Miranda AF, Wrede D, Kadali K, Gujar A, *et al*. Fungal-assisted algal flocculation: Application in wastewater treatment and biofuel production. Biotechnol Biofuels. 2015;8(24). https://doi.org/10.1186/s13068-015-0210-6.
76. Bhattacharya A, Mathur M, Kumar P, Prajapati SK, Malik A. A rapid method for fungal assisted algal flocculation: Critical parameters & mechanism insights. Algal Res. 2017;21:42–51. https://doi.org/10.1016/j.algal.2016.10.022.
77. Wang Q-R, Hong Y, Li L-H. Insights into differences between spore-assisted and pellet-assisted microalgae harvesting using a highly efficient fungus: Efficiency, high-value substances, and mechanisms. Sci Total Environ. 2023;877:162945. https://doi.org/10.1016/j.scitotenv.2023.162945.
78. Chu R, Li S, Yin Z, Hu D, Zhang L, Xiang M, *et al*. A fungal immobilization technique for efficient harvesting of oleaginous microalgae: Key parameter optimization, mechanism exploration and spent medium recycling. Sci Total Environ. 2021;790:148174. https://doi.org/10.1016/j.scitotenv.2021.148174.
79. Laezza C, Salbitani G, Carfagna S. Fungal contamination in microalgal cultivation: Biological and biotechnological aspects of fungi-microalgae interaction. J Fungi. 2022;8(10):1099. https://doi.org/10.3390/jof8101099.
80. Xiao Y, Chen R, Chen L, Yang B, Jiang L, Fang J. Endophytic gungus *Talaromyces* sp. MR1 promotes the growth and cadmium uptake of *Arabidopsis thaliana* L. under

cadmium stress. Curr Microbiol. 2023;80(11):346. https://doi.org/10.1007/s00284-023-03453-3.
81. Krespach MKC, García-Altares M, Flak M, Hanno Schoeler, Scherlach K, Netzker T, *et al*. Lichen-like association of *Chlamydomonas reinhardtii* and *Aspergillus nidulans* protects algal cells from bacteria. ISME J. 2020;14(11):2794–805. https://doi.org/10.1038/s41396-020-0731-2.
82. Du Z-Y, Zienkiewicz K, Pol NV, Ostrom NE, Benning C, Bonito GM. Algal-fungal symbiosis leads to photosynthetic mycelium. Front Plant Sci. 2019;12. https://doi.org/10.7554/eLife.47815.001.
83. Ogbonna JC, Tanaka H. Production of pure photosynthetic cell biomass for environmental biosensors. Mater Sci Eng C. 2000;12(1–2):9–15. https://doi.org/10.1016/S0928-4931(00)00150-8.
84. Yoshida N, Ikeda R, Okuno T. Identification and characterization of heavy metal-resistant unicellular alga isolated from soil and its potential for phytoremediation. Bioresour Technol. 2006;97(15):1843–9. https://doi.org/10.1016/j.biortech.2005.08.021.
85. Khatiwada B, Sunna A, Nevalainen H. Molecular tools and applications of *Euglena gracilis* : From biorefineries to bioremediation. Biotechnol Bioeng. 2020;117(12):3952–67. https://doi.org/10.1002/bit.27516.
86. Khatiwada B, Hasan MT, Sun A, Kamath KS, Mirzaei M, Sunna A, *et al*. Proteomic response of *Euglena gracilis* to heavy metal exposure – Identification of key proteins involved in heavy metal tolerance and accumulation. Algal Res. 2020;45:101764. https://doi.org/10.1016/j.algal.2019.101764.
87. Abreu AP, Fernandes B, Vicente AA, Teixeira J, Dragone G. Mixotrophic cultivation of *Chlorella vulgaris* using industrial dairy waste as organic carbon source. Bioresour Technol. 2012;118:61–6. https://doi.org/10.1016/j.biortech.2012.05.055.
88. Li B, Zhang T, Yang Z. Immobilizing unicellular microalga on pellet-forming filamentous fungus: Can this provide new insights into the remediation of arsenic from contaminated water? Bioresour Technol. 2019;284:231–9. https://doi.org/10.1016/j.biortech.2019.03.128.
89. Mendoza-Cozatl D, Devars S, Loza-Tavera H, Moreno-Sánchez R. Cadmium accumulation in the chloroplast of *Euglena gracilis*. Physiol Plant. 2002;115(2):276–83. https://doi.org/10.1034/j.1399-3054.2002.1150214.x.
90. Rodríguez-Zavala JS, García-García JD, Ortiz-Cruz MA, Moreno-Sánchez R. Molecular mechanisms of resistance to heavy metals in the protist *Euglena gracilis*. J Environ Sci Health Part A. 2007;42(10):1365–78. https://doi.org/10.1080/10934520701480326.
91. Zhang L, Xu X, Sun Y, Huang Y, Yang Z. Metabolic plasticity endows mixotrophic organisms with high tolerance to cadmium and special potential for recovering cadmium-contaminated aquatic environment. Appl Environ Microbiol. 2023;89(7):e00228-23. https://doi.org/10.1128/aem.00228-23.
92. Khatiwada B, Hasan MT, Sun A, Kamath KS, Mirzaei M, Sunna A, *et al*. Probing the role of the chloroplasts in heavy metal tolerance and accumulation in *Euglena gracilis*. Microorganisms. 2020;8(1):115. https://doi.org/10.3390/microorganisms8010115.

93. Guerra Sierra BE, Arteaga-Figueroa LA, Sierra-Pelaéz S, Alvarez JC. *Talaromyces santanderensis*: A new cadmium-tolerant fungus from cacao soils in Colombia. J Fungi. 2022;8(10):1042. https://doi.org/10.3390/jof8101042.
94. Romero MC, Reinoso EH, Urrutia MI, Keiran AM. Biosorption of heavy metals by *Talaromyces helicus*: A trained fungus for copper and biphenyl detoxification. Electron J Biotechnol. 2006;9(3):221–6. https://doi.org/10.2225/vol9-issue3-fulltext-11.
95. Lu X, Yamaji K, Haruma T, Doyama K, Masuya H. Root endophytic *Phialocephala fortinii* and *Talaromyces verruculosus* enhance growth and affect heavy metal tolerance of *Miscanthus sinensis* Andersson growing naturally at a mine site. J Plant Interact. 2024;19(1):2370980. https://doi.org/10.1080/17429145.2024.2370980.
96. Nam I-H, Murugesan K, Ryu J, Kim JH. Arsenic (As) removal using *Talaromyces* sp. KM-31 isolated from As-contaminated mine soil. Minerals. 2019;9(10):568. https://doi.org/10.3390/min9100568.
97. Buck KR, Barry JP, Hallam SJ. *Thioploca* spp. sheaths as niches for bacterial and protistan assemblages. Mar Ecol. 2014;35(3):395–400. https://doi.org/10.1111/maec.12076.
98. Akya A, Pointon A, Thomas C. *Listeria monocytogenes* does not survive ingestion by Acanthamoeba polyphaga. Microbiol Read Engl. 2009;156:809–18. https://doi.org/10.1099/mic.0.031146-0.
99. Kawafune K, Hongoh Y, Hamaji T, Nozaki H. Molecular identification of rickettsial endosymbionts in the non-phagotrophic volvocalean green algae. PLOS ON*E.* 2012;7(2):e31749. https://doi.org/10.1371/journal.pone.0031749.
100. Maruyama S, Kim *E.* A modern descendant of early green algal phagotrophs. Curr Biol. 2013;23(12):1081–4. https://doi.org/10.1016/j.cub.2013.04.063.
101. Shin W, Boo SM, Fritz L. Endonuclear bacteria in *Euglena* hemichromata (Euglenophyceae): A proposed pathway to endonucleobiosis. Phycologia. 2003;42(2):198–203. https://doi.org/10.2216/i0031-8884-42-2-198.1.
102. Willey RL, Walne PL, Kivic P, Patterson DJ. Phagotrophy and the origins of the euglenoid flagellates. Crit Rev Plant Sci. 1988;7(4):303–40. https://doi.org/10.1080/07352688809382268.
103. Henze K, Badr A, Wettern M, Cerff R, Martin W. A nuclear gene of eubacterial origin in *Euglena gracilis* reflects cryptic endosymbioses during protist evolution. Proc Natl Acad Sci. 1995;92(20):9122–6. https://doi.org/10.1073/pnas.92.20.9122.
104. Zakryś B, Milanowski R, Karnkowska A. Evolutionary origin of *Euglena*. In: Schwartzbach SD, Shigeoka S, editors. *Euglena*: Biochemistry, Cell and Molecular Biology. Cham: Springer International Publishing; 2017. p. 3–17.
105. Hahn MW, Höfle MG. Grazing of protozoa and its effect on populations of aquatic bacteria. FEMS Microbiol Ecol. 2001;35(2):113–21. https://doi.org/10.1111/j.1574-6941.2001.tb00794.x.
106. Amaro F, Martín-González A. Microbial warfare in the wild—the impact of protists on the evolution and virulence of bacterial pathogens. Int Microbiol. 2021;24(4):559–71. https://doi.org/10.1007/s10123-021-00192-y.
107. Gong J, Qing Y, Zou S, Fu R, Su L, Zhang X, *et al*. Protist-bacteria associations: gammaproteobacteria and alphaproteobacteria are prevalent as digestion-resistant bacteria in ciliated protozoa. Front Microbiol. 2016;7. https://doi.org/10.3389/fmicb.2016.00498.

108. Ebenezer TE, Low RS, O'Neill EC, Huang I, DeSimone A, Farrow SC, *et al*. *Euglena* International Network (EIN): Driving euglenoid biotechnology for the benefit of a challenged world. Biol Open. 2022;11(11):bio059561. https://doi.org/10.1242/bio.059561.
109. Thompson MD, Copertino DW, Thompson E, Favreau MR, Hallick RB. Evidence for the late origin of introns in chloroplast genes from an evolutionary analysis of the genus *Euglena*. Nucleic Acids Res. 1995;23(23):4745–52. https://doi.org/10.1093/nar/23.23.4745.
110. Kuhne AM, Morrison EN, Sultana T, Kisiala AB, Horlock-Roberts K, Noble A, *et al*. Cultivation of heterotrophic *Euglena gracilis*: The effects of recycled media on culture growth and associations with growth regulating phytohormone profiles. J Appl Phycol. 2023;35(5):2161–75. https://doi.org/10.1007/s10811-023-03062-4.
111. Noble A, Kisiala A, Galer A, Clysdale D, Emery RJN. *Euglena gracilis* (Euglenophyceae) produces abscisic acid and cytokinins and responds to their exogenous application singly and in combination with other growth regulators. Eur J Phycol. 2014;49(2):244–54. https://doi.org/10.1080/09670262.2014.911353.
112. Swaminathan S, Bock RM. Isolation and identification of cytokinins from *Euglena gracilis* transfer ribonucleic acid. Biochemistry. 1977;16(7):1355–60. https://doi.org/10.1021/bi00626a018.
113. Bean KM, Kisiala AB, Morrison EN, Emery RJN. *Trichoderma* synthesizes cytokinins and alters cytokinin dynamics of inoculated *Arabidopsis* seedlings. J Plant Growth Regul. 2021;(0123456789). https://doi.org/10.1007/s00344-021-10466-4.
114. Anand G, Gupta R, Marash I, Leibman-Markus M, Bar M. Cytokinin production and sensing in fungi. Microbiol Res. 2022;262:127103. https://doi.org/10.1016/j.micres.2022.127103.
115. Hinsch J, Galuszka P, Tudzynski P. Functional characterization of the first filamentous fungal tRNA-isopentenyltransferase and its role in the virulence of *Claviceps purpurea*. New Phytol. 2016;211(3):980–92. https://doi.org/10.1111/nph.13960.
116. Hinsch J, Vrabka J, Oeser B, Novák O, Galuszka P, Tudzynski P. *De novo* biosynthesis of cytokinins in the biotrophic fungus *C laviceps purpurea*. Environ Microbiol. 2015;17(8):2935–51. https://doi.org/10.1111/1462-2920.12838.
117. Zhang X, Chen Y, Lin X, Hong X, Zhu Y, Li W, *et al*. Adenine phosphoribosyl transferase 1 is a key enzyme catalyzing cytokinin conversion from nucleobases to nucleotides in *Arabidopsis*. Mol Plant. 2013;6(5):1661–72. https://doi.org/10.1093/mp/sst071.
118. Gibb M, Kisiala AB, Morrison EN, Emery RJN. The origins and roles of methylthiolated cytokinins: Evidence from among life kingdoms. Front Cell Dev Biol. 2020;8:605672. https://doi.org/10.3389/fcell.2020.605672.
119. Kambhampati S, Kurepin LV, Kisiala AB, Bruce KE, Cober ER, Morrison MJ, *et al*. Yield associated traits correlate with cytokinin profiles in developing pods and seeds of field-grown soybean cultivars. Field Crops Res. 2017;214:175–84. https://doi.org/10.1016/j.fcr.2017.09.009.
120. Jorge GL, Kisiala A, Morrison E, Aoki M, Nogueira APO, Emery RJN. Endosymbiotic *Methylobacterium oryzae* mitigates the impact of limited water availability in lentil (*Lens culinaris* Medik.) by increasing plant cytokinin levels.

Environ Exp Bot. 2019;162:525–40. https://doi.org/10.1016/j.envexpbot.2019.03.028.
121. Prerostova S, Rezek J, Jarosova J, Lacek J, Dobrev P, Marsik P, *et al*. Cytokinins act synergistically with heat acclimation to enhance rice thermotolerance affecting hormonal dynamics, gene expression and volatile emission. Plant Physiol Biochem. 2023;198:107683. https://doi.org/10.1016/j.plaphy.2023.107683.
122. Radhika V, Ueda N, Tsuboi Y, Kojima M, Kikuchi J, Kudo T, *et al*. Methylated cytokinins from the phytopathogen *Rhodococcus fascians* mimic plant hormone activity. Plant Physiol. 2015;169(2):1118–26. https://doi.org/10.1104/pp.15.00787.
123. Morrison EN, Knowles S, Hayward A, Greg Thorn R, Saville BJ, Emery RJN. Detection of phytohormones in temperate forest fungi predicts consistent abscisic acid production and a common pathway for cytokinin biosynthesis. Mycologia. 2015;107(2). https://doi.org/10.3852/14-157.
124. Derkx MPM, Vermeer E, Karssen CM. Gibberellins in seeds of *Arabidopsis thaliana*: Biological activities, identification and effects of light and chilling on endogenous levels. Plant Growth Regul. 1994;15(3):223–34. https://doi.org/10.1007/BF00029895.
125. Leitão AL, Enguita FJ. Gibberellins in *Penicillium* strains: Challenges for endophyte-plant host interactions under salinity stress. Microbiol Res. 2016;183:8–18. https://doi.org/10.1016/j.micres.2015.11.004.
126. Bralczyk J, Wielgat B, Wasilewska-Dabrowska LD, Kleczkowski K. Growth accelerating response of *Euglena gracilis* Z. to gibberellic acid. Plant Sci Lett. 1978;12(3–4):265–71. https://doi.org/10.1016/0304-4211(78)90077-9.
127. Khan A, Lee I-J. Endophytic *Penicillium funiculosum* LHL06 secretes gibberellin that reprograms *Glycine max* L. growth during copper stress. BMC Plant Biol. 2013;13(1):86. https://doi.org/10.1186/1471-2229-13-86.
128. El-Shahir AA, El-Tayeh NA, Ali OM, Abdel Latef AAH, Loutfy N. The effect of endophytic *Talaromyces pinophilus* on growth, absorption and accumulation of heavy metals of *Triticum aestivum* grown on sandy soil amended by sewage sludge. Plants. 2021;10(12):2659. https://doi.org/10.3390/plants10122659.
129. Li L, Li C-B, Wu Y-H, Li B, Wu Y-R, Yan Z-Y. Combining metabolomics and metagenomics to analyze the biosynthetic potential of culturable endophytic fungi isolated from *Salvia miltiorrhiza*. Appl Biochem Microbiol. 2023;59(5):659–72. https://doi.org/10.1134/S0003683823050095.
130. Salazar-Cerezo S, Martinez-Montiel N, Cruz-Lopez MDC, Martinez-Contreras RD. Fungal diversity and community composition of culturable fungi in *Stanhopea trigrina* cast gibberellin producers. Front Microbiol. 2018;9:612. https://doi.org/10.3389/fmicb.2018.00612.
131. Leitão AL, Enguita FJ. Gibberellins in *Penicillium* strains: Challenges for endophyte-plant host interactions under salinity stress. Microbiol Res. 2016;183:8–18. https://doi.org/10.1016/j.micres.2015.11.004.
132. Sun T, Gubler F. Molecular mechanism of gibberellin signaling in plants. Annu Rev Plant Biol. 2004;55(1):197–223. https://doi.org/10.1146/annurev.arplant.55.031903.141753.
133. He J, Xin P, Ma X, Chu J, Wang G. Gibberellin metabolism in flowering plants: An update and perspectives. Front Plant Sci. 2020;11:532. https://doi.org/10.3389/fpls.2020.00532.

134. Fernández-Martn R, Reyes F, Domenech CE, Cabrera E, Bramley PM, Barrero AF, *et al*. Gibberellin biosynthesis in *gib* mutants of *Gibberella fujikuroi*. J Biol Chem. 1995;270(25):14970–4. https://doi.org/10.1074/jbc.270.25.14970.
135. Ahmad N, Hamayun M, Khan SA, Khan AL, Lee I-J, Shin D-H. Gibberellin-producing endophytic fungi isolated from *Monochoria vaginalis*. J Microbiol Biotechnol. 2010;20(12):1744–9.
136. Salazar-Cerezo S, Martinez-Montiel N, Cruz-Lopez MDC, Martinez-Contreras RD. Fungal diversity and community composition of culturable fungi in *Stanhopea trigrina* cast gibberellin producers. Front Microbiol. 2018;9:612. https://doi.org/10.3389/fmicb.2018.00612.
137. Hedden P. The current status of research on gibberellin biosynthesis. Plant Cell Physiol. 2020;61(11):1832–49. https://doi.org/10.1093/pcp/pcaa092.
138. Cen Y-K, Lin J-G, Wang Y-L, Wang J-Y, Liu Z-Q, Zheng Y-G. The gibberellin producer *Fusarium fujikuroi*: Methods and technologies in the current toolkit. Front Bioeng Biotechnol. 2020;8. https://doi.org/10.3389/fbioe.2020.00232.
139. Chen C-Y, Chen S-Y, Liu C-W, Wu D-H, Kuo C-C, Lin C-C, *et al*. Invasion and colonization pattern of *Fusarium fujikuroi* in rice. Phytopathology. 2020;110(12):1934–45. https://doi.org/10.1094/PHYTO-03-20-0068-R.
140. Wang J, Song L, Gong X, Xu J, Li M. Functions of jasmonic acid in plant regulation and response to abiotic stress. Int J Mol Sci. 2020;21(4):1446. https://doi.org/10.3390/ijms21041446.
141. Ruan J, Zhou Y, Zhou M, Yan J, Khurshid M, Weng W, *et al*. Jasmonic acid signaling pathway in plants. Int J Mol Sci. 2019;20(10):2479. https://doi.org/10.3390/ijms20102479.
142. Zhao S, Ma Q, Xu X, Li G, Hao L. Tomato jasmonic acid-deficient mutant spr2 seedling response to cadmium stress. J Plant Growth Regul. 2016;35(3):603–10. https://doi.org/10.1007/s00344-015-9563-0.
143. Ueda J, Miyamoto K, Sato T, Momotani Y. Identification of jasmonic Acid from *Euglena gracilis* Z as a plant growth regulator. Agric Biol Chem. 1991;55(1):275–6. https://doi.org/10.1080/00021369.1991.10870547.
144. Eng F, Marin JE, Zienkiewicz K, Gutiérrez-Rojas M, Favela-Torres E, Feussner I. Jasmonic acid biosynthesis by fungi: derivatives, first evidence on biochemical pathways and culture conditions for production. PeerJ. 2021;9:e10873. https://doi.org/10.7717/peerj.10873.
145. Scartazza A, Picciarelli P, Mariotti L, Curadi M, Barsanti L, Gualtieri P. The role of *Euglena gracilis* paramylon in modulating xylem hormone levels, photosynthesis and water-use efficiency in *Solanum lycopersicum* L. Physiol Plant. 2017;161(4):486–501. https://doi.org/10.1111/ppl.12611.
146. Kilaru A, Bailey BA, Hasenstein KH. *Moniliophthora perniciosa* produces hormones and alters endogenous auxin and salicylic acid in infected cocoa leaves. FEMS Microbiol Lett. 2007;274(2):238–44. https://doi.org/10.1111/j.1574-6968.2007.00837.x.
147. Chanclud E, Morel J-B. Plant hormones: A fungal point of view. Mol Plant Pathol. 2016;17(8):1289–97. https://doi.org/10.1111/mpp.12393.
148. Bari R, Jones JDG. Role of plant hormones in plant defence responses. Plant Mol Biol. 2009;69(4):473–88. https://doi.org/10.1007/s11103-008-9435-0.

149. Mishra AK, Baek K-H. Salicylic acid biosynthesis and metabolism: A divergent pathway for plants and bacteria. Biomolecules. 2021;11(5):705. https://doi.org/10.3390/biom11050705.
150. Zhang T, Shi M, Yan H, Li C. Effects of salicylic acid on heavy metal resistance in eukaryotic algae and its mechanisms. Int J Environ Res Public Health. 2022;19(20):13415. https://doi.org/10.3390/ijerph192013415.

CHAPTER 4

4.1 PREFACE

Title: Integrated transcriptomic and hormonomic insights into cadmium tolerance of a *Euglena mutabilis* fungal-algal-bacterial (FAB) consortium

Authors: Emma Kaszecki, Zeynab Azimychetabi, R. J. Neil Emery, Barry J. Saville

Reference: This chapter has been submitted to the journal *Microbiology* to be reviewed for publication. The published version may appear different than presented here.

Contributions: Study conception, experimental design, material preparation, data collection, and analysis were carried out by EK. ZA processed samples using HPLC-MS/MS data and scored peak area for phytohormone calculations. RJNE and BJS contributed to experimental design and funding. The manuscript was written by EK with edits from RJNE and BJS. All authors have approved the final version of the manuscript.

CHAPTER 4

Integrated transcriptomic and hormonomic insights into cadmium tolerance of a *Euglena mutabilis* fungal-algal-bacterial (FAB) consortium

4.2 ABSTRACT

Background: Acidic, metal-contaminated environments such as mine tailings ponds harbor specialized microbial communities capable of surviving extreme physicochemical stress. Among these, *Euglena mutabilis* is a resilient, acidophilic protist, often persisting as part of a facultative fungal- algal–bacterial (FAB) consortium. However, the molecular mechanisms driving heavy metal tolerance, particularly in naturally cohabiting consortia, remain poorly characterized.

Results: We investigated transcriptomic, hormonal, structural, and taxonomic responses of an environmental *E. mutabilis* culture containing *Talaromyces* and *Acidiphilium acidophilum* exposed to cadmium (Cd). RNA-seq identified differential expression of metal transporters, particularly ZIP and CDF family proteins, supporting a shift from Cd uptake to intracellular sequestration over time. TEM imaging confirmed Cd compartmentalization within chloroplasts and increased paramylon accumulation. Cd exposure also led to suppression of light-harvesting complex (LHC) genes and formate/nitrite transporters, while maintaining core photosynthetic function. Hormone profiling revealed near-complete suppression of bioactive auxin (IAA) and cytokinin (CK) free bases, coupled with increased CK nucleotide accumulation. This hormonal dormancy aligned with downregulation of CK biosynthetic (IPT) and activation (LOG) genes.

Metagenomic analysis showed enrichment of *Talaromyces* and *Acidiphilium* under Cd exposure, suggesting their supportive roles in detoxification and stress signaling.

Conclusions: Our results reveal a coordinated stress response in *E. mutabilis* involving early Cd uptake, chloroplast-based detoxification, metabolic buffering via paramylon, suppression of growth-promoting hormones, and community-mediated resilience. This study demonstrates that natural microbial consortia not only enhance metal tolerance through physical and metabolic buffering but also modulate host transcriptional and hormonal pathways, highlighting their potential as biotechnological tools for sustainable bioremediation.

Keywords: *Euglena*; FAB consortium; heavy metal stress; transcriptome; hormones; RNA-seq; bioremediation

4.3 BACKGROUND

Mining activities have profoundly altered landscapes worldwide, leaving behind long-lasting environmental legacies in the form of acid mine drainage (AMD), heavy metal (HM) contamination, and chemically unstable tailings ponds [1,2]. These engineered reservoirs often remain biologically degraded for decades, resisting natural recovery due to their acrid, metal-laden conditions [3–5]. Conventional strategies for remediating HM polluted environments – such as chemical neutralizing agents, passive treatment systems, and biological sulfate-reducing systems – are expensive and technically demanding [6], prompting growing interest in biological approaches that leverage the adaptive capacities of extremophilic microorganisms [7,8].

Microorganisms can metabolize, immobilize, or transform toxic pollutants into less harmful forms [9,10]. While monoculture systems offer reproducibility, they often underperform in complex environments due to limited metabolic flexibility [11,12]. In contrast, co-culture systems enhance tolerance, functional breadth, and stability by exploiting complementary pathways and interspecies interactions [13–15]. For instance, acidophilic algae co-cultivated with bacteria or fungi have demonstrated improved metal uptake and detoxification in AMD waters [16–18]. Such synergistic strategies position microbial consortia as a promising frontier for sustainable bioremediation of AMD and tailing ponds.

Among extremophilic algae, *Euglena mutabilis* has emerged as a particularly compelling organism. This acidophilic, facultatively autotrophic protist is considered an indicator species of AMD and can be found in acidic aquatic environments such as peat bogs and volcanic lakes [19]. *E. mutabilis* demonstrates remarkable resilience to low pH and high metal loads and is often observed within complex microbial mats or biofilms where it coexists with acidophilic bacteria and fungi [20,21]. These associations are thought to contribute to its survival and functional stability in extreme environments. For instance, a culture of *E. mutabilis* isolated from gold mine tailings in Ontario, Canada was found to be maintained as part of a stable facultative fungal-algal-bacterial (FAB) consortium alongside *Acidiphilium acidophilum* and *Talaromyces* [20]. Disrupting these microbial partners using antibiotic and antifungal treatments resulted in a significant reduction in Cd tolerance, suggesting that interspecies interactions are essential for *E. mutabilis*' enhanced stress response [20].

Despite its ecological importance, *E. mutabilis* remains relatively understudied at the molecular level compared to its close relative and model species, *Euglena gracilis*. *E. gracilis* has been widely explored for its metabolic plasticity, genome structure, and potential in biotechnological applications [22–24]. Though, recent studies demonstrate that *E. mutabilis* possesses substantially greater physiological resilience to Cd stress, maintaining cellular viability at concentrations that severely impair *E. gracilis* [25,26]. In *Euglena*, the uptake and intracellular compartmentalization of HMs is strongly influenced by metabolic state and environmental conditions. Under photoautotrophic growth, Cd tends to accumulate in chloroplasts, whereas in heterotrophic or dark-grown cells, Cd is more often sequestered in mitochondria [27]. These redistribution patterns likely reflect dynamic detoxification strategies based on energy status. Additionally, *Euglena* stores carbon as paramylon, a β-1,3-glucan polymer that has been implicated in oxidative stress regulation and energy buffering [28,29]. Paramylon accumulation may also contribute to metal stress tolerance, though its role in heavy metal detoxification remains underexplored [28,29].

An emerging aspect of microalgal stress response involves the production and regulation of phytohormones. Although traditionally associated with plant development, signaling molecules such as auxins and cytokinins (CKs) have been detected in bacteria [30], fungi [31], and algae [32,33], where they influence growth, metabolism, and interspecies communication. In eukaryotic microalgae, hormone biosynthesis and signaling are increasingly recognized as evolutionarily conserved systems with potential roles in modulating metal stress responses [34]. However, few studies have integrated hormone profiling with gene expression data to explore these pathways—particularly in complex microbial consortia or extremophilic systems such as *E. mutabilis*.

To address this gap, we investigated the transcriptomic, chemical, structural, and taxonomic responses of an *E. mutabilis* FAB culture exposed to Cd stress over a 21-day time course. RNA-sequencing was used to identify differentially expressed genes (DEGs) at three timepoints, followed by functional annotation using gene ontology (GO), KEGG pathways, and clusters of orthologous genes (COG) classifications. We complemented this molecular analysis with targeted quantification of extracellular phytohormones to assess their involvement in stress signaling. To explore potential shifts in community structure, we also profiled microbial taxa using Kraken2 and Bracken-based metagenomics. Finally, transmission electron microscopy (TEM) was used to assess Cd-induced ultrastructural changes in *E. mutabilis* cells, with a particular focus on organelle integrity and paramylon accumulation. Together, this integrative approach provides new insight into the transcriptional and physiological strategies underlying HM tolerance in *E. mutabilis* and highlights the role of microbial partnerships and phytohormones in shaping stress resilience in mixed algal cultures.

4.4 METHODS

Culture selection and growth of *E. mutabilis*

Field samples of *Euglena mutabilis* were sourced from the Canadian Phycological Culture Centre (CPCC) at the University of Waterloo, Canada. The strain selected (CPCC 657) is composed of *E. mutabilis* which maintains a seemingly symbiotic relationship with a *Talaromyces* species fungus and the bacterium *Acidiphilium acidophilum*. Stock cultures were maintained in modified acid medium (MAM) [35], following CPCC-recommended adjustments, and the pH was set to 4.3 [36]. After autoclaving, the medium was allowed to

cool before the addition of filter-sterilized F/2 vitamins. Cultures were grown autotrophically in 250 mL Pyrex Erlenmeyer flasks, sealed with foam stoppers wrapped in aluminum foil, and aerated at 100 RPM using a Thermo Fisher Scientific MaxQ 3000 shaker. Growth conditions included a 16:8 light-dark cycle with controlled temperature (260 μmol s^{-1} m^{-1}; 24 ± 0.5°C during light and 18 ± 0.5°C during dark) using a Conviron PCG20 environmental chamber.

Pre-growth and Cd exposure with *E. mutabilis*

Euglena mutabilis cultures were exposed to $CdCl_2$ following the protocol outlined by Kennedy *et al* [25], with modifications. In brief, 21 stock cultures were grown in MAM in 250 mL Erlenmeyer flasks, each containing 120 mL of MAM and inoculated at a density of 20,000 cells/mL. Cultures were maintained under the same environmental conditions as the original stock cultures. Cell densities were monitored on days 7 and 14 post-inoculation using a hemocytometer (Hausser Scientific) at 10x magnification. By day 14, cell concentrations exceeded 200,000 cells/mL in all flasks. At this point, each culture was divided into two conditions: a control (MAM only) and a treatment (MAM + 100 μM $CdCl_2$), resulting in a total of 42 flasks. Each flask contained 60 mL of MAM, with or without Cd, and a concentration of 200,000 *E. mutabilis* cells/mL. These were maintained under the same growth conditions as the pre-treatment phase. On days 7, 14, and 21 post-treatment, seven pairs of control and treated cultures were sampled to assess growth and viability, extract RNA, quantify hormone concentrations in the supernatant, and measure cellular Cd accumulation. Time points for analysis were chosen based on previous work by Kennedy *et al* [25], designed to expose cells to Cd over extended periods in order to assess adaptability.

Euglena cell growth and viability after Cd exposure

Every 7-, 14-, and 21-days post-inoculation, 100 µL aliquots were taken from each flask being assessed that day and diluted with 100 µL of a 0.4% Trypan Blue solution (Bioshop Cat. No. TRY477.100) in PBS (Bioshop, Cat. No. PBS404.100). Cell counts were determined using a hemocytometer (Hausser Scientific) at 10x magnification to assess the viability of *E. mutabilis* visually by counting the number of cells that had taken up the Trypan Blue stain.

Cellular Cd accumulation

Cellular Cd accumulation was assessed in treatment flasks 7-, 14-, and 21-days after inoculation. Sample preparation followed the protocol outlined by Metcalfe *et al* [37], with modifications. A 1.0 mL aliquot was taken from each culture flask and transferred into 1.5 mL microcentrifuge tubes. After centrifuging at 3,824 RCF for 10 minutes, the supernatant was carefully removed using a pipette. The remaining cell pellets were washed three times by resuspension in 2.0 mL of sterile deionized water (dH_2O), followed by centrifugation and supernatant removal after each wash. Following the final rinse, 300 µL of 70% (v/v) nitric acid (HNO_3; Fisher Scientific Cat. No. A509P500) was added to each sample. Tubes were then incubated on a heat block at 95°C for 20 minutes to facilitate digestion. The digested samples were diluted with 10.2 mL of sterile dH_2O to achieve a final acid concentration of 2% (v/v) HNO_3. Each sample was subsequently passed through a 0.45 µm polytetrafluoroethylene (PTFE) syringe filter (VWR Cat. No. 76479-004) into a sterile 15 mL Falcon tube. Seven media blanks of the treatment condition were processed in parallel.

Elemental quantification was performed using an Agilent 8900 triple quadrupole inductively coupled plasma mass spectrometer (ICP-QQQ-MS) at the Water Quality Centre (Trent University, Peterborough, Canada). Samples were introduced via a MicroMist nebulizer (nominal uptake: 400 µL/min) attached to a Scott-type double-pass spray chamber, optimizing aerosol generation. The ICP-MS was run under the General-Purpose Plasma Preset with a radio frequency (RF) power setting of 1550 W and a carrier gas flow rate of 1.05 L/min. The sample introduction depth was fixed at 10 mm, and an X-type extraction lens was employed to enhance ion focusing. Standard nickel cones (sampler and skimmer) facilitated ion transmission to the plasma. Cadmium (Cd) was detected in single quadrupole mode using helium (He) as the collision gas. Calibration standards were made by serial dilution from 1000 ng/mL single-element stock solutions in 2% HNO_3. Rhodium was used as an internal standard and delivered inline continuously during measurement.

Transmission electron microscopy

A 1 mL aliquot of cultures grown in either MAM or MAM + 100 µM $CdCl_2$ was transferred into 1.5 mL microcentrifuge tubes. Following centrifugation, the supernatant was carefully removed using a pipette, and the resulting pellet was resuspended in 500 µL of 2.5% glutaraldehyde (Sigma Aldrich, Cat. No. G5882-100ML) prepared in 0.1 M phosphate buffer (pH 7.2). Samples were fixed at room temperature for 24 hours. All subsequent preparation and embedding steps were carried out by the Cellular and Molecular Electron Microscopy Core Facility at The Hospital for Sick Children (Toronto, Canada). Fixed samples were cut into 2 mm cubes and rinsed in 0.1 M sodium cacodylate buffer containing 0.2 M sucrose (pH 7.3) for 10 minutes. Post-fixation was performed in 1% osmium tetroxide in the same buffer for 1.5 hours, followed by a second rinse in the

sucrose-buffer solution. Samples were dehydrated through a graded ethanol series (70%, 90%, and three changes of 100% ethanol), then washed twice with propylene oxide. Infiltration was carried out using a 1:1 mixture of propylene oxide and Spurr resin for 1 hour, followed by two incubations in pure Spurr resin (1 hour and overnight). Samples were then embedded in molds and polymerized overnight at 65 °C. Ultrathin sections (90 nm) were cut using a diamond knife on an ultramicrotome, mounted on copper grids, and stained with uranyl acetate and lead citrate prior to imaging with a Hitachi HT7800 transmission electron microscope.

All solutions were prepared using ultrapure water (18.2 MΩ·cm) and trace-metal grade HNO_3 to minimize contamination.

Hormone profiling

Solid phase extraction and purification of hormones

Supernatant from culture samples (12 mL) were harvested from each flask at 7-, 14-, and 21-days following inoculation and filtered through a 0.2 μm polyethersulfone (PES) syringe filter (Fisher Scientific, Cat. No. 13-1001-06) into 50 mL Falcon tubes. Media controls underwent the same processing. All processed samples were flash-frozen in liquid nitrogen, lyophilized using a LabConco FreeZone freeze dryer (Kansas City, MO, USA), and stored at −80°C until extraction.

A sequential extraction strategy, adapted from previously described protocols [38,39], was used to isolate distinct hormone classes from a single sample. This approach allowed for the recovery of 39 cytokinins (CKs) and acidic hormones, including abscisic acid (ABA),

indole-3-acetic acid (IAA), salicylic acid (SA), jasmonic acid (JA), and five key gibberellins (GA_1, GA_4, GA_7, GA_9, GA_{20}) (Table S4.1).

To enable isotope dilution-based quantification, each sample was spiked with deuterated internal standards (IS) in 2 mL of ice-cold 50% acetonitrile (ACN). These included $^2H_4$-ABA (60.9 ng; PBI, Saskatoon, Canada), 10 ng each of $^2H_5$-IAA and $^2H_6$-SA (OLChemim, Czech Republic), and 10 ng each of the $^2H_2$-gibberellins GA_1, GA_4, GA_7, GA_9, and GA_{20}. An additional 10 ng of ^2H-labeled CK standards, encompassing aromatic, methylthiolated, and glucoside derivatives, were also added. The CKs scanned for comprised benzyladenine (BA), benzyladenine riboside (BAR), kinetin (KIN), *cis*-Zeatin (*c*Z) and its derivatives (*c*ZR, *c*Z9G, *c*ZNT, *c*ZOG, *c*ZROG), dihydroZeatin (DZ) and derivatives (DZNT, DZOG, DZR, DZROG, DZ9G), isopentenyladenine (iP) and its forms (iPNT, iP9G, iPR), along with methylthiolated and *trans*-Zeatin forms (2MeSiP, 2MeSiPR, 2MeSZ, 2MeSZR, *t*Z, *t*ZR, *t*Z9G, *t*ZNT, *t*ZOG, *t*ZROG) (Table S4.1). Although a specific JA standard was not included, $^2H_4$-ABA was used for JA quantification.

Supernatants and media controls were resuspended in 1.5 mL 50% acetonitrile and vortexed to ensure homogeneity. Samples were centrifuged (maximum speed for 10 minutes), and the resulting supernatant was split equally: 750 µL for acidic hormone analysis and 750 µL for CK analysis. Seven method blanks were processed concurrently.

Extraction and solid phase purification of acidic hormones

Samples were purified using HLB solid-phase extraction (SPE) cartridges (Canadian Life Sciences, Cat. No. VO34445). Columns were sequentially conditioned with

methanol, B-Pure water (18.2 MΩ·cm), and 50% aqueous acetonitrile. After centrifugation, supernatants were applied to the cartridges and eluted by gravity into 5 mL tubes, followed by a final rinse with 2 mL of 30% aqueous acetonitrile. The eluates were dried using a Savant UVS400 vacuum concentrator at room temperature. Dried acidic hormone samples were derivatized by adding 75 µL of 1-propanol, 20 µL of B-Pure water, 5 µL of 500 mM bromocholine in 70% ACN (TCI America, Cat. No. B0577), and 1 µL triethylamine (Fisher Scientific, Cat. No. O4884-100). Samples were incubated in an 80°C water bath for 130 minutes, cooled on ice for 1 hour, then dried again (Savant UVS400 vacuum) and stored at −20°C.

Extraction and solid phase purification of cytokinins

CK fractions were dissolved in 1 mL of 1M formic acid and loaded onto MCX SPE cartridges (Canadian Life Sciences, Cat. No. VO54445) preconditioned with 5 mL of methanol and 5 mL of formic acid. After sample application, columns were sequentially washed and eluted. The first elution (5 mL of 0.35M ammonium hydroxide) contained nucleotide forms (NT), while the second (5 mL of 0.35M ammonium hydroxide in 60% methanol) contained freebase (FB) and riboside (RB) forms. Both eluates were dried by vacuum centrifugation. FB and RB samples were stored at −20°C until analysis.

NT fractions were further processed to allow detection by mass spectrometry. These dried samples were reconstituted in 1 mL of 0.1M ethanolamine (Sigma Aldrich, Cat. No. E9508-100) with 12 µL (3 units) of a phosphatase enzyme mix (New England Biolabs, Cat. No. M0525L) and incubated overnight at 37°C. The resulting mixture was dried and reconstituted in 1.5 mL B-Pure water for a final purification using C18 cartridges (Canadian

Life Sciences, Cat. No. IS72006). Columns were conditioned with methanol and water, and the sample supernatant was loaded and eluted by gravity. After a water rinse, CKs were recovered by washing with 1.25 mL of 80% methanol into 2 mL tubes. These samples were dried again and stored at −20°C.

Prior to analysis, all hormone samples were reconstituted in 300 µL of 0.08% acetic acid (CH_3COOH) in 5% acetonitrile, vortexed, and centrifuged at 3,724 × g for 10 minutes to remove particulates. A 250 µL aliquot of each was transferred into clear MS vials with 300 µL glass inserts.

Hormone analysis by UHPLC-ESI-MS/MS

Hormone fractions were analyzed using ultra high-performance liquid chromatography-electrospray ionization tandem mass spectrometry (UHPLC-ESI-MS/MS) on a Thermo Q-Exactive quadrupole Orbitrap mass spectrometer coupled to a Thermo Dionex Ultimate 3000 UHPLC system, following a previously established method [38]. Separation was achieved on a Kinetex C18 column (2.1 mm × 50 mm, 2.6 µm particle size; Phenomenex, Torrance, CA, USA), with the column maintained near room temperature (22°C). A 25 µL injection volume was used. The mobile phase consisted by ddH_2O with 0.08% acetic acid (Solvent A) and acetonitrile with 0.08% acetic acid (Solvent B). Elution was performed at 0.5 $mL \cdot min^{-1}$ with the following gradient: 5% B for 0.5 min, linearly increasing to 45% B over 4.5 min, then to 95% B over 6.5 min, held for 1 min, and returned to initial conditions for 2 min, resulting in a total run time of 8.2 minutes. Chromeleon 6.8 (ThermoFisher Scientific, Ottawa, ON, Canada) was used for instrument control and data acquisition.

Hormone quantification

Hormone quantification was performed using Xcalibur 3.0.63 (ThermoFisher Scientific). Peaks were identified based on accurate monoisotopic $[M+H]^+$ masses and comparison of retention times with internal standards. Extracted ion chromatograms (XICs) were constructed using the precursor ion and the two most intense fragment ions, applying a mass tolerance of 3 ppm. Quantification was based on peak areas from XICs. Supernatant hormone concentrations were normalized to the number of *E. mutabilis* cells per 12 mL of media to establish the concentration per cell.

RNA-sequencing analysis and bioinformatics

RNA isolation and DNase1 treatment

RNA from seven control and seven treatment cultures across three timepoints (Days 7, 14, and 21) were isolated for a total of 42 samples. 50 mL of culture from each flask was transferred to a sterile Falcon tube, centrifuged and the supernatant was collected for hormone analysis. The cells were then resuspended in 2 mL of TRIzol™ Reagent (Invitrogen™). Samples were transferred to Lysing Matrix C tubes (MP Biomedicals Cat. No. 1169120-CF) and lysed using an MP Biomedicals Fast Prep-24 (6.5 Hz for 45 seconds). RNA was initially precipitated by adding 250 µL of a solution containing 0.8 M disodium citrate and 1.2 M NaCl, along with 250 µL of isopropanol. Following this, genomic DNA was removed via DNase1 treatment. A second round of RNA precipitation was then carried out using the same disodium citrate/NaCl solution and isopropanol. The integrity and quality of the RNA were evaluated by electrophoresis on a 1.5% BPTE agarose gel after glyoxal denaturation. DNase-treated RNA samples and a single-stranded RNA ladder (New

England BioLabs, Whitby, Canada) were loaded onto the gels for visualization (Figure S4.1).

cDNA library preparation and RNA-sequencing

20 µL aliquots of DNase-treated RNA were submitted to the Centre for Applied Genomics (TCAG) at the Hospital for Sick Children (Toronto, Canada) for quality assessment, cDNA library preparation, and RNA sequencing. RNA quality was evaluated using an Agilent 2100 Bioanalyzer (Agilent Technologies), which provided both the RNA Integrity Number (RIN) and DV200%. Given the fragmented nature of *Euglena* RNA [47], emphasis was placed on DV200% as the primary quality metric. All 42 samples exhibited high RNA quality (DV200% > 90%) and were selected for cDNA library construction. Poly(A)-enriched RNA was isolated using oligo(dT) beads, and cDNA libraries were prepared using the NEBNext Ultra Directional RNA Library Prep Kit for Illumina (New England BioLabs). In total, 42 barcoded libraries were generated, pooled, and sequenced across one lane of an S4 flowcell on the Illumina NovaSeq 6000 platform, yielding 2 x 150 bp paired-end (PE) reads.

Read quality assessment, pre-processing, and transcriptome assembly

Bioinformatic analysis including pre-processing, transcriptome assembly, differential gene expression (DGE), gene ontology (GO-term), and metagenomic analysis following RNA-sequencing was carried out by the TCAG at the Hospital for Sick Children (Toronto, Canada). Raw sequencing reads in FASTQ format were assessed for quality using FastQC v0.11.5 [48]. Adapter trimming and quality filtering were performed with Trim Galore v0.5.0 [49], which incorporates Cutadapt v1.10 [50], using the following

parameters: -q 25 for 3′ end quality trimming, --stringency 5 to require a minimum of 5 bp overlap with adapter sequences, --length 20 to discard short reads, and --paired to retain only properly paired reads. Adapter sequences were automatically detected from the first million reads. The quality of the trimmed reads was reassessed using FastQC.

To ensure no contamination, reads were screened against the hg38 human genome and UniVec database using FastQ-Screen v0.10.0 [51]. Results from FastQC and FastQ-Screen for both raw and processed reads were compiled into a consolidated report using MultiQC v1.14 [52].

All high-quality, trimmed reads from the 42 RNA-seq libraries were combined and used to generate a single *de novo* transcriptome assembly with Trinity v2.15.2 [53], using the --SS_lib_type RF option to accommodate strand-specific reads and enabling --normalize_by_read_set to normalize read coverage across libraries. Following assembly, each library's trimmed reads were aligned back to the assembled transcriptome using Bowtie2 v2.5.4 [54], and transcript abundances were estimated with RSEM v1.3.3 [55].

Differential gene expression and GO-term analysis

Differential gene expression (DGE) analysis was performed using both DESeq2 (v1.26.0) [49] and edgeR (v3.28.1) [50] within R v3.6.1 [51]. Gene count data generated by RSEM were filtered to exclude genes with fewer than 50 reads in at least six samples. DESeq2 analyses were conducted using default parameters with cooksCutoff=TRUE, independentFiltering=TRUE, alpha=0.05, and p-value adjustment via the Benjamini-Hochberg method (pAdjustMethod="BH"). Exploratory principal component analysis

(PCA) was generated using rlog-transformed counts to visualize sample grouping. One control sample (MAM Control 8; Day 14) was identified as an outlier and was removed along with its paired Cd-treated sample (MAM + 100 µM Cd Treatment 8; Day 14) to maintain the integrity of paired comparisons (Figure S4.2a). To further account for sample variability, surrogate variables were identified using Surrogate Variable Analysis (SVA) [52] and included in the DESeq2 model for comparisons between control and treatment samples at each time point. DGE testing in edgeR was performed using the TMM normalization method (calcNormFactors) followed by quasi-likelihood F-tests via glmLRT. Volcano plots and Euler diagrams were generated in RStudio (v2024.12.0+467) after filtering padj and $\log_2$ fold change (padj < 0.05; $|\log_2 FC| > 1$) accounting for overlapping DGEs between DESeq2 and edgeR.

To functionally characterize differentially expressed genes (DEGs), nucleotide sequences corresponding to each DEG were retrieved from the Trinity-assembled transcriptome and analyzed using BLASTx against protein databases from *Homo sapiens*, *Arabidopsis thaliana*, *Chlamydomonas reinhardtii*, and *Synechocystis* sp. (GCA_000478825), using Ensembl 113 as the reference and an E-value threshold of $1e^{-5}$. No dedicated databases exist for *Euglena* because its genomes have not been fully sequenced or annotated; however, partial transcripts are available through BLASTx and Ensembl 113, with other databases serving as comparators. For each DEG, the top BLASTx hit with an associated Gene Ontology (GO) annotation was retained, and corresponding gene symbols were assigned. These curated gene sets were used for GO enrichment analysis with the PANTHER Classification System (version 19.0, accessed 2025-06-12; https://pantherdb.org/), based on the GO database release dated 2025-03-16 [53].

Enrichment was performed using Fisher's Exact Test with False Discovery Rate (FDR) correction, and only gene lists containing a minimum of five annotated genes were included to ensure statistical reliability. For each species, DEGs from all relevant comparisons were grouped together to streamline interpretation, and enrichment results for biological process (BP), molecular function (MF), and cellular component (CC) ontologies were summarized for downstream analysis. The PANTHER database used for GO annotation is independent of the transcriptome assembly, ensuring consistency across species and comparisons.

Metagenomic sequencing and taxonomic analysis

The RNA-seq reads from 42 samples were subjected to metatranscriptomic taxonomic analysis to identify co-cultured microbial species. After sequencing, raw reads were quality-checked using FastQC (v0.11.5) [48], and adapter trimming was performed using Trim Galore (v0.5.0) [49] with Cutadapt (v1.10) [50]. Trimmed reads were re-evaluated for quality, screened for human and vector contaminants with FastQ Screen (v0.10.0) [51], and summarized using MultiQC (v1.14) [52]. Taxonomic classification of RNA-seq reads was performed using Kraken2 (v2.1.3) [61] with a core nucleotide (core_nt) database built on 2024-12-28 and a confidence threshold of 0.5. Kraken2 assigned reads to operational taxonomic units (OTUs) based on k-mer matches and lowest common ancestor (LCA) principles. For refined species-level resolution, Bracken (v2.8) [62] was used to re-estimate taxonomic abundances using a 75 bp k-mer database and a read threshold of 10 to filter low-abundance taxa. Bracken output included both absolute and relative abundance data. Relative abundance bar plots were generated in R (v4.4.2) using the Bracken reports.

Statistical analysis

Differences in viable *E. mutabilis* cell counts and hormone content at each timepoint were evaluated after outlier removal and using an F-test of equality of variances, followed by Student's t-test ($p < 0.05$) with appropriate consideration of variance structure.

A Mann-Whiney U-test was used to identify microbial taxa that were differentially abundant between control and Cd-treated cultures. Count data were derived from Bracken-refined Kraken2 classifications and aggregated into a sample-wise species-level count matrix. To correct for multiple testing, FDR adjustment was applied using the Benjamini-Hochberg procedure, and taxa with padj < 0.05 were considered statistically significant. Log_2 fold changes were calculated to quantify the direction and magnitude of change in relative abundance between conditions.

4.5 RESULTS

E. mutabilis cell viability after $CdCl_2$ exposure

Cd exposure significantly reduced *E. mutabilis* cell proliferation at all sampling times (Figure 4.1). In control cultures (0 µM Cd), cell counts increased steadily from approximately 3.0×10^5 cells/mL on day 7 to 5.3×10^5 cells/mL by day 21 – representing a 72% increase. In contrast, cultures exposed to 100 µM $CdCl_2$ consistently exhibited lower cell densities at all timepoints. By day 7, Cd-treated cultures showed a significant reduction in cell counts compared to controls ($p < 0.01$). This trend persisted through day 14 ($p < 0.001$) and day 21, where the difference became more pronounced ($p < 0.001$), despite continued growth in the treated group – representing a more modest 58% increase.

Despite reduced proliferation, cell viability remained high in all treatments. Trypan Blue staining revealed minimal *E. mutabilis* cell death across timepoints, with Cd-treated cultures exhibiting only a slight increase in the proportion of non-viable cells over 21-days ([# dead cells / total cell count] * 100%; Table 4.1).

Cellular Cd accumulation

Following exposure to 100 µM Cd, cellular Cd concentrations in *E. mutabilis* increased steadily over the 21-day period (Figure 4.2). On day 7, the average cellular Cd content was 161 ng/10^5 cells, which rose to 204 ng on day 14, and 322 ng by day 21. When scaled to the total number of cells per 60 mL culture, this corresponded to approximately 22,800 ng, 37,900 ng, and 72,000 ng of total cellular Cd on days 7, 14, and 21, respectively. Relative to the initial 674,000 ng dose, these values represent approximately 3%, 6%, and 11% uptake, indicating progressive accumulation by *E. mutabilis*. However, direct ICP-MS measurements of the treatment culture media (MAM + 100 µM Cd with no cells) showed only 500,000 ng remaining after 7-days, 525,000 ng after 14-days, and 491,000 ng by 21-days which increases sequestration efficiency to 5%, 7%, and 15%, respectively. This indicates that a fraction of Cd was lost through abiotic processes. Cd ions are prone to adsorbing to glassware surfaces [56] and forming insoluble precipitates within media components such as phosphate and sulfate [57], which would reduce the dissolved fraction available for detection and may explain the discrepancy between the amount of Cd introduced and the lower concentrations quantified.

Transmission electron microscopy (TEM) revealed distinct ultrastructural differences between *E. mutabilis* cells grown in control conditions and those exposed to

100 µM Cd (Figure 4.3). In control cells (MAM) grown for 21-days, organelles including chloroplasts, Golgi bodies, mitochondria, the nucleus, and vacuoles appeared intact, with paramylon granules and a clearly defined pellicle. In contrast, Cd-treated cells displayed notable structural alterations, including the accumulation of electron-dense deposits within chloroplasts which appear limited in control cells, although this was not quantified. Additionally, Cd-treated cells exhibited increased vacuolization and a higher abundance of paramylon bodies. The appearance of these electron-dense inclusions correlates with the observed increase in cellular Cd accumulation over time.

Hormone Profiles

Identification and quantification of hormones in *E. mutabilis* culture supernatants revealed clear differences between control and Cd-treated conditions over the 21-day experimental period (Table 4.2). Of the hormones screened for, seven were detected six of which were CKs, (including one methylthiolated CK) and the other was IAA. No hormones were detected in culture media blanks.

CK free bases showed distinct patterns between control and Cd-treated conditions. In control cultures, *c*Z rose steadily from 33 fmol/100,000 *Euglena* cells on day 7 to 147 fmol/100,000 *Euglena* cells on day 14, reaching 761 fmol/100,000 cells by day 21. In contrast, *c*Z was only detectable in Cd-treated cultures at day 7, in significantly lower concentrations than the control, with levels falling below detection thereafter. A similar trend was observed for iP, which peaked in control conditions on day 14 (18.1 ± 0.8 fmol/100,000 *Euglena* cells) but was significantly lower in Cd-treated samples on day 7 and undetectable at subsequent time points. The total concentration of CK free bases in

control sample increased nearly 18-fold over 21-days of growth, while Cd-exposed cultures exhibited a sharp decline in free base detection after day 7 resulting in no detectable free bases at 21-days.

Riboside forms of CKs, such as *c*ZR, remained consistently detectable in control cultures. Like *c*Z, it followed a similar increasing trend over 21-days, peaking at 30 fmol/100,000 *Euglena* cells (Table 4.2). In Cd-treated cultures, however, *c*ZR was observed only on day 7. Among nucleotide forms, *c*ZNT remained detectable throughout all timepoints in both control and treatment conditions. In control cultures, *c*ZNT peaked on day 14 (308.0 ± 5.8 fmol/100,000 *Euglena* cells). Cd-treated samples also showed their highest *c*ZNT concentration on day 14 (325.9 ± 8.0 fmol/100,000 *Euglena* cells), which was significantly higher than the control, although by day 21 the concentration of *c*ZNT was significantly higher in the control. By contrast, iPNT was not detected in control cultures but was present in Cd-treated samples on both day 14 (495.1 ± 27.9 fmol/100,000 *Euglena* cells) and day 21 (991.9 ± 78.3 fmol/100,000 *Euglena* cells). Overall, total nucleotide concentrations were consistently higher in Cd-treated cultures compared to controls at all time points.

IAA was exclusively detected in control cultures and declined over time, with concentrations decreasing from 1022.1 ± 132.7 pmol/100,000 cells on day 7 to 665.2 ± 86.4 pmol/100,000 *Euglena* cells by day 14. IAA was not detected in any Cd-treated cultures at any time point.

RNA-sequencing and *de novo* transcriptome assembly

RNA-sequencing was performed on *E. mutabilis* cultures grown in MAM and MAM supplemented with 100 µM Cd after 7, 14, and 21 days of exposure. For each condition, seven biological replicates were sequenced, resulting in a total of 42 samples with an average of 65.1 million raw paired-end (PE) reads per sample. After removal of adapter sequences and low-quality reads, an average of 64.7 million PE reads remained per sample (Table S4.2).

Due to the large dataset (over 966 million reads), *de novo* transcriptome assembly was conducted using Trinity with *in silico* normalization (--normalize_by_read_set), which used approximately 11.48% of total reads (110,931,566 of 966,374,998). The resulting assembly consisted of approximately 1.2 million transcripts with an N50 of 816, representing 639,820 Trinity genes. Because the assembly reflected a mixed transcriptome from multiple organisms, BUSCO completeness analysis was not performed. Instead, RNA-seq reads were mapped back to the assembly, revealing that over 90% of all reads aligned to the transcriptome (Table S4.3).

To reduce noise from low-abundance transcripts, genes with fewer than 20 read counts in fewer than 8 samples (20%) were excluded, yielding a filtered gene set of 78,302. Exploratory PCA revealed that one sample – Control 8 (Day 14) – was an outlier and was removed along with its paired Cd-treated sample from downstream analysis (Figure S4.2).

Comparative transcriptome analysis of *E. mutabilis* grown in the absence and presence of cadmium

Differential gene expression (DGE) analysis was conducted using both DESeq2 and edgeR. DESeq2 identified 108,064 differentially expressed genes (DEGs), while edgeR identified 26,355 DEGs (adjusted p-value < 0.05; Table S4.4). After applying a fold-change threshold ($|\log_2 FC| > 1$), the number of DEGs was reduced to 23,119 in DESeq2 and 17,967 in edgeR. Of these, 4,596 DEGs were shared between both methods and were used in all subsequent analyses.

Pairwise comparisons between control and Cd-treated cultures at each timepoint revealed 480 unique DEGs on day 7, 352 on day 14, and 751 on day 21, with 427 genes differentially expressed across all three timepoints (Figure 4.4a). Specifically, day 7 cultures had 676 upregulated and 416 downregulated genes (Figure 4.4b); day 14 showed 680 upregulated and 336 downregulated genes (Figure 4.4c); and day 21 had 1,003 upregulated and 469 downregulated genes (Figure 4.4d). Pairwise comparisons were also conducted within each treatment group – control and Cd – to assess DEGs across timepoints (Day 7 vs 14, Day 7 vs 21, and Day 14 vs 21) (Table S4.5; Figures S4.3, S4.4).

There is no complete and annotated genome for *E. mutabilis*, therefore functional annotation was conducted using well-annotated databases, some of which contain partial transcripts from *Euglena*. To identify potential gene encoding proteins that were associated with transcript level changes, a BLASTX search was conducted using the NCBI non-redundant protein database, SWISS-Prot database, and Ensembl 113 databases for *Homo sapiens*, *Arabidopsis thaliana*, *Chlamydomonas reinhardtii*, and *Synechocystis* sp. (GCA_000478825). BLASTX results indicated that most DEGs lacked functional assignment (Table S4.6). Notably, BLASTX-based protein classification was primarily

observed in DEGs identified from comparisons between control and Cd-treated samples at each timepoint. The predominant differences between control and Cd-treated cultures at each time point were inorganic ion transport and metabolism (P), signal transduction mechanisms (T), posttranslational modification, protein turnover, and chaperones (O), and energy production and conversion (C).

Genes in clusters of orthologous genes (COG) P exhibited prominent regulation, particularly those encoding formate/nitrite transporters and metal-binding proteins. Most formate and nitrite-related transporters were downregulated across all days (Table S4.6). In contrast, several zinc transporters and metal homeostasis genes were upregulated. Genes within COG T were predominantly upregulated, including multiple histidine kinases, cyclases, and serine/threonine protein kinases. In COG O, upregulation of E3 ubiquitin ligases and protein kinases indicated increased protein turnover and posttranslational remodeling. Notably, COG C contained both up- and downregulated genes. While core photosynthetic genes such as ATP synthase subunits and PSII components were upregulated, light-harvesting complex (LHC) proteins were downregulated. In contrast, a substantial portion of DEGs across all timepoints belonged to COG S (function unknown). While not interpretable in function, the prevalence of unknown annotations highlights the unique or poorly characterized genomic responses of *E. mutabilis* to Cd.

Additionally, BLASTX-based protein annotation revealed temporal differences in the functional classification of DEGs in Cd-treated cultures (Table S4.7). While most DEGs identified between Days 7 and 14, and between Days 7 and 21, lacked functional assignment, comparison between Days 14 and 21 yielded 931 COG classifications

corresponding to 882 DEGs. Different from comparisons between control and Cd-treated cultures over time, the predominant differences between cultures exposed to Cd after 14 and 21 days were related to signal transduction mechanisms (T), posttranslational modification, protein turnover, and chaperones (O), RNA processing and modification (A), lipid transport and metabolism (I), and inorganic ion transport and metabolism (P).

Genes within COG T were broadly upregulated between Cd-treated cultures at Day 21, including several histidine kinases, adenylyl/guanylyl cyclases, and serine/threonine protein kinases. In COG A, genes associated with RNA recognition, splicing, and processing were also upregulated. Genes assigned to COG O were primarily involved in protein degradation and posttranslational control, with upregulation of ubiquitin-conjugating enzymes and RING-type ligases. Additionally, several genes in COG I related to lipid metabolism, such as carboxylesterases and acyltransferases, were upregulated. Notably, upregulated genes in COG P included zinc transporters, cation efflux proteins, and ABC phosphate transporters, whereas formate/nitrite transporters were predominantly downregulated.

DEGs were further assessed to identify gene ontology (GO) terms using the PANTHER classification system. A total of 369 significant genes (FDR < 0.05) were annotated with GO terms and species information across all timepoints: 105 on Day 7, 115 on Day 14, and 149 on Day 21. Of the 369 genes, 211 were unique while 158 were significantly expressed at multiple timepoints. These genes were associated with 1,377 GO term annotations (Appendix I: Days) representing 39 unique GO terms (Table 4.3; Figure S4.5) in 419 gene-GO term combinations. Importantly, these annotated GO terms meet the

significance threshold for classification as overrepresented biological functions, cellular components, or molecular processes enriched among the DEGs.

By contrast, only 124 significant genes (FDR < 0.05) were annotated with GO terms comparing Cd-treated cultures after 14 and 21 days of exposure (Table 4.4; Figure S4.6) of which 78 were unique. These genes were associated with 264 GO term annotations representing 24 GO annotations (Appendix I: 14vs21). Notably, there were no significant genes (FDR < 0.05) annotated when comparing Cd-grown cultures after 7 and 14 days of growth or 7 and 21 days of growth.

Integrating analysis of transcripts and hormones

Annotated genes were initially filtered based on specific keywords from SPROT BLASTX results, transcript predicted functions, and KEGG identifiers associated with phytohormone biosynthesis (Table S4.8). A total of 357 unique genes were identified and found to be consistently present across Days 7, 14, and 21. Of these, 34, 46, and 68 genes were deemed statistically significant (padj < 0.05) at Days 7, 14, and 21, respectively, while only 6, 5, and 4 genes met the threshold for differential expression ($|\log_2$ fold change$| > 1$) at the corresponding time points (Appendix I: Hormones - Days).

Transcriptomic analysis across Days 7, 14, and 21 revealed modest but statistically significant changes in the expression of several genes associated with phytohormone biosynthesis, particularly within the auxin and CK pathways. Several genes linked to the tryptophan-dependent auxin biosynthesis pathway showed differential expression (padj < 0.05), although most exhibited low-magnitude shifts ($|\log_2$ fold change$| < 1$). At Day 14, a

gene annotated with KEGG ortholog K00820 (tryptophan synthase beta chain) was identified, suggesting potential upregulation of tryptophan synthesis, a precursor to IAA. By Day 21, additional genes with annotations consistent with aminotransferase activity were detected, which may represent TAA1-like enzymes that convert tryptophan to indole-3-pyruvate. Furthermore, flavin monooxygenase-like genes, potentially corresponding to the YUC family of enzymes, were also observed.

However, quantification of IAA in the culture supernatant did not mirror these expression patterns. Under control conditions, IAA levels in the supernatant decreased from 1022.1 ± 132.7 pmol/100,000 cells at Day 7 to 665.2 ± 86.4 pmol/100,000 cells at Day 14 and were not detectable at Day 21 (Table 4.2). IAA was absent at all timepoints in Cd-treated cultures. This apparent disconnect suggests that auxin biosynthesis may have occurred predominantly within the cellular fraction, with limited export or stability in the extracellular medium.

In contrast, CK-related gene expression aligned more clearly with metabolite profiles. Genes annotated as tRNA isopentenyltransferase (IPT) (K00591), the LONELY GUY (LOG) enzyme cytokinin riboside 5′-monophosphate phosphoribohydrolase (K00588), homocysteine S-methyltransferases, and O-methyltransferases were differentially expressed, particularly at Days 14 and 21, and displayed statistically significant changes in expression (Appendix I: Hormones – Days). Although fold changes were modest, the downregulation of these genes suggests transcriptional deactivation of the CK biosynthetic pathways. Supporting this, supernatant CK nucleotide levels, including *c*ZNT and iPNT, increased over time in Cd-treated cultures, reaching 1227.4 ± 82.3

fmol/100,000 cells at Day 21 while bioactive CKs and methylthiolated CKs remained undetectable (Table 2). These data demonstrated consistent downregulation of CK-related pathways at both the transcriptomic and metabolite levels.

Compared to the time course under control conditions, a greater number of hormone-related genes were differentially expressed, and the magnitude of expression changes was more pronounced when comparing cultures grown in Cd over time (Appendix I: Hormones – Cd). Comparisons between Days 7 and 14 under Cd treatment revealed 99 genes matching auxin or CK biosynthetic pathways showed significant changes in expression. Among these, the maximum fold change reached 2.17, indicating substantial transcriptional modulation of specific genes. Genes related to tryptophan biosynthesis and transferases with possible roles in the TAA1/YUC auxin pathway were among those identified, although the majority of fold changes were moderate.

Between Day 7 and Day 21 under Cd treatment, 193 hormone-related genes displayed statistically significant expression differences, though only one showed a fold change exceeding 1. The broader representation of hormone-related annotations suggests persistent, low-magnitude transcriptional modulation under prolonged Cd exposure. 3 genes encoding methyltransferases were among those identified, consistent with activation of CK biosynthesis and modification pathways.

Comparisons between Days 14 and 21 under Cd treatment uncovered 115 hormone-related genes that were statistically significant (padj < 0.05), with a maximum fold change of 1.66. This includes genes encoding CK riboside 5′-monophosphate

phosphoribohydrolase (LOG; K00588) and tRNA IPT (K00591), both of which were modestly upregulated, supporting continued CK pathway activation.

Metagenomic analysis

Kraken2 classified an average of 15% and 14% of reads at the genus level in control and Cd-treated samples, respectively. At the species level, the average classification was 14% for control samples and Cd-treated samples. Bracken refinement revealed *E. gracilis* as the most abundant taxa across all samples on average (99.2%; Figure 4.5).

Differential abundance analysis revealed a subset of taxa that were significantly enriched in either control or Cd-treated cultures (Table S4.9; Figure S4.7). For example, *Talaromyces amestolkiae* and *Exophiala oligosperma* exhibited strong enrichment under Cd exposure, with $\log_2$ fold changes exceeding 8 and FDR-adjusted p-values < 0.001. In contrast, *Corynebacterium simulans* was significantly more abundant in control samples ($\log_2$ fold change = –2.32; padj = 0.01).

4.6 DISCUSSION

This study highlights the stress resilience of *E. mutabilis* and its associated microbial partners under Cd exposure, revealing a coordinated response that spans molecular, physiological, and community levels. Rather than simply tolerating toxicity, the FAB consortium actively modulates gene expression, hormone biosynthesis, and

ultrastructural organization to manage HM stress, which underscores the adaptive capacity of co-cultured extremophiles in severe environments.

Cd tolerance and accumulation of *E. mutabilis*

Cd is a non-essential and toxic metal for microalgae, known to disrupt photosynthetic processes and respiration [58–61]. In this study, *E. mutabilis* demonstrated exceptional resilience to Cd stress, tolerating concentrations that are lethal to most freshwater microalgae. After 21 days of exposure to 100 μM Cd (approximately 11.2 mg/L), *E. mutabilis* maintained cell densities exceeding 3.7×10^5 cells/mL and viability above 97%. In contrast, *Chlorella* sp. and *Ankistrodesmus* sp. exhibit sharp declines in both growth and viability at Cd levels above 8.0 mg/L and 5.4 mg/L, respectively, within a shorter timeframe [62]. Even *Scenedesmus*, often considered more tolerant, shows growth inhibition at 10–15 mg/L Cd within 12 days [62]. Notably, the related euglenoid *E. gracilis* demonstrates high sensitivity to Cd under autotrophic growth, with severe growth inhibition at concentrations far below those tolerated by *E. mutabilis* [25,26,63,64].

Alongside superior viability, *E. mutabilis* accumulated cellular Cd at levels that surpassed those reported in most freshwater algal species. By day 21, approximately 15% of total Cd added to the culture had been internalized. In comparison, *Chlorella vulgaris* [65] and *Scenedesmus obliquus* [66] exhibit cellular Cd accumulation of approximately 5% and 8%, with most metal ions remaining adsorbed on the cell surface after shorter exposures. Studies of diatoms such as *Thalassiosira weissflogii* indicate that cellular Cd accumulation typically plateaus within hours rather than over weeks [67]. In *E. mutabilis*,

however, accumulation increased steadily over three weeks, suggesting efficient and sustained uptake or sequestration mechanisms. This ability to internalize and compartmentalize Cd likely underpins *E. mutabilis*' tolerance. Intracellular accumulation and organelle sequestration are critical detoxification mechanisms in algae, preventing free Cd^{2+} from disrupting photosynthesis and metabolism [68]. Thus, *E. mutabilis*' capacity for sustained Cd uptake and sequestration may directly contribute to its high viability under Cd stress, setting it apart from more sensitive taxa.

TEM ultrastructural observations support this finding, revealing electron-dense deposits within chloroplasts of Cd-treated cells. These deposits are consistent with Cd sequestration [69,70], and their presence suggests that chloroplasts may act as key intracellular compartments for Cd storage in *E. mutabilis*, similar to patterns observed in *E. gracilis* under autotrophic conditions [71]; however, the sustained and increasing intracellular uptake observed in *E. mutabilis* stands in contrast to *E. gracilis*. While capable of accumulating Cd, *E. gracilis* often exhibits stress-related growth inhibition and reduced metal uptake over time, particularly under photoautotrophic conditions. For instance, in *E. gracilis*, cellular Cd accumulation at 100 µM typically results in significant growth inhibition (59–81%) within 4 days, with sequestration largely occurring in organelles such as chloroplasts or mitochondria depending on trophic state [26,64]. In contrast, *E. mutabilis* steadily increased Cd accumulation reaching levels that represent a higher proportion of total Cd introduced to the system than is commonly reported in *E. gracilis* or other freshwater microalgae.

TEM also suggested a greater presence of paramylon granules in Cd-treated cells, although this was not quantified. This qualitative observation aligns with prior studies showing elevated paramylon content in *E. gracilis* under Cd [28], chromium (Cr) [72,73], and osmotic stress [29,74]. Under autotrophic growth, paramylon accumulation is minimal, but stress can promote its synthesis as an alternative energy reserve [75,76]. Thus, the apparent increase in paramylon may reflect a metabolic adjustment to compensate for impaired photosynthetic carbon fixation under Cd stress.

Transcriptomic data further revealed molecular adaptations consistent with these physiological responses. DEGs related to metal transport (COG P), including zinc and cation efflux proteins, suggest active regulation of ion homeostasis. Similar metal transport systems including cation diffusion facilitators (CDFs), metal tolerance proteins (MTPs), ABC transporters, and P-type ATPases play key roles in Cd detoxification in green microalgae such as *Chlamydomonas reinhardtii* and *Auxenochlorella protothecoides* [77–79]. In *C. reinhardtii*, for instance, MTP1 and MTP4 are upregulated in response to Cd stress and localized to acidic vacuoles to aid in metal sequestration [79]. Similarly, upregulation of ABC transporters and cation exchange (CE) proteins has been observed in *Auxenochlorella protothecoides* and *C. reinhardtii* under HM stress, where they facilitate cellular efflux of Cd and Hg ions, respectively [77,78]. While *E. mutabilis* showed mixed expression of these genes, including some downregulation of ATP-binding (GO:0005737) and ABC transporter genes (GO:0140359), alternative or lineage-specific detoxification pathways may be at play.

Notably, genes associated with photosynthesis and energy production (COG C) including ATP synthase subunits and photosystem II components were upregulated under Cd stress. This suggests that *E. mutabilis* maintains chloroplast function and energy production despite metal exposure. Interestingly, LHC genes were downregulated a phenomenon also observed in *C. reinhardtii* under metal stress and interpreted as a strategy to reduce photooxidative damage when photosystem integrity is compromised [80]. Together, these patterns point to a strategic rebalancing of photosynthetic activity to sustain core energy production while limiting photodamage.

Finally, enrichment of GO terms related to catalytic activity and carbohydrate metabolism (GO:0003824) supports the hypothesis of metabolic reorganization under stress. Although direct annotation of β-1,3-glucan metabolism genes was lacking, the increased paramylon observed in TEM (Figure 4.3) suggests a shift toward energy conservation and stress buffering. The coordinated upregulation of genes supporting energy metabolism, metal transport, and chloroplast resilience alongside increased paramylon storage indicates an integrated survival response in *E. mutabilis* that is both metabolically flexible and stress adapted [74].

The exceptional Cd tolerance observed in *E. mutabilis* is likely not the result of algal physiology alone but may be reinforced by its microbial partners within the FAB consortium. Previous studies have shown that disrupting this consortium through antifungal or antibiotic treatments significantly impairs Cd tolerance, suggesting that cohabiting microbes play a functional role in stress adaptation [20]. Microbial partners such as *Talaromyces* and *Acidiphilium* may enhance metal resistance through several mechanisms

including modifying local pH, producing metal-chelating compounds, or facilitating redox transformations that alter Cd speciation and reduce bioavailability [81–84]. Additionally, members of the FAB community may themselves sequester Cd or stimulate algal signaling pathways that modulate detoxification responses. For instance, engineered fungal–bacterial biofilms composed of *Trichoderma harzianum* and *Bacillus subtilis* reduced soil Cd, Pb, and zinc (Zn) available content by approximately 76–78%, outperforming individual strains under greenhouse conditions [85].

Although the transcriptomic data in this study reflect predominantly *E. mutabilis* gene expression, the functional outcome observed including sustained cell viability, high Cd uptake, and metabolic resilience likely emerges from synergistic interactions within the FAB system. These findings support the growing consensus that microbial consortia offer metabolic plasticity, niche complementarity, and environmental buffering not attainable by monocultures, particularly in extreme conditions.

Hormones as regulators of Cd toxicity

Cytokinins

Transcriptome and hormone analyses suggest that the *E. mutabilis* FAB engages a coordinated, hormone-mediated response to Cd, reflecting a strategic regulatory shift that deprioritizes growth and reallocates metabolic energy toward survival. The near-complete suppression of CK free bases and ribosides – the forms directly involved in active signaling [86] – suggests a deliberate downscaling of growth-promoting pathways in response to HM exposure. This suppression aligns with the observed transcriptional downregulation of key

CK biosynthetic and activation genes, including IPT and LOG, which are responsible for CK nucleotide production and subsequent conversion to active forms, respectively.

In *Euglena*, CKs are primarily synthesized via the tRNA degradation pathway, in which IPT enzymes transfer an isopentyl group from dimethylallyl pyrophosphate (DMAPP) to adenine at position 37 of tRNA molecules, producing isopentenylated tRNAs [87,88]. Upon degradation, these modified tRNAs release inactive CK nucleotides which are then activated by LOG enzymes through cleavage of the riboside monophosphate moiety, yielding free base CKs [89]. Further modification is carried out using S-adenosylmethionine (SAM), iron (Fe), and cysteine (Cys) which are required for the methylthiolation of CKs from the tRNA degradation pathway [90]. The observed downregulation of genes involved in SAM and O-methyltransferase biosynthesis under Cd stress suggests a key shift in methylation dynamics that may directly affect hormonal regulation and metabolic prioritization. SAM is a universal methyl donor in the synthesis of methylthiolated CKs, particularly 2-methylthio derivatives such as MeSZR [91]. Methionine and SAM metabolism are tightly regulated under abiotic stress, where increased methionine synthesis can suppress CK signaling in favor of stress adaptation [91]. In contrast, the reduction of SAM and methyltransferase activity in *E. mutabilis* under Cd exposure implies a deliberate suppression of methylthiolated CK biosynthesis which has not been characterized in other systems as a response to environmental stressors. Downregulation of these genes under Cd stress suggests an adaptive hormonal checkpoint. While the biosynthetic machinery may still be producing precursor CK nucleotides, the conversion to active signaling molecules is intentionally restricted.

Interestingly, comparisons between cultures exposed to Cd after 21 days against cultures exposed for 14 days show modest upregulation of genes encoding LOG enzymes and SAM-dependent methyltransferases. This pattern implies that the *E. mutabilis* FAB system does not maintain a static suppression of CK signaling under stress, but rather dynamically modulates its hormonal machinery in response to environmental duration and intensity. Initially, suppressing CK activation and methylthiolated derivative synthesis may serve to halt energy-expensive processes such as cell division and metabolic stimulation. However, after prolonged exposure, the observed transcriptional activation of LOG and SAM genes may indicate a priming response, in which the system prepares for re-entry into growth or detoxification states once sufficient acclimation has occurred. Similar regulatory strategies have been documented in higher plants, where overexpression of LOG genes enhances recovery from abiotic stress by promoting controlled reactivation of CK signaling pathways during late-stage adaptation [92]. The reactivation of SAM metabolism may further support methylation-related processes tied to antioxidant production and hormone biosynthesis [93]. Although methylthiolated CKs are the least characterized group of CKs, this evidence suggests they may play a role in tempering stress responses [90].

This hormonal modulation appears to serve as a protective mechanism. Rather than allowing uncontrolled cell division or resource allocation during metal-induced stress, *E. mutabilis* may maintain CKs in their inactive nucleotide form, effectively buffering the signaling capacity while minimizing metabolic risk. Similar trends have been observed in higher plants. In *Oryza sativa*, overexpression of LOG enhances tolerance to drought and salinity by promoting sustained growth and recovery capacity, whereas reduced expression limits growth under stress [92]. In *Gossypium hirsutum*, LOG expression is regulated by

salt stress, with elevated LOG activity promoting root development and stress mitigation, while knockdown lines show heightened stress sensitivity [94].

The concurrent accumulation of CK nucleotides in Cd-treated *E. mutabilis* cultures supports this model. Although biosynthesis is not fully halted, hormonal signaling output is restrained. This is likely not a passive outcome of cellular damage, but an active regulatory strategy to balance energy demands, limit oxidative damage, and maintain hormonal readiness for post-stress recovery [95].

Auxins

The complete absence of extracellular IAA in Cd-exposed cultures, despite modest transcriptional activation of upstream biosynthetic genes, points to a similarly strategic suppression. Although transcripts linked the tryptophan-dependent IAA biosynthesis pathway – including a putative tryptophan synthase β subunit and genes with aminotransferase- or flavin monooxygenase-like annotations [96] – were weakly upregulated, their precise functional identity remains uncertain. These enzymes could represent early steps in IAA biosynthesis but given the broad metabolic roles of tryptophan and the ambiguity of annotations, the evidence for a direct auxin pathway is inconclusive. Notably, these modest transcript increases did not correspond to detectable extracellular IAA. This may reflect intracellular retention of IAA, the degradation of IAA under stress conditions, or the diversion of tryptophan towards alternative pathways. Such a response could limit oxidative risk, as IAA is redox-active and can exacerbate ROS generation when present in excess [97].

In other systems, similar reductions in auxin production or export have been correlated with improved tolerance to abiotic stressors such as salinity, drought, and HM exposure. For example, seedlings of *Pisum sativum* L. exposed to Cd and copper (Cu) exhibited elevated IAA oxidase activity – an enzyme associated with degradation of IAA resulting in decreased concentrations of auxin and impeded growth [98]. In *S. obliquus*, the concentration of intracellular IAA was reduced by 33% after being exposed to Pb which contributed to reduced cell proliferation [99]. However, IAA supplementation alleviated oxidative stress by boosting antioxidant defenses such as phytochelatin and glutathione production, suggesting that IAA can either exacerbate or mitigate ROS-related damage depending on context and concentration [99]. The *E. mutabilis* response likely mirrors these adaptive strategies, prioritizing redox balance and metabolic stability while continuing to proliferate in the face of Cd stress.

Considering the possible lack of alignment between IAA hormone profiles and possible related genes identified in transcriptomic analyses could be explained if IAA remained sequestered intracellularly or was rapidly metabolized to prevent redox imbalance. Supporting this, auxin has been shown to passively diffuse through the cell wall and accumulate within algal cells without requiring active export, as seen in *Scenedesmus* exposed to Pb [99]. Alternatively, the lack of IAA in the media may reflect suppressed microbial auxin production. Previous work identified that IAA production by co-cultured bacteria enhanced growth in *E. gracilis*, suggesting that auxin may function as a cross-kingdom signaling molecule in microbial consortia [100]. In the present study, however, the fungal and bacterial partners may not have contributed to extracellular auxin pools, or the overall biosynthetic activity may have been suppressed by Cd exposure. Whether auxin

signaling occurred entirely within *E. mutabilis* or through localized microenvironmental interactions remains unclear, but the strategic absence of extracellular IAA under stress likely reflects a controlled adaptation to avoid unnecessary growth signaling or oxidative activation.

The shift away from canonical hormone signaling aligns with broader transcriptomic and cellular trends in the *E. mutabilis* FAB: increased paramylon storage, suppressed LHC expression, and sustained chloroplast function under Cd stress. Together, these observations support a model in which *E. mutabilis*, possibly in concert with its microbial partners, transitions into a metabolically buffered state characterized by hormonal restraint, energy conservation, and enhanced detoxification capacity. In *E. mutabilis*, this may manifest as a culture-wide metabolic shift that enables prolonged survival and functional stability despite metal toxicity.

Microbial contributions and community-level adaptation

The functional success of the FAB system under Cd stress cannot be attributed to *E. mutabilis* alone. Community profiling revealed a shift in associated microbial assemblages under Cd exposure, with several fungal and bacterial taxa showing increased relative abundance. While some annotations suggested specific genera, it is important to note that metatranscriptomic pipelines are prone to taxonomic misassignments, particularly for fungi, where databases are often incomplete, markers lack phylogenetic resolution, and non-model organisms have a greater risk of spurious matches even to non-microbial lineages such as amphibians or humans [101–103]. Consequently, these identifications should be interpreted at a broad taxonomic level, with emphasis on functional potential

rather than species-specific roles. This aligns with earlier work using phylogenetically certified sequences that confirmed FAB associations in the consortium [20].

Rather than attributing detoxification to individual strains, the observed community-level adaptation is consistent with microbial partners contributing general functions widely distributed across microbial kingdoms such as biosorption, chelation, and pH regulation [7,104]. Fungal associations, for example, are known in plants to buffer oxidative stress and alter nutrient mobility under HM exposure [105], while bacteria such as acidophiles adjust pH and redox conditions in extreme environments [82]. The increased abundance of certain fungi in Cd-exposed cultures may therefore reflect general adaptive traits favoring persistence under metal stress, without requiring precise species-level assignment. In this regard, *Euglena* itself is exemplary. As a euglenoid, it harbours genes with similarities to plants and bacteria [106,107] making taxonomic and functional assignments particularly challenging. Thus, the community's apparent contributions to FAB resilience under Cd stress are best interpreted as cross-kingdom functional strategies rather than discrete activities of any single identified species.

Insights into Cd tolerance of *E. mutabilis* from transcriptome analysis

GO-term enrichment analysis revealed a suite of transcriptional adjustments in response to Cd stress, highlighting genes associated with heavy metal detoxification, ion homeostasis, and oxidative stress mitigation. This included the upregulation in genes involved in "metabolism", "chloroplast thylakoid membrane", and "thylakoid" while those linked to "chloroplast", "photosynthesis, light harvesting", "transmembrane transporter activity" and "formate transmembrane transporter activity" were consistently

downregulated. Notably, genes annotated for ZIP (ZRT/IRT-like Protein) family transporters and cellular zinc homeostasis were significantly upregulated at all timepoints. In plants and microalgae, ZIP and IRT transporters mediate the uptake and intracellular transport of divalent metal ions, including Zn^{2+}, Fe^{2+}, and Cd^{2+}, across membranes [108,109]. Under metal stress, ZIP proteins may also function in detoxification, reducing metal accumulation by facilitating redistribution or efflux [110–112]. In *E. gracilis*, ZIP transporters have been implicated in mediating Cd accumulation within chloroplasts [27,59], consistent with the electron-dense Cd deposits observed in chloroplasts of *E. mutabilis* in TEM images.

Although DGE analysis revealed upregulation of ZIP transporters when comparing control and Cd-treated cultures, a different pattern emerged when Cd-treated cultures were compared over time. Between Days 14 and 21, GO-terms related to “membrane” functions were notably enriched, particularly those associated with cation transmembrane transporters and cation efflux family proteins (CDF). Unlike ZIP transporters, which primarily involve divalent cations into the cytoplasm, cation efflux proteins of the CDF family mediate transport of metals from the cytosol into organelles such as vacuoles or out of the cell entirely [113,114]. Both ZIP and CDF transporters have been implicated in Cd translocation into chloroplast of *E. gracilis* [115], and in *C. reinhardtii* the overexpression of a CDF transporter enhanced Cd uptake and tolerance [116]. Interestingly, naturally Cd-adapted chlorophyte strains still outperformed engineered *C. reinhardtii*, suggesting that complex mechanisms underpin long-term adaptation. Taken together, the expression of both ZIP and CDF transporters in *E. mutabilis* suggests a coordinated strategy of Cd uptake

and compartmentalization, which may contribute to its exceptional tolerance under sustained Cd stress.

The contrast between early ZIP upregulation and later activation of efflux-related pathways in *E. mutabilis* may indicate a shift in detoxification strategy from initial metal internalization and compartmentalization, toward long-term management through vacuolar sequestration or extracellular export. This shift may be reflective of a multi-tiered detoxification model in which early uptake is buffered by cellular organelles, and later response mechanisms aim to clear accumulated intracellular Cd as oxidative stress and metal saturation increase.

Unlike many microalgae, *E. mutabilis* did not exhibit increased expression of phytochelatin or glutathione synthesis genes, highlighting a potential unique detoxification mechanism among euglenoids. One possibility is the formation or compartmentalization of Cd-phosphate complexes. This is supported by the upregulation of a proton-phosphate symporter, potentially indicating enhanced phosphate import. Phosphorus not only forms insoluble Cd-phosphate precipitates that reduce Cd bioavailability, but also enhances antioxidant enzyme activity, aiding in ROS detoxification and mitigating oxidative damage. [117,118]. In *Saccharomyces cerevisiae*, the interaction between phosphate and Cd has been shown to affect ROS sensitivity, where excess phosphate suppresses antioxidant defenses and exacerbates Cd toxicity [119]. Yet, in other systems, phosphate can act as a protective agent. In *Citrobacter* sp., Cd-phosphate precipitates form on the cell surface when both Cd and phosphate are present in the medium, reducing intracellular Cd burden [120]. Similarly, in *Chlorella*, extracellular polyphosphates have been shown to complex

with Cd, providing a non-enzymatic barrier to uptake [121]. Although *E. mutabilis* was not cultured in phosphate-rich media, the simultaneous upregulation of phosphate transport, ZIP-family genes, and CDF transport raises the possibility of a detoxification strategy in which Cd is exported or redistributed and neutralized through phosphate complexation, either intra- or extracellularly. These findings suggest that even in non-phosphate-enriched environments, *E. mutabilis* may activate latent phosphate-based detoxification strategies as an alternative to classical phytochelatin-mediated pathways.

If *E. mutabilis* is attempting to detoxify Cd, it is not without exhibiting stress. Under Cd stress, *E. mutabilis* displays a complex transcriptional strategy that reflects a balancing act between sustaining essential chloroplast function and minimizing oxidative damage. Upregulation of genes encoding core photosynthetic components such as cytochrome b6, ATP synthase β-subunit, and photosystem II (PSII) reaction center proteins suggests an attempt to maintain electron transport and ATP generation despite the known inhibitory effects of Cd on photosynthetic proteins. Cd is known to displace essential metal cofactors like Mg^{2+} or Fe^{2+} in photosystem complexes, which can impair electron transport and lead to excessive ROS production [115,122]. Thus, the increased expression of these core genes likely represents a compensatory mechanism to repair or replace damaged complexes, consistent with similar observations in higher plants and algae under metal stress [123–125]. Supporting this, ATPases associated with ion regulation and energy production were also upregulated, indicating increased metabolic demand – likely tied to detoxification, redox balancing, and maintenance of ion gradients within the chloroplast.

Although HM exposure is widely known to impair photosynthesis, the upregulation of photosynthesis-related genes in this study may reflect compensatory responses rather than functional enhancement. Cd, for instance, can substitute for magnesium (Mg) in the porphyrin ring of chlorophyll, but this substitution produces structurally unstable and photosynthetically inactive chlorophyll analogs, ultimately impairing light capture and energy transfer [126]. Similar trends have been observed in other extremophilic microalgae such as *Chlamydomonas acidophila*, which upregulated genes associated with photosynthesis and metabolism under high copper (Cu) concentrations [125]. These responses were interpreted as part of an adaptive strategy that allows the alga to tolerate and adjust to toxic environments, potentially through enhanced repair or detoxification mechanisms [127]. In *E. mutabilis*, the upregulation of core chloroplast genes likely reflects an inherent stress-adaptive strategy aimed at repairing or stabilizing damaged photosynthetic complexes and mitigating oxidative damage, rather than enhancing photosynthetic efficiency or incorporating Cd into functional components of the photosynthetic apparatus.

At the same time, transcripts encoding the LHC proteins were significantly downregulated. This aligns with a well-characterized photoprotective response wherein LHCs are suppressed to reduce light capture and minimize photooxidative stress during periods of photosystem instability [122,128]. In a damaged PSII environment, continued light harvesting exacerbates ROS generation. By shrinking the antennae size, *E. mutabilis* reduces excitation pressure on its photosystems, thus mitigating potential oxidative damage [129,130]. This response, sometimes described as “hardening” in plant systems [131,132],

supports the hypothesis that *E. mutabilis* prioritizes minimal but stable photosynthetic output under extreme stress.

This is supported with the observed downregulation of formate/nitrite transporters in *E. mutabilis* under Cd stress, whereby limiting nitrite influx helps prevent the formation of reactive nitrogen species (RNS) and simultaneously conserves reducing power for antioxidant defense systems [133,134]. Likewise, suppression of formate transport may serve to moderate cellular NADH levels, as formate oxidation via formate dehydrogenase generates NADH, which can overstimulate the electron transport chain and increase ROS formation through electron leakage [134,135]. By curbing formate uptake, *E. mutabilis* may reduce the burden on redox buffering systems, preventing excess ROS accumulation and maintaining intracellular redox homeostasis.

Together, these transcriptional patterns suggest that *E. mutabilis* is engaging in a deliberate overcompensation or functional prioritization strategy under HM stress: preserving core photosynthetic infrastructure, reinforcing detoxification pathways, and downregulating auxiliary metabolic functions that could exacerbate oxidative damage or drain cellular resources. Importantly, the upregulation of chloroplast thylakoid-associated GO-terms despite downregulation of LHC and undefined chloroplast genes implies that membrane integrity and photosystem core complexes are preserved, while light input and metabolic outflow are tightly regulated. Contrary to any suggestion that *Euglena* might be using Cd in place of Mg^{2+} in chlorophyll biosynthesis, such substitution is biochemically disruptive and would be maladaptive; instead, the observed upregulation more likely reflects a repair or stabilization response to metal-induced chloroplast stress. Collectively,

this pattern points to a sophisticated ROS mitigation and energy conservation mechanism that enables *E. mutabilis* to endure and function in metal polluted environments.

These molecular, metabolic, and structural responses support a unified model of Cd tolerance in the *E. mutabilis* FAB consortium (Figure 7). This model encompasses (1) early Cd uptake via ZIP transporters, (2) intracellular detoxification through chloroplast sequestration and efflux mechanisms, (3) strategic downregulation of light harvesting and nitrogen transport to reduce ROS, (4) paramylon accumulation as a metabolic buffer, and (5) hormone suppression to pause growth signaling. The enrichment of *Talaromyces* and *Acidiphilium* under Cd stress suggests that microbial associates further support stress adaptation through chemical signaling and environmental modulation. This integrative response underpins the long-term stability and functional resilience of the consortium in metal polluted environments.

4.7 CONCLUSIONS

This study reveals the unique molecular and physiological adaptations of a naturally occurring *E. mutabilis* FAB consortium to Cd stress, integrating transcriptomics, hormone profiling, structural imaging, and community analysis. Notably, the combined response of *E. mutabilis* and its microbial partners involves a transition from early metal uptake to intracellular detoxification, strategic suppression of ROS-generating pathways, metabolic reorganization, and hormone downregulation to maintain cellular stability.

The novelty of this work lies in the holistic demonstration that natural microbial consortia – rather than isolated monocultures or synthetic co-cultures – coordinate at

multiple biological levels to achieve extreme stress resilience. By preserving photosynthetic function, activating detoxification pathways, and dynamically modulating hormone metabolism, this system offers a blueprint for leveraging ecological interactions in engineered biotechnologies. The *E. mutabilis* FAB consortium represents a compelling model for designing biologically robust, adaptive remediation systems for acidic and metal-laden environments. These findings underscore the potential of co-cultured extremophiles in shaping the next generation of sustainable bioremediation strategies.

4.8 FIGURES AND TABLES

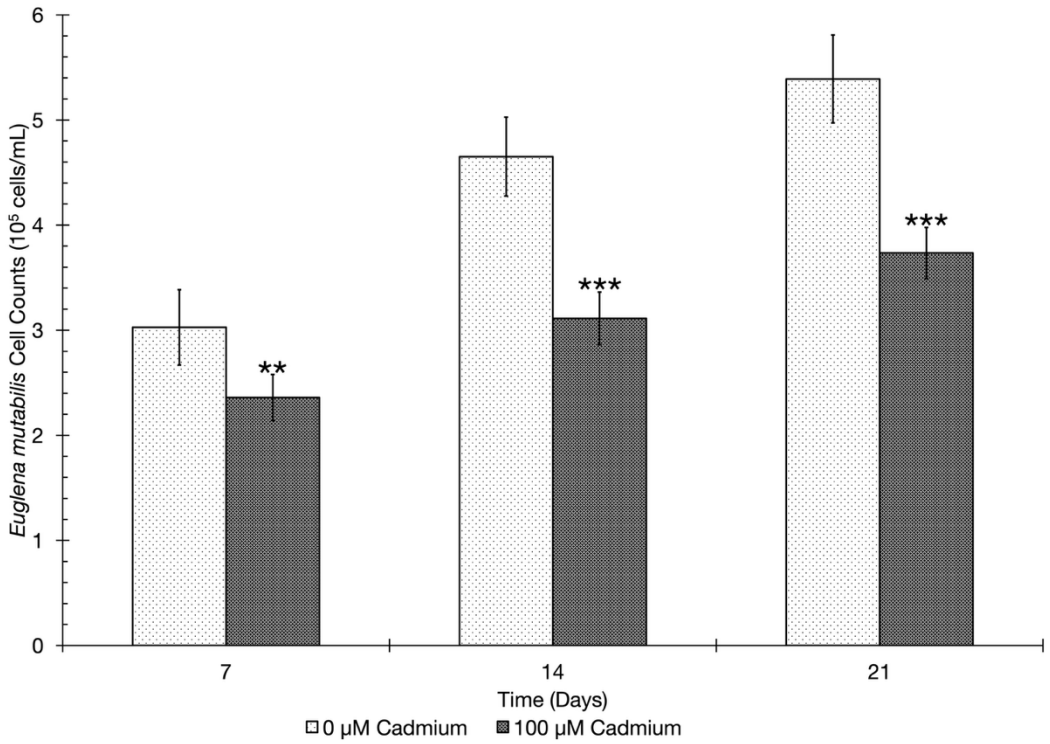

Figure 4.1: Assessment of Cd tolerance of *E. mutabilis*. Growth of *E. mutabilis* over 21-days in 100 µM $CdCl_2$ revealed significant decreases in cell counts compared to *E. mutabilis* cells grown in MAM only. Error bars represent standard deviation between biological replicates ($n = 7$), and asterisks represents significant difference between 0 µM and 100 µM Cd on each day (* = $p < 0.05$; ** = $p < 0.01$; *** = $p < 0.001$) as determined by an F-test for variance and Student's t-test.

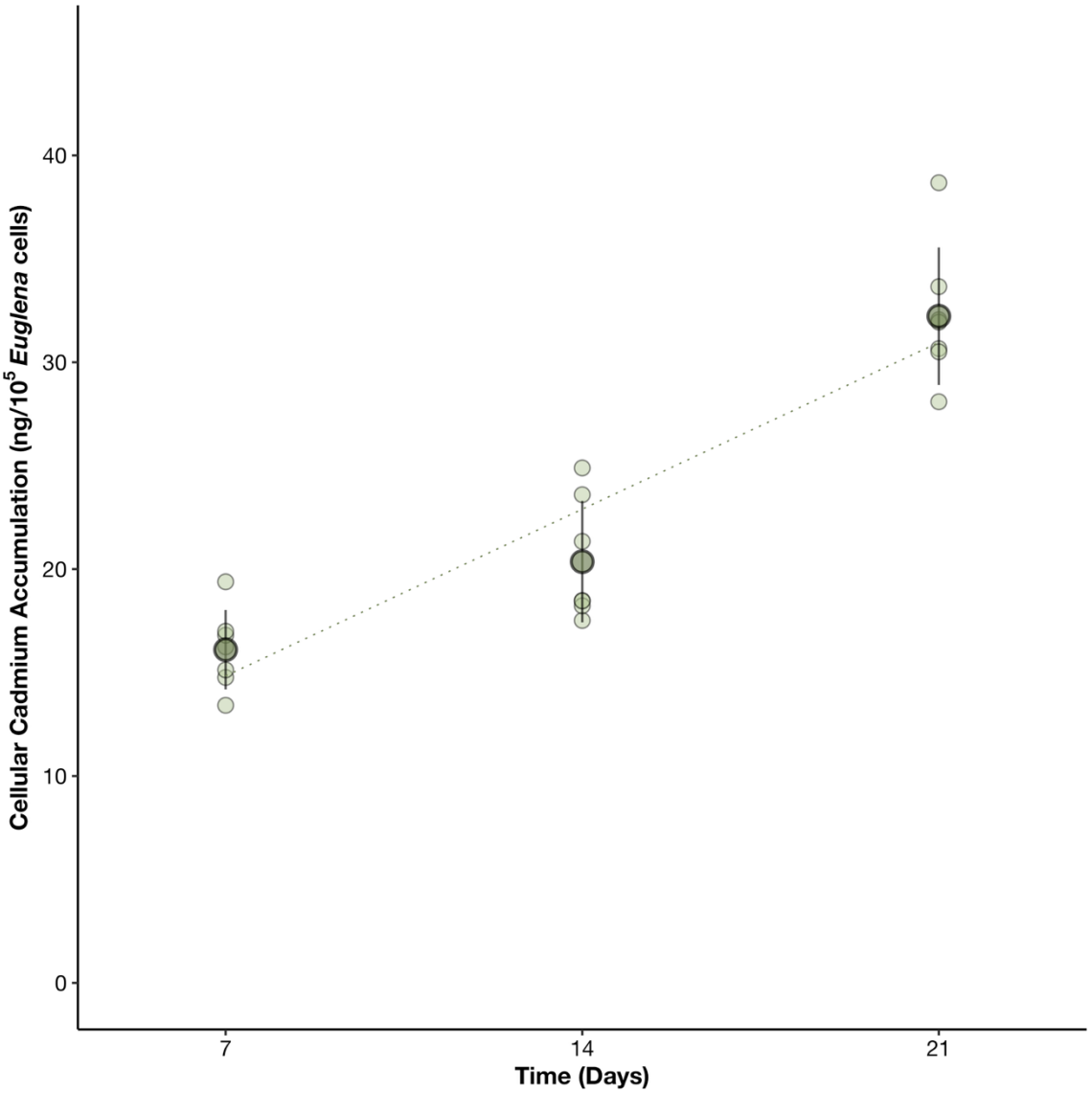

Figure 4.2: Cellular $CdCl_2$ accumulation increases progressively over the 21-day exposure to Cd. Each light green dot represents an individual biological replicate (n = 7) while the dark green point represents the average ± standard deviation (black error bars). The dotted line illustrates the overall trend of increasing average Cd accumulation over time (R^2 = 0.93; $y = 11.5x + 67.8$). Based on the initial Cd dosing (674,000 ng per 60 mL culture flask), intracellular uptake accounted for 3-11% over time. Background media controls indicated abiotic Cd losses where 500,000 ng, 525,000 ng, and 491,000 ng remained after 7-, 14-, and 21-days, respectively. This raised the effective sequestration efficiencies to 5-15%.

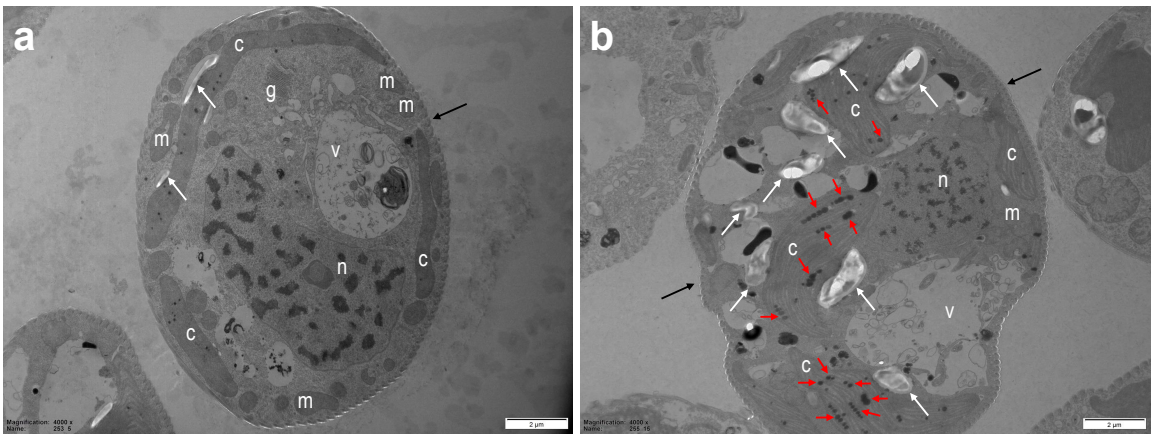

Figure 4.3: Transmission electron microscopy of *E. mutabilis* cells points to an elevated presence of paramylon and Cd accumulation after 21-days of growth. Representative cross-sections of *E. mutabilis* grown in (a) MAM and (b) MAM + 100 µM $CdCl_2$ display chloroplasts (c), Golgi bodies (g), mitochondria (m), the nucleus (n) vacuoles (v), the pellicle (black arrows), paramylon granules (white arrows), and electron-dense bodies within the chloroplast (red arrows). While not measured, paramylon granules appeared more numerous in Cd-treated cells. The scale bar on each image is 2 µm.

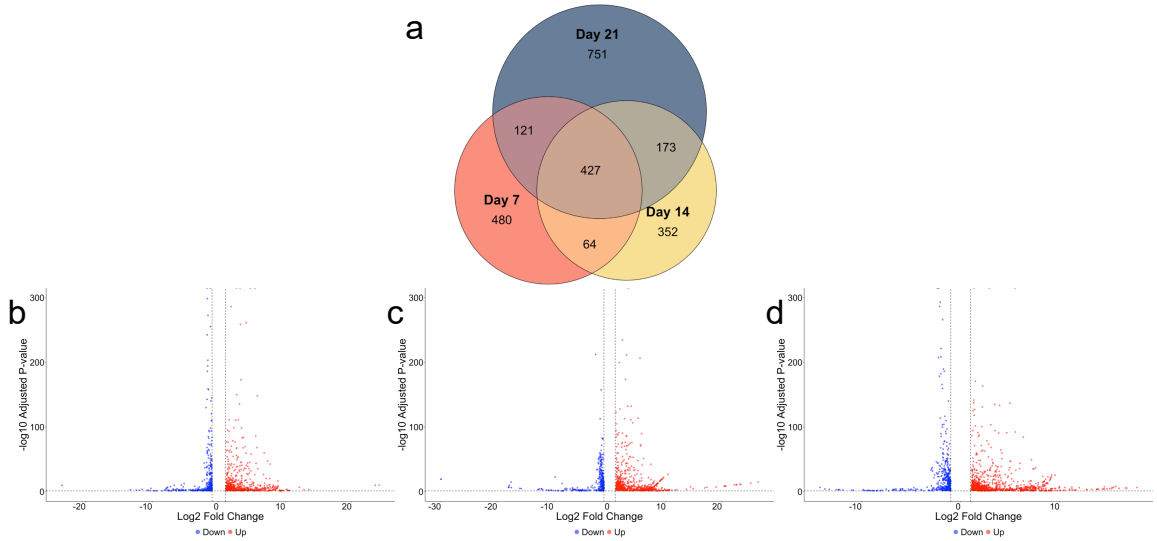

Figure 4.4: Gene expression when *E. mutabilis* is grown in 100 µM Cd changes over time. A Euler diagram (a) displays the number of unique DEGs between control and Cd-treated cultures after 7 (red), 14 (yellow), and 21 (blue) days growing in the presence of 100 µM Cd. Volcano plot comparing the $\log_2$ fold change (*x*-axis) and $-\log_{10}$ adjusted *p*-value (*y*-axis) illustrate the distribution of DEGs which are significantly (padj < 0.05; $|\log_2$ fold change$| > 1$) upregulated (red) and downregulated (blue) after 7 (b), 14 (c), and 21 (d) days of growth with Cd.

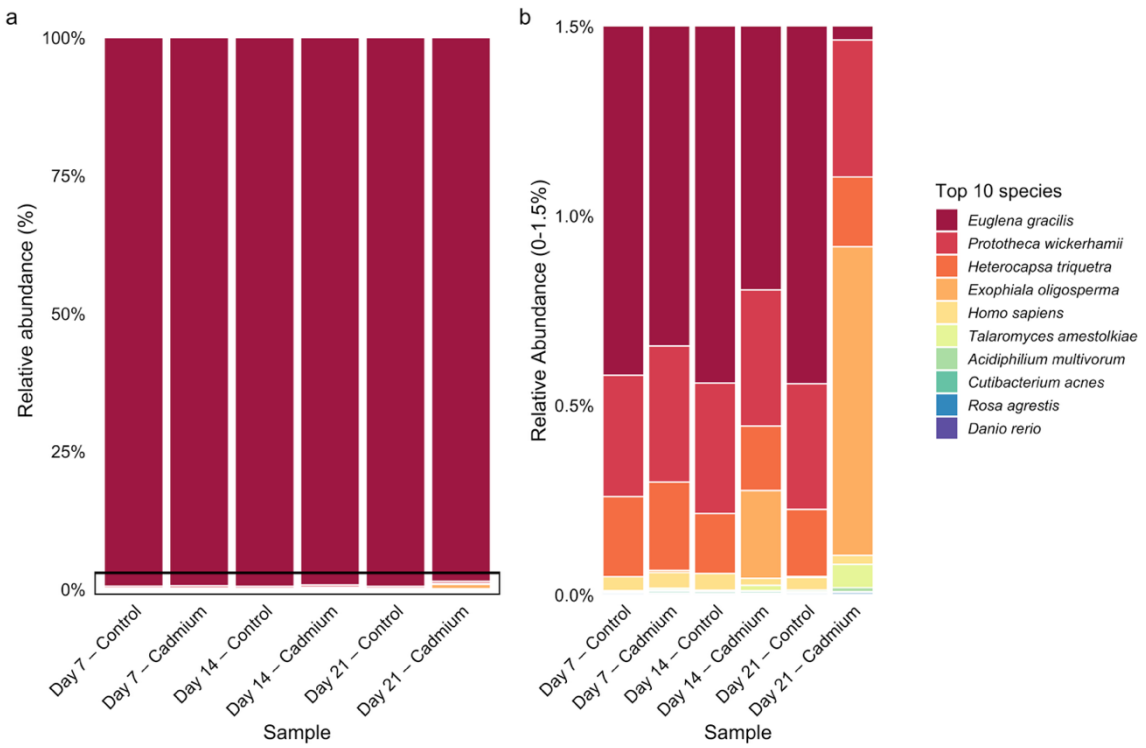

Figure 4.5: Relative abundance of the top 10 most abundant species identified in metatranscriptomic samples across timepoints and treatment conditions using Kraken2 classification with Bracken refinement. (a) Full-scale relative abundance showing that *Euglena gracilis* overwhelmingly dominated all samples across control and Cd-treated cultures at Days 7, 14, and 21. (b) Expanded view (0–1.5% scale) highlighting low-abundance taxa, including *Prototheca wickerhamii*, *Heterocapsa triquetra*, *Exophiala oligosperma*, *Homo sapiens*, and others. The analysis was performed at the species level, and values represent the estimated fraction of reads assigned to each species normalized by Bracken. Bars represent the average relative abundance across replicates (n = 7) for each condition.

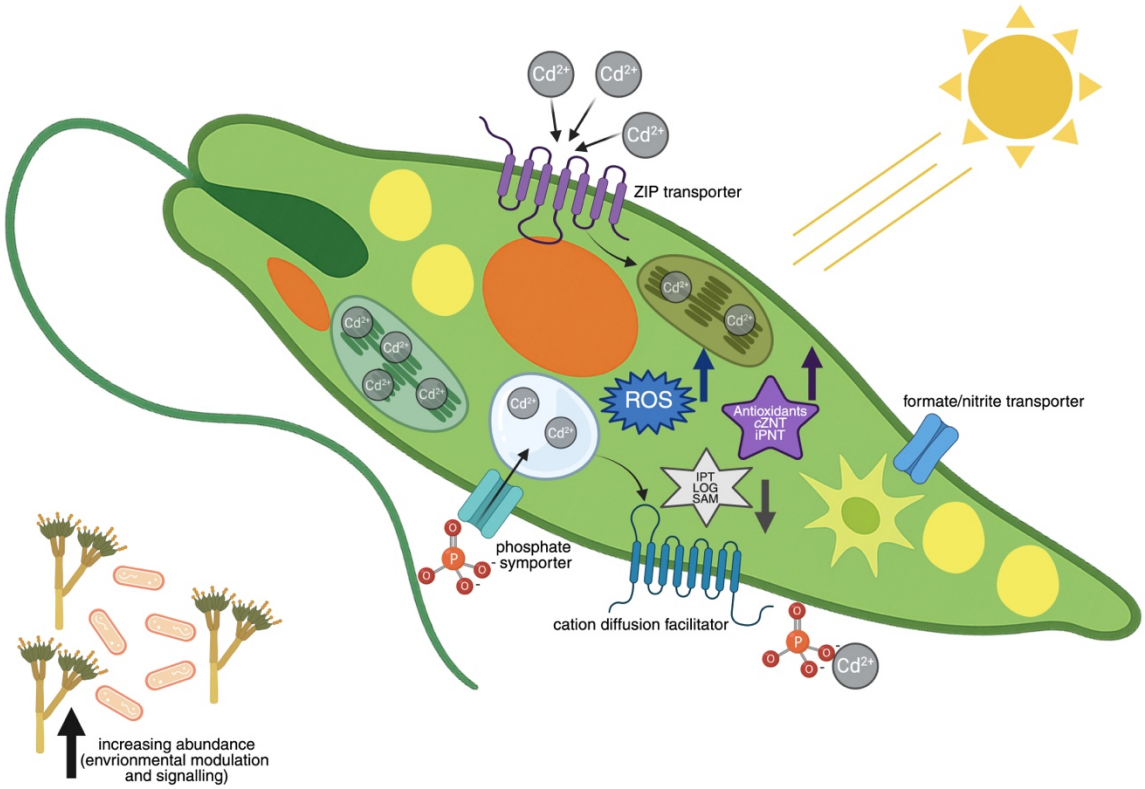

Figure 4.6: Conceptual model of the multifaceted response of the *Euglena mutabilis* FAB consortium to Cd stress, integrating metal handling, metabolic regulation, antioxidant defense, and hormonal modulation. Cd uptake is initially mediated by ZIP family transporters, followed by upregulation of cation diffusion facilitators and CDF transporters to support intracellular sequestration or export. Chloroplasts may serve as key detoxification compartments, limiting damage to other organelles. Cd exposure induces ROS (blue shape and up arrow), prompting downregulation of LHC and formate/nitrite transporter genes to reduce light harvesting and electron leakage. Despite suppressed photosystem activity, upregulation of ATP synthase and PSII core components suggests maintenance of basal photosynthetic function (depicted as dark pigmented chlorophyll). Paramylon accumulation (yellow) provides metabolic buffering under prolonged stress. Hormone responses include suppressed active CKs and auxin with the downregulation of IPT and LOG (grey star and down arrow) but increased CK nucleotide forms (purple star and up arrow), indicating a shift toward hormonal dormancy. Symbiotic partners such as *Talaromyces* and *Acidiphilium acidophilum* may further enhance tolerance via metal chelation, pH stabilization, and phytohormone signaling. Together, the model highlights a coordinated strategy for survival in metal-contaminated environments. Figure was made using BioRender.com.

Table 4.1: Comparison between the frequency of non-viable cells in control and Cd treated cells after 21-days of growth ($n = 7$). Dead cell frequency was assessed by staining with Trypan Blue and counting on a haemocytometer at 10x magnification. The frequency of dead cells was determined using the formula: (# dead cells / total cell count) * 100% = frequence of dead cells.

	Day 7		Day 14		Day 21	
	Total Cell Counts (cell/mL)	Frequency of Dead Cells (%)	Total Cell Counts (cell/mL)	Frequency of Dead Cells (%)	Total Cell Counts (cell/mL)	Frequency of Dead Cells (%)
0 µM Cd	302,678	0	465,104	0	538,988	0
100 µM Cd	237,648	0.69	318,228	2.25	379,910	1.75

Table 4.2: Concentrations of hormones detected in the culture supernatant of *E. mutabilis* under control and Cd-treated conditions over 21 days. Hormone levels are reported as mean ± standard error (SE) in picomolar per 100,000 cells (pmol/100,000 cells) or femtomolar per 100,000 cells (fmol/100,000 cells). CKs are grouped into free bases, ribosides, and nucleotides, with total concentrations provided for each class where applicable. A dagger (†) indicates significant difference in hormone concentration between control and Cd-treated cultures at each timepoint using an F-test to assess variance followed by Student's t-test ($n = 7$).

Supernatant (pmol/100,000 cells ± SE)		0 µM Control			100 µM Cadmium		
	Compound	Day 7	Day 14	Day 21	Day 7	Day 14	Day 21
	IAA	1022.124 ± 132.706	665.174 ± 86.362	n.d.	n.d.	n.d.	n.d.
Supernatant (fmol/100,000 cells ± SE)		0 µM Control			100 µM Cadmium		
	Compound	Day 7	Day 14	Day 21	Day 7	Day 14	Day 21
Free bases	*c*Z	32.753 ± 8.503	146.646 ± 7.823	761.035 ± 41.450	507.937 ± 59.590†	n.d.	n.d.
	iP	10.975 ± 1.463	18.084 ± 0.836	10.226 ± 0.585	13.872 ± 3.219†	n.d.	n.d.
Total		**43.728 ± 9.966**	**164.73 ± 8.659**	**771.261 ± 42.035**	**521.809 ± 62.809**	**0**	**0**
Ribosides	*c*ZR	8.845 ± 1.792	25.164 ± 3.540	29.162 ± 4.970	20.257 ± 2.595	n.d.	n.d.
Nucleotides	*c*ZNT	125.712 ± 5.994	308.041 ± 5.780	290.031 ± 17.981	301.741 ± 11.426†	325.904 ± 8.042†	235.569 ± 4.015†
	iPNT	n.d.	n.d.	n.d.	n.d.	495.101 ± 27.895†	991.867 ± 78.298†
Total		**125.712 ± 5.994**	**308.041 ± 5.780**	**290.031 ± 17.981**	**301.741 ± 11.426**	**821.005 ± 35.937**	**1,227.436 ± 82.313**
Methylthiols	MeSZR	1689.148 ± 50.541	1099.257 ± 32.891	1164.213 ± 31.045	641.495 ± 6.141†	778.509 ± 13.023†	487.250 ± 18.076†

Table 4.3: Identification of unique GO terms in the presence of Cd. 39 statistically overexpressed (FDR < 0.05) gene ontology (GO) terms were identified from the list of DEGs using the PANTHER classification system when *E. mutabilis* cultures grown in MAM were compared to cultures grown in MAM + 100 µM Cd. Databases for GO term identification include *Homo sapiens, Arabidopsis thaliana, Chlamydomonas reinhardtii,* and *Synechocystis sp.* in relation to clusters of orthologous genes (COGs) identified using BLASTX.

Ontology	GO Term	Gene Count	Average FDR	COG Classification(s)
Biological Process	Photosynthesis, light harvesting (GO:0009765)	178	7.09×10^{-9}	C, P, Unclassified
	Photosynthesis (GO:0015979)	22	6.13×10^{-6}	S, Unclassified
	Translation (GO:0006412)	19	8.36×10^{-3}	J, Unclassified
	Cyclic nucleotide biosynthetic process (GO:0009190)	8	3.68×10^{-3}	P, T, Unclassified
	Photosynthesis, light reaction (GO:0019684)	6	4.58×10^{-7}	C
	Nucleotide metabolic process (GO:0009117)	4	2.12×10^{-2}	F
	Response to light stimulus (GO:0009416)	3	1.91×10^{-8}	BDLTU
	Translational elongation (GO:0006414)	1	3.22×10^{-5}	Unclassified
	Proton transmembrane transport (GO:1902600)	1	4.74×10^{-2}	Unclassified
Cellular Component	Cytoplasm (GO:0005737)	276	6.98×10^{-4}	E, F, J, N, O, Q, S, T, UY, V, Z, Unclassified
	Chloroplast (GO:0009507)	228	1.47×10^{-2}	C, E, J, P, S, Unclassified
	Membrane (GO:0016020)	218	2.45×10^{-3}	BDLTU, C, DKT, E, J, P, Q, S, V, Z, Unclassified
	Photosystem I (GO:0009522)	95	4.04×10^{-9}	C, P, S, Unclassified
	Chloroplast thylakoid membrane (GO:0009535)	50	2.43×10^{-6}	C, S, Unclassified
	Cytosol (GO:0005829)	48	3.86×10^{-2}	B, E, F, G, H, O, T, Z, Unclassified
	Plasma membrane (GO:0005886)	41	1.28×10^{-4}	P, PQ, Q, T, U, V, Z, Unclassified
	Extracellular region (GO:0005576)	14	7.39×10^{-3}	E, O, Q, Z, Unclassified
	Plastid (GO:0009536)	10	4.00×10^{-3}	E, G, Unclassified
	Ribosome (GO:0005840)	9	5.94×10^{-3}	J, Unclassified
	Photosystem (GO:0009521)	6	6.10×10^{-3}	C
	Thylakoid (GO:0009579)	6	5.60×10^{-3}	S
	Small ribosomal subunit (GO:0015935)	5	1.93×10^{-2}	J, Unclassified
	Photosystem II (GO:0009523)	5	4.35×10^{-9}	C, Unclassified
	Extracellular exosome (GO:0070062)	5	1.34×10^{-4}	E, Unclassified
	Protein-containing complex (GO:0032991)	4	8.74×10^{-3}	Unclassified
	Plastoglobule (GO:0010287)	3	1.23×10^{-2}	S
	Thylakoid membrane (GO:0042651)	3	4.43×10^{-3}	Unclassified
	Extracellular space (GO:0005615)	2	3.91×10^{-3}	Unclassified
	Mitochondrial nucleoid (GO:0042645)	1	3.75×10^{-2}	Unclassified
	Cytosolic ribosome (GO:0022626)	1	3.70×10^{-2}	Unclassified
	Chloroplast envelope (GO:0009941)	1	1.37×10^{-2}	E
Molecular Function	Transmembrane transporter activity (GO:0022857)	46	4.38×10^{-2}	E, P, Unclassified
	ABC-type transporter activity (GO:0140359)	21	3.39×10^{-2}	Q, V, Unclassified
	Translation elongation factor activity (GO:0003746)	15	7.79×10^{-7}	J, Unclassified
	Proton-transporting ATP synthase activity, rotational mechanism (GO:0046933)	9	6.32×10^{-3}	C, Unclassified
	Chlorophyll binding (GO:0016168)	6	2.50×10^{-6}	C
	Hydrolase activity (GO:0016787)	4	1.41×10^{-2}	T, Unclassified
	Formate transmembrane transporter activity (GO:0015499)	2	5.85×10^{-4}	P
	Nucleotide binding (GO:0000166)	1	1.45×10^{-3}	Unclassified

Table 4.4: Identification of unique GO terms from cultures grown in Cd. 24 statistically overexpressed (FDR < 0.05) gene ontology (GO) terms were identified from the list of DEGs using the PANTHER classification system when *E. mutabilis* cultures grown in 100 µM Cd for 14 days were compared to cultures in 100 µM Cd for 21 days. Databases for GO term identification include *Homo sapiens, Arabidopsis thaliana, Chlamydomonas reinhardtii,* and *Synechocystis sp.* in relation to clusters of orthologous genes (COGs) identified using BLASTX.

Ontology	GO Term	Gene Count	Average FDR	COG Classification(s)
Biological Process	Cyclic nucleotide biosynthetic process (GO:0009190)	9	3.68×10^{-3}	C, T
	Photosynthesis, light harvesting (GO:0009765)	3	7.09×10^{-9}	S, Unknown
	Translation (GO:0006412)	2	8.36×10^{-3}	J, Unknown
	Response to light stimulus (GO:0009416)	1	1.91×10^{-8}	LT
Cellular Component	Cytoplasm (GO:0005737)	23	6.98×10^{-4}	C, H, I, J, L, LT, O, Q, S, T, Unknown
	Membrane (GO:0016020)	18	2.45×10^{-3}	DO, EG, I, J, P, Q, S, T, Unknown
	Plasma membrane (GO:0005886)	16	1.28×10^{-4}	C, O, P, PQ, S, T, U, Unknown
	Cytosol (GO:0005829)	12	3.86×10^{-2}	DO, F, G, H, J, O, S, Z, Unknown
	Extracellular region (GO:0005576)	8	7.39×10^{-3}	E, G, I, O, Q, S, Unknown
	Chloroplast (GO:0009507)	6	1.47×10^{-2}	I, O, S, Unknown
	Photosystem I (GO:0009522)	3	4.04×10^{-9}	S, Unknown
	Ribosome (GO:0005840)	2	5.94×10^{-3}	J, Unknown
	Photosystem II (GO:0009523)	2	4.35×10^{-9}	S, Unknown
	Chloroplast thylakoid membrane (GO:0009535)	2	2.43×10^{-6}	S, Unknown
	Plastoglobule (GO:0010287)	2	1.23×10^{-2}	I, S
	Extracellular exosome (GO:0070062)	2	1.34×10^{-4}	C, G
	Extracellular space (GO:0005615)	1	3.91×10^{-3}	O
	Chloroplast envelope (GO:0009941)	1	1.37×10^{-2}	S
	Protein-containing complex (GO:0032991)	1	8.74×10^{-3}	S
Molecular Function	Nucleotide binding (GO:0000166)	3	1.45×10^{-3}	H, LT, Unknown
	Hydrolase activity (GO:0016787)	3	1.41×10^{-2}	F, I, M
	Chlorophyll binding (GO:0016168)	2	2.50×10^{-6}	S, Unknown
	Catalytic activity (GO:0003824)	1	3.97×10^{-3}	I
	Transmembrane transporter activity (GO:0022857)	1	4.38×10^{-2}	P

4.9 SUPPLEMENTARY MATERIAL

Table S4.1: Hormones, listed in order of retention time (minutes) included in the UHPLC-MS/MS method using PRM mode. 29 CKs (freebase, riboside, glucoside, methylated, and aromatic forms) and 8 acidic hormones were analyzed directly while 4 CK nucleotides were analyzed in their dephosphorylated riboside state

Group	Analyte	Abbreviation	Labelled Analyte
Freebases	*trans*-Zeatin	*t*Z	*t*Z-d_5
	cis-Zeatin	*c*Z	
	Dihydrozeatin	DZ	DZ-d_3
	Isopentyladenine	iP	iP-d_6
Ribosides	*trans*-Zeatin riboside	*t*ZR	*t*ZR-d_5
	cis-Zeatin riboside	*c*ZR	
	Dihydrozeatin riboside	DZR	DZR-d_3
	Isopentyladenosine	iPR	iPR-d_6
Nucleotides	*trans*-zeatin riboside-5′-monophosphate	*t*ZNT	*t*ZR-d_5
	cis-zeatin riboside-5′-monophosphate	*c*ZNT	
	Dihydrozeatin riboside -5′-monophosphate	DZNT	DZR-d_3
	Isopentyladenosine-5′monophosphate	iPNT	iPR-d_6
Methylthiols	2-Methylthio-*trans*-zeatin	MeSZ	MeSZ-d_5
	2-Methylthio-*trans*-zeatin riboside	MeSZR	MeSZR-d_5
	2-Methylthio-isopentyladenine	MeSiP	MeSiP-d_6
	2-Methylthio-isopentyladenosine	MeSiPR	MeSiPR-d_6
Glucosides	*trans*-zeatin-O-glucoside	*t*ZOG	*t*ZOG-d_5
	cis-zeatin-O-glucoside	*c*ZOG	
	Dihydrozeatin-O-glucoside riboside	DZOG	DZOG-d_7
	trans-zeatin-7-glucoside	*t*Z7G	*t*Z7G-d_5
	cis-zeatin-7-glucoside		
	trans-zeatin-9-glucoside	*t*Z9G	*t*Z9G-d_5
	cis-zeatin-9-glucoside	*c*Z9G	
	Dihydrozeatin-9-glucoside	DZ9G	DZ9G-d_3
	Isopentenyladenine-7-glucoside	iP7G	iP7G-d_6
	Isopentenyladenine-9-glucoside	iP9G	iP7G-d_6
Aromatic CKs	Benzylaminopurine	BA	BA-d_7
	Benzylaminopurine riboside	BAR	BAR-d_7
Acids	Abscisic acid	ABA	ABA-d_6
	Gibberellin 1	GA1	GA1-d_2
	Gibberellin 3	GA3	GA3-d_2
	Gibberellic acid 4	GA4	GA4-d_2
	Gibberellin 7	GA7	GA7-d_2
	Indole-3-acetic acid	IAA	IAA-d_5
	Salicylic acid	SA	SA-d_6
	Jasmonic acid	JA	ABA-d_6

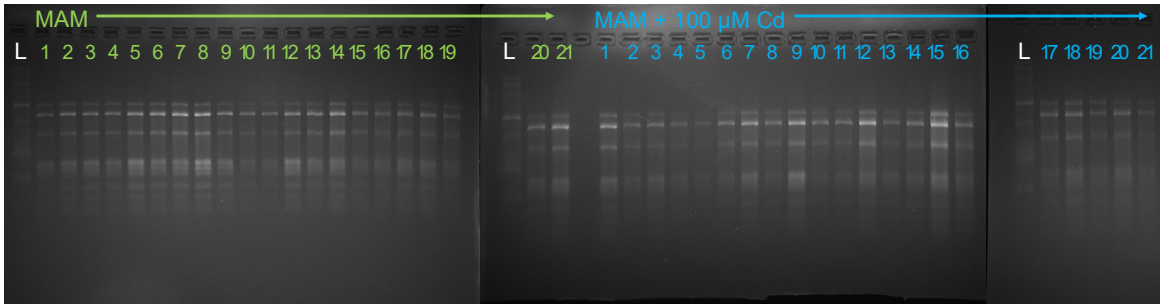

Figure S4.1: Visualization of DNAase-treated RNA samples. Integrity and quality of DNAse-treated RNA was visualized by electrophoresis on a 1.5% BPTE agarose gel after glyoxal denaturation. A single-stranded RNA ladder ("L"; New England BioLabs, Whitby, Canada) was used as a reference. The rRNA of *Euglena* is fragmented, consisting of approximately 14 RNA molecules [1], which accounts for its distinct appearance on the gel. Control (MAM; green lettering) and treatment (MAM + 100 µM Cd; blue lettering) samples are numbered sequentially: samples 1-7 were analyzed after 7-days of growth, samples 8-14 were analyzed after 14-days of growth, and samples 15-21 were analyzed after 21-days of growth.

Table S4.2: Average number of raw and quality-trimmed reads (n = 7) obtained from RNA-sequencing of *E. mutabilis* cultures exposed to 0 µM or 100 µM Cd across three time points. Read counts represent the average per condition after initial sequencing and post-trimming quality control.

Day	Treatment	Number of Raw Reads	Number of Trimmed Reads
7	0 µM Cd	67,720,090	67,238,647
	100 µM Cd	64,913,563	64,400,546
14	0 µM Cd	68,959,057	68,521,184
	100 µM Cd	66,754,179	66,287,454
21	0 µM Cd	61,359,308	60,879,526
	100 µM Cd	61,135,707	60,607,572

Table S4.3: Average number of reads (n = 7) assigned to genes and isoforms in cultures treated with 0 µM or 100 µM Cd across Days 7, 14, and 21. Reads were quantified at both the gene and isoform levels to assess mapping efficiency to the assembly.

Day	Treatment	Reads Assigned to Genes	Reads Assigned to Isoforms
7	0 µM Cd	54,577,857	54,577,686
	100 µM Cd	50,818,499	50,818,525
14	0 µM Cd	56,623,113	56,623,089
	100 µM Cd	51,624,278	51,624,363
21	0 µM Cd	49,228,679	49,228,640
	100 µM Cd	45,873,166	45,873,322

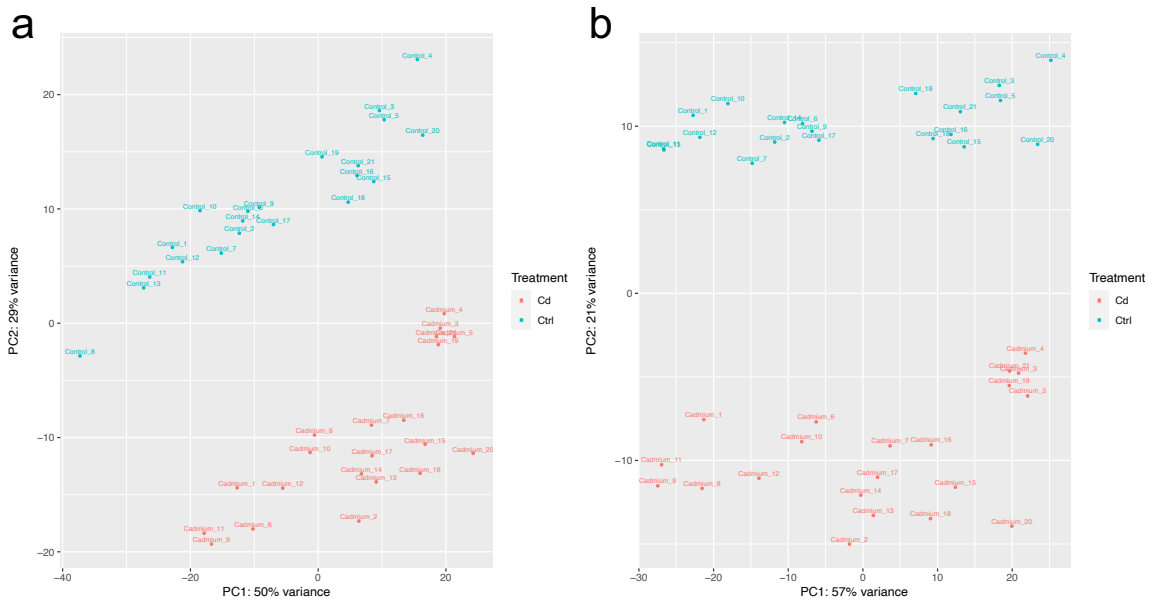

Figure S4.2: Principal component analysis (PCA) of differentially expressed genes in control (0 µM Cd) and Cd-treated (100 µM Cd) cultures. (a) PCA including all samples, with Control 8 appearing as an outlier along PC1. (b) PCA with Control 8 removed, resulting in clearer clustering by treatment group. Variance explained by each principal component is indicated on the axes

Table S4.4: Summary of differentially expressed genes (DEGs) identified by DESeq2 and edgeR across treatment and timepoint comparisons. The number of DEGs with an adjusted p-value (Padj) < 0.05 and those with both Padj < 0.05 and $|\log_2$ fold change$| > 1$ are reported for each method. The final two columns show the overlap in DEGs identified by both DESeq2 and edgeR using the same thresholds. Comparisons include control vs. Cd treatment and intra-treatment changes over time.

Comparison	**DESeq2**		**edgeR**		**Overlap of DESeq2 & edgeR**	
	Padj < 0.05	Padj < 0.05; $\|\log_2FC\| > 1$	Padj < 0.05	Padj < 0.05; $\|\log_2FC\| > 1$	Padj < 0.05	Padj < 0.05; $\|\log_2FC\| > 1$
Control vs Cd Day 7	7,503	1,980	3,578	1,880	2,700	1,092
Control vs Cd Day 14	8,202	2,378	4,170	1,745	2,893	1,016
Control vs Cd Day 21	12,981	2,908	4,087	2,286	3,192	1,472
Control Day 7 vs 14	13,832	5,304	66	65	23	23
Control Day 7 vs 21	10,877	846	122	121	42	42
Control Day 14 vs 21	16,457	3,758	101	101	31	31
Cd Day 7 vs 14	10,540	3,239	143	142	33	32
Cd Day 7 vs 21	15,481	1,016	32	30	6	6
Cd Day 14 vs 21	12,191	1,690	14,056	11,597	5,212	882

Table S4.5: Overlap of differentially expressed genes (DEGs) across control vs Cd comparisons at days 7, 14, and 21. Genes were identified using both DESeq2 and edgeR with padj < 0.05 and |log2 fold change| > 1. The table shows the number of DEGs unique to each day and those shared between two or all three timepoints.

Overlap Group	Number of Genes
Day 7 only	480
Day 14 only	352
Day 21 only	751
Day 7 & 14	64
Day 7 & 21	121
Day 14 & 21	173
All three days	427

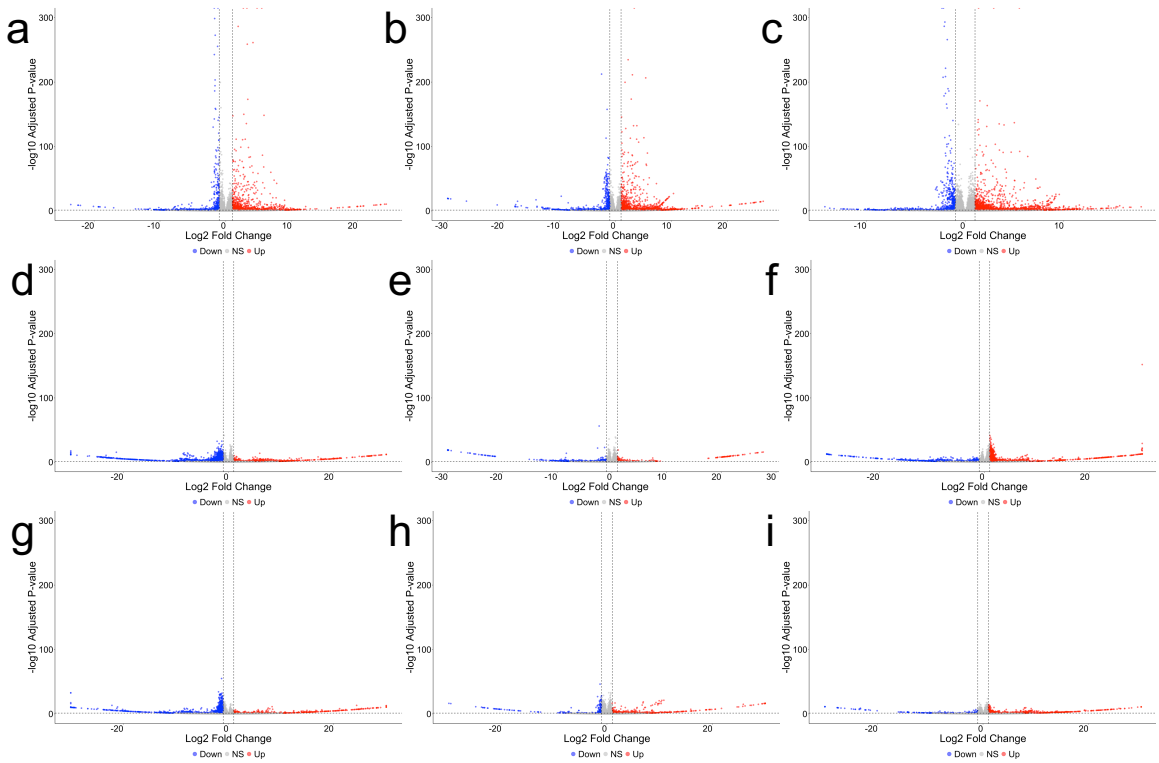

Figure S4.3: Volcano plots depicting differential gene expression across growth conditions, as identified using DESeq2. Comparisons include control vs. Cd-treated cultures after 7 days (a), 14 days (b), and 21 days (c) of growth. Additional comparisons were made within control cultures between days 7 and 14 (d), days 7 and 21 (e), and days 14 and 21 (f). Cd-treated cultures were compared across days 7 and 14 (g), 7 and 21 (h), and 14 and 21 (i). Genes highlighted in red are significantly upregulated (padj < 0.05; $\log_2$ fold change > 1), blue are significantly downregulated (padj < 0.05; $\log_2$ fold change < –1), and grey indicate genes not meeting significance thresholds.

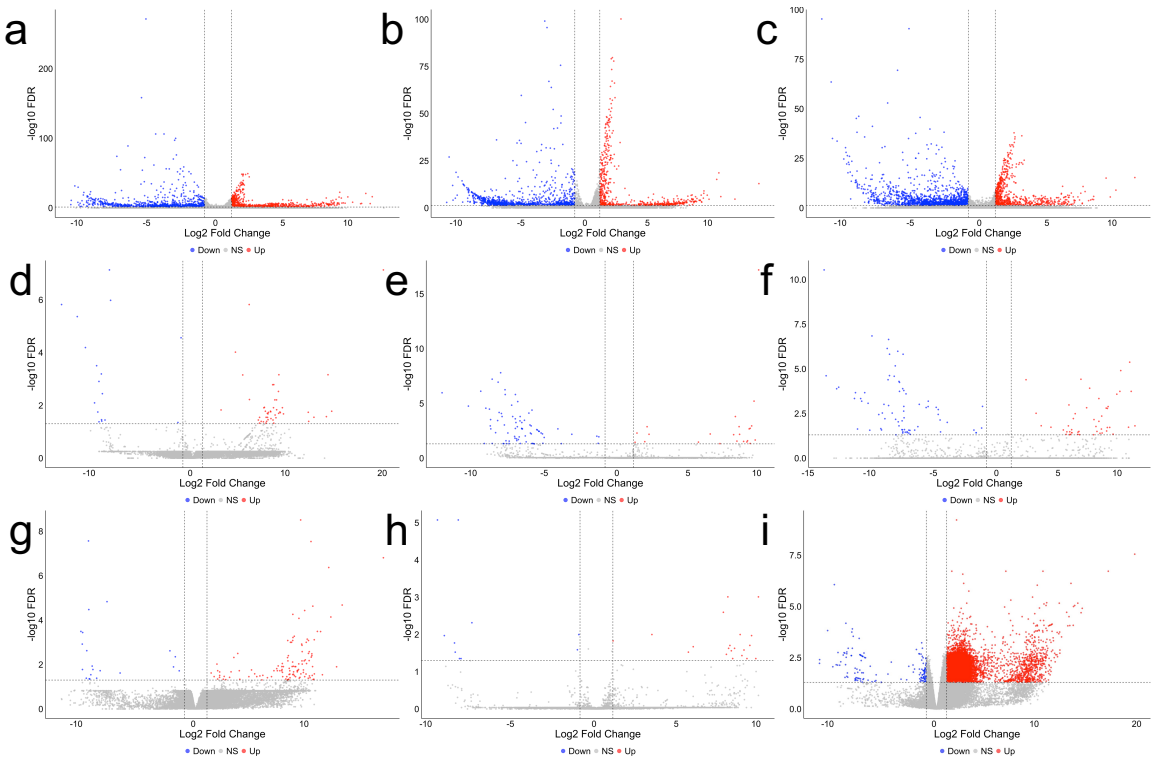

Figure S4.4: Volcano plots depicting differential gene expression across growth conditions, as identified using edgeR. Comparisons include control vs. Cd-treated cultures after 7 days (a), 14 days (b), and 21 days (c) of growth. Additional comparisons were made within control cultures between days 7 and 14 (d), days 7 and 21 (e), and days 14 and 21 (f). Cd-treated cultures were compared across days 7 and 14 (g), 7 and 21 (h), and 14 and 21 (i). Genes highlighted in red are significantly upregulated (padj < 0.05; $\log_2$ fold change > 1), blue are significantly downregulated (padj < 0.05; $\log_2$ fold change < –1), and grey indicate genes not meeting significance thresholds.

Table S4.6: Functional classification of differentially expressed genes (DEGs) identified from comparisons between control and Cd-treated *E. mutabilis* cultures across days 7, 14, and 21. Functional annotation was conducted via BLASTX searches against the NCBI non-redundant protein database, SWISS-Prot, and Ensembl 113 databases for *Homo sapiens*, *Arabidopsis thaliana*, *Chlamydomonas reinhardtii*, and *Synechocystis* sp. The majority of DEGs lacked functional assignment; however, annotated genes were grouped into clusters of orthologous genes (COG). Some genes may be assigned to more than one COG, accounting for the discrepancy between the number of COGs identified and the number of DEGs.

	Day			
COG	**7**	**14**	**21**	**Classification**
.	1017	917	1331	Not assigned
S	16	16	30	Function unknown
P	15	24	27	Inorganic ion transport and metabolism
T	14	9	15	Signal transduction mechanisms
O	8	10	12	Posttranslational modification, protein turnover, chaperones
C	8	11	17	Energy production and conversion
D	4	2	4	Cell cycle control, cell division, chromosome partitioning
L	4	4	3	Replication, recombination, and repair
F	3	2	2	Nucleotide transport and metabolism
K	3	1	3	Transcription
J	3	5	7	Translation, ribosomal structure and biogenesis
B	2	7	6	Chromatin structure and dynamics
U	2	3	2	Intracellular trafficking, secretion, and vesicular transport
G	2	1	1	Carbohydrate transport and metabolism
H	2	3	3	Coenzyme transport and metabolism
Z	1	1	2	Cytoskeleton
W	1	1	1	Extracellular structures
V	1	1	3	Defence mechanisms
E	1	9	9	Amino acid transport and metabolism
Y	1	0	0	Nuclear structure
Q	0	4	10	Secondary metabolites biosynthesis, transport and catabolism
N	0	1	1	Cell motility
I	0	1	1	Lipide transport and metabolism
A	0	0	1	RNA processing and modification
Total	1108	1033	1491	
# of DEGs	1092	1016	1472	

Table S4.7: Functional classification of differentially expressed genes (DEGs) identified from comparisons between cultures of *E. mutabilis* grown in 100 µM Cd over 7-, 14-, and 21-days. Functional annotation was conducted via BLASTX searches against the NCBI non-redundant protein database, SWISS-Prot, and Ensembl 113 databases for *Homo sapiens*, *Arabidopsis thaliana*, *Chlamydomonas reinhardtii*, and *Synechocystis* sp. Some genes may be assigned to more than one COG, accounting for the discrepancy between the number of COGs identified and the number of DEGs.

COG	Comparison			Classification
	Day 7 vs 14	**Day 7 vs 21**	**Day 14 vs 21**	
.	31	6	756	Not assigned
L	1	0	6	Replication, recombination, and repair
S	0	0	33	Function unknown
T	0	0	29	Signal transduction mechanisms
O	0	0	17	Posttranslational modification, protein turnover, chaperones
A	0	0	10	RNA processing and modification
I	0	0	8	Lipide transport and metabolism
P	0	0	8	Inorganic ion transport and metabolism
H	0	0	7	Coenzyme transport and metabolism
Q	0	0	7	Secondary metabolites biosynthesis, transport and catabolism
E	0	0	6	Amino acid transport and metabolism
D	0	0	5	Cell cycle control, cell division, chromosome partitioning
J	0	0	5	Translation, ribosomal structure and biogenesis
G	0	0	5	Carbohydrate transport and metabolism
B	0	0	4	Chromatin structure and dynamics
K	0	0	4	Transcription
C	0	0	4	Energy production and conversion
F	0	0	3	Nucleotide transport and metabolism
M	0	0	3	Cell wall/membrane/envelope biogenesis
Z	0	0	3	Cytoskeleton
U	0	0	3	Intracellular trafficking, secretion, and vesicular transport
N	0	0	2	Cell motility
W	0	0	1	Extracellular structures
V	0	0	1	Defence mechanisms
Y	0	0	1	Nuclear structure
Total	32	6	931	
# of DEGs	32	6	882	

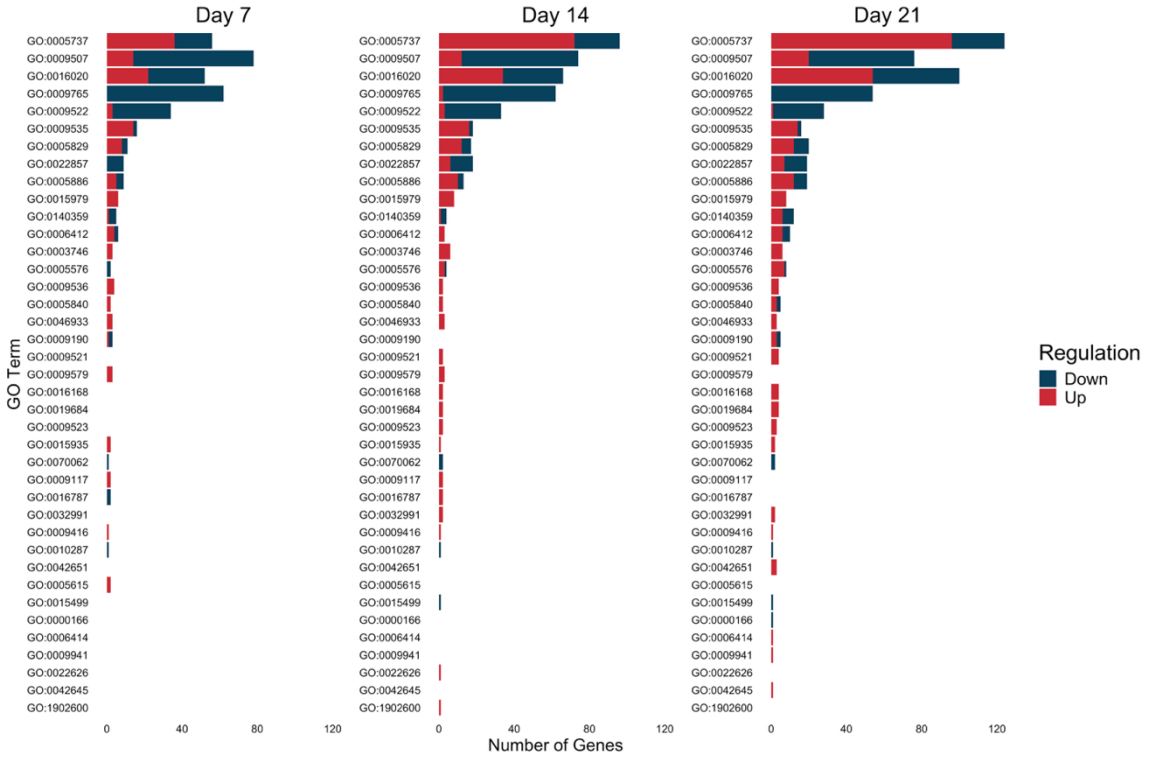

Figure S4.5: Gene Ontology (GO) term enrichment of differentially expressed genes (DEGs) in *E. mutabilis* cultures exposed to Cd. DEGs were annotated using the PANTHER classification system, resulting in 1,377 GO term associations across 369 significant genes (FDR < 0.05) identified over three timepoints: 105 genes on Day 7, 115 on Day 14, and 149 on Day 21. Of these, 211 genes were unique and 158 were shared across multiple timepoints. Bar plots show the number of upregulated (red) and downregulated (blue) DEGs associated with the top GO terms at each timepoint. In total, 39 unique GO terms were represented.

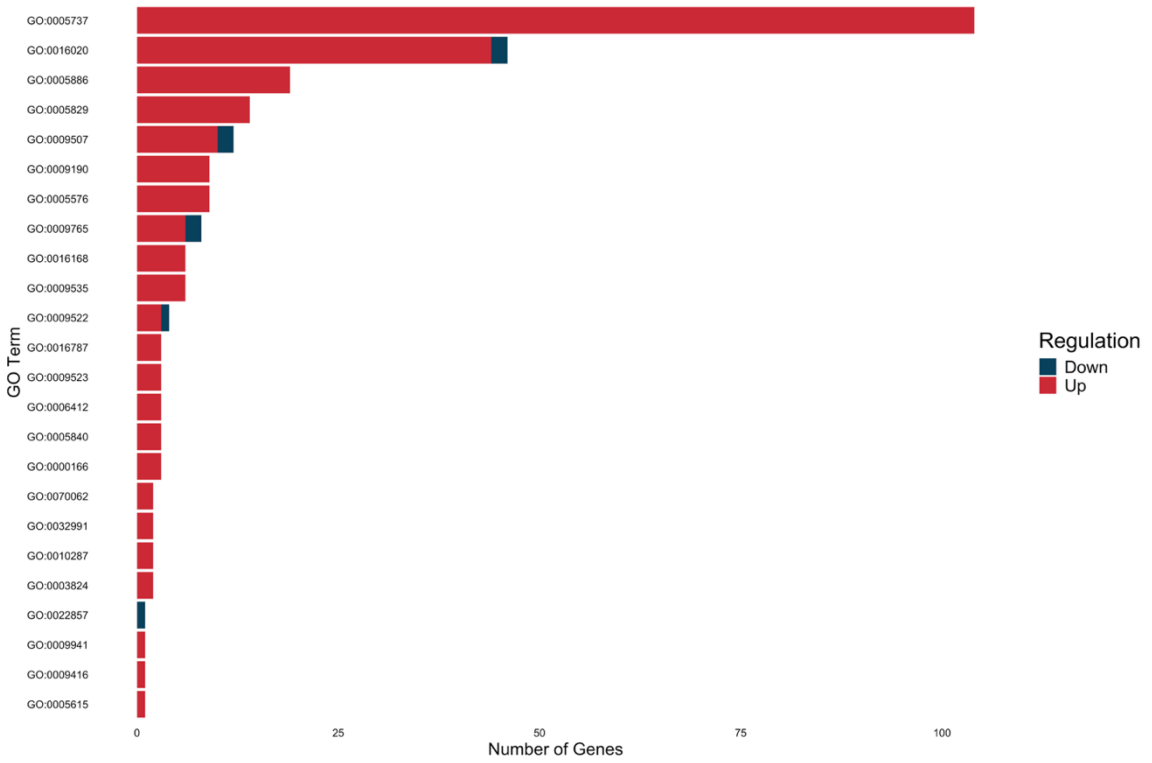

Figure S4.6: Gene Ontology (GO) term enrichment of differentially expressed genes (DEGs) in *E. mutabilis* after prolonged Cd exposure. GO terms associated with DEGs identified in cultures treated with cadmium for 21 days compared to 14 days were annotated using the PANTHER classification system. A total of 124 significant genes (FDR < 0.05) were annotated, of which 78 were unique. These genes were associated with 264 GO term annotations encompassing 24 unique GO categories. Bars indicate the number of upregulated (red) and downregulated (blue) DEGs linked to each GO term.

Table S4.8: Keyword and KEGG classification framework used to identify genes involved in phytohormone biosynthesis. Keywords and KEGG identifiers related to auxin and cytokinin (CK) biosynthetic pathways were compiled and used to filter annotated genes derived from SPROT BLASTX results, transcript-predicted functions, and KEGG orthology assignments. This strategy enabled the targeted identification of transcripts potentially involved in phytohormone production and regulation.

Phytohormone Classification	Keyword	Description
Auxin	IAA	Indole-3-acetic acid
	Auxin	Class of phytohormone
	Tryptophan	Required for IAA biosynthesis
	TAA1	Tryptophan animotransferase converts tryptophan to IPA (indole-3-pyruvate)
	YUC	YUC1-11 converts IPA to IAA
	AMI1	Amidase converts indole-3-acetamide to IAA
	NIT	Nitrilase converts indole-3-acetamide to IAA
Cytokinin	Cytokinin	Class of phytohormone
	Zeatin	Class of cytokinin
	iP	Isopentenyladenine
	cZ	cis-Zeatin
	cZR	cis-Zeatin riboside
	LOG	Cytokinin nucelotidase converts cZNT to cZR to cZ
	IPT	tRNA isopentenyltransferase adds isopentenyl group to tRNA-bound adenosine
	Methyltransferase	Cytokinin methyltransferase performs methylation of cZR to MeSZR
	tRNA isopentenyltransferase	tRNA -IPT gene adds isopentenyl group to tRNA-bound adenosine
	KEGG Classification	
Auxin	K00465	Tryptophan monooxygenase (EC 1.13.12.3)
	K00466	Indoleacetamide hydrolase (EC 3.5.1.4)
	K00128	YUC (Flavin monooxygenase)
	K01814	Aminotransferases (converting Trp to IPA)
	K01749	Aldehyde dehydrogenase (for IAA-aldehyde to IAA)
	K00002	Tryptophan aminotransferase-related proteins (TARs)
Cytokinin	K10742	Adenylate isopentenyltransferase (IPT) (EC 2.5.1.27) produces iPMP
	K19327	Cytokinin riboside 5'-monophosphate phosphoribohydrolase (LOG) (EC 3.1.3.91) activates cytokinins
	K00820	tRNA isopentenyltransferase (EC 2.5.1.8) produces cis-zeatin (cZ)
	K00682	UDP-glucosyltransferase (glucosylation of CKs; stabilizes storage forms like cZNT and iPNT)
	K00591	Cytokinin oxidase/dehydrogenase (CKX) (EC 1.5.99.12) degrades active cytokinins
	K08211	O-methyltransferases may be involved in methylated derivatives like
	K00588	Xanthosine synthase (purine metabolism crossover)

Table S4.9: Differential abundance of taxa in control and Cd-treated cultures. A Mann–Whitney U test was used to identify significantly enriched taxa between treatment groups. The table includes the taxon name, raw *p*-value, log_2 fold change (Log_2 FC), and adjusted *p*-value (Padj). Positive log_2FC values indicate enrichment in Cd-treated cultures, while negative values indicate enrichment in control cultures. Taxa are ordered from most to least statistically significant (Padj < 0.05) from the top of the table down.

Taxon	***p*-value**	**Log_2FC**	**Padj**
Talaromyces amestolkiae	2.68×10^{-7}	10.3	1.23×10^{-5}
Exophiala oligosperma	1.68×10^{-6}	8.57	3.87×10^{-5}
Picea glauca	1.12×10^{-5}	6.13	1.72×10^{-4}
Exophiala xenobiotica	2.96×10^{-5}	6.24	3.40×10^{-4}
Danio rerio	8.82×10^{-4}	0.58	8.11×10^{-3}
Corynebacterium simulans	1.30×10^{-3}	-2.32	1.00×10^{-2}
Rhagoletis zephyria	2.76×10^{-3}	2.60	1.81×10^{-2}
Staphylococcus lugdunensis	6.27×10^{-3}	-1.99	3.61×10^{-2}
Homo sapiens	9.57×10^{-3}	-0.58	4.89×10^{-2}
Deinococcus sp. VB142	3.38×10^{-2}	-2.02	0.16
Malassezia restricta	4.81×10^{-2}	-2.54	0.20
Euglena gracilis	5.27×10^{-2}	-0.09	0.20
Rosa agrestis	5.91×10^{-2}	0.14	0.21
Sus scrofa	8.08×10^{-2}	-2.24	0.27
Cutibacterium modestum	0.14	-1.36	0.42
Boleophthalmus pectinirostris	0.34	0.93	0.42
Timema genevievae	0.19	0.60	0.42
Acidiphilium cryptum	0.31	1.67	0.42
Exophiala dermatitidis	0.34	0.74	0.42
Exophiala mesophila	0.34	0.70	0.42
Talaromyces stipitatus	0.34	0.61	0.42
Mus musculus	0.34	4.70	0.42
Oncorhynchus keta	0.34	-3.22	0.42
Cutibacterium granulosum	0.16	-1.63	0.42
Corynebacterium kefirresidentii	0.34	-1.28	0.42
Staphylococcus epidermidis	0.34	-2.47	0.42
Staphylococcus capitis	0.34	-1.25	0.42
Pseudomonas putida	0.34	-3.80	0.42
Halomonas sp. NyZ770	0.34	-2.80	0.42
Methylorubrum populi	0.34	-1.56	0.42
Bradyrhizobium sp. PSBB068	0.34	-1.58	0.42
Acidovorax temperans	0.34	-3.11	0.42
Herbaspirillum huttiense	0.34	-2.54	0.42
Burkholderia multivorans	0.34	-1.56	0.42
Deinococcus wulumuqiensis	0.34	-1.10	0.42
Rathayibacter festucae	0.34	-3.57	0.42
Triticum aestivum	0.34	-4.47	0.42
Moraxella osloensis	0.40	-0.99	0.48
Astyanax mexicanus	0.52	-0.45	0.61
Prototheca wickerhamii	0.78	0.03	0.88
Heterocapsa triquetra	0.80	0.01	0.88
Acidiphilium multivorum	0.81	0.42	0.88
Cutibacterium acnes	0.84	-0.13	0.90
Euglena longa	0.98	6.36×10^{-3}	1
Corynebacterium sp. SCR221107	1	0.38	1
Mammaliicoccus sciuri	0.97	0.66	1

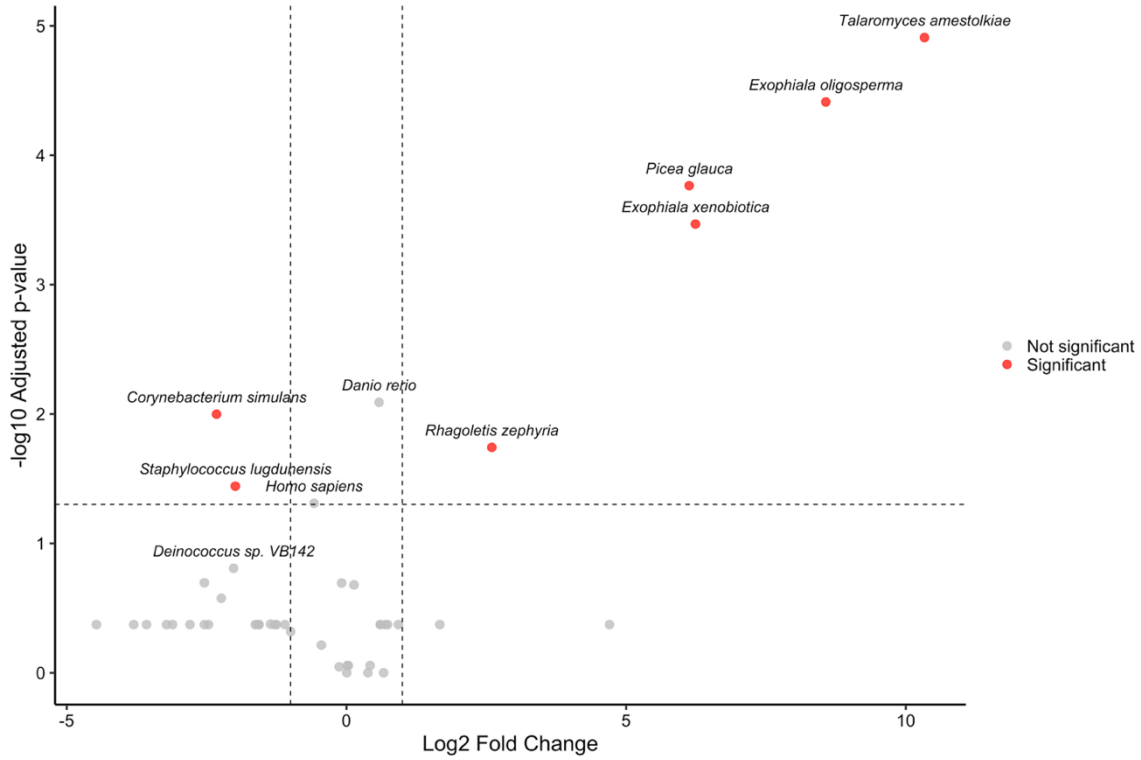

Figure S4.7: Volcano plot showing differential taxonomic abundance between Cd-treated and control samples. Each point represents a species identified in the metagenomic data. The x-axis indicates the $\log_2$ fold change in abundance between conditions, and the y-axis represents the $-\log_{10}$ of the padj. Vertical dashed lines correspond to $\pm$ 1 $\log_2$ fold change, and the horizontal dashed line marks the threshold for statistical significance (padj < 0.05). Species labeled in italics represent the top differentially abundant taxa based on both statistical significance and fold change. Red points indicate significantly different taxa, while gray points are not significant.

4.10 REFERENCES

1. Akcil A, Koldas S. Acid mine drainage (AMD): Causes, treatment and case studies. J Clean Prod. 2006;14(12-13 SPEC. ISS.):1139–45. https://doi.org/10.1016/j.jclepro.2004.09.006.
2. Haghighizadeh A, Rajabi O, Nezarat A, Hajyani Z, Haghmohammadi M, Hedayatikhah S, *et al*. Comprehensive analysis of heavy metal soil contamination in mining environments: Impacts, monitoring techniques, and remediation strategies. Arab J Chem. 2024;17(6):105777. https://doi.org/10.1016/j.arabjc.2024.105777.
3. Willis CE, St. Louis VL, Kirk JL, St. Pierre KA, Dodge C. Tailings ponds of the Athabasca Oil Sands Region, Alberta, Canada, are likely not significant sources of total mercury and methylmercury to nearby ground and surface waters. Sci Total Environ. 2019;647:1604–10. https://doi.org/10.1016/j.scitotenv.2018.08.083.
4. Kossoff D, Dubbin WE, Alfredsson M, Edwards SJ, Macklin MG, Hudson-Edwards KA. Mine tailings dams: Characteristics, failure, environmental impacts, and remediation. Appl Geochem. 2014;51:229–45. https://doi.org/10.1016/j.apgeochem.2014.09.010.
5. Kastury F, Besedin J, Betts AR, Asamoah R, Herde C, Netherway P, *et al*. Arsenic, cadmium, lead, antimony bioaccessibility and relative bioavailability in legacy gold mining waste. J Hazard Mater. 2024;469:133948. https://doi.org/10.1016/j.jhazmat.2024.133948.
6. Taylor MP, Mould SA, Kristensen LJ, Rouillon M. Environmental arsenic, cadmium and lead dust emissions from metal mine operations: Implications for environmental management, monitoring and human health. Environ Res. 2014;135:296–303. https://doi.org/10.1016/j.envres.2014.08.036.
7. Courchesne B, Schindler M, Mykytczuk NCS. relationships between the microbial composition and the geochemistry and mineralogy of the cobalt-bearing legacy mine tailings in northeastern Ontario. Front Microbiol. 2021;12:660190. https://doi.org/10.3389/fmicb.2021.660190.
8. Seervi V, Yadav HL, Srivastav SK, Jamal A. Overview of active and passive systems for treating acid mine drainage. IARJSET. 2017;4(5):131–7. https://doi.org/10.17148/iarjset.2017.4525.
9. Yadav HL, Jamal A. Removal of heavy metals from acid mine drainage: A review. 2015;2(3).
10. Abbasi, M, Khan I, Rehman A, Hayat A, Ur Rehman M, Shah TA, *et al*. Bioremediation of heavy metals contaminated soil by using indigenous metallotolerant bacterial isolates. Appl Ecol Environ Res. 2024;22(2):1623–48. https://doi.org/10.15666/aeer/2202_16231648.
11. Das PK, Rani J, Rawat S, Kumar S. Microalgal co-cultivation for biofuel production and bioremediation: Current status and benefits. BioEnergy Res. 2022;15:1–26. https://doi.org/10.1007/s12155-021-10254-8/Published.
12. Das BK, Roy A, Koschorreck M, Mandal SM, Wendt-Potthoff K, Bhattacharya J. Occurrence and role of algae and fungi in acid mine drainage environment with special reference to metals and sulfate immobilization. Water Res. 2009;43(4):883–94. https://doi.org/10.1016/j.watres.2008.11.046.

13. Qattan SYA. Harnessing bacterial consortia for effective bioremediation: Targeted removal of heavy metals, hydrocarbons, and persistent pollutants. Environ Sci Eur. 2025;37(1):85. https://doi.org/10.1186/s12302-025-01103-y.
14. Pande V, Pandey SC, Sati D, Bhatt P, Samant M. Microbial interventions in bioremediation of heavy metal contaminants in agroecosystem. Front Microbiol. 2022;13. https://doi.org/10.3389/fmicb.2022.824084.
15. Wang J, Chen C. Biosorbents for heavy metals removal and their future. Biotechnol Adv. 2009;27(2):195–226. https://doi.org/10.1016/j.biotechadv.2008.11.002.
16. Gadd GM. Metals, minerals and microbes: geomicrobiology and bioremediation. Microbiology. 2010;156(3):609–43. https://doi.org/10.1099/mic.0.037143-0.
17. Aravind MK, Vignesh NS, Gayathri S, Anjitha N, Athira KM, Gunaseelan S, *et al*. Review on rewiring of microalgal strategies for the heavy metal remediation - A metal specific logistics and tactics. Chemosphere. 2023;313:137310. https://doi.org/10.1016/j.chemosphere.2022.137310.
18. Al-Jabri H, Das P, Khan S, Thaher M, AbdulQuadir M. Treatment of wastewaters by microalgae and the potential applications of the produced biomass—A review. Water. 2021;13(1):27. https://doi.org/10.3390/w13010027.
19. Song H, Ding M-Z, Jia X-Q, Ma Q, Yuan Y-J. Synthetic microbial consortia: From systematic analysis to construction and applications. Chem Soc Rev. 2014;43(20):6954–81. https://doi.org/10.1039/c4cs00114a.
20. Li X, Wu S, Dong Y, Fan H, Bai Z, Zhuang X. Engineering microbial consortia towards bioremediation. water. 2021;13(20):2928. https://doi.org/10.3390/w13202928.
21. Perera IA, Abinandan S, Panneerselvan L, Subashchandrabose SR, Venkateswarlu K, Naidu R, *et al*. Co-culturing of microalgae and bacteria in real wastewaters alters indigenous bacterial communities enhancing effluent bioremediation. Algal Res. 2022;64:102705. https://doi.org/10.1016/j.algal.2022.102705.
22. Wang J, Chen R, Fan L, Cui L, Zhang Y, Cheng J, *et al*. Construction of fungi-microalgae symbiotic system and adsorption study of heavy metal ions. Sep Purif Technol. 2021;268(April):118689. https://doi.org/10.1016/j.seppur.2021.118689.
23. Sahoo H, Senapati D, Thakur IS, Naik UC. Integrated bacteria-algal bioreactor for removal of toxic metals in acid mine drainage from iron ore mines. Bioresour Technol Rep. 2020;11:100422. https://doi.org/10.1016/J.BITEB.2020.100422.
24. Yu Q, Chen J, Ye M, Wei Y, Zhang C, Ge Y. N-acyl homoserine lactones (AHLs) enhanced removal of cadmium and other pollutants by algae-bacteria consortia. J Environ Manage. 2024;366:121792. https://doi.org/10.1016/j.jenvman.2024.121792.
25. Halter D, Goulhen-Chollet F, Gallien S, Casiot C, Hamelin J, Gilard F, *et al*. In situ proteo-metabolomics reveals metabolite secretion by the acid mine drainage bio-indicator, *Euglena mutabilis*. ISME J. 2012;6(7):1391–402. https://doi.org/10.1038/ismej.2011.198.
26. Nakatsu C, Hutchinson TC. Extreme metal and acid tolerance of *Euglena mutabilis* and an associated yeast from Smoking Hills, Northwest Territories, and their apparent mutualism. Microb Ecol. 1988;16(2):213–31. https://doi.org/10.1007/BF02018915.

27. Kaszecki E, Palberg D, Grant M, Griffin S, Dhanjal C, Capperauld M, *et al*. *Euglena mutabilis* exists in a FAB consortium with microbes that enhance cadmium tolerance. Int Microbiol. 2024. https://doi.org/10.1007/s10123-023-00474-7.
28. Ebenezer TE, Zoltner M, Burrell A, Nenarokova A, Novák Vanclová AMG, Prasad B, *et al*. Transcriptome, proteome and draft genome of *Euglena gracilis*. BMC Biol. 2019;17(1):1–23. https://doi.org/10.1186/s12915-019-0626-8.
29. Ebenezer TE, Low RS, O'Neill EC, Huang I, DeSimone A, Farrow SC, *et al*. *Euglena* International Network (EIN): Driving euglenoid biotechnology for the benefit of a challenged world. Biol Open. 2022;11(11):bio059561. https://doi.org/10.1242/bio.059561.
30. Kaszecki E, Kennedy V, Shah M, Maciszewski K, Karnkowska A, Linton E, *et al*. Meeting report: Euglenids in the age of symbiogenesis: Origins, innovations, and prospects, November 8–11, 2021. Protist. 2022;173(4):125894. https://doi.org/10.1016/j.protis.2022.125894.
31. Kennedy V, Kaszecki E, Donaldson ME, Saville BJ. The impact of elevated sulfur and nitrogen levels on cadmium tolerance in *Euglena* species. Sci Rep. 2024;14(1):11734. https://doi.org/10.1038/s41598-024-61964-w.
32. Avilés C, Loza-Tavera H, Terry N, Moreno-Sánchez R. Mercury pretreatment selects an enhanced cadmium-accumulating phenotype in *Euglena gracilis*. Arch Microbiol. 2003;180(1):1–10. https://doi.org/10.1007/s00203-003-0547-2.
33. Rodríguez-Zavala JS, García-García JD, Ortiz-Cruz MA, Moreno-Sánchez R. Molecular mechanisms of resistance to heavy metals in the protist *Euglena gracilis*. J Environ Sci Health Part A. 2007;42(10):1365–78. https://doi.org/10.1080/10934520701480326.
34. He J, Liu C, Du M, Zhou X, Hu Z, Lei A, *et al*. Metabolic responses of a model green microalga *Euglena gracilis* to different environmental stresses. Front Bioeng Biotechnol. 2021;9:662655. https://doi.org/10.3389/fbioe.2021.662655.
35. Zhang K, Wan M, Bai W, Bao Z, Duan X, Wang W, *et al*. A novel heterotrophic cultivation process of *Euglena gracilis* based on NaCl stress significantly increases the paramylon production. Algal Res. 2024;78:103391. https://doi.org/10.1016/j.algal.2024.103391.
36. Kudoyarova G, Arkhipova T, Korshunova T, Bakaeva M, Loginov O, Dodd IC. Phytohormone mediation of interactions between plants and non-symbiotic growth promoting bacteria under edaphic stresses. Front Plant Sci. 2019;10. https://doi.org/10.3389/fpls.2019.01368.
37. Morrison EN, Knowles S, Hayward A, Greg Thorn R, Saville BJ, Emery RJN. Detection of phytohormones in temperate forest fungi predicts consistent abscisic acid production and a common pathway for cytokinin biosynthesis. Mycologia. 2015;107(2). https://doi.org/10.3852/14-157.
38. Nguyen HN, Kisiala AB, Emery RJN. The roles of phytohormones in metal stress regulation in microalgae. J Appl Phycol. 2020;32(6):3817–29. https://doi.org/10.1007/s10811-020-02271-5.
39. Tarakhovskaya ER, Maslov YI, Shishova MF. Phytohormones in algae. Russ J Plant Physiol. 2007;54(2):163–70. https://doi.org/10.1134/S1021443707020021.
40. Noble A, Kisiala A, Galer A, Clysdale D, Emery RJN. *Euglena gracilis* (Euglenophyceae) produces abscisic acid and cytokinins and responds to their

exogenous application singly and in combination with other growth regulators. Eur J Phycol. 2014;49(2):244–54. https://doi.org/10.1080/09670262.2014.911353.
41. Schmidt V, Skokan R, Depaepe T, Kurtović K, Haluška S, Vosolsobě S, *et al*. Phytohormone profiling in an evolutionary framework. Nat Commun. 2024;15(1):3875. https://doi.org/10.1038/s41467-024-47753-z.
42. Olaveson MM, Stokes PM. Reponses of the acidiphilic alga *Euglena* mutablilis (Euglenophyceae) to carbon enrichment at pH 3. J Phycol. 1989;25(3):529–39. https://doi.org/10.1111/j.1529-8817.1989.tb00259.x.
43. Canadian Phycological Culture Centre. Modified acid medium (MAM). University of Waterloo. 2017. https://uwaterloo.ca/canadian-phycological-culture-centre/cultures/culture-media/modified-acid-medium.
44. Metcalfe CD, Sultana T, Martin J, Newman K, Helm P, Kleywegt S, *et al*. Silver near municipal wastewater discharges into western Lake Ontario, Canada. Environ Monit Assess. 2018;190(9):555. https://doi.org/10.1007/s10661-018-6922-x.
45. Kisiala A, Kambhampati S, Stock NL, Aoki M, Emery RJN. Quantification of cytokinins using high-resolution accurate-mass orbitrap mass spectrometry and parallel reaction monitoring (PRM). Anal Chem. 2019;91(23):15049–56. https://doi.org/10.1021/acs.analchem.9b03728.
46. Šimura J, Antoniadi I, Široká J, Tarkowská D, Strnad M, Ljung K, *et al*. Plant hormonomics: Multiple phytohormone profiling by targeted metabolomics. Plant Physiol. 2018;177(2):476–89. https://doi.org/10.1104/pp.18.00293.
47. Spencer DF, Gray MW. Ribosomal RNA genes in *Euglena gracilis* mitochondrial DNA: Fragmented genes in a seemingly fragmented genome. Mol Genet Genomics. 2011;285(1):19–31. https://doi.org/10.1007/s00438-010-0585-9.
48. Babraham Bioinformatics - FastQC A quality control tool for high throughput sequence data. https://www.bioinformatics.babraham.ac.uk/projects/fastqc/ (accessed July 7, 2025).
49. Babraham Bioinformatics - Trim Galore! https://www.bioinformatics.babraham.ac.uk/projects/trim_galore/ (accessed July 7, 2025).
50. Martin M. Cutadapt removes adapter sequences from high-throughput sequencing reads. EMBnet.journal. 2011;17(1):10. https://doi.org/10.14806/ej.17.1.200.
51. Babraham Bioinformatics - FastQ Screen. https://www.bioinformatics.babraham.ac.uk/projects/fastq_screen/ (accessed July 7, 2025).
52. MultiQC | Seqera. https://seqera.io/multiqc/ (accessed July 7, 2025).
53. Grabherr MG, Haas BJ, Yassour M, Levin JZ, Thompson DA, Amit I, *et al*. Trinity: Reconstructing a full-length transcriptome without a genome from RNA-Seq data. Nat Biotechnol. 2011;29(7):644–52. https://doi.org/10.1038/nbt.1883.
54. Langmead B, Salzberg SL. Fast gapped-read alignment with Bowtie 2. Nat Methods. 2012;9(4):357–9. https://doi.org/10.1038/nmeth.1923.
55. Li B, Dewey CN. RSEM: Accurate transcript quantification from RNA-Seq data with or without a reference genome. BMC Bioinformatics. 2011;12(1):323. https://doi.org/10.1186/1471-2105-12-323.
56. Michael Love SA. DESeq2. 2017.
57. Yunshun Chen <Yuchen@Wehi. Edu.Au> ALEA. edgeR. 2017.

58. R: The R Project for Statistical Computing. https://www.r-project.org/ (accessed July 7, 2025).
59. Jeffrey T. Leek <Jtleek@Gmail. Com> WEJ*E.* sva. 2017.
60. Carbon S, Mungall C. Gene Ontology Data Archive. 2025.
61. Lu J, Rincon N, Wood DE, Breitwieser FP, Pockrandt C, Langmead B, *et al*. Metagenome analysis using the Kraken software suite. Nat Protoc. 2022;17(12):2815–39. https://doi.org/10.1038/s41596-022-00738-y.
62. Lu J, Breitwieser FP, Thielen P, Salzberg SL. Bracken: estimating species abundance in metagenomics data. PeerJ Comput Sci. 2017;3:e104. https://doi.org/10.7717/peerj-cs.104.
63. Mendoza Cozatl D, Devars S, Loza-Tavera H, Moreno-Sanchez R. Cadmium accumulation in the chloroplast of *Euglena gracilis*. Physiol Plant. 2002;115:276–83. https://doi.org/10.1034/j.1399-3054.2002.1150214.x.
64. Mendoza-Cózatl DG, Moreno-Sánchez R. Cd^{2+} transport and storage in the chloroplast of *Euglena gracilis*. Biochim Biophys Acta BBA - Bioenerg. 2005;1706(1–2):88–97. https://doi.org/10.1016/j.bbabio.2004.09.010.
65. Nagel K, Adelmeier U, Voigt J. Subcellular distribution of cadmium in the unicellular green alga *Chlamydomonas reinhardtii*. J Plant Physiol. 1996;149(1–2):86–90. https://doi.org/10.1016/S0176-1617(96)80178-7.
66. Perales-Vela HV, Peña-Castro JM, Cañizares-Villanueva RO. Heavy metal detoxification in eukaryotic microalgae. Chemosphere. 2006;64(1):1–10. https://doi.org/10.1016/j.chemosphere.2005.11.024.
67. Duque-Granda D, Montoya-Vallejo C, Botero-Botero LR. Cadmium (Cd) tolerance evaluation of three strains of microalgae of the genus *Ankistrodesmus*, *Chlorella* and *Scenedesmus*. Rev Fac Ing Univ Antioquia. 2019;(92):88–95. https://doi.org/10.17533/udea.redin.20190523.
68. Suresh Kumar K, Dahms H-U, Won E-J, Lee J-S, Shin K-H. Microalgae – A promising tool for heavy metal remediation. Ecotoxicol Environ Saf. 2015;113:329–52. https://doi.org/10.1016/j.ecoenv.2014.12.019.
69. Monteiro C, Castro P, Malcata F. Cadmium removal by two strains of *Desmodesmus pleiomorphus* cells. Water Air Soil Pollut. 2009;208:17–27. https://doi.org/10.1007/s11270-009-0146-1.
70. Bernard E, Guéguen C. Molecular changes in phenolic compounds in *Euglena gracilis* cells grown under metal stress. Front Plant Sci. 2023;14:1099375. https://doi.org/10.3389/fpls.2023.1099375.
71. Devars S, Hernández R, Moreno-Sánchez R. Enhanced heavy metal tolerance in two strains of photosynthetic *Euglena gracilis* by preexposure to mercury or cadmium. Arch Environ Contam Toxicol. 1998;34(2):128–35. https://doi.org/10.1007/s002449900296.
72. Liu S, Jiang M, Wu J, Li X, Zhu J. Mechanism of biological transport and transformation of copper, cadmium, and zinc in water by *Chlorella*. Water. 2024;16(13):1906. https://doi.org/10.3390/w16131906.
73. Xu P, Tu X, An Z, Mi W, Wan D, Bi Y, *et al*. Cadmium-induced physiological responses, biosorption and bioaccumulation in *Scenedesmus obliquus*. Toxics. 2024;12(4):262. https://doi.org/10.3390/toxics12040262.

74. Wu Y, Guo Z, Zhang W, Tan Q, Zhang L, Ge X, *et al*. Quantitative relationship between cadmium uptake and the kinetics of phytochelatin induction by cadmium in a marine diatom. Sci Rep. 2016;6(1):35935. https://doi.org/10.1038/srep35935.
75. Jiang HM, Yang JC, Zhang JF. Effects of external phosphorus on the cell ultrastructure and the chlorophyll content of maize under cadmium and zinc stress. Environ Pollut. 2007;147(3):750–6. https://doi.org/10.1016/j.envpol.2006.09.006.
76. Samadani M, Perreault F, Oukarroum A, Dewez D. Effect of cadmium accumulation on green algae *Chlamydomonas reinhardtii* and acid-tolerant *Chlamydomonas* CPCC 121. Chemosphere. 2018;191:174–82. https://doi.org/10.1016/j.chemosphere.2017.10.017.
77. Khatiwada B, Hasan MT, Sun A, Kamath KS, Mirzaei M, Sunna A, *et al*. Probing the role of the chloroplasts in heavy metal tolerance and accumulation in *Euglena gracilis*. Microorganisms. 2020;8(1). https://doi.org/10.3390/microorganisms8010115.
78. Rocchetta I, Mazzuca M, Conforti V, Balzaretti V, Molina M del CR de. Chromium induced stress conditions in heterotrophic and auxotrophic strains of *Euglena gracilis*. Ecotoxicol Environ Saf. 2012;84:147–54. https://doi.org/10.1016/j.ecoenv.2012.07.020.
79. Rocchetta I, Ruiz LB, Rios De Molina MC, Conforti V. Chromium toxicity to *Euglena gracilis* strains depending on the physiocochemical properties of the culture medium. Bull Environ Contam Toxicol. 2006;76(3):512–21. https://doi.org/10.1007/s00128-006-0950-x.
80. Kanna SD, Domonkos I, Kóbori TO, Dergez Á, Böde K, Nagyapáti S, *et al*. Salt stress induces paramylon accumulation and fine-tuning of the macro-organization of thylakoid membranes in *Euglena gracilis* cells. Front Plant Sci. 2021;12. https://doi.org/10.3389/fpls.2021.725699.
81. Grimm P, Risse JM, Cholewa D, Müller JM, Beshay U, Friehs K, *et al*. Applicability of *Euglena gracilis* for biorefineries demonstrated by the production of α-tocopherol and paramylon followed by anaerobic digestion. J Biotechnol. 2015;215:72–9. https://doi.org/10.1016/j.jbiotec.2015.04.004.
82. Inui H, Ishikawa T, Tamoi M. Wax ester fermentation and its application for biofuel production. In: Schwartzbach SD, Shigeoka S, editors. *Euglena*: Biochemistry, Cell and Molecular Biology. Cham: Springer International Publishing; 2017. p. 269–83.
83. Lu J, Ma Y, Xing G, Li W, Kong X, Li J, *et al*. Revelation of microalgae's lipid production and resistance mechanism to ultra-high Cd stress by integrated transcriptome and physiochemical analyses. Environ Pollut. 2019;250:186–95. https://doi.org/10.1016/j.envpol.2019.04.018.
84. Beauvais-Flück R, Slaveykova VI, Cosio C. Transcriptomic and physiological responses of the green microalga *Chlamydomonas reinhardtii* during short-term exposure to subnanomolar methylmercury concentrations. Environ Sci Technol. 2016;50(13):7126–34. https://doi.org/10.1021/acs.est.6b00403.
85. Tripathi S, Poluri KM. Heavy metal detoxification mechanisms by microalgae: Insights from transcriptomics analysis. Environ Pollut. 2021;285:117443. https://doi.org/10.1016/j.envpol.2021.117443.
86. Thiriet-Rupert S, Gain G, Jadoul A, Vigneron A, Bosman B, Carnol M, *et al*. Long-term acclimation to cadmium exposure reveals extensive phenotypic plasticity in

Chlamydomonas. Plant Physiol. 2021;187(3):1653–78. https://doi.org/10.1093/plphys/kiab375.
87. Johnson DB, Bridge TAM. Reduction of ferric iron by acidophilic heterotrophic bacteria: evidence for constitutive and inducible enzyme systems in *Acidiphilium* spp. J Appl Microbiol. 2002;92(2):315–21. https://doi.org/10.1046/j.1365-2672.2002.01535.x.
88. Li L, Liu Z, Zhang M, Meng D, Liu X, Wang P, *et al*. Insights into the metabolism and evolution of the genus *Acidiphilium*, a typical acidophile in acid mine drainage. mSystems. 2020;5(6):10.1128/msystems.00867-20. https://doi.org/10.1128/msystems.00867-20.
89. Johnson DB, Hedrich S, Pakostova *E.* Indirect redox transformations of iron, copper, and chromium catalyzed by extremely acidophilic bacteria. Front Microbiol. 2017;8. https://doi.org/10.3389/fmicb.2017.00211.
90. Xiao Y, Chen R, Chen L, Yang B, Jiang L, Fang J. Endophytic fungus *Talaromyces* sp. mr1 promotes the growth and cadmium uptake of *Arabidopsis thaliana* l. under cadmium stress. Curr Microbiol. 2023;80(11):346. https://doi.org/10.1007/s00284-023-03453-3.
91. Henagamage AP, Peries CM, Seneviratne G. Fungal-bacterial biofilm mediated heavy metal rhizo-remediation. World J Microbiol Biotechnol. 2022;38(5):1–13. https://doi.org/10.1007/s11274-022-03267-8.
92. Swaminathan S, Bock RM. Isolation and identification of cytokinins from *Euglena gracilis* transfer ribonucleic acid. Biochemistry. 1977;16(7):1355–60. https://doi.org/10.1021/bi00626a018.
93. Hrtyan M, Šliková E, Hejátko J, Růžička K. RNA processing in auxin and cytokinin pathways. J Exp Bot. 2015;66(16):4897–912. https://doi.org/10.1093/jxb/erv189.
94. Kuroha T, Tokunaga H, Kojima M, Ueda N, Ishida T, Nagawa S, *et al*. Functional analyses of LONELY GUY cytokinin-activating enzymes reveal the importance of the direct activation pathway in *Arabidopsis*. Plant Cell. 2009;21(10):3152–69. https://doi.org/10.1105/tpc.109.068676.
95. Gibb M, Kisiala AB, Morrison EN, Emery RJN. The origins and roles of methylthiolated cytokinins: Evidence from among life kingdoms. Front Cell Dev Biol. 2020;8:605672. https://doi.org/10.3389/fcell.2020.605672.
96. Shi B, Li K, Xu R, Zhang F, Yu Z, Ding Z, *et al*. Methionine-mediated trade-off between plant growth and salt tolerance. Plant Physiol. 2025;197. https://doi.org/10.1093/plphys/kiaf074.
97. Rathore RS, Mishra M, Pareek A, Singla-Pareek SL. Concurrent improvement of rice grain yield and abiotic stress tolerance by overexpression of cytokinin activating enzyme LONELY GUY (OsLOG). Plant Physiol Biochem. 2024;211:108635. https://doi.org/10.1016/j.plaphy.2024.108635.
98. Ma C, Wang Y, Gu D, Nan J, Chen S, Li H. Overexpression of s-adenosyl-l-methionine synthetase 2 from sugar beet m14 increased *Arabidopsis* tolerance to salt and oxidative stress. Int J Mol Sci. 2017;18(4):847. https://doi.org/10.3390/ijms18040847.
99. Wang R, Liu L, Kong Z, Li S, Lu L, Nosheen kabir, *et al*. Identification of *GhLOG* gene family revealed that *GhLOG3* is involved in regulating salinity tolerance in cotton (*Gossypium hirsutum* L.). Plant Physiol Biochem. 2021;166:328–40. https://doi.org/10.1016/j.plaphy.2021.06.011.

100. Won C, Shen X, Mashiguchi K, Zheng Z, Dai X, Cheng Y, *et al*. Conversion of tryptophan to indole-3-acetic acid by tryptophan aminotransferases of *Arabidopsis* and yuccas in *Arabidopsis*. Proc Natl Acad Sci. 2011;108(45):18518–23. https://doi.org/10.1073/pnas.1108436108.
101. Peer WA, Cheng Y, Murphy AS. Evidence of oxidative attenuation of auxin signalling. J Exp Bot. 2013;64(9):2629–39. https://doi.org/10.1093/jxb/ert152.
102. Chaoui A, El Ferjani *E.* Effects of cadmium and copper on antioxidant capacities, lignification and auxin degradation in leaves of pea (*Pisum sativum* L.) seedlings. C R Biol. 2005;328(1):23–31. https://doi.org/10.1016/j.crvi.2004.10.001.
103. Piotrowska-Niczyporuk A, Bajguz A, Kotowska U, Zambrzycka-Szelewa E, Sienkiewicz A. Auxins and cytokinins regulate phytohormone homeostasis and thiol-mediated detoxification in the green alga *Acutodesmus obliquus* exposed to lead stress. Sci Rep. 2020;10(1):10193. https://doi.org/10.1038/s41598-020-67085-4.
104. Kim JY, Oh J-J, Jeon MS, Kim G-H, Choi Y-*E.* Improvement of *Euglena gracilis* paramylon production through a cocultivation strategy with the indole-3-acetic acid-producing bacterium *Vibrio natriegens*. Appl Environ Microbiol. 2019;85(19):e01548-19. https://doi.org/10.1128/AEM.01548-19.
105. Guerra Sierra BE, Arteaga-Figueroa LA, Sierra-Pelaéz S, Alvarez JC. *Talaromyces santanderensis*: A new cadmium-tolerant fungus from cacao soils in Colombia. J Fungi. 2022;8(10):1042. https://doi.org/10.3390/jof8101042.
106. Nam I-H, Murugesan K, Ryu J, Kim JH. Arsenic (As) removal using *Talaromyces* sp. km-31 isolated from as-contaminated mine soil. Minerals. 2019;9(10):568. https://doi.org/10.3390/min9100568.
107. Priyanka, Dwivedi SK. Hexavalent chromium (Cr^{+6}) detoxification potential and stress response of fungus *Talaromyces pinophillus* isolated from tannery wastewater. Environ Adv. 2023;13:100417. https://doi.org/10.1016/j.envadv.2023.100417.
108. Abbas A, Ali S, Mubeen M, Hussain A, Gutumsary KA, Hussain B, *et al*. *Talaromyces* spp. are promising biocontrol agents for sustainable agriculture. microbial biocontrol techniques. Springer, Singapore; 2024. p. 245–80.
109. Hussain I, Irshad M, Hussain A, Qadir M, Mehmood A, Urrehman M, *et al*. Enhancing phosphorus uptake and mitigating lead stress in maize using the rhizospheric fungus *Talaromyces purpureogenus* PH7. CLEAN – Soil Air Water. 2025;53(2):e70006. https://doi.org/10.1002/clen.70006.
110. Pastirčáková K, Baková K, Adamčíková K, Barta M, Lalík M, Pavlík M, *et al*. Fungi associated with ambrosia beetle *Xylosandrus germanus* in Slovakia. Biologia (Bratisl). 2024;79(8):2387–400. https://doi.org/10.1007/s11756-024-01712-7.
111. Nicoletti R, Bellavita R, Falanga A. The outstanding chemodiversity of marine-derived *Talaromyces*. Biomolecules. 2023;13(7):1021. https://doi.org/10.3390/biom13071021.
112. Ajeesh Krishna TP, Maharajan T, Victor Roch G, Ignacimuthu S, Antony Ceasar S. structure, function, regulation and phylogenetic relationship of ZIP family transporters of plants. Front Plant Sci. 2020;11. https://doi.org/10.3389/fpls.2020.00662.
113. Ivanov R, Bauer P. Sequence and coexpression analysis of iron-regulated ZIP transporter genes reveals crossing points between iron acquisition strategies in green

algae and land plants. Plant Soil. 2017;418(1/2):61–73. http://doi.org/10.1007/s11104-016-3128-2.
114. Liu XS, Feng SJ, Zhang BQ, Wang MQ, Cao HW, Rono JK, *et al*. OsZIP1 functions as a metal efflux transporter limiting excess zinc, copper and cadmium accumulation in rice. BMC Plant Biol. 2019;19(1):283. https://doi.org/10.1186/s12870-019-1899-3.
115. Tian S, Liang S, Qiao K, Wang F, Zhang Y, Chai T. Co-expression of multiple heavy metal transporters changes the translocation, accumulation, and potential oxidative stress of Cd and Zn in rice (*Oryza sativa*). J Hazard Mater. 2019;380:120853. https://doi.org/10.1016/j.jhazmat.2019.120853.
116. Zhang H, Zhao S, Li D, Xu X, Li C. Genome-wide analysis of the ZRT, IRT-Like Protein (ZIP) family and their responses to metal stress in *Populus trichocarpa*. Plant Mol Biol Report. 2017;35(5):534–49. https://doi.org/10.1007/s11105-017-1042-2.
117. Haney C, Grass G, Franke S, Rensing C. New developments in the understanding of the cation diffusion facilitator family. J Ind Microbiol Biotechnol. 2005;32:215–26. https://doi.org/10.1007/s10295-005-0224-3.
118. Montanini B, Blaudez D, Jeandroz S, Sanders D, Chalot M. Phylogenetic and functional analysis of the Cation Diffusion Facilitator (CDF) family: Improved signature and prediction of substrate specificity. BMC Genomics. 2007;8:107. https://doi.org/10.1186/1471-2164-8-107.
119. Pfeiffer T, Ivna Š, Špoljarić Maronić D, Maksimovic I. Regulation of photosynthesis in algae under metal stress. In: Singh VP, Sungh S, authors. Environment and Photosynthesis: A Future Prospect. Stadium Press; 2017. p. 261-86.
120. Ibuot A, Dean AP, McIntosh OA, Pittman JK. Metal bioremediation by *CrMTP4* over-expressing *Chlamydomonas reinhardtii* in comparison to natural wastewater-tolerant microalgae strains. Algal Res. 2017;24:89–96. https://doi.org/10.1016/j.algal.2017.03.002.
121. Lennicke C, Cochemé HM. Redox metabolism: ROS as specific molecular regulators of cell signaling and function. Mol Cell. 2021;81(18):3691–707. https://doi.org/10.1016/j.molcel.2021.08.018.
122. Lynch JP. Root phenes for enhanced soil exploration and phosphorus acquisition: Tools for future crops. Plant Physiol. 2011;156(3):1041–9. https://doi.org/10.1104/pp.111.175414.
123. Kerdsomboon K, Techo T, Limcharoensuk T, Tatip S, Auesukaree C. Low phosphate mitigates cadmium-induced oxidative stress in *Saccharomyces cerevisiae* by enhancing endogenous antioxidant defence system. Environ Microbiol. 2022;24(2):707–20. https://doi.org/10.1111/1462-2920.15875.
124. Macaskie LE, Dean ACR, Cheetham AK, Jakeman RJB, Skarnulis AJ. Cadmium accumulation by a *Citrobacter* sp.: The chemical nature of the accumulated metal precipitate and its location on the bacterial cells. Microbiology. 1987;133(3):539–44. https://doi.org/10.1099/00221287-133-3-539.
125. Sianoudis J, Küsel AC, Mayer A, Grimme LH, Leibfritz D. Distribution of polyphosphates in cell-compartments of *Chlorella fusca* as measured by ^{31}P-NMR-spectroscopy. Arch Microbiol. 1986;144(1):48–54. https://doi.org/10.1007/BF00454955.
126. Nowicka B. Heavy metal–induced stress in eukaryotic algae—Mechanisms of heavy metal toxicity and tolerance with particular emphasis on oxidative stress in exposed

cells and the role of antioxidant response. Environ Sci Pollut Res. 2022;29:1–52. https://doi.org/10.1007/s11356-021-18419-w.
127. Singh S, Parihar P, Singh R, Singh VP, Prasad SM. Heavy metal tolerance in plants: Role of transcriptomics, proteomics, metabolomics, and ionomics. Front Plant Sci. 2016;6:1143. https://doi.org/10.3389/fpls.2015.01143.
128. Semane B, Dupae J, Cuypers A, Noben J-P, Tuomainen M, Tervahauta A, *et al*. Leaf proteome responses of *Arabidopsis thaliana* exposed to mild cadmium stress. J Plant Physiol. 2010;167(4):247–54. https://doi.org/10.1016/j.jplph.2009.09.015.
129. Olsson S, Puente-Sánchez F, Gomez M, Aguilera A. Transcriptional response to copper excess and identification of genes involved in heavy metal tolerance in the extremophilic microalga *Chlamydomonas acidophila*. Extrem Life Extreme Cond. 2015;19. https://doi.org/10.1007/s00792-015-0746-1.
130. Küpper H, Küpper F, Spiller M. Environmental relevance of heavy metal-substituted chlorophylls using the example of water plants. J Exp Bot. 1996;47(2):259–66. https://doi.org/10.1093/jxb/47.2.259.
131. Aguilera A, Amils R. Tolerance to cadmium in *Chlamydomonas* sp. (Chlorophyta) strains isolated from an extreme acidic environment, the Tinto River (SW, Spain). Aquat Toxicol. 2005;75(4):316–29. https://doi.org/10.1016/j.aquatox.2005.09.002.
132. Dalal VK, Tripathy BC. Water-stress induced downsizing of light-harvesting antenna complex protects developing rice seedlings from photo-oxidative damage. Sci Rep. 2018;8(1):5955. https://doi.org/10.1038/s41598-017-14419-4.
133. Negi S, Perrine Z, Friedland N, Kumar A, Tokutsu R, Minagawa J, *et al*. Light regulation of light-harvesting antenna size substantially enhances photosynthetic efficiency and biomass yield in green algae. Plant J. 2020;103(2):584–603. https://doi.org/10.1111/tpj.14751.
134. Kanna SD, Domonkos I, Kóbori TO, Dergez Á, Böde K, Nagyapáti S, *et al*. Salt stress induces paramylon accumulation and fine-tuning of the macro-organization of thylakoid membranes in *Euglena gracilis* cells. Front Plant Sci. 2021;12:725699. https://doi.org/10.3389/fpls.2021.725699.
135. Crosatti C, Rizza F, Badeck FW, Mazzucotelli E, Cattivelli L. Harden the chloroplast to protect the plant. Physiol Plant. 2013;147(1):55–63. https://doi.org/10.1111/j.1399-3054.2012.01689.x.
136. Popov VN, Astakhova NV. Ultrastructural changes in chloroplasts of *Cucumis sativus* l. and *Secale cereale* l. during low-temperature hardening. Russ J Plant Physiol. 2021;68(4):678–87. https://doi.org/10.1134/S1021443721040130.
137. Gupta KJ, Igamberdiev AU. Reactive nitrogen species in mitochondria and their implications in plant energy status and hypoxic stress tolerance. Front Plant Sci. 2016;7. https://doi.org/10.3389/fpls.2016.00369.
138. Farnese FS, Menezes-Silva PE, Gusman GS, Oliveira JA. When bad guys become good ones: The key role of reactive oxygen species and nitric oxide in the plant responses to abiotic stress. Front Plant Sci. 2016;7. https://doi.org/10.3389/fpls.2016.00471.
139. Jiang J, Li X, Yang K, Wang W, Cao X, Li C. Photosynthetic cultivation of *Chlamydomonas reinhardtii* with formate as a novel carbon source to the protein production. Chem Eng J. 2024;493:152518. https://doi.org/10.1016/j.cej.2024.152518.

4.11 SUPPLEMENTARY REFERENCES

1. Spencer DF, Gray MW. Ribosomal RNA genes in *Euglena gracilis* mitochondrial DNA: fragmented genes in a seemingly fragmented genome. Mol Genet Genomics. 2011;285(1):19–31. https://doi.org/10.1007/s00438-010-0585-9.

CHAPTER 5

5.1 PREFACE

Title: General Discussion

Author: Emma Kaszecki

CHAPTER 5

5.2 GENERAL CONCLUSIONS

Criticism of bioremediation as a viable alternative to chemical or engineering-based restoration strategies often stems from perceptions of inefficiency and unpredictability. Traditional chemical amendments offer immediate, quantifiable outcomes: pH can be neutralized within hours, metals precipitated in days [1]. In contrast, bioremediation strategies are viewed as slow, contingent, and biologically "messy," requiring weeks or months to yield measurable improvements [2]. These perceptions, coupled with the logistical simplicity of deploying chemical neutralizers, impart the impression that bioremediation is impractical for large-scale applications, particularly in environments as extreme as acid mine drainage (AMD) or metal-contaminated tailings ponds. Yet, such a view rests on what may be called the "direct intervention fallacy" – the belief that environmental remediation is most effective when pollutants are addressed in isolation, stripped from their ecological context, and neutralized by force. This approach, while producing rapid chemical transformations, often does so at the expense of ecological resilience, leaving behind depauperate systems vulnerable to relapse once interventions cease [3].

Mine tailings and AMD epitomize such challenges. Their harsh physicochemical regimes – high acidity, elevated metal loads, low organic carbon – not only impose severe stress on native biota but also suppress the ecological processes necessary for long-term recovery. Conventional wisdom would predict such habitats to be barren, yet they are consistently colonized by highly specialized microbial communities. The persistence of these consortia under conditions lethal to most organisms challenges the assumption that

biological activity is fragile in the face of contamination. Instead, it suggests that microbial robustness is not only possible but can be harnessed – if we are willing to broaden our conception of what constitutes a "remediating agent."

In this thesis, *Euglena mutabilis* emerges as a symbol of ecological robustness. Long regarded as merely an indicator species of AMD, *E. mutabilis* is often overlooked as an agent of change in its own right. Yet the work presented here demonstrates that its survival in extreme environments is neither incidental nor solitary. Rather, the alga persists as the nucleus of a fungal–algal–bacterial (FAB) consortium, in which physiological burden is distributed across kingdoms of life, and survival emerges from cooperative rather than individualistic strategies.

In Chapter 2, experimental disruption of the FAB revealed the indispensability of microbial partners: Cd tolerance collapsed when fungal and bacterial associates were suppressed (Figure 2.5), underscoring that tolerance cannot be attributed to *E. mutabilis* alone. Chapter 3 showed that this consortium is not static but reorganizes in response to resource availability. Glucose supplementation triggered dense fungal hyphae, bacterial proliferation, and pronounced flocculation (Figure 3.2; Figure 3.5), enhancing the growth and survival of *E. mutabilis* under Cd stress. Hormone profiling revealed that these structural changes coincided with coordinated shifts in cytokinin (CK), gibberellin, jasmonic acid (JA), and salicylic acid (SA) (Figure 3.6-3.10; Table S3.3-3.10), suggesting that carbon availability not only fuels growth but also modulates a distributed hormonal network spanning multiple partners.

Chapter 4 integrated transcriptomic, hormonal, and ultrastructural analyses to reveal how *E. mutabilis* itself contributes to this tolerance. Under Cd exposure, the alga upregulated transporters involved in metal homeostasis (Appendix I: Days), compartmentalized Cd into chloroplasts (Figure 4.3), and accumulated paramylon granules (Figure 4.3), likely as a metabolic buffer against impaired photosynthesis. Hormonal profiles indicated suppression of growth-promoting auxins and CKs in their bioactive forms (Table 4.2), coupled with accumulation of nucleotide precursors (Table 4.2), consistent with a shift into metabolic dormancy. These cellular and molecular strategies were mirrored by community-level responses, including the enrichment of fungal and bacterial constituents, pointing to a multi-layered adaptation where gene expression, metabolism, and community composition act in concert.

Appendix II further demonstrated that the FAB is more than a survival mechanism; it is also a reservoir of novel chemistry. Molecular networking revealed that *E. mutabilis* consortia unlock biosynthetic pathways that remain silent in monocultures, yielding unique secondary metabolites shaped by nutrient regime and microbial composition (Figure II.2). Some of these compounds were traced to *Acidiphilium* or *Talaromyces* partners, highlighting that natural product discovery is itself an emergent property of the consortium. In this sense, the FAB exemplifies how microbial partnerships not only sustain survival in extreme environments but also generate novel biochemical diversity with potential biotechnological relevance.

Together, these findings illustrate that *E. mutabilis* heavy metal tolerance emerges at multiple scales: through intracellular sequestration and metabolic buffering, through

hormonally coordinated restructuring of the consortium, and through community-level interactions that unlock hidden genetic potential. The FAB is not simply a collection of hardy organisms but an integrated system whose properties cannot be reduced to the sum of its parts.

This challenges conventional paradigms of bioremediation, which have historically privileged individual isolates with desirable traits – "the metal-tolerant fungus" [4] and "the biosorptive bacterium" [5] – and sought to optimize them in isolation. The FAB consortium offers an alternative model, one in which emergent properties arise from interaction: fungal hyphae providing structural scaffolding for algal flocculation, bacterial partners contributing metabolic breadth, and hormonal cross-signaling aligning community-level responses to stress. By definition, emergent properties are lost when systems are dismantled into their parts. In this model, remediation is not a matter of deploying a single organism with an engineered trait, but of fostering conditions under which complex microbial partnerships can enact their collective survival strategies. This multiscale coordination is the hallmark of a consortium that behaves less as an assemblage of species and more as a single adaptive unit – a microbial superorganism.

5.3 *Euglena mutabilis* SUPERORGANISM

Biology has long wrestled with the question of what constitutes an individual. In many cases, the answer seems simple: an entity with clear boundaries, integrated organs, and a single genome. Yet nature repeatedly unsettles this assumption. Ant colonies coordinate foraging, defense, and temperature regulation with the cohesion of a single body [6]. Corals are not solitary animals but composites of polyps, algae, and bacteria, together

forming one of Earth's most productive ecosystems [7]. Lichens, once dismissed as accidents of cohabitation, are now celebrated as true symbiotic organisms in which fungi and algae fuse to create something new [8]. These examples illustrate the principle of the superorganism: an assemblage of individuals whose interactions are so cohesive, and whose division of labor so refined, that the group behaves as if it were a single organism [9]. In such cases, individuality blurs into collective function, and natural selection may act most strongly on the whole rather than its parts.

The evidence presented in this thesis suggests that the FAB consortium anchored by *E. mutabilis* should be understood in the same way. While *E. mutabilis* has long been described as an unusually hardy protist, thriving in acidic and metal polluted environments, its resilience cannot be reduced to individual physiology. Rather, it emerges from the integration of fungal and bacterial partners (Chapter 2). When these partners are suppressed, the system loses its characteristic tolerance to Cd (Chapter 2). When glucose is introduced, the consortium does not merely grow faster but reorganizes structurally and biochemically: fungal hyphae weave *Euglena* cells into dense flocs, bacteria proliferate in concert, and hormones are secreted into the extracellular space with a coordination that resembles a shared physiology (Chapter 3). These patterns are more than association; they are the hallmarks of collective integration.

What distinguishes the FAB from a loose symbiosis is the degree to which its members function as a single adaptive entity. Fungal hyphae provide physical scaffolds that protect the alga and may adsorb metals (Figure 3.5); bacterial associates expand metabolic capacity and possibly contribute novel biosynthetic products (Appendix II); *Euglena* itself

provides carbon through photosynthesis and serves as the physical nucleus of the community (Figure 3.1; Figure 3.5). Regulation is distributed across partners rather than centralized. Hormones traditionally associated with plants, such as *trans*-Zeatin (*t*Z) and gibberellins (GA), are produced by the fungus (Chapter 3), while methylthiolated CKs, JA, and SA originate from the alga (Chapter 3; Table 4.2). This arrangement creates a consortium-wide endocrine system in which no one species alone dictates the response, y*et al*l contribute to a unified outcome. Even the boundaries between species are porous, as transmission electron microscopy revealed bacterial-like bodies within *Euglena* vacuoles (Figure 3.6), suggesting that partners may shift between extracellular collaborators and intracellular residents. The consortium flexibly reorganizes according to environmental conditions, retreating into dormancy under nutrient limitation and expanding into dense mats when glucose is available. In every sense, its behavior reflects that of a self-regulating organism rather than a mere community.

The holobiont concept provides a useful comparison. Holobionts are defined as hosts with their associated microorganisms functioning together as ecological and evolutionary units, as in the case of corals, cows, or humans [9]. By this definition, the FAB can be seen as a holobiont, with *E. mutabilis* as the host and its microbial associates providing accessory functions. Yet the FAB also challenges the hierarchical framing implicit in the holobiont. In many host-microbiome systems, the host remains the central locus of selection, while microbes are treated as appendages. In the FAB, this distinction dissolves. Fungal, algal, and bacterial partners are so tightly interwoven that none can be regarded as accessory; all are indispensable. The consortium is not simply a host with symbionts, but a community in which the identity of the host itself becomes blurred. In this

sense, the FAB exceeds the holobiont model and approaches the definition of a true microbial superorganism, where the unit of survival, adaptation, and perhaps selection is the consortium itself.

Recognizing the FAB as a superorganism reframes both ecological interpretation and applied potential. It shifts attention away from searching for singular "metal-tolerant isolates" or "resistance genes" toward appreciating emergent properties that only exist in the collective. It demonstrates that tolerance to extreme environments can be understood as a product of integration, not independence. Additionally, this suggests that strategies for bioremediation may find their strongest models not in monocultures or engineered strains, but in naturally evolved microbial superorganisms. The division of labor, signaling networks, and structural organization of these natural microbial associations have already been refined by evolution to withstand precisely the conditions of toxicity and stress that challenge human remediation efforts.

5.4 CHALLENGES AND FUTURE DIRECTIONS

While this thesis has established the FAB consortium as a model microbial superorganism, several challenges remain before these insights can be fully translated into ecological theory or applied bioremediation strategies. Chief among them is the difficulty of dissecting causality in such highly integrated systems. The results presented here reveal coordinated shifts in structure, hormone production, and Cd tolerance, but it remains unclear whether specific metabolic exchanges or signaling molecules are necessary and sufficient for these outcomes. Without a fully annotated *E. mutabilis* genome, functional interpretation of transcriptomic data remains restricted, and the precise genetic basis of

hormone biosynthesis, metal transport, and stress signaling cannot yet be mapped with certainty. Similarly, although metagenomic analysis suggests that *Talaromyces* and *Acidiphilium* contribute biosynthetic and regulatory functions, their roles remain inferred rather than proven by direct gene-function assays.

Another challenge lies in the complexity of replicating the FAB's ecological context under laboratory conditions. Cultures maintained in modified acid medium (MAM) provide a simplified environment that cannot capture the fluctuating geochemistry, microbial diversity, and resource limitations of mine tailings and AMD. The FAB consortium likely interacts with a wider network of acidophiles, protists, and fungi *in situ*, raising the possibility that its performance in the field may be shaped by interactions beyond those tested here. Scaling from controlled flasks to field applications will require careful evaluation of how consortium behavior changes in the presence of competing or antagonistic species, fluctuating redox conditions, and the heterogeneity of abandoned tailings sites – current challenges that face bioremediation scale-up [10,11].

The very features that make the FAB consortium a compelling superorganism also create challenges for its study and application. Efforts to dissect partner-specific roles using antibiotic suppression or nutrient perturbation can yield insights, but they risk disrupting the community's collective dynamics and emergent properties. Progress will require reconstructing synthetic FAB consortia under controlled conditions, systematically adding or removing partners while monitoring survival, hormone signaling, and metal handling. For instance, a synthetic consortium combining *Aspergillus fumigatus* with *Synechocystis* sp. PCC6803 under Cd stress enhanced Cd removal with up to 98.9% efficiency, largely

through stress-induced changes in extracellular polymeric substances [12]. In this case, *A. fumigatus* and *Synechocystis* were selected for their complementary traits, where the fungus offers structural stability and metal-binding potential while the cyanobacterium offers photosynthetic and tolerance to heavy metals, rather than on any prior guarantee that the two would function optimally in a consortium. Such "trial-and-error" approaches underscore both the promise and the pitfalls of synthetic consortium design. Research on natural bacterial consortia has shown that dismantling and reassembling communities from their isolated members can impair the ability to degrade chlorimuron-ethyl [13]. Although the core degraders were retained, the "auxiliary" partners and their metabolic cross-feeding disrupted the community's functional balance, illustrating how emergent properties can vanish once natural structures are disturbed. More broadly, microbial consortia engineering studies emphasize that synthetic combinations often fail because of competition, inhibitory metabolites, or missing facilitative interactions destabilize performance under stress [14]. Together, these findings suggest that while engineering pairings can sometimes succeed, advancing bioremediation will require close attention to the stability and emergent properties of naturally co-evolving partnerships, rather than assuming that any set of organisms can be forced to function together.

Advances in microfluidics and co-culture platforms may provide the fine-scale resolution necessary to observe microbial interactions as they unfold. For instance, microfluidic devices have enabled direct, time-resolved imaging of root-bacteria colonization [15] and encapsulation of microbial subcommunities for network interference [16]. Equally pressing is the challenge of tracing nutrient and metal flow within the consortium. Techniques such as single-cell stable isotope probing (SC-SIP) combine

isotopic labelling with high-resolution imaging, such as Raman or NanoSIMS, to map substrate assimilation at the cellular level [17]. In parallel, metal stable isotope tracers have been used to resolve metal fluxes and speciation in environmental systems [18]. Although this thesis demonstrates that glucose supplementation alters structural organization, hormone production, and Cd accumulation, the precise distribution of carbon and metals among partners remains unresolved. Bulk measurements of cellular Cd or extracellular hormone pools offer only community-level snapshots, obscuring which member is responsible for uptake, storage, or secretion, and how these processes shift over time.

Moving forward, several avenues for advancing FAB consortium research stand out. The first is the development of genomic and transcriptomic resources. A high-quality genome for *E. mutabilis* would permit precise annotation of metal transporters, hormone biosynthetic pathways, and symbiosis-related genes, and would clarify how these are regulated under stress. When coupled with fungal and bacterial genomes, such resources would enable network-level modeling of interspecies interactions across the consortium. The second is optimization of synthetic reconstruction. Building defined FAB consortia based on natural interactions could allow causal roles for hormones, metabolites, and structural interactions to be disentangled without losing the emergent properties of the intact system. The third is nutrient and metal tracking. New approaches such as stable isotope labeling, NanoSIMS, or single-cell ICP-MS could reveal how carbon and Cd are partitioned among partners, and how these flows shift across time and environmental regimes. A fourth avenue is natural product discovery. Molecular networking has already shown that the FAB can unlock otherwise silent biosynthetic pathways (Appendix II); targeted characterization of these metabolites may yield novel compounds that mitigate

stress. Finally, field validation is essential. Deploying FAB consortia into mesocosms or pilot remediation sites would test whether the emergent properties observed in the laboratory translates to complex environments, and whether superorganismal properties provide the stability required for sustainable bioremediation. At the same time, it is important to recognize that FABs do not operate in isolation: their organization and function are shaped by environmental context such as pH, nutrient composition, and media characteristics. As shown in this thesis, glucose supplementation altered consortium structure, signalling, and Cd accumulation. Thus, the FAB should be viewed not only as a microbial superorganism but also as a micro-ecosystem whose emergent properties depend on both biological partnerships and environmental conditions.

Beyond specific experiments, the greatest challenge may be conceptual. The FAB forces us to reconsider what constitutes an organism, and by extension, what constitutes a viable unit of remediation. If resilience to heavy metals in extreme environments is an emergent property of microbial superorganisms, then efforts to harness these systems must move beyond the search for singular traits in isolated strains. Instead, future research should focus on the ecological and evolutionary principles that allow collectives like the FAB to persist. By embracing the consortium itself as the relevant level of analysis, we may begin to design biotechnologies that echo nature's own solutions: communities that thrive not in spite of adversity, but because of it.

5.5 REFERENCES

1. Akcil A, Koldas S. Acid mine drainage (AMD): Causes, treatment and case studies. J Clean Prod. 2006;14(12-13 SPEC. ISS.):1139–45. https://doi.org/10.1016/j.jclepro.2004.09.006.
2. Hassan Z ul, Ali S, Rizwan M, Ibrahim M, Nafees M, Waseem M. Role of bioremediation agents (bacteria, fungi, and algae) in alleviating heavy metal toxicity. In: Kumar V, Kumar M, Sharma S, Prasad R, editors. Probiotics in Agroecosystem. 2017. p. 517–37.
3. Tate RL, Klein DA, editors. Soil reclamation processes: microbiological analyses and applications. Boca Raton, FL: CRC Press; 2020.
4. Dell'Anno F, Rastelli E, Buschi E, Barone G, Beolchini F, Dell'Anno A. Fungi can be more effective than bacteria for the bioremediation of marine sediments highly contaminated with heavy metals. Microorganisms. 2022;10(5):993. https://doi.org/10.3390/microorganisms10050993.
5. Abbasi, M, Khan I, Rehman A, Hayat A, Ur Rehman M, Shah TA, *et al*. Bioremediation of heavy metals contaminated soil by using indigenous metallotolerant bacterial isolates. Appl Ecol Environ Res. 2024;22(2):1623–48. https://doi.org/10.15666/aeer/2202_16231648.
6. Wenseleers T. The Superorganism Revisited. BioScience. 2009;59(8):702–5. https://doi.org/10.1525/bio.2009.59.8.12.
7. Roth MS. The engine of the reef: Photobiology of the coral-algal symbiosis. Front Microbiol. 2014;5. https://doi.org/10.3389/fmicb.2014.00422.
8. Griffiths D. Queer theory for lichens. UnderCurrents. 2015;19(1):36–45.
9. Youle M, Knowlton N, Rohwer F, Gordon J, Relman D. Superorganisms and holobionts. Microbe Mag. 2013;8:152–3. https://doi.org/10.1128/microbe.8.152.1.
10. Nandy S, Andraskar J, Lanjewar K, Kapley A. Challenges in bioremediation: From lab to land. Bioremediation for Environmental Sustainability. Elsevier; 2021. p. 561–83.
11. Vishwakarma GS, Bhattacharjee G, Gohil N, Singh V. Current status, challenges and future of bioremediation. Bioremediation of Pollutants. Elsevier; 2020. p. 403–15.
12. Wang J, Chen R, Fan L, Cui L, Zhang Y, Cheng J, *et al*. Construction of fungi-microalgae symbiotic system and adsorption study of heavy metal ions. Sep Purif Technol. 2021;268(April):118689. https://doi.org/10.1016/j.seppur.2021.118689.
13. Li X, Lu C, Dai Y, Yu Z, Gu W, Li T, *et al*. Characterizing the microbial consortium l1 capable of efficiently degrading chlorimuron-ethyl via metagenome combining 16S rDNA sequencing. Front Microbiol. 2022;13:912312. https://doi.org/10.3389/fmicb.2022.912312.
14. Li X, Wu S, Dong Y, Fan H, Bai Z, Zhuang X. Engineering microbial consortia towards bioremediation. Water. 2021;13(20):2928. https://doi.org/10.3390/w13202928.
15. Massalha H, Korenblum E, Malitsky S, Shapiro OH, Aharoni A. Live imaging of root–bacteria interactions in a microfluidics setup. Proc Natl Acad Sci. 2017;114(17):4549–54. https://doi.org/10.1073/pnas.1618584114.
16. Hsu RH, Clark RL, Tan JW, Ahn JC, Gupta S, Romero PA, *et al*. Microbial interaction network inference in microfluidic droplets. Cell Syst. 2019;9(3):229-242.e4. https://doi.org/10.1016/j.cels.2019.06.008.

17. Alcolombri U, Pioli R, Stocker R, Berry D. Single-cell stable isotope probing in microbial ecology. ISME Commun. 2022;2(1):55. https://doi.org/10.1038/s43705-022-00142-3.
18. Wiederhold JG. Metal stable isotope signatures as tracers in environmental geochemistry. Environ Sci Technol. 2015;49(5):2606–24. https://doi.org/10.1021/es504683e.

APPENDIX I

I.1 PREFACE

Title: Supplementary Material

Purpose: This appendix is an Excel file of Trinity identities to supplement results from Chapter 4 of this thesis. The file name of this Excel file is "Appendix I_Supplementary File_Chapter 4.xlsx".

Reference: This file was generated in conjunction with Chapter 4 of this thesis as part of publication preparation. The published version may appear different than presented here.

Author: Emma Kaszecki

APPENDIX II

II.1 PREFACE

Title: Uncovering natural products of *Euglena mutabilis* environmental consortia using MS/MS based molecular networking

Authors: Emma Kaszecki, Harrison T. J. Leedham, James W. C. Barnwell, Eve T. Roxborough, Barry J. Saville, R. J. Neil Emery, Ellis C. O'Neill

Reference: This chapter is under review for publication in the journal *Communications Biology*. The published version may appear different than presented here.

Contributions: ECO contributed the study conception, experimental design, and funding. Experimental design, material preparation, data collection, and analysis were performed by EK with assistance from HTJL. JWCB carried out antiSMASH analysis. Scale-up and purification were conducted by JWCB with assistance from HTJL and ETR. ETR contributed to metabolite extraction method development and data collection. The first draft of the manuscript was written by EK and HTJL with edits made by BJS, RJNE, and ECO. All authors commented on subsequent versions of the manuscript and have approved the final version.

Uncovering natural products of *Euglena mutabilis* environmental consortia using MS/MS based molecular networking

II.2 ABSTRACT

Natural products (NPs) are a vital source of antibiotics and bioactive compounds, yet monoculture-based discovery often yields known metabolites. Natural microbial consortia provide an alternative by activating silent biosynthetic pathways. *Euglena mutabilis*, an extremophilic alga that naturally associates with bacteria and fungi, represents a promising platform for NP discovery. We investigated three *E. mutabilis* consortia compared to axenic *E. gracilis* controls, grown under varying nutrient conditions and sampled over time. Molecular networking of 720 LC-MS/MS profiles yielded 7,469 molecular features, including 202 reproducible nodes, most unique to *E. mutabilis*. NP diversity was strongly influenced by medium, solvent, and culture duration, with nutrient-rich conditions and butanol extraction producing the most complex profiles. Consortia consistently outperformed controls, and metagenomic sequencing with antiSMASH identified diverse biosynthetic gene clusters, primarily from *Acidiphilium*. One fungal metabolite related to a known *Talaromyces* compound was confirmed by NMR. These results establish *E. mutabilis* consortia as productive sources of novel secondary metabolites.

II.3 INTRODUCTION

Specialised metabolites (SMs) are compounds produced by an organism that are not essential to their growth and development [1]. Often referred to as natural products (NPs), these molecules allow interaction with other organisms and have historically been a rich source of antimicrobial and pharmaceutical agents [2]. This could be a defensive response

to competition or stress, promotion of growth and development, mediation of mutualistic interactions, or facilitation of transport [3,4]. Out of the constellation of NPs and their derivatives produced, some demonstrate critical bioactivity; however, their overuse has stimulated resistance through selective pressure, contributing to the rise in antimicrobial resistance [5]. In response, researchers are attempting to uncover novel bioactive compounds.

Historically, NPs and their derivatives that have been used in drug and antimicrobial therapies were discovered from a single source organism, such as penicillin from *Penicillium notatum* [6] or morphine from *Papaver somniferum* [7]. This began with Selman Waksman's systematic study in the 1930s to uncover microbes with inhibitory properties [8]. The rapid discovery of bioactive NPs led to the development of over half the pharmaceutical drugs available today, which are either derived from or inspired by natural sources [2]. This was achieved using "top-down" bioprospecting workflows directly extracting, analyzing, isolating, and screening abundant agents with reproducible activity [9]. Although this approach was effective for the early discovery of bioactive NPs, several factors now make it challenging to utilize. The steady decline in the discovery of novel products increases the likelihood of re-identifying previously characterized compounds [10]. This challenge is amplified by the fact that many identical compounds are produced by multiple organisms [11]. Proprietary databases, such as the Dictionary of Natural Products (DNP) and the Global Natural Product Social (GNPS) molecular networking platform, help mitigate dereplication [10,11]; however, no single database comprehensively catalogs tandem mass spectrometry (MS/MS) data for all NPs [10]. Because newly identified compounds are often produced in low quantities—making isolation and scale-up

both time- and cost-intensive (around $50,000 USD and three months per novel NP) [11,12] – NP discovery is increasingly shifting toward “bottom-up” bioprospecting workflows [9] and co-cultivation [13].

Rather than continuing to employ MS-based methods for the discovery of novel products, the advancement of bioinformatic and molecular biological techniques enables researchers to identify and characterize potential NP gene clusters. Tools such as antibiotics & Secondary Metabolite Analysis Shell (antiSMASH) [14] and emerging artificial intelligence (AI) algorithms [15] offer assistance by streamlining the identification of potentially bioactive BGCs [16]; however, many prospective compounds identified in this way cannot be produced under traditional laboratory conditions [17]. Indeed, an organism’s NP production varies when silent genes are triggered in response to changing surroundings. For example, modifying the nutrient availability of marine *Salinispora* and *Streptomyces* produced NPs characterized in 15 molecular families [18]. Changes are also observed when other organisms are introduced to the environment. Novel antimicrobial compounds were isolated from a co-culture of the fungus *Cladosporium* with the bacterium *Bacillus subtilis* [19], and the algacidal bacterium *Streptomyces iranensis* produces azalomycin F in the presence of *Chlamydomonas reinhardtii* [20]. Co-cultivation has proven to be a promising strategy for discovering novel NPs and increasing their yield [21]. Integrating co-cultivation, symbiotically or parasitically, with bioinformatic tools could provide insight into how silent BGCs can be expressed without molecular intervention [22].

The photosynthetic protist (alga) *Euglena* has previously been investigated for its production of paramylon, a β-1,3 glucan which has demonstrated antibacterial activity

against *Escherichia coli* and *Staphylococcus aureus* [23]. Recent research has revealed that *E. gracilis*, *E. mutabilis*, and *E. sanguinea* produce a class of compounds known as euglenatides [24], large compounds comprised of five cyclic lipopeptides containing β-aminoisobutyric acid and dihydroxynorvaline with a hydroxylated lipid tail [25]. Their bioactivity demonstrated cytotoxic effects in MCF-7 breast cancer cells and antimicrobial activity against *Aspergillus* and *Caenorhabditis elegans* [24].

Euglenatides are the first reported high value NP from *E. mutabilis*, an extremophilic euglenoid frequently found in harsh, metal-contaminated, and acidic environments such as acid mine drainage (AMD), volcanic lakes, and peat bogs [26]. Its remarkable tolerance to low pH and high concentrations of heavy metals has led to its recognition as a bioindicator species for AMD-impacted ecosystems [26]. In these environments, *E. mutabilis* often occurs within complex microbial consortia, forming biofilms alongside bacteria and fungi [27]. Previous studies have reported persistent associations between *E. mutabilis*, extremophilic bacteria, and specific fungal species, including *Cryptococcus* and *Talaromyces*, which appear to contribute to its survival under stress [28,29]. These studies suggest the microbial partnerships rely on *E. mutabilis* photosynthate for nutrients and may reflect mutualistic interactions that enhance metal tolerance. These organisms can therefore be considered components of a true microbiome, sustained by the primary productivity of *E. mutabilis* in otherwise carbon-limited environments. This tight metabolic coupling, especially under extreme geochemical stress, positions the *E. mutabilis* microbiome as a promising system for studying microbial adaptation and evolution. Moreover, given that extremophilic microorganisms often produce structurally unique and bioactive NPs as part of their survival strategies [30], this

system offers an underexplored reservoir of potential new chemistry with biotechnological or pharmaceutical relevance.

The objective of the presented research was to investigate NP production by environmental *E. mutabilis* consortia containing fungi and bacteria. Synthetic biology and bioengineering have been used to manipulate metabolic pathways for SM production in well-defined single organisms; however, these approaches often fall short when applied to complex systems, where the tools may not function reliably [21]. As a result, there has been growing interest in co-culture engineering as a more accessible and cost-effective strategy – not only for enhancing the yield and efficiency of known SMs, but also for uncovering novel NPs, without the technical demands of synthetic biology [22]. We employed a systematic approach using "top-down" and "bottom-up" methods to culturing and extracting metabolites in three environmental microbiomes of *E. mutabilis*. Our findings suggest that culture composition and nutrient availability play a role in NP production. Further, the results of our study highlight diverse NP production utilizing various culture media, extraction solvents, and sample time in algal consortia. This study is the first to examine NP production of environmental microbiomes containing *Euglena* and emphasizes the importance of natural microbial consortia for novel compound discovery.

II.4 METHODS

Selection of *E. mutabilis* and *E. gracilis* strains & culture conditions

Field samples of *E. mutabilis* were obtained from the Canadian Phycological Culture Centre (CPCC, University of Waterloo, Canada). CPCC 452 was isolated from a nickel mine (Levack, Ontario, Canada) and contained *E. mutabilis* and unidentified bacteria. CPCC 657 was isolated from a gold mine (Timmins, Ontario, Canada) and contained *E. mutabilis* with bacteria and fungi previously identified as *Acidiphilium acidophilum* and *Talaromyces* sp., respectively [29]. CPCC 658 was isolated from the same gold mine (Timmins, Ontario, Canada) and contained *E. mutabilis* with unidentified bacteria and fungi. The CPCC did not have an axenic culture of *E. mutabilis*, therefore an axenic culture of *E. gracilis* (CPCC 95) was obtained to act as an experimental control.

Cultures were grown in T75 tissue culture flasks (Sarstedt Inc. Cat. No. 83-3911-502) under standard aeration (75 RPM on a Stuart mini orbital shaker SSM1) and temperature (25 °C ± 0.5 °C) while cycling light (16:8 LD cycle at 45 μmol/m^2/s) in an LMS 1200NP incubator. Stock cultures were grown autotrophically in modified acid medium (MAM), a defined inorganic medium, with modifications recommended by the CPCC and adjusted to a pH of 4.3 [31]. Filter sterilized F/2 vitamin mix was added to autoclaved medium once it cooled.

Cell counts of *Euglena* from stock cultures were performed using a hemocytometer (Reichert Bright-Line). A volume of culture was aliquoted into 2 mL microfuge tubes from each stock which equated to 600,000 cells. Microfuge tubes were centrifuged (6000 RCF for 10 minutes) and the supernatant was removed using a micropipette. The pelleted cells were inoculated into T25 tissue culture flasks (Sarstedt Inc. Cat. No. 83-3910-502) containing 30 mL of media. Cultures were grown in MAM, MAM with 20 g/L glucose

(Fisher Scientific Cat. No.10141520) (MAM+G), *Euglena gracilis* Medium (EG), Jaworski's Medium (JM), and EG:JM [32]. Modifications to EG include substituting Lab-Lemco powder and tryptone with casamino acids (3 g/L). Additionally, the vitamin in JM was substituted for the f/2 vitamin found in MAM and was added to cooled autoclaved medium. All media types were made using Milli Q (MQ) water (18.2MΩ·cm) and adjusted to a pH of 4.3 with diluted hydrochloric acid (HCl).

Cells were grown in the LMS 1200NP incubator under the same temperature and light conditions as the stock cultures with aeration (70 RPM on a Stuart mini gyro-rocker SSM3) for 7 days. Cell counts of *Euglena* were assessed 1-, 4-, and 7-days post-inoculation using a hemocytometer, and 5 mL of culture was aliquoted into scintillation vials (DWK Life Sciences Cat. No. 986546) for metabolite extractions. Aliquots of cultures were also taken 1- and 7-days post-inoculation to assess the growth recovery of the culture to quantify *Euglena* and constituent organisms which could not be counted using a hemocytometer. The outlined experiment was executed using all 4 *Euglena* strains and replicated 4 times in each medium.

Cultures selected for scale-up were grown in T250 tissue culture flasks **(**Fisher Scientific Cat. No. 10527161) under the same conditions as previously described. 160 mL of culture, containing 500,000 cells, was inoculated into 5 L volumetric cylinders filled with media to a final volume of 4 L. Cultures were incubated for 14 days prior to purification.

Growth recovery check

Recovery of *E. mutabilis*, *E. gracilis*, and constituent organisms after 1 and 7 days of growth in their respective media was assessed by plating on non-selective media plates. Malt extract (VWR Cat. No. 84618.0500) plates were prepared using a 1.4% (w/v) agar mixture. Malt agar was autoclaved to sterilize, and 15 mL of media was added to each plate (Greiner Bio-One Cat. No. 633181). Aliquots of 100 µL were taken from each sample, diluted with 900 µL of sterile 0.9% NaCl, and 50 µL of the diluted sample was added to an agar plate. All plates were sealed with parafilm and incubated for 7 days under the same growth conditions as the stock cultures.

Statistical analysis

Differences in *Euglena* cell counts after 7 days of growth were compared within each strain using a one-way ANOVA ($p < 0.05$) followed by Tukey's Honest Significant Difference (HSD) test.

Metabolite extraction process

Sequential metabolite extractions were performed on the culture aliquots in the scintillation vials. Briefly, using a glass pipette (Fisher Scientific Cat. No. 1154-6963), 5 mL of ethyl acetate (EtOAc) (Fisher Scientific Cat. No. E/0900/PB17) was added to each sample, quickly vortexed to mix and left to separate. The organic layer was transferred to a new scintillation vial, and the EtOAc extraction was repeated. Following the second extraction, 2 mL of MQ was added to the scintillation vial containing the organic fraction, vortexed to mix, and left to separate. The aqueous layer was then transferred back to the original scintillation vial and the extracted EtOAc vial was left to evaporate in a fume hood. This extraction process was repeated by adding 5 mL of butan-1-ol (BuOH) (Fisher

Scientific Cat. No. B/4800/PB17) to the original scintillation vial and transferring the organic layer to a new scintillation vial. Once the extractions were completed, the scintillation vials were dried using a freeze dryer and the BuOH samples were dried using a rotary evaporator under reduced pressure at 50 °C. Dried samples were reconstituted in 2 mL of methanol (MeOH) (Fisher Scientific Cat. No. M/4000/PB17) and transferred into 2 mL microfuge tubes (Fisher Scientific Cat. No. 11321934). The microfuge tubes were centrifuged for 2 minutes at maximum speed and 1.5 mL of supernatant was transferred to HPLC vials (Restek Part No. SR-0100802-CL). Samples were stored at -80 °C ahead of LC-HRMS/MS analysis.

Liquid chromatography & high-resolution tandem mass spectrometry (LC-HRMS/MS)

Samples were analysed using a Bruker Daltonics Impact Mass Spectrometer (MS/MS) equipped with a Dionex Ultimate 3000 Ultra-High-Performance Liquid Chromatography (uHPLC) system using a Kinetex reverse-phase C18 column (2.6 µm pore, 150 x 2.1 mm). Injection volume was set to 1 µL. Solvents used were MQ water and LC-MS grade MeCN (VWR Chemicals Cat. No. 83640.320 with 0.1 % formic acid) at a flow rate of 0.5 mL/min. LC was used under the following conditions: 0-2 min (10% MeCN in H_2O), 2-12 min (10-100% MeCN), 12-14 min (100% MeCN), 14-20 min (10% MeCN). 0.4 mM HCOONa was injected for the first 2 min to calibrate the MS, during which the divert valve was set to waste. Q-TOF MS settings during the LC gradient were as follows: positive ion mode, mass range 100-1500 m/z for MS1, 300-1500 m/z for MS2 selection, 100-1500 m/z for MS2, MS scan rate 4/s, number of precursors selected for MS2 3, fixed

collision energy 10 eV, source gas temperature 250 °C, gas flow 8 L/min, nebulizer pressure 3 Bar.

Semi-preparative high-performance liquid chromatography (HPLC)

Samples were purified using an Agilent 1260 Infinity II HPLC system equipped with a Kinetex Axia packed preparative column (5 µm, 100 × 21.2 mm). The mobile phases consisted of Milli-Q water and HPLC-grade acetonitrile containing 0.1% formic acid (VWR Chemicals, Cat. No. 83640.320), delivered at a flow rate of 5 mL/min. Each run involved a manual injection of 2 mL of sample. The gradient elution was as follows: 0–2 min at 69.5% MeCN in water, followed by a linear increase to 72.5% MeCN from 2–11.5 min. Absorbance was monitored at 210, 275, and 360 nm, and 1.5 mL fractions were collected between 2 and 11.5 minutes.

Molecular networking and data analysis

All MS/MS data files were converted from Bruker data format (.d) to .mzML file format using MSConvert 3.0.24075 [33]. Converted files were transferred onto the GNPS server (gnps.ucsd.edu) using WinSCP, and molecular networking was performed using the standard GNPS data analysis workflow [34]. Sample attributes were linked to the data (2 *Euglena* species, 4 culture strains, 5 media types, 3 timepoints, 3 locations, 3 solvents). The chosen parameters for molecular networking were as follows: minimum cosine score 0.7, minimum number of matched fragment peaks 6, precursor mass tolerance 2.0 Da, minimum cluster size 2, maximum cluster size 100. The network was then imported into Cytoscape 3.10.2 (https://cytoscape.org) [35] and visualised using the force-directed layout. All nodes containing ions present in the media and nodes within the same cluster as media nodes were

subtracted to facilitate analysis. Nodes represent parent masses, and edge stroke colour denotes cosine score. The data is publicly accessible as MassIVE data sets (MSV000098947). Euler diagrams were produced using the eulerr package (https://cran.r-project.org/web/packages/eulerr/index.html) [36] and abundance plots were produced using ggplot2 (https://cran.r-project.org/web/packages/ggplot2/index.html) in RStudio 2024.12.0+467 (https://posit.co/download/rstudio-desktop) [37] using R v4.4.2 (https://www.r-project.org) [38].

DNA isolation and whole genome shotgun metagenomics

Samples of *E. mutabilis* (CPCC 452, 657, 658) grown in MAM were to Novogene (UK) Company Limited for DNA extraction and whole genome shotgun metagenomics. Each sample was snap frozen and contained a concentration of 5 x 10^6 *Euglena* cells in a 2 mL Eppendorf tube. DNA was extraction was performed by Novogene and quality was checked using an Agilent 5400. Library construction and whole genome sequencing using a NovaSeq X Plus (PE150) were carried out by Novogene. Sequencing was carried out in triplicate for each strain.

Bioinformatic analysis

Fastp v0.23.1 was used for preprocessing cleanup of raw Illumina reads [39] while Bowtie2 v2.2.4 was used to filter out possible host contamination [40,41], although this is limited because the genome of *Euglena* has not been full sequenced or annotated. Paired reads were discarded if base quality was < 5. Metagenomes were assembled using MEGAHIT software v1.2.9 discarding scaftigs < 500 bp [42]. Remaining scaftigs were selected for Open Reading Frame (ORF) prediction using MetaGeneMark, excluding ORFs

< 100 bp [43]. CD-HIT software was used to eliminate ORF prediction redundancy (identity at 95% and coverage at 90%) [44,45] and clean data was mapped using Bowtie2 to quantify gene abundance [43,44]. The gene catalogue (unigenes) was identified by filtering out genes with reads <= 2 in each sample [45]. Gene abundance was calculated using the number of mapped reads and gene length [40] and used to perform statistics, core-pan gene analysis, correlation analysis, and Venn diagram analysis in R. Species annotation was carried out using DIAMOND software to align unigene sequences with the NCBI's NR database, inclusive of sequences from bacteria, fungi, archaea, and viruses [46]. Assembled genomes were analyzed using the default parameters of the bacterial and fungal modules in antiSMASH v7.0 [14] to identify potentially encoding BGCs. Additional analyses included active site finder, knownclusterBLAST, RRE finder, TFBS finder. Outputs were manually curated for genes of interest.

II.5 RESULTS

Growth of *Euglena* in different media

E. gracilis and *E. mutabilis* growth could be assessed by direct cell counting and revealed differences in growth across media types. Although showing a slight increase above the initial $2x10^4$, none of the cultures grew substantially in the JM media, despite its wide application in the growth of freshwater algae (Figure II.1). All cultures grew very well in the EG:JM media, substantially more than for the EG media on its own, which barely supported any growth of the axenic *E. gracilis* (CPCC 95). Despite being the maintenance media for these algae MAM only supports minor growth for the *E. mutabilis* strains and moderate growth for *E. gracilis*. Interestingly, addition of glucose to MAM did not support the growth of *E. mutabilis* CPCC 657 and 658, the cultures that contain both fungal and

bacterial organisms with *Euglena*, whilst enhancing the growth of CPCC 452, which only contains bacteria and *Euglena*, and axenic *E. gracilis.*

The growth of *E. gracilis*, *E. mutabilis*, and constituent organisms were also assessed by plating on malt agar media and counting number of colony forming units (CFUs). The plates were incubated under the same autotrophic conditions the cultures were grown in (25 °C; 16L:8D cycling light) and CFUs were counted after 7 days. Bacterial CFUs were not recorded since they were too numerous and often confluent. Consistent with cell count data, all algal cells produced colonies, mostly aligning with the cell count data, notably higher than would be suggested for the JM media (Table II.1) The associated fungus in CPCC 657 and 658 also exhibited the greatest recovery after being grown in EG:JM, suggesting that EG:JM supports fungal growth in the consortia. Interestingly, no fungal colonies were observed after being grown in MAM or JM, despite clearly being present in the maintenance cultures grown in MAM.

Molecular networks of natural products

Global metabolite profiles of field samples of *E. mutabilis* and a laboratory culture of *E. gracilis* were obtained using well-established HPLC-MS/MS methods [18]. Each culture was grown as described before and sampled after 1, 4, and 7 days of growth. In total, 720 culture samples and 135 blanks were analysed to generate approximately 310,000 MS2 spectra that were processed according to a standard GNPS molecular networking workflow [34]. A comprehensive network was generated consisting of 7,469 nodes (Figure SII.1), 4,933 of which were from or connected to media blanks and removed (Figure II.2). Of the remaining 2,538 nodes, 1,348 were identified as unique to one culture strain. 444

nodes were unique to CPCC 95, 226 to CPCC 452, 194 to CPCC 657, and 484 to CPCC 658. All nodes were independently investigated and manually filtered to determine their potential as new natural products. Nodes were considered as "leads" based on the following criteria: 1) The peak of interest fell within an RT of 77.5 and 720 seconds, 2) the node was not connected to a node of another strain, 3) the peak was present at an intensity of at least 1000, 4) the peak was present in at least 2 biological replicates, and 5) the spectrum associated with the node did not match a previously identified compound in the GNPS database. After filtering, a total of 202 nodes were identified as leads, having met the criteria, consisting of 45 nodes from CPCC 95, 42 from CPCC 452, 15 from CPCC 657, and 100 from CPCC 658.

The lead nodes can be further analysed according to the additional attributes including extraction method, timepoint, and media type (Figure II.3). Several trends related to these additional attributes exhibited inverse effects when comparing *E. gracilis* (CPCC 95) to *E. mutabilis* consortia (CPCC 452, 657, 658). The greatest number of nodes were found in the BuOH fraction, composing 56.4% of the 202 nodes, including the majority of nodes from each *E. mutabilis* culture and, only 13% (6) of the nodes produced by CPCC 95. Rather, the majority of lead nodes from CPCC 95 were found in the MeOH fraction (53%; 24), which contained the fewest unique nodes from the *E. mutabilis* consortia.

Likewise, the timing of sampling influenced NP production (Figure II.3b). CPCC 95 yielded the fewest unique lead nodes after 1 day but the most after 7 days, whereas CPCC 452, 657, and 658 exhibited the opposite pattern, generating the most unique nodes after 1 day and the fewest after 7 days. Across all strains, the lowest number of unique

nodes was observed after 4 days of growth, with half of the lead nodes produced after 1 or 7 days of growth alone, each generating 53 nodes. This suggests there is not a gradual build-up of these compounds over the growth, and some are lost over time.

Different growth media displayed variations in lead node distribution (Figure II.3c). The minimal media (JM, MAM) generated the fewest unique lead nodes, while media supplemented with a carbon source (MAM + G, EG, EG:JM) produced the highest number of nodes. Among the 202 reproducible lead nodes, only 17 (8%) were exclusively produced in minimal media, 64 (31.6%) were generated in MAM + G, and 155 (76.7%) from media containing EG. The highest number of lead nodes were produced in EG:JM media across all strains (115; 56.7%). Whilst there is significant overlap between related media, over half of the lead nodes are only produced in a single media type.

These results emphasise the importance of varying extraction solvent, growth time and media type to improve the production of the most promising lead compounds from these cultures. Overall, if the *E. mutabilis* microbiomes produce novel bioactive compounds, they are more likely to do so when grown in nutrient-rich media.

Metagenome sequencing

To understand the members of the microbial microbiome, their contribution to the consortia and their potential for NP biosynthesis, we performed metagenomic sequencing. The relative microbial abundance of three *E. mutabilis* metagenomes was analyzed at various taxonomic levels. The predominant non-redundant genes were associated with the domains Archaea, Eukaryota, Bacteria, and Viruses (Figure II.4, Table SII.2). Given that

the genome of *E. mutabilis* has not been sequenced or annotated, abundance was normalized for each strain at every taxonomic level to account for the removal of "other" non-redundant genes. The high abundance of "other" sequences (86-93%) from each sample were not classified to a specific taxonomic level likely because they represent sequences from *Euglena* that have not been previously characterized, so this approach provided a clearer representation of microbial diversity.

Although CPCC 452 is thought to contain only *E. mutabilis* and associated bacteria, it exhibited the lowest number of non-redundant bacterial gene hits. Additionally, phylum-level analysis revealed the presence of fungal genes in higher abundance then CPCC 657 and 658 (Figure II.5a, Table SII.3), which are believed to contain *E. mutabilis* along with associated bacteria and fungi. At the family level, bacterial genes were more prevalent than fungal genes across all strains (Figure II.5b, Table SII.4). When analyzing the relative abundance of each sample in a strain, the top 10 most abundant microbes at the phylum level remain consistent (Figure II.5c, Table SII.3), while the family level reveals nominal diversity (Figure II.5d, Table SII.5). Taxonomic analysis using NCBI indicated that the majority of read alignments in each sample originated from bacteria, with the highest number aligning to *Acidiphilium acidophilum* (37-79%; Table SII.6). The Ascomycota reads map most closely to T*alaromyces*, consistent with previous work [29].

Given the different locations these three strains were isolated, it is notable that all three microbiomes contain the same extremophilic bacterium adapted to acidic, heavy metal-rich conditions and that two strains contain a fungal contributor from the same genus.

The consistent composition and maintenance of these microbial consortia suggest they are important for the ecology of *E. mutabilis* and are not artifacts of the culture collection.

Prediction of secondary metabolite biosynthetic gene clusters (BGCs)

Analysis of sequence assemblies using bacterial and fungal antiSMASH databases identified 14 secondary metabolite regions from 68 bacterial BGCs and 20 fungal BGCs (Figure II.6). As of April 2025, 56 of the identified bacterial BGCs (Table SII.7) and 17 of the identified fungal BGCs (Table SII.8) display no cluster similarity within the antiSMASH database. Terpenes were the most common cluster type among bacterial and fungal outputs (30 and 12, respectively). Each strain produced acyl amino acid, aryl polyene, ectoine, non-ribosomal peptide synthase (NRPS) or NRPS-like, ranthipeptide, redox cofactor, RiPP recognition element (RRE), type I polyketide synthase (T1PKS), and type III polyketide synthase (T3PKS) clusters identified through the bacterial database. Interestingly, analysis using the fungal antiSMASH database also identified the same ectoine biosynthetic clusters in each strain.

Clusters within regions identified using antiSMASH with biosynthetic, biosynthetic – additional, or transport related functions were further analyzed using NCBI Protein BLAST. These results yielded little insight into the holistic function of the gene clusters as most of the functions within a region were not related to biosynthesis or transport. Nonetheless, Protein BLAST results suggested that an *Acidiphilium* species is likely the predominant bacterium in each strain. Among the top BLAST hits, 85%, 81%, and 70% of sequences in identified BGCs from CPCC 452, 657, and 658, respectively, were predicted to originate from *Acidiphilium* species. Interestingly, Protein BLAST results from BGCs

identified using the fungal antiSMASH database did not yield any fungal matches. Instead, the majority of hits (88%, 70%, and 67% from CPCC 452, 657, and 658, respectively) were attributed to *Acidiphilium* species. Other bacterial hits included *Acidibrevibacterium fodinaquatile* (9%, 7%, and 10% from CPCC 452, 657, and 658, respectively) and *Metallibacterium scheffleri* (9% from CPCC 658). All strains also shared at least one BGC sequence identified as similar to phytoene synthase from *E. gracilis* which may originate from the *E. mutabilis*.

Purification and characterization of a fungal secondary metabolite

From molecular networks produced, a node was identified containing an m/z (413.16) matching the $[M+H]^+$ of a SM previously identified in *Talaromyces*, 3-(9a-methyl-3-octanoyl-2,9-dioxofuro[3,2-g]isochromen-6-yl)prop-2-enoic acid [47]. The MS/MS of the node corresponded to many fragments which could be produced from this metabolite (Figure SI.4). Following identification of the metabolite, purification was conducted to confirm the reported structure via NMR. HMBC, HSQC, and TOCSY experiments reported similar shifts to those previously reported (Table II.2) [47].

After scaling up to 4 L cultures, a new molecular network was generated containing solely scale-up samples, in which GNPS identified 3-(9a-methyl-3-octanoyl-2,9-dioxofuro[3,2-g]isochromen-6-yl)prop-2-enoic acid within a cluster. Other nodes connected included a library match, whereas numerous had no reported structure (Figure II.8).

II.6 DISCUSSION

Recently, the shift towards co-culture engineering has gained popularity for increasing the production and efficiency of known SMs [48], for the discovery of novel NPs [49], and as an inexpensive alternative to the technical expertise and equipment required for synthetic biology [22].

Our work supports the growing recognition that microbial interactions in natural microbiomes can stimulate or unlock biosynthetic potential that remains silent in monoculture. This is important for discovering novel SMs and NPs, as different media and nutrient conditions influence microbial interactions, altering the metabolites produced by the organisms [50]. Specifically, our discovery of differences in growth between two minimal media, MAM and JM, is noteworthy. JM is meant to be a neutral media – intentionally decreasing the pH of JM resulted in poor growth and recovery of *Euglena* in nutrient-rich plates relative to MAM, likely spurred by an enhanced trace metal toxicity by increasing their solubility [51]. Importantly, recovery of fungal colonies was not reproducible in malt for either nutrient-minimum medium likely because of the absence of an adequate carbon source for the fungi. This is a significant finding, as fungi are well-known metabolite reservoirs, and their presence may enhance biosynthetic activity when grown with *Euglena*. However, under altered pH conditions, these genes may remain inactive, or alternatively, antiSMASH may not effectively detect biosynthetic genes from *Talaromyces* species.

Further, our work supports existing literature which indicates that the available carbon source plays a significant role in not only the health of the culture, but the

differential growth of the system partners, and the SM output. For example, the greatest accumulation of cell density was different for *E. gracilis* and *E. mutabilis* depending on the available carbon source. While *Euglena* generally can catabolize both glucose and acetate, previous research suggests a preference for acetate under mixotrophic and heterotrophic conditions [52,53]. In the absence of glucose, *Euglena* can catabolise acetate through the glyoxylate cycle, yet CPCC 95 departed from this expected behaviour by exhibiting an order of magnitude greater growth in MAM + G, when compared to previous studies [54]. These results may be attributable to downstream metabolic side effects of the glyoxylate cycle, including the wholesale bypass of the decarboxylation steps of the TCA cycle leading to decreased electron transporters (NADH, $FADH_2$) and ATP synthesis [55,56]. Fungi and bacteria also preferentially metabolize glucose and do so more rapidly than *Euglena*, likely explaining the lower *E. mutabilis* cell density observed in MAM + G compared to EG:JM. *Euglena* cells grown in EG media also showed signs of stress – reduced size and a more rounded morphology (Figure SII.2) – compared to growth in EG:JM. EG contains 0.1% (w/v) acetate, which is lethal to *Euglena* below pH 5.0 [52]; dilution in EG:JM halves this concentration, supporting higher cell density.

The importance of carbon source was a consistent trait, even in experiments involving malt agar. The primary carbon source in malt agar, maltose, is widely considered selective for culturing acidophilic organisms. Metabolism of maltose is slower relative to glucose because it first needs to be hydrolyzed to become bioavailable [57]. In the presence of alternative carbon sources, fungi and bacteria selectively utilize glucose by repressing the synthesis of enzymes used in the catabolism of other carbon sources [57,58]. The time and energy required to adjust from metabolizing glucose to maltose – mainly driven by an

ATP binding cassette transporter subunit - may explain why *Euglena* and fungal recovery on malt agar was stunted. The lag in growth, however, was not observed in cultures previously grown in EG:JM which were subsequently transferred to malt agar.

On malt agar, the *E. mutabilis* microbiomes with fungi and bacteria revealed changes in fungal pigmentation, uniformly between protist strains (Figure SII.3). It is widely known that fungi can produce pigmented SMs which vary in colour and intensity based on environmental conditions [59]. Previous research established that the fungi present in CPCC 657 produces a red pigmentation – proposed by either the repression of the *ade2* gene, or the production of anthraquinones – in response to stress and carbon availability [29]. Indeed, purification of the red pigment producing compound 3-(9a-methyl-3-octanoyl-2,9-dioxofuro[3,2-g]isochromen-6-yl)prop-2-enoic acid was from upscaled conditions only, which may be indicative of a stress-related response due to a shift in nutrients or growth environment. Production of azaphilone compounds in *Talaromyces* is well documented, although their exact metabolic functions are not well understood [60]. A host of azaphilone compounds are reported to exhibit various biological activities, although no data has been reported for the compound in question, so further bioactivity testing on fully purified extracts may yield new insights into its role [61].

Though CPCC 657 and 658 exhibit similar trends in growth and pigmentation response, the evidence for their differences is highlighted in the antiSMASH analysis. Although they produce many of the same classes of compounds, BLAST results suggest that these compounds are generated at different locations within the WGS assemblies and at varying frequencies (Table SII.7, SII.8). This suggests that each of the strains may be

exploited for both greater and diversified spectrum of SM production differently by a wide range of biotic and abiotic inputs and challenges.

Interestingly, among the *E. mutabilis* microbiomes, *Acidiphilium* appears as the predominant bacterium present. Given that these environmental strains were isolated from mining sites, the presence of an extremophilic bacterium adapted to acidic, heavy metal-rich conditions is unsurprising – though it may be of little relevance from an antimicrobial perspective [62]. Terpenes can have bioactive properties, though the terpenes identified here are associated with squalene and carotenoid biosynthesis likely related to cell membrane structure and function [63]. Extremophilic bacteria produce ectoine and aryl polyenes in response to environmental stressors, though they have more applications in biotechnology than pharmaceuticals [64,65]. The most likely candidates for novel antimicrobial BGCs are those that code for NRPS and NRPS-like compounds. Many clinical drugs today, including penicillin and vancomycin, have been synthesized in whole or part from non-ribosomal peptides isolated from bacteria, fungi, and cyanobacteria [66]. The complexity of non-ribosomal peptides makes it difficult to study their bioactivity, but their structural diversity provides a promising start for the development and bioengineering of pharmaceuticals [67]. Given that the large NRPS BGCs identified in CPCC 657 and 658 are not related to known clusters suggest that the cultures may be producing a novel bioactive compound. BLAST results indicated that some regions within the NRPS BGCs align with *Acidiphilium*, however, the lipophilic region in euglenatides are structurally similar to nemamides – the metazoan PKS-NRPS metabolite [24]. Future work should attempt to isolate these NRPS compounds, determine their structures, and assess their bioactivity. Unexpectedly however, antiSMASH analysis did not reveal evidence of

bioactive compounds of fungal origin. Rather, matches from the fungal antiSMASH database indicated activity associated with *Acidiphilium* species. The inability to support fungal colonization in minimal media may have limited the detection of fungal BGC-related sequence. This is further supported by the limited fungal representation in the WGS data beyond the phylum level. The only bioactivity linked to *Euglena* was associated with phytoene synthase – a rate-limiting enzyme in the carotenoid biosynthesis pathway related to chlorophyll production, whose activity is influenced by light intensity [68]. Integrating these findings with the molecular networking data suggests that if the *E. mutabilis* consortia produce novel bioactive compounds, they are more likely to do so when grown in nutrient-rich media.

Each strain, as well as each microbiome organism, likely has distinct physiological requirements that influence metabolite production. Generally, previous research investigating NPs suggests that changing culture conditions by altering growth media and nutrient profiles can have significant impacts on SM production [10]. While our findings confirm that glucose is the preferred carbon source for *Euglena*, acetate-based growth in EG and EG:JM resulted in a greater number of unique nodes, highlighting the significant influence of culture composition on NP diversity and dynamics in *Euglena* consortia.

Crucially, in addition to nutrient composition of the growth medium, the presence of other organisms had an impact on NP biosynthesis. Most of the unique nodes were generated by one of the three *E. mutabilis* microbiomes rather than the *E. gracilis* axenic culture. Although synthetic biology has traditionally been used to manipulate metabolic pathways for SM production, the complexity, cost, and technical challenges of

bioengineering are increasingly driving researchers toward co-culture approaches to elicit SM production and unlock bioactive potential [21,48]. The strong performance of CPCC 658, particularly after 7-days, suggests that strain-specific microbial interplay contribute to enhanced NP diversity. This highlights the importance of using co-culture strategies not only for activating biosynthetic pathways, but also for exploring the ecological dynamics that shape SM production. Further investigation into the microbial composition and metabolic interactions within the microbiomes could reveal new insights into how these relationships drive NP biosynthesis. It may also uncover the specific compounds extracted in each solvent fraction of the consortia. By integrating GNPS and antiSMASH analyses, it is plausible that some of the nodes extracted from consortia in the BuOH fraction represent novel NRPS-derived compounds [69]. A review of fungal co-cultures reported the production of 19 PKS and PKS-NRPS compounds when fungi were co-cultured with bacteria [22]. Similarly, in a competitive co-culture involving the cyanobacterium *Nodularia spumigena*, the diatom *Phaeodactylum tricornutum*, and the cryptomonad *Rhodomonas salina*, researchers observed up to a fivefold increase in NRP compound production by *N. spumigena* [70]. Some of these compounds were detected extracellularly, coinciding with suppressed growth of *P. tricornutum*, suggesting chemically mediated interactions within the community. Taken together, these findings emphasize that co-cultivation not only enhances chemical diversity but may also influence the polarity, abundance, and ecological roles of the natural products produced – making co-culture strategies a powerful tool for uncovering novel bioactive metabolites and understanding the microbial interactions that drive their biosynthesis.

I.7 CONCLUSIONS

This study explored the SM potential of environmental *E. mutabilis* microbiomes using a combination of genome mining and molecular networking. The results show that natural microbial co-cultivation, extraction method, and growth time all influence the diversity and reproducibility of NPs produced. Most of the reproducible features came from the *E. mutabilis* strains, especially CPCC 658, which produced the highest number of unique nodes after 7-days. These patterns suggest that both microbial interactions and strain-specific factors contribute to metabolite output, and that timing plays a key role in when certain compounds are expressed.

More than half of the lead compounds were extracted from the BuOH fraction – consistent with the types of compounds expected from NRPS-like and RiPP clusters. AntiSMASH results and Protein BLAST hits suggest that associated *Acidiphilium* species are likely contributing to biosynthetic activity, though more work is needed to confirm the origin and structure of specific compounds.

This work demonstrates that naturally occurring microbial consortia of *E. mutabilis* – rather than synthetic co-cultures – are powerful, ecologically grounded systems for accessing novel chemistry While synthetic biology has made significant progress, it can prove insufficient for complex or poorly understood pathways. Natural microbiomes offer a simpler and often more ecologically relevant alternative. The results here suggest that even without genetic modification or high-throughput screening, meaningful chemical diversity can be uncovered using relatively accessible methods. This work provides a starting point for deeper exploration of not only *E. mutabilis* and its microbiomes, but algal

consortia in general, as a source of novel metabolites. Future studies might focus on identifying the compounds responsible for the most promising nodes, tracking changes in metabolic output across more refined time points, or exploring the functional role of specific microbial partners in shaping metabolite production.

II.8 FIGURES AND TABLES

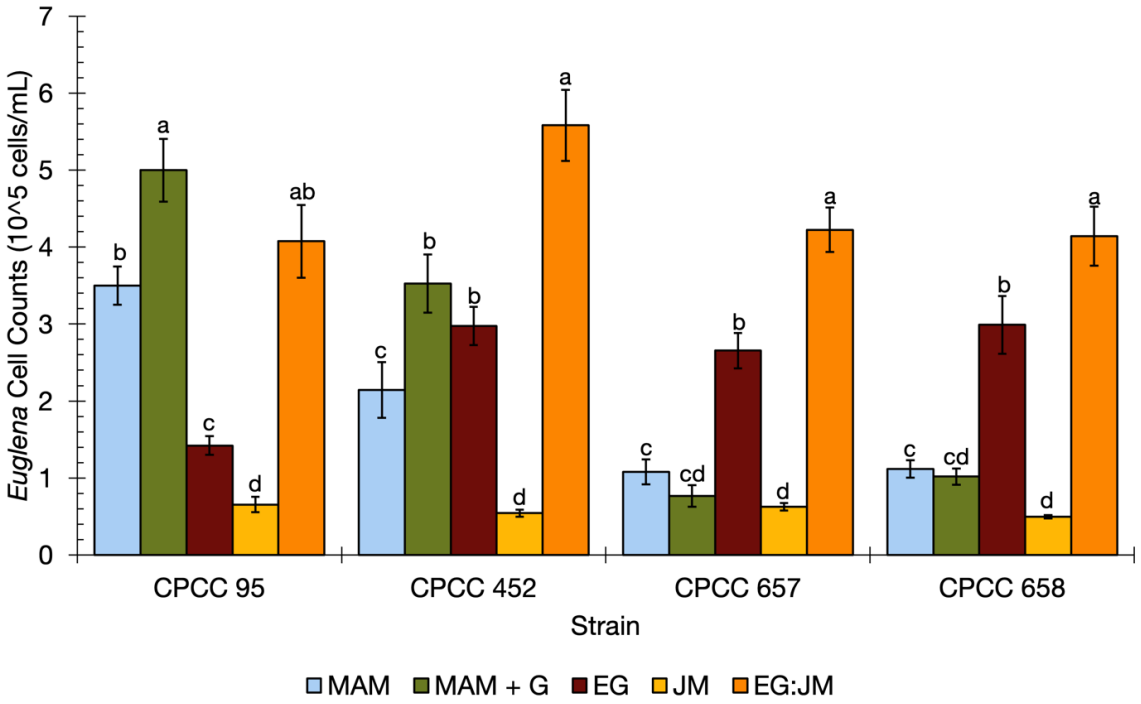

Figure II.1: The growth of *E. gracilis* and *E. mutabilis* vary across different medium. Cultures were grown for 7 days in five different types of media. Differences in cell concentrations within each strain were determined using a one-way ANOVA ($p < 0.05$) with a Tukey HSD. Error bars represent standard deviation ($n = 4$).

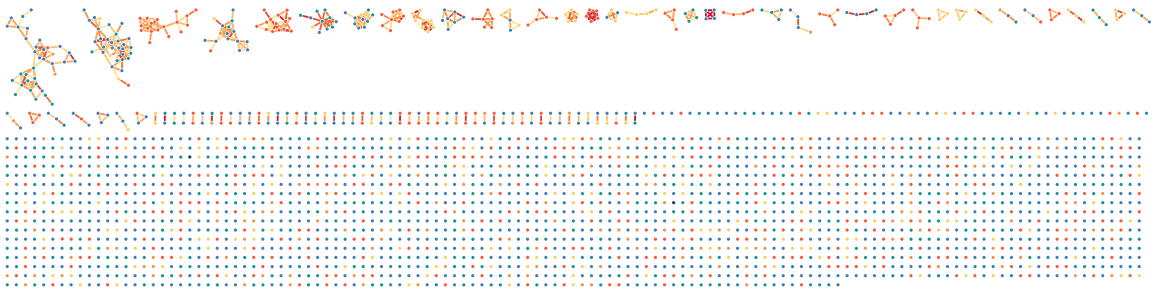

Figure II.2: Molecular network with media removed. Turquoise nodes represent ions unique to CPCC 95, yellow nodes represent ions unique to CPCC 452, orange nodes represent ions unique to CPCC 657, and red nodes represent ions unique to CPCC 658. Blue nodes indicate that an ion was present in multiple samples. The full molecular network consisted of 7,469 nodes (Figure S1). However, after removing nodes associated with and connected to media blanks, 2,538 nodes remained from samples.

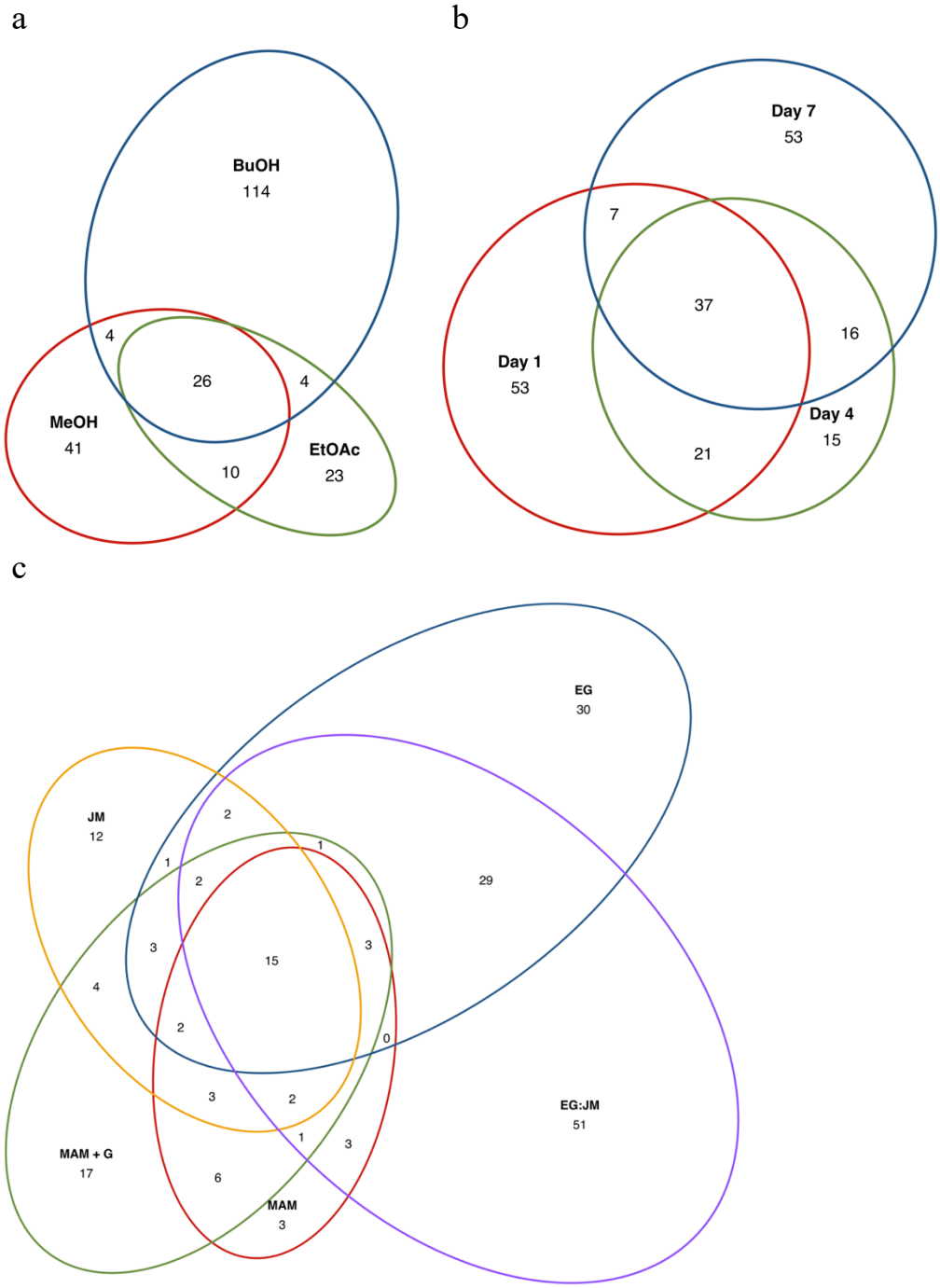

Figure II.3: Additional attributes play a role in the diversity of compounds present in the molecular network. Euler diagrams display the distribution of 202 reproducible nodes from 540 *Euglena* culture samples across extraction solvents (a), timepoints (b), and types of media (c).

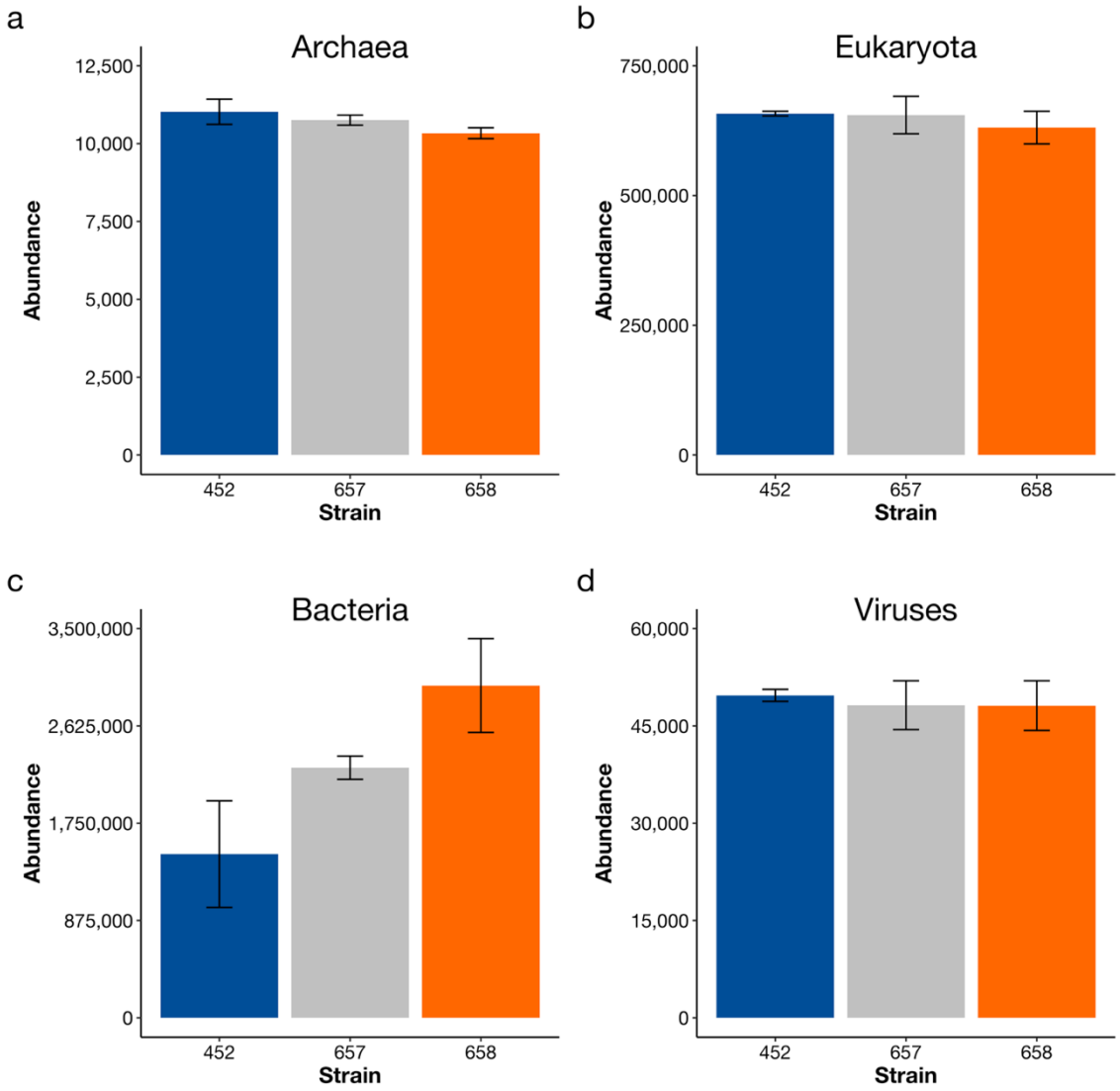

Figure II.4: Average microbial abundance at the domain level assigned taxonomically by non-redundant genes across three strains of environmental *E. mutabilis* consortia. Error bars represent the standard deviation of the number of non-redundant genes ($n = 3$).

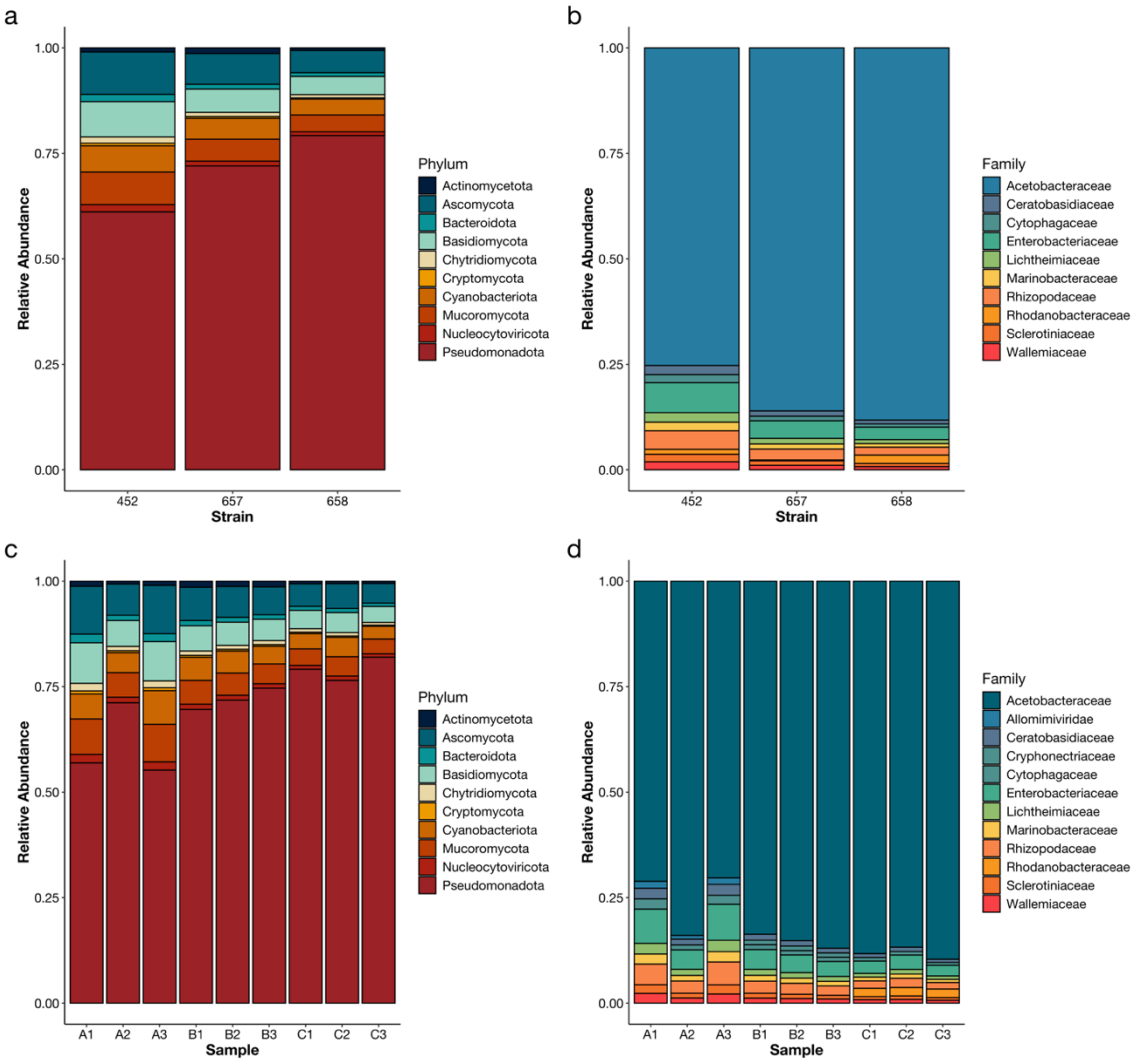

Figure II.5: Relative microbial abundance assigned taxonomically by non-redundant genes of the average top 10 most abundant microbes at phylum (a) and family (b) levels compared to top 10 most abundant microbes in each sample (A samples = CPCC 452, B samples = CPCC 657, C samples = CPCC 658) across three strains of natural *E. mutabilis* consortia.

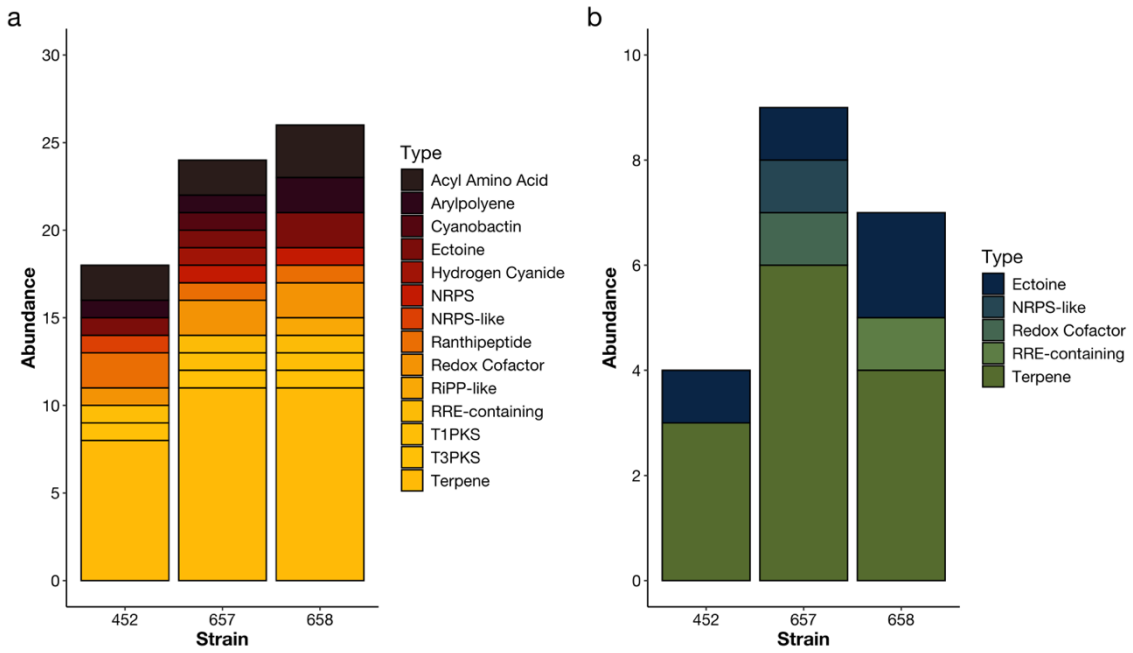

Figure II.6: Abundance of secondary metabolite regions identified using bacterial (a) and fungal (b) versions of antiSMASH v7.0 for each strain of natural *E. mutabilis* consortia.

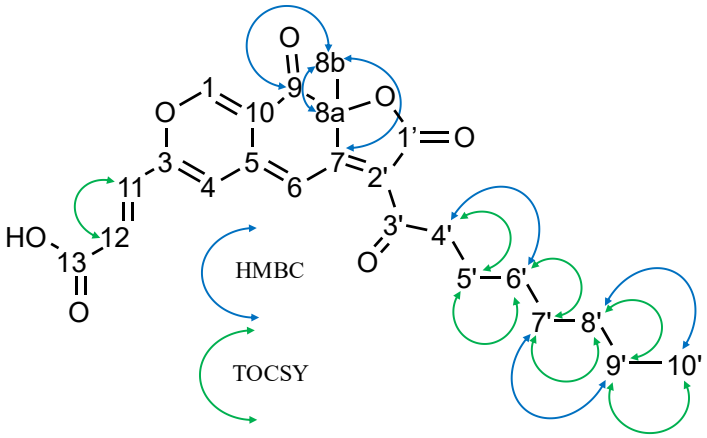

Figure II.7: Assigned atoms for NMR shifts detected in 3-(9a-methyl-3-octanoyl-2,9-dioxofuro[3,2-g]isochromen-6-yl)prop-2-enoic acid. Arrows denote shifts detected via Heteronuclear Multiple Bond Correlation (HMBC) or Total Correlation Spectroscopy (TOCSY).

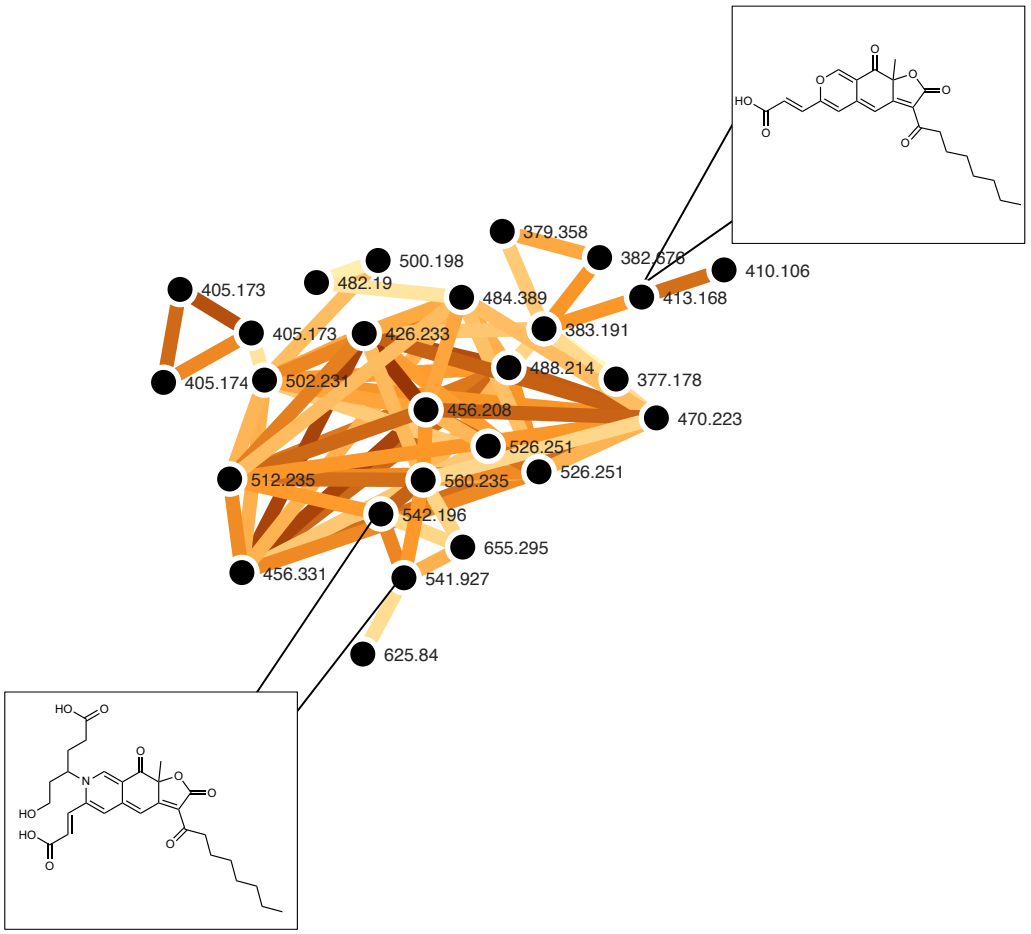

Figure II.8: Cluster containing metabolites of interest related to *Talaromyces* furanochromenes. Each node is annotated with its m/z. Associated nodes have been annotated with either their corresponding library match or their confirmed structure.

Table II.1: Cell viability test (n = 4) comparing colony forming units of *E. gracilis* (CPCC 95), *E. mutabilis* (CPCC 452, 657, 658), and fungus after 7 days of incubation on malt agar at 25°C cycling light and dark (16:8). Before plating, samples were grown in their respective media types for 7 days.

Strain	Organism	MAM	MAM + G	EG	JM	EG:JM
CPCC 95	*E. gracilis*	+++	++	+	++	++
CPCC 452	*E. mutabilis*	+	++	++	++	+++
CPCC 657	Fungus	-	+	+	-	+++
	E. mutabilis	++	++	++	++	+++
CPCC 658	Fungus	-	+	+	-	+++
	E. mutabilis	+	+	++	++	+++

Bacterial CFUs were excluded as they were too numerous to count.
"-" no CFU; "+" if < 50 CFU; "++" if 50><250 CFU; "+++" if >250 CFU or if a complete lawn is present and CFU count is impossible.

Table II.2: NMR shift comparison between the expected and observed values for 3-(9a-methyl-3-octanoyl-2,9-dioxofuro[3,2-g]isochromen-6-yl)prop-2-enoic acid.

Position	Expected		Observed	
	δ_H	δ_C	δ_H	δ_C
1	7.87, s	152.6	7.70, s	147.9
3	-	153.1	-	n.i
4	6.53, s	117.6	6.79, s	116.6
5	-	138.9	-	n.i
6	7.02, s	107.5	6.96, s	115.4
7	-	170.5	-	172.4
8a	-	86.1	-	86.6
8b	1.72, s	27.9	1.73, s	27.0
9	-	190.9	-	190.5
10	-	116.3	-	n.i
11	7.23, d (15.5)	135.3	7.91, s	130.1
12	6.52, d	125.6	7.2, d	120.0
13	-	169.6	-	n.i
1’	-	168.8	-	n.i
2’	-	116.0	-	n.i
3’	-	197.4	-	n.i
4’	2.90-3.00, m	42.0	2.9, m	40.8
5’	1.59-1.61, m	23.7	1.61, m	23.6
6’	1.26-1.30, m	29.3	1.23-1.36, m	29.2
7’	1.26-1.30, m	29.3	1.23-1.36, m	29.2
8’	1.26-1.30, m	31.9	1.23-1.36, m	29.2
9’	1.26-1.30, m	22.8	1.23-1.36, m	29.2
10’	0.88, t	14.2	0.91, t	12.9

II.9 SUPPLEMENTARY MATERIAL

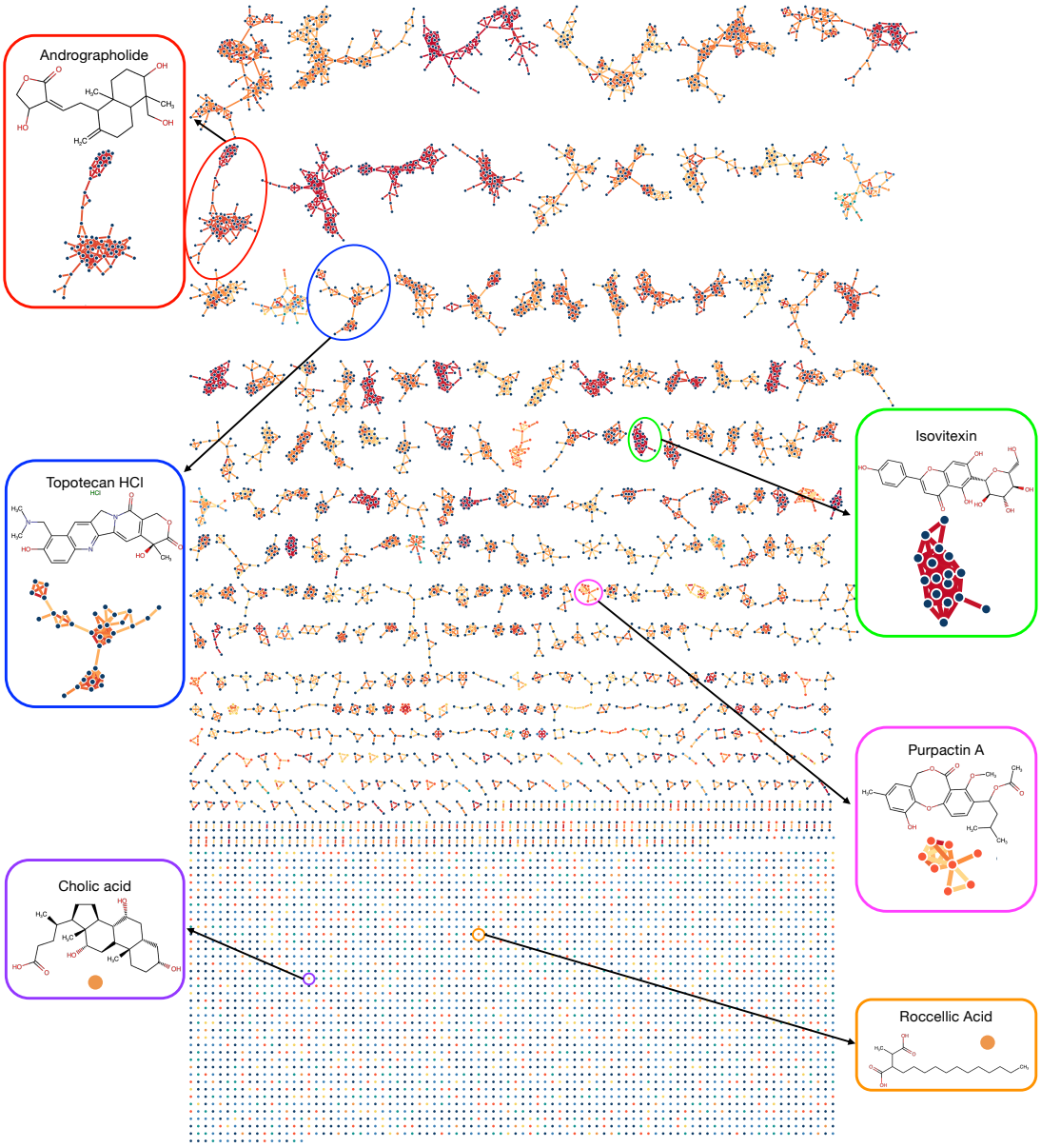

Figure SII.1: Complete molecular network from all samples and blanks. Turquoise nodes represent ions unique to CPCC 95, yellow nodes represent ions unique to CPCC 452, orange nodes represent ions unique to CPCC 657, and red nodes represent ions unique to CPCC 658. Blue nodes indicate that an ion was present in multiple samples. The 6 highlighted compounds were identified as library hits from the GNPS database and have been previously characterized as having pharmaceutical or antimicrobial properties (Table SI.1).

Table S1I.1: Overview of GNPS library matches from the full molecular network that have been previously characterized as having pharmaceutical or antimicrobial properties.

Compound Name	NP Class	Molecular Formula	Mean Retention Time	m/z Measured	Theoretical m/z	Adduct	GNPS Score	GNPS Library ID	Strains Detected	Solvent	Media	Growth Time (Days)
Andrographolide [1]	Labdane diterpenoids	C20H30O5	639.3486667	372.27	373.2	[M+Na]+	0.73	CCMSLIB00006562591	CPCC658	MeOH, EtOAc	EG, MAM+G, MAM	1, 4, 7
Cholic Acid [2]	Cholane steroids	C24H40O5	532.1365	373.27	373.27	M-2H2O+H	0.81	CCMSLIB00005435975	CPCC657	BuOH	EG:JM	7
Isovitexin [3]	Flavanols	C21H20O10	663.328	430.39	431.1	M-H	0.76	CCMSLIB00003137358	CPCC657	EtOAc, BuOH	EG:JM, MAM	1, 4 ,7
Purpactin A [4]	Depsidones	C23H26O7	644.0587778	437.15	437.16	[M+Na]+	0.93	CCMSLIB00004691898	CPCC658	EtOAc	EG, EG:JM	4, 7
Roccellic Acid [5]	Branched fatty acids; Dicarboxylic acids	C17H32O4	186.823	300.26	299.21	M-H	0.71	CCMSLIB00004751359	CPCC657	BuOH	EG:JM	7
Topotecan HCl [6]	Pyrroloquinoline alkaloids	C23H24ClN3O5	572.8618	421.31	422.17	M+H	0.82	CCMSLIB00000004934	CPCC658, CPCC657	MeOH, EtOAc, BuOH	EG, EG:JM, MAM	1, 4 ,7

Table SII.2: Non-redundant genes present in each *E. mutabilis* sample at the domain level. A samples are replicates of CPCC 452, B samples are replicates of CPCC 657, and C samples are replicates of CPCC 658.

	CPCC 452			CPCC 657			CPCC 658		
	A1	A2	A3	B1	B2	B3	C1	C2	C3
Archaea	11490.797	10788.9973	10793.3032	10668.4006	10653.7613	10940.6116	10516.2745	10167.3694	10320.4755
Eukaryota	659857.966	652677.413	661050.253	685384.831	664530.521	615196.252	595268.333	654586.549	642968.687
Bacteria	1184643.67	2025675.13	1205600.14	2135125.93	2270975.4	2340419.89	2767870.98	2721410.86	3474381.11
Viruses	50582.3854	49776.7396	48747.0791	51376.7685	49161.0039	44039.2989	43886.4828	51335.8702	49154.2086
Others	29035139.2	28202795.7	29015523.2	28059158.1	27946393.3	27931117.9	27524171.9	27504213.3	26764889.5

Table SII.3: Average 10 top phyla based on non-redundant genes present in each *E. mutabilis* sample. A samples are replicates of CPCC 452, B samples are replicates of CPCC 657, and C samples are replicates of CPCC 658.

	CPCC 452			CPCC 657			CPCC 658		
	A1	A2	A3	B1	B2	B3	C1	C2	C3
Pseudomonadota	901387.969	1714678.77	879428.523	1762822.01	1903016	2005631.76	2448824.7	2362677.09	3144899.03
Ascomycota	179517.569	178360.801	182025.981	199705.473	194174.873	177319.231	165626.76	180902.398	178528.496
Basidiomycota	152529.374	147735.579	148018.323	152145.213	145813.587	135746.316	135117.996	146608.944	145131.617
Mucoromycota	133164.424	139923.873	142184.124	143046.748	139643.988	126678.011	121056.343	141756.071	133889.925
Cyanobacteriota	93960.3522	114212.128	126965.631	138820.009	138075.124	113010.71	112827.709	141108.189	116234.813
Actinomycetota	19040.3644	16269.5522	15988.2506	36494.3798	33381.101	36690.996	19476.0409	18498.1679	21151.1162
Bacteroidota	32691.4222	29788.9419	29976.6804	31231.2562	30073.4429	28717.2737	29119.1585	30362.3271	30058.0265
Nucleocytoviricota	31590.8989	30813.7664	30308.0636	31545.7148	30250.1744	27377.0148	27395.5369	31446.6566	30243.055
Chytridiomycota	27994.3771	25302.378	25910.6006	25572.9025	25202.5087	25536.5318	24960.8575	24574.3087	24800.9398
Cryptomycota	11291.6564	10869.1275	10913.2559	11201.6305	10647.5787	10051.2329	9915.05558	10680.9234	10626.3188
Others	29294736.3	28471952.5	29286716	28343781.2	28227705.2	28193428	27787544.2	27790278.2	27043367.5

Table SII.4: Average 10 top families based on non-redundant genes present in each *E. mutabilis* sample. A samples are replicates of CPCC 452, B samples are replicates of CPCC 657, and C samples are replicates of CPCC 658.

	CPCC 452			CPCC 657			CPCC 658		
	A1	A2	A3	B1	B2	B3	C1	C2	C3
Acetobacteraceae	669285.862	1419503.31	647331.332	1443604.08	1578245.47	1679489.71	2066270.58	1975934.1	2685711.96
Enterobacteriaceae	76479.4023	78098.749	78687.2464	81008.1875	77351.3478	69126.3482	68543.4921	77510.3803	76495.1657
Rhodanobacteraceae	12627.1847	14297.5555	12046.9359	4853.54317	3636.53273	2651.94508	46081.163	45384.5003	61189.7453
Rhizopodaceae	45824.5665	48905.9287	50043.5984	49512.3362	48224.2377	43015.8228	41264.5015	49914.4978	46613.0973
Lichtheimiaceae	23685.7936	24801.03	24808.3448	24695.7291	24387.595	22006.8227	21299.801	24954.0758	23652.8613
Ceratobasidiaceae	23639.1166	23565.1939	24002.7013	24210.0342	23382.9788	21754.0348	21301.8696	23475.8243	22888.3078
Marinobacteraceae	22548.2687	21938.9666	22358.9295	23297.2079	22323.3023	20832.4299	20504.1745	22667.1659	22021.6675
Cytophagaceae	22845.0766	19605.7408	19348.101	20013.8333	19182.2489	18916.6835	19206.8464	19066.578	19992.664
Wallemiaceae	21872.8356	20470.4522	20062.7016	20459.88	20030.1759	18879.9774	19049.3842	20170.8755	20385.0603
Sclerotiniaceae	19214.6633	19395.3473	19862.0786	20116.1615	19133.9673	17135.4483	17129.8741	18875.1457	18645.1538
Others	29619681.1	28861127.6	29636401.2	28774388.1	28661326.6	28607491.2	28208908.4	28237416.8	27519345.5

Table SII.5: Actual 10 top families based on non-redundant genes present in each *E. mutabilis* sample. A samples are replicates of CPCC 452, B samples are replicates of CPCC 657, and C samples are replicates of CPCC 658.

	CPCC 452			CPCC 657			CPCC 658		
	A1	A2	A3	B1	B2	B3	C1	C2	C3
Acetobacteraceae	669285.862	1419503.31	647331.332	1443604.08	1578245.47	1679489.71	2066270.58	1975934.1	2685711.96
Enterobacteriaceae	76479.4023	78098.749	78687.2464	81008.1875	77351.3478	69126.3482	68543.4921	77510.3803	76495.1657
Rhodanobacteraceae	-	-	-	-	-	-	46081.163	45384.5003	61189.7453
Rhizopodaceae	45824.5665	48905.9287	50043.5984	49512.3362	48224.2377	43015.8228	41264.5015	49914.4978	46613.0973
Lichtheimiaceae	23685.7936	24801.03	24808.3448	24695.7291	24387.595	22006.8227	21299.801	24954.0758	23652.8613
Ceratobasidiaceae	23639.1166	23565.1939	24002.7013	24210.0342	23382.9788	21754.0348	21301.8696	23475.8243	22888.3078
Marinobacteraceae	22548.2687	21938.9666	22358.9295	23297.2079	22323.3023	20832.4299	20504.1745	22667.1659	22021.6675
Cytophagaceae	22845.0766	19605.7408	19348.101	20013.8333	19182.2489	18916.6835	19206.8464	19066.578	19992.664
Wallemiaceae	21872.8356	20470.4522	20062.7016	20459.88	20030.1759	18879.9774	19049.3842	20170.8755	20385.0603
Sclerotiniaceae	19214.6633	19395.3473	19862.0786	20116.1615	19133.9673	17135.4483	17129.8741	18875.1457	18645.1538
Allomimiviridae	15549.3915	14329.506	14101.934	-	-	-	-	-	-
Cryphonectriaceae	-	-	-	18323.6672	20032.2751	19517.4787	-	-	-
Others	29294736.3	28471952.5	29286716	28343781.2	28227705.2	28193428	27787544.2	27790278.2	27043367.5

Table SII.6: Spot count of top 10 hits from NCBI taxonomic analysis for each *E. mutabilis* sample. A samples are replicates of CPCC 452, B samples are replicates of CPCC 657, and C samples are replicates of CPCC 658.

	CPCC 452			CPCC 657			CPCC 658		
	A1	A2	A3	B1	B2	B3	C1	C2	C3
Acidibrevibacterium fodinaquatile	60675	86230	57429	5706	-	5392	9381	7844	10119
Acidocella aminolytica 101 = DSM 11237	-	-	-	-	-	-	7660	6861	8178
Acidiphilium acidophilum	125177	229295	139809	1100702	945019	1042106	1026915	949216	1224555
Acidiphilium cryptum JF-5	20882	40765	23144	39688	46191	43788	55165	46296	65642
Acidiphilium multivorum AIU301	-	4895	-	-	-	-	-	-	-
Acidiphilium sp.	80675	152599	80519	132525	156746	158246	192673	167404	230554
Acidiphilium sp. C61	-	5520	-	4871	5729	5542	6893	-	8232
Acidiphilium sp. JA12-A1	9873	19432	9797	16663	20138	19626	24291	22154	30012
Acidiphilium sp. PA	-	4561	2970	12609	11292	12432	22048	20279	25479
Acidiphilium sp. PM	5093	9648	4960	8240	10180	10174	12452	10839	15529
Klebsiella pneumoniae	-	-	-	7617	6896	6663	-	-	-
Metallibacterium scheffleri	22354	25054	24444	-	-	-	92837	80239	113371
Methylosoma difficile	3460	-	4981	5490	5460	-	-	-	-
Salarias fasciatus	-	-	-	-	21082	22098	-	18790	-
Salvelinus namaycush	3675	-	3440	-	-	-	-	-	-
Triticum	3681	-	-	-	-	-	-	-	-

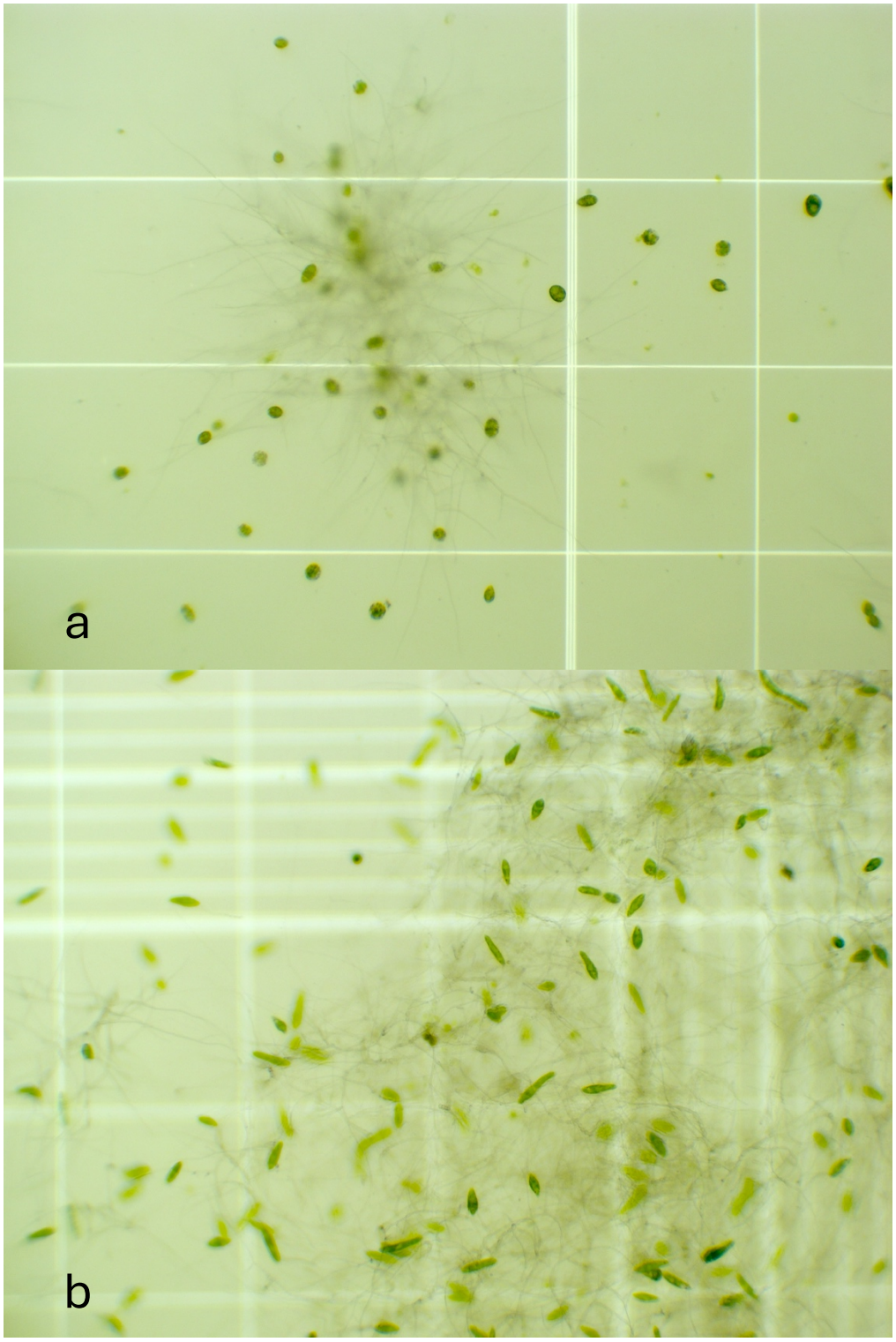

Figure SII.2: Growth of *E. mutabilis* (CPCC 658) after 7 days of growth in EG (a) and EG:JM (b) media at 10x magnification.

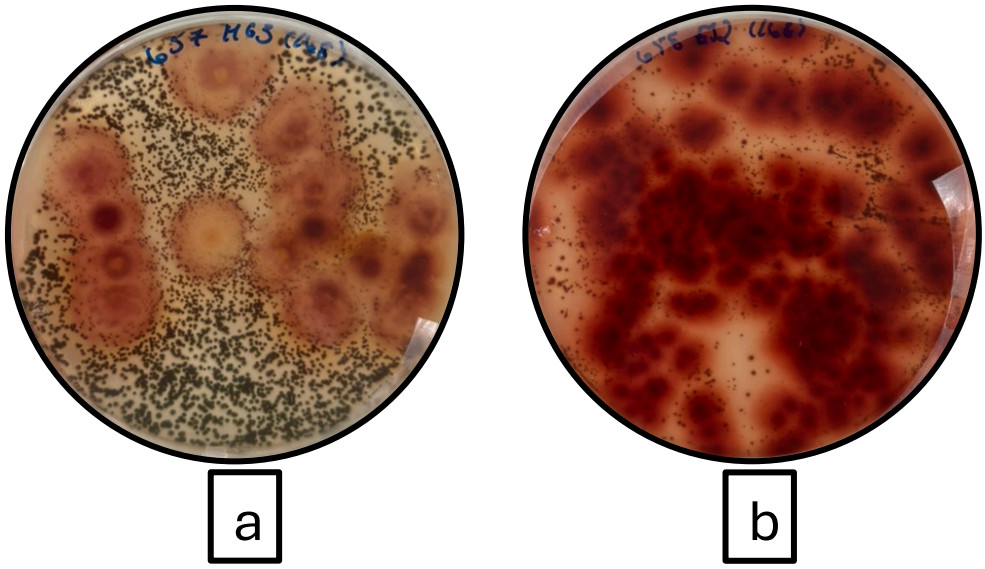

Figure SII.3: Plate photographs of an *E. mutabilis* co-culture (CPCC 657) after 7 days on malt agar following 7 days of growth in MAM + G (a) and of an *E. mutabilis* co-culture (CPCC 658) after 7 days on malt agar following 7 days of growth in EG:JM (b).

Table SII.7: BGC predicted using the bacterial antiSMASH database for *E. mutabilis* co-cultures. The percentage (%) indicates the proportion of gene similarities to predicted clusters. T1PKS: type I polyketide synthase; T3PKS: type III polyketide synthase; NRPS: non-ribosomal peptide synthase; RiPP-like: Ribosomally synthesized and post-translationally modified peptides; RRE-containing: RiPP recognition element.

Results from Bacterial antiSMASH Database				
Strain	Gene Type	Span [nt]		Most Similar Biosynthetic Gene Cluster
		From	To	
452	Acyl Amino Acid	1	1,058	
	Acyl Amino Acid	90,223	141,655	
	Aryl polyene	1	1,903	
	Ectoine	142,365	152,763	Ectoine (66%)
	NRPS-like	1	2,685	
	Ranthipeptide	1	7,895	
	Ranthipeptide	1	1,392	
	Redox Cofactor	7,602	29,732	
	T1PKS	1	2,829	
	T3PKS	1	6,646	
	Terpene	1	1,255	
	Terpene	1	5,004	
	Terpene	1	7,870	
	Terpene	1	9,578	Carotenoid (100%)
	Terpene	1	10,055	
	Terpene	4,352	25,413	Carotenoid (100%)
	Terpene	8,749	30,457	
	Terpene	80,211	102,160	
657	Acyl Amino Acid	1	4,244	
	Acyl Amino Acid	90,223	141,655	
	Aryl polyene	1	5,279	
	Cyanobactin	1	1,592	
	Ectoine	142,365	152,763	Ectoine (66%)
	Hydrogen Cyanide	1	5,132	
	NRPS	1,762	45,700	
	Ranthipeptide	1	3,388	
	Redox Cofactor	1	21,493	
	Redox Cofactor	7,602	29,732	
	RRE-containing	1	1,430	
	T1PKS	1	2,858	
	T3PKS	47,015	88,142	Thaxteramide C (11%)

	Terpene	1	1,742	
	Terpene	1	1,810	
	Terpene	1	2,901	
	Terpene	1	3,573	
	Terpene	1	3,715	
	Terpene	4,352	25,413	Carotenoid (100%)
	Terpene	8,749	30,457	
	Terpene	20,952	42,904	
	Terpene	41,049	62,113	Carotenoid (100%)
	Terpene	41,904	63,600	
	Terpene	80,211	102,160	
	Acyl Amino Acid	1	2,149	
	Acyl Amino Acid	1	4,463	
	Acyl Amino Acid	90,223	141,655	
	Aryl polyene	1	7,474	
	Aryl polyene	1	24,434	
	Ectoine	3,753	13,779	Ectoine (66%)
	Ectoine	142,365	152,763	Ectoine (66%)
	NRPS	9,819	53,266	
	Ranthipeptide	1	6,237	
	Redox Cofactor	7,602	29,732	
	Redox Cofactor	9,295	30,784	
	RiPP-like	37,446	48,360	
658	RRE-containing	1	3,509	
	T1PKS	1	2,857	
	T3PKS	1	38,804	Thaxteramide C (11%)
	Terpene	1	2,025	
	Terpene	1	2,384	
	Terpene	1	3,006	
	Terpene	1	3,446	
	Terpene	1	8,387	
	Terpene	1	11,232	
	Terpene	4,492	25,559	Carotenoid (100%)
	Terpene	8,749	30,457	
	Terpene	22,474	44,417	
	Terpene	41,693	62,757	Carotenoid (100%)
	Terpene	80,211	102,160	

Table SII.8: BGC predicted using the fungal antiSMASH database for *E. mutabilis* co-cultures. The percentage (%) indicates the proportion of gene similarities to predicted clusters. NRPS: non-ribosomal peptide synthase; RRE-containing: RiPP recognition element.

Results from Fungal antiSMASH Database				
Strain	Gene Type	Span [nt]		Most Similar Biosynthetic Gene Cluster
		From	To	
452	Ectoine	142,365	155,391	Ectoine (33%)
	Terpene	1	9,578	
	Terpene	8,749	30,457	
	Terpene	80,211	102,160	
657	Ectoine	142,365	155,391	Ectoine (40%)
	NRPS-like	1	2,089	
	Redox Cofactor	1	23,824	
	Terpene	1	3,573	
	Terpene	1	1,742	
	Terpene	1	1,810	
	Terpene	8,749	30,457	
	Terpene	41,578	64,829	
	Terpene	80,211	102,160	
658	Ectoine	39	13,779	
	Ectoine	142,365	155,391	Ectoine (33%)
	Redox Cofactor	6,964	30,784	
	RRE-containing	1	3,509	
	Terpene	1	2,025	
	Terpene	8,749	30,457	
	Terpene	80,211	102,160	

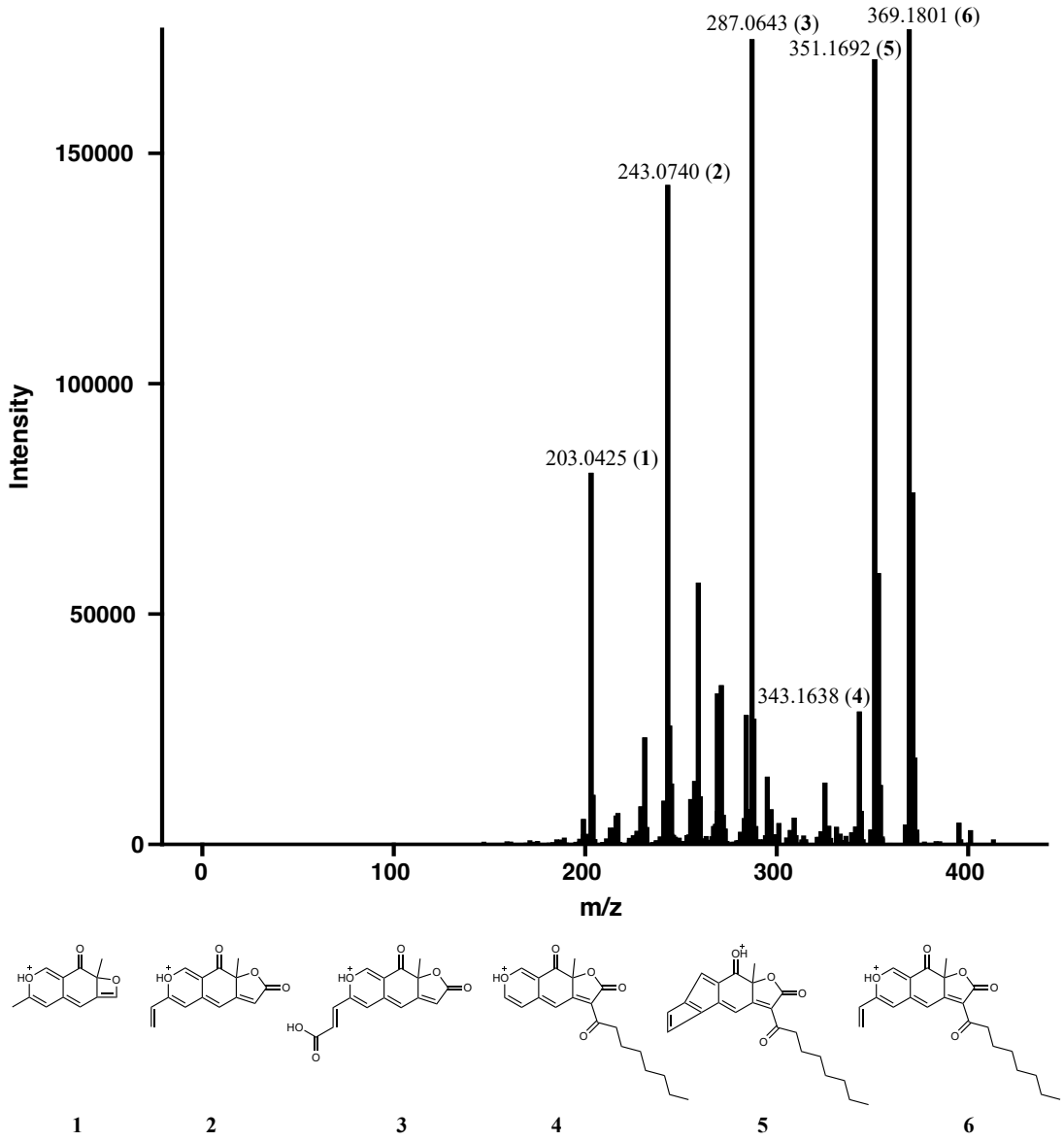

Figure SII.4: MS/MS assignment for precursor m/z 413.16. Predicted structures are shown below assigned peaks

II.10 REFERENCES

1. Maplestone RA, Stone MJ, Williams DH. The evolutionary role of secondary metabolites — a review. Gene. 1992;115(1–2):151–7. https://doi.org/10.1016/0378-1119(92)90553-2.
2. Newman DJ, Cragg GM. Natural products as sources of new drugs over the nearly four decades from 01/1981 to 09/2019. J Nat Prod. 2020;83(3):770–803. https://doi.org/10.1021/acs.jnatprod.9b01285.
3. Suresh PS, Kumari S, Sahal D, Sharma U. Innate functions of natural products: A promising path for the identification of novel therapeutics. Eur J Med Chem. 2023;260:115748. https://doi.org/10.1016/j.ejmech.2023.115748.
4. Scherlach K, Hertweck C. Mediators of mutualistic microbe–microbe interactions. Nat Prod Rep. 2018;35(4):303–8. https://doi.org/10.1039/C7NP00035A.
5. Murray CJL, Ikuta KS, Sharara F, Swetschinski L, Robles Aguilar G, Gray A, *et al*. Global burden of bacterial antimicrobial resistance in 2019: A systematic analysis. The Lancet. 2022;399(10325):629–55. https://doi.org/10.1016/S0140-6736(21)02724-0.
6. Ligon BL. Penicillin: Its discovery and early development. Semin Pediatr Infect Dis. 2004;15(1):52–7. https://doi.org/10.1053/j.spid.2004.02.001.
7. Gümüşçü A, Arslan N, Sarıhan EO. Evaluation of selected poppy (*Papaver somniferum* L.) lines by their morphine and other alkaloids contents. Eur Food Res Technol. 2008;226(5):1213–20. https://doi.org/10.1007/s00217-007-0739-0.
8. Hutchings MI, Truman AW, Wilkinson B. Antibiotics: Past, present and future. Curr Opin Microbiol. 2019;51:72–80. https://doi.org/10.1016/j.mib.2019.10.008.
9. Schneider YK. Bacterial natural product drug discovery for new antibiotics: Strategies for tackling the problem of antibiotic resistance by efficient bioprospecting. Antibiotics. 2021;10(7):842. https://doi.org/10.3390/antibiotics10070842.
10. Atanasov AG, Zotchev SB, Dirsch VM, the International Natural Product Sciences Taskforce, Orhan IE, Banach M, *et al*. Natural products in drug discovery: Advances and opportunities. Nat Rev Drug Discov. 2021;20(3):200–16. https://doi.org/10.1038/s41573-020-00114-z.
11. Dias DA, Urban S, Roessner U. A historical overview of natural products in drug discovery. Metabolites. 2012;2(2):303–36. https://doi.org/10.3390/metabo2020303.
12. Cordell GA, Shin YG. Finding the needle in the haystack. The dereplication of natural product extracts. Pure Appl Chem. 1999;71(6):1089–94. https://doi.org/10.1351/pac199971061089.
13. Zhuang L, Zhang H. Utilizing cross-species co-cultures for discovery of novel natural products. Curr Opin Biotechnol. 2021;69:252–62. https://doi.org/10.1016/j.copbio.2021.01.023.
14. Blin K, Shaw S, Augustijn HE, Reitz ZL, Biermann F, Alanjary M, *et al*. antiSMASH 7.0: New and improved predictions for detection, regulation, chemical structures and visualisation. Nucleic Acids Res. 2023;51(W1):W46–50. https://doi.org/10.1093/nar/gkad344.

15. Mullowney MW, Duncan KR, Elsayed SS, Garg N, Van Der Hooft JJJ, Martin NI, *et al*. Artificial intelligence for natural product drug discovery. Nat Rev Drug Discov. 2023;22(11):895–916. https://doi.org/10.1038/s41573-023-00774-7.
16. De França P, Costa JH, Fill TP, Lancellotti M, Ruiz ALTG, Fantinatti-Garboggini F. Genome mining reveals secondary metabolites of Antarctic bacterium *Streptomyces albidoflavus* related to antimicrobial and antiproliferative activities. Arch Microbiol. 2023;205(11):354. https://doi.org/10.1007/s00203-023-03691-w.
17. Tong CY, Honda K, Derek CJC. A review on microalgal-bacterial co-culture: The multifaceted role of beneficial bacteria towards enhancement of microalgal metabolite production. Environ Res. 2023;228:115872. https://doi.org/10.1016/j.envres.2023.115872.
18. Crüsemann M, O'Neill EC, Larson CB, Melnik AV, Floros DJ, Da Silva RR, *et al*. Prioritizing natural product diversity in a collection of 146 bacterial strains based on growth and extraction protocols. J Nat Prod. 2017;80(3):588–97. https://doi.org/10.1021/acs.jnatprod.6b00722.
19. Shi Y, Pan C, Wang K, Chen X, Wu X, Chen CA, *et al*. Synthetic multispecies microbial communities reveals shifts in secondary metabolism and facilitates cryptic natural product discovery. Environ Microbiol. 2017;19(9):3606–18. https://doi.org/10.1111/1462-2920.13858.
20. Krespach MKC, García-Altares M, Flak M, Hanno Schoeler, Scherlach K, Netzker T, *et al*. Lichen-like association of *Chlamydomonas reinhardtii* and *Aspergillus nidulans* protects algal cells from bacteria. ISME J. 2020;14(11):2794–805. https://doi.org/10.1038/s41396-020-0731-2.
21. Wang R, Zhao S, Wang Z, Koffas MA. Recent advances in modular co-culture engineering for synthesis of natural products. Curr Opin Biotechnol. 2020;62:65–71. https://doi.org/10.1016/j.copbio.2019.09.004.
22. Xu S, Li M, Hu Z, Shao Y, Ying J, Zhang H. The potential use of fungal co-culture strategy for discovery of new secondary metabolites. Microorganisms. 2023;11(2):464. https://doi.org/10.3390/microorganisms11020464.
23. Gao L, Zhao X, Liu M, Zhao X. Characterization and antibacterial activities of carboxymethylated paramylon from *Euglena gracilis*. Polymers. 2022;14(15):3022. https://doi.org/10.3390/polym14153022.
24. Aldholmi M, Ahmad R, Carretero-Molina D, Pérez-Victoria I, Martín J, Reyes F, *et al*. Euglenatides, potent antiproliferative cyclic peptides isolated from the freshwater photosynthetic microalga *Euglena gracilis*. Angew Chem Int Ed. 2022;61(23):e202203175. https://doi.org/10.1002/anie.202203175.
25. Bedard S, Roxborough E, O'Neill E, Mangal V. The biomolecules of *Euglena gracilis*: Harnessing biology for natural solutions to future problems. Protist. 2024;175(4):126044. https://doi.org/10.1016/j.protis.2024.126044.
26. Halter D, Goulhen-Chollet F, Gallien S, Casiot C, Hamelin J, Gilard F, *et al*. In situ proteo-metabolomics reveals metabolite secretion by the acid mine drainage bio-indicator, *Euglena mutabilis*. ISME J. 2012;6(7):1391–402. https://doi.org/10.1038/ismej.2011.198.
27. Brake SS, Hasiotis ST, Dannelly HK. Diatoms in acid mine drainage and their role in the formation of iron-rich stromatolites. Geomicrobiol J. 2004;21(5):331–40. https://doi.org/10.1080/01490450490454074.

28. Nakatsu C, Hutchinson TC. Extreme metal and acid tolerance of *Euglena mutabilis* and an associated yeast from Smoking Hills, Northwest Territories, and their apparent mutualism. Microb Ecol. 1988;16(2):213–31. https://doi.org/10.1007/BF02018915.
29. Kaszecki E, Palberg D, Grant M, Griffin S, Dhanjal C, Capperauld M, *et al*. *Euglena mutabilis* exists in a FAB consortium with microbes that enhance cadmium tolerance. Int Microbiol. 2024. https://doi.org/10.1007/s10123-023-00474-7.
30. Kumar R, Patel DD, Bansal DD, Mishra S, Mohammed A, Arora R, *et al*. Extremophiles: Sustainable resource of natural compounds-extremolytes. In: Singh OV, Harvey SP, editors. Sustainable Biotechnology. Dordrecht: Springer Netherlands; 2010. p. 279–94.
31. Canadian Phycological Culture Centre. Modified acid medium (MAM). University of Waterloo. 2017. https://uwaterloo.ca/canadian-phycological-culture-centre/cultures/culture-media/modified-acid-medium.
32. Culture Collection of Algae and Protozoa. EG:JM. 2019. https://www.ccap.ac.uk/wp-content/uploads/MR_EG_JM.pdf.
33. Adusumilli R, Mallick P. Data conversion with ProteoWizard msConvert. Methods Mol Biol Clifton NJ. 2017;1550:339–68. https://doi.org/10.1007/978-1-4939-6747-6_23.
34. Wang M, Carver JJ, Phelan VV, Sanchez LM, Garg N, Peng Y, *et al*. Sharing and community curation of mass spectrometry data with Global Natural Products Social Molecular Networking. Nat Biotechnol. 2016;34(8):828–37. https://doi.org/10.1038/nbt.3597.
35. Cline MS, Smoot M, Cerami E, Kuchinsky A, Landys N, Workman C, *et al*. Integration of biological networks and gene expression data using Cytoscape. Nat Protoc. 2007;2(10):2366–82. https://doi.org/10.1038/nprot.2007.324.
36. Larsson J, Godfrey AJR, Gustafsson P, algorithms) DHE (geometric, code) EH (root solver, Privé F. eulerr: Area-Proportional Euler and Venn Diagrams with Ellipses. 2022.
37. RStudio Team. RStudio: Integrated development environment for R. Boston, MA: RStudio, PBC.; 2020.
38. R Core Team. R: A language and environment for statistical computing. Vienna, Austria: R Foundation for Statistical Computing; 2024.
39. Chen S. Ultrafast one-pass FASTQ data preprocessing, quality control, and deduplication using fastp. iMeta. 2023;2(2):e107. https://doi.org/10.1002/imt2.107.
40. Karlsson FH, Fåk F, Nookaew I, Tremaroli V, Fagerberg B, Petranovic D, *et al*. Symptomatic atherosclerosis is associated with an altered gut metagenome. Nat Commun. 2012;3(1):1245. https://doi.org/10.1038/ncomms2266.
41. Karlsson FH, Tremaroli V, Nookaew I, Bergström G, Behre CJ, Fagerberg B, *et al*. Gut metagenome in European women with normal, impaired and diabetic glucose control. Nature. 2013;498(7452):99–103. https://doi.org/10.1038/nature12198.
42. Qin N, Yang F, Li A, Prifti E, Chen Y, Shao L, *et al*. Alterations of the human gut microbiome in liver cirrhosis. Nature. 2014;513(7516):59–64. https://doi.org/10.1038/nature13568.
43. Qin J, Li R, Raes J, Arumugam M, Burgdorf KS, Manichanh C, *et al*. A human gut microbial gene catalogue established by metagenomic sequencing. Nature. 2010;464(7285):59–65. https://doi.org/10.1038/nature08821.

44. Li J, Jia H, Cai X, Zhong H, Feng Q, Sunagawa S, *et al*. An integrated catalog of reference genes in the human gut microbiome. Nat Biotechnol. 2014;32(8):834–41. https://doi.org/10.1038/nbt.2942.
45. Zeller G, Tap J, Voigt AY, Sunagawa S, Kultima JR, Costea PI, *et al*. Potential of fecal microbiota for early-stage detection of colorectal cancer. Mol Syst Biol. 2014;10(11):766. https://doi.org/10.15252/msb.20145645.
46. Buchfink B, Xie C, Huson DH. Fast and sensitive protein alignment using DIAMOND. Nat Methods. 2015;12(1):59–60. https://doi.org/10.1038/nmeth.3176.
47. Venkatachalam M, Zelena M, Cacciola F, Ceslova L, Girard-Valenciennes E, Clerc P, *et al*. Partial characterization of the pigments produced by the marine-derived fungus *Talaromyces albobiverticillius* 30548. Towards a new fungal red colorant for the food industry. J Food Compos Anal. 2018;67:38–47. https://doi.org/10.1016/j.jfca.2017.12.036.
48. Li Y-Z, Zhang W-Q, Hu P-F, Yang Q-Q, Molnár I, Xu P, *et al*. Harnessing microbial co-culture to increase the production of known secondary metabolites. Nat Prod Rep. 2025;42(3):623–37. https://doi.org/10.1039/D4NP00052H.
49. Peng X-Y, Wu J-T, Shao C-L, Li Z-Y, Chen M, Wang C-Y. Co-culture: Stimulate the metabolic potential and explore the molecular diversity of natural products from microorganisms. Mar Life Sci Technol. 2021;3(3):363–74. https://doi.org/10.1007/s42995-020-00077-5.
50. Urui M, Yamada Y, Ikeda Y, Nakagawa A, Sato F, Minami H, *et al*. Establishment of a co-culture system using *Escherichia coli* and *Pichia pastoris* (Komagataella phaffii) for valuable alkaloid production. Microb Cell Factories. 2021;20(1):200. https://doi.org/10.1186/s12934-021-01687-z.
51. Jaworski GHM, Talling JF, Heaney SI. The influence of carbon dioxide-depletion on growth and sinking rate of two planktonic diatoms in culture. Br Phycol J. 1981;16(4):395–410. https://doi.org/10.1080/00071618100650461.
52. Bates RC, Hurlbert R*E.* The effect of acetate on *Euglena gracilis* var. bacillaris as a function of environmental conditions. J Protozool. 1970;17(1):134–8. https://doi.org/10.1111/j.1550-7408.1970.tb05172.x.
53. Nicolas P, Freyssinet G, Nigon V. Effect of light on glucose utilization by *Euglena gracilis*. Plant Physiol. 1980;65(4):631–4. https://doi.org/10.1104/pp.65.4.631.
54. Cook JR, Heinrich B. Glucose vs. acetate metabolism in *Euglena*. J Protozool. 1965;12(4):581–4. https://doi.org/10.1111/j.1550-7408.1965.tb03258.x.
55. Goo E, Kang Y, Lim JY, Ham H, Hwang I. Lethal consequences of overcoming metabolic restrictions imposed on a cooperative bacterial population. mBio. 2017;8(1):e00042-17. https://doi.org/10.1128/mBio.00042-17.
56. Gonçalves IL, Mielniczki-Pereira AA, Piovezan Borges AC, Valduga AT. Metabolic modeling and comparative biochemistry in glyoxylate cycle. Acta Sci Biol Sci. 2016;38(1):1. https://doi.org/10.4025/actascibiolsci.v38i1.24597.
57. Boos W, Shuman H. Maltose/maltodextrin system of *Escherichia coli*: Transport, metabolism, and regulation. Microbiol Mol Biol Rev. 1998;62(1):204–29. https://doi.org/10.1128/MMBR.62.1.204-229.1998.
58. Gancedo JM. Yeast carbon catabolite repression. Microbiol Mol Biol Rev. 1998;62(2):334–61. https://doi.org/10.1128/MMBR.62.2.334-361.1998.

59. Kalra R, Conlan XA, Goel M. Fungi as a potential source of pigments: Harnessing filamentous fungi. Front Chem. 2020;8:369. https://doi.org/10.3389/fchem.2020.00369.
60. Pimenta LPS, Gomes DC, Cardoso PG, Takahashi JA. Recent findings in azaphilone pigments. J Fungi. 2021;7(7):541. https://doi.org/10.3390/jof7070541.
61. Chen C, Tao H, Chen W, Yang B, Zhou X, Luo X, *et al*. Recent advances in the chemistry and biology of azaphilones. RSC Adv. 2020;10(17):10197–220. https://doi.org/10.1039/D0RA00894J.
62. Li L, Liu Z, Zhang M, Meng D, Liu X, Wang P, *et al*. Insights into the metabolism and evolution of the genus *Acidiphilium*, a typical acidophile in acid mine drainage. mSystems. 2020;5(6):e00867-20. https://doi.org/10.1128/mSystems.00867-20.
63. Santana-Molina C, Rivas-Marin E, Rojas AM, Devos DP. Origin and evolution of polycyclic triterpene synthesis. Mol Biol Evol. 2020;37(7):1925–41. https://doi.org/10.1093/molbev/msaa054.
64. Chen J, Qiao D, Yuan T, Feng Y, Zhang P, Wang X, *et al*. Biotechnological production of ectoine: Current status and prospects. Folia Microbiol (Praha). 2024;69(2):247–58. https://doi.org/10.1007/s12223-023-01105-4.
65. Schöner TA, Gassel S, Osawa A, Tobias NJ, Okuno Y, Sakakibara Y, *et al*. Aryl polyenes, a highly abundant class of bacterial natural products, are functionally related to antioxidative carotenoids. ChemBioChem. 2016;17(3):247–53. https://doi.org/10.1002/cbic.201500474.
66. Liu Y. Nonribosomal antibacterial peptides that target multidrug-resistant bacteria. Nat Prod Rep. 2019. https://doi.org/10.1039/C8NP00031J.
67. Agrawal S, Acharya D, Adholeya A, Barrow CJ, Deshmukh SK. Nonribosomal peptides from marine microbes and their antimicrobial and anticancer potential. Front Pharmacol. 2017;8:828. https://doi.org/10.3389/fphar.2017.00828.
68. Kato S, Soshino M, Takaichi S, Ishikawa T, Nagata N, Asahina M, *et al*. Suppression of the phytoene synthase gene (EgcrtB) alters carotenoid content and intracellular structure of *Euglena gracilis*. BMC Plant Biol. 2017;17:125. https://doi.org/10.1186/s12870-017-1066-7.
69. Prado-Alonso L, Pérez-Victoria I, Malmierca MG, Montero I, Rioja-Blanco E, Martín J, *et al*. Colibrimycins, Novel halogenated hybrid polyketide synthase-nonribosomal peptide synthetase (PKS-NRPS) compounds produced by *Streptomyces* sp. strain CS147. Appl Environ Microbiol. 2022;88(1):e0183921. https://doi.org/10.1128/AEM.01839-21.
70. Lage S, Mazur-Marzec H, Gorokhova *E.* Interspecific interactions drive nonribosomal peptide production in *Nodularia spumigena*. Appl Environ Microbiol. 2022;88(15):e00966-22. https://doi.org/10.1128/aem.00966-22.

II.11 SUPPLEMENTARY MATRIAL REFERENCES

1. Banerjee M, Parai D, Chattopadhyay S, Mukherjee SK. Andrographolide:Antibacterial activity against common bacteria of human health concern and possible mechanism of action. Folia Microbiol (Praha). 2017;62(3):237–44. https://doi.org/10.1007/s12223-017-0496-9.
2. Savage PB, Li C. Cholic acid derivatives: Novel antimicrobials. Expert Opin Investig Drugs. 2000;9(2):263–72. https://doi.org/10.1517/13543784.9.2.263.
3. Xiang H, Yang P, Wang L, Li J, Wang T, Xue J, *et al*. Isovitexin is a direct inhibitor of *Staphylococcus aureus* Coagulase. J Microbiol Biotechnol. 2021;31(10):1350–7. https://doi.org/10.4014/jmb.2105.05013.
4. Salvatore MM, Nicoletti R, Fiorito F, Andolfi A. Penicillides from *Penicillium* and *Talaromyces*: Chemical structures, occurrence and bioactivities. Molecules. 2024;29(16):3888. https://doi.org/10.3390/molecules29163888.
5. Mishra T, Shukla S, Meena S, Singh R, Pal M, Upreti DK, *et al*. Isolation and identification of cytotoxic compounds from a fruticose lichen *Roccella montagnei*, and it's *in silico* docking study against CDK-10. Rev Bras Farmacogn. 2017;27(6):724–8. https://doi.org/10.1016/j.bjp.2017.07.006.
6. Patel K, Craig SB, McBride MG, Palepu NR. Microbial inhibitory properties and stability of topotecan hydrochloride injection. Am J Health Syst Pharm. 1998;55(15):1584–7. https://doi.org/10.1093/ajhp/55.15.1584.